Amine hydrochloride salts: a problem in polyurethane synthesis

Emma K Gibson

For the degree of Doctor of Philosophy

Department of Chemistry

UNIVERSITY
of
GLASGOW

July 2007

Declaration

The work contained in this thesis, submitted for the degree of Doctor of Philosophy is my own original work, except where due reference is made to other authors and has not been previously submitted for a degree at this or any other university.

Emma K Gibson

Abstract

A major problem encountered during the industrial synthesis of isocyanates, is the loss of amine starting material through reaction with the hydrogen chloride (HCl) by-product. HCl is formed by the phosgenation of polymeric amines and also by the subsequent decomposition of the carbamyl chloride, Equation (1). HCl readily reacts with the polymeric amine to form an unwanted and highly insoluble amine hydrochloride salt.

$$\begin{aligned} R{-}NH_2 + COCl_2 &\longrightarrow R{-}NHCOCl + HCl \\ R{-}NHCOCl &\rightleftharpoons R{-}NCO + HCl \\ R{-}NH_2 + HCl &\longrightarrow R{-}NH_3Cl \end{aligned} \qquad (1)$$

Methylene dianiline (MDA) and 4-benzylaniline (4-BA) were used as models for the industrial amine starting material with their hydrochloride counterparts methylene dianiline dihydrochloride (MDA.2HCl) and 4-benzylaniline hydrochloride (4-BA.HCl) as models for the industrial waste material. To understand the forces controlling the structure and stability of these solid amine hydrochloride salts the solid state structures of MDA, MDA.2HCl, methylene dianiline monohydrochloride (MDA.HCl), 4-BA and 4-BA.HCl were investigated using single crystal X-ray diffraction which led to the determination of their lattice energies. The XRD studies were also used as a basis for Density Functional Theory (DFT) calculations, which were validated against Inelastic Neutron Scattering (INS) spectra. These calculations facilitated the assignment of the vibrational modes in FTIR spectra.

The information obtained from the solid state structures, combined with an investigation of the solution phase behaviour of 4-BA.$HCl_{(s)}$, resulted in the determination of a kinetic model for the recovery of amine starting material. The solution phase was investigated using quantitative ^1H NMR spectroscopy, for which a pre-saturation pulse programme had been developed. The proposed reaction scheme describes the conditions under which the dissociation of 4-BA.$HCl_{(s)}$ can occur. Reaction in a closed system shows no amine production while reaction in an open system permits, within solubility limits, the complete consumption of solid waste to produce free amine. From these two extremes the conversion of waste hydrochloride salt in the industrial reactor can be rationalised.

Acknowledgements

I would like to thank everyone who has contributed to this project and whose help and support has been very much appreciated.

- A special thanks to my supervisors Prof John Winfield and Dr. David Lennon who have been a constant source of guidance and encouragement. Thank you also for your patience and sound advice over the past four years.

- Huntsman Polyurethanes and my supervisors Dr Rob Carr and Dr Archie Eaglesham. Your informative and friendly discussions made our many project meetings a pleasure. Thanks also for a new found love of Belgian beer.

- The crystallography studies were a great experience thanks to the immense knowledge and patience of Dr Ken Muir.

- Dr Stewart Parker at the Rutherford Appleton Laboratory for the INS, calculations and understanding of the vibrational spectra.

- Dr David Rycroft and Jim Gall for all their help with the NMR and especially Dr David Adam for his help with the pulse program.

- Prof A Gavezzotti for the calculations of the lattice energies.

- Dr Alice Miller for being cajoled into doing maths over your Christmas holidays.

- Ally, Iain, Neil and June for the great times I've had in the lab, cheers. And a big thanks to my mates for all the advice, singing lessons and unwavering belief that one day I'll learn some grammar.

- Finally, but most importantly, a huge thanks to Mum and Doreen. Your infinite common sense and great humour *usually* keeps me sane. And I promise to get a proper job some day.

Contents

List of Figures

Abbreviations

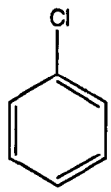	MCB	chlorobenzene
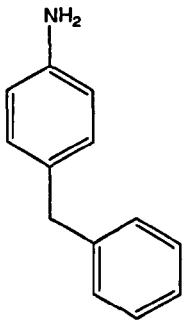	4-BA	4-benzylaniline
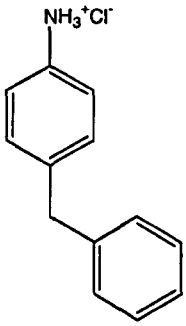	4-BA.HCl	4-benzylaniline hydrochloride
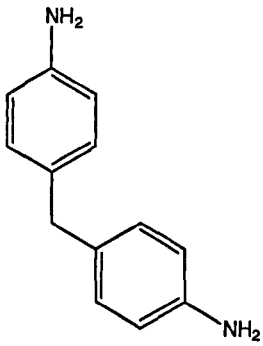	MDA	Methylene dianiline
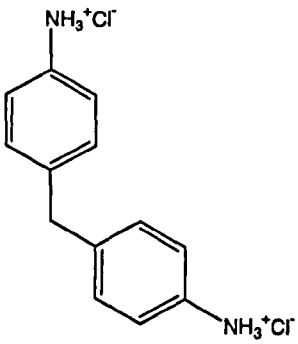	MDA.2HCl	Methylene dianiline dihyrochloride

Chapter 1

Introduction

1 Introduction

This project, sponsored by Huntsman Polyurethanes, has focused on the fundamental chemistry that underlies a major problem encountered during the industrial synthesis of isocyanates: the loss of amine starting material through reaction with the hydrogen chloride (HCl) by-product. The manufacture of polyurethanes is a multi-billion dollar industry and is the Huntsman Corporation's largest business section earning the company almost $3.3 billion in sales in 2006.[1]

1.1 A problem encountered in isocyanate synthesis

During the industrial manufacture of methylene diphenyl diisocyanate (MDI) ($C_{15}H_{10}N_2O_2$), hydrogen chloride (HCl) is formed as a by-product by the phosgenation of polymeric amines and also by the subsequent decomposition of the carbamyl chloride, Equation (2).[2] HCl readily reacts with the polymeric amine to form an unwanted and highly insoluble amine hydrochloride salt.

$$\begin{aligned} R{-}NH_2 + COCl_2 &\longrightarrow R{-}NHCOCl + HCl \\ R{-}NHCOCl &\rightleftharpoons R{-}NCO + HCl \\ R{-}NH_2 + HCl &\longrightarrow R{-}NH_3Cl \end{aligned} \qquad (2)$$

The reaction between amines and HCl in the solution phase to form an amine hydrochloride is a side reaction in the manufacture of isocyanates which causes loss of starting material and so extensive reprocessing is required.

At first glance this is a simple acid plus base reaction to form a salt. However, there are added complications from the strong intermolecular interactions which inhibit dissolution of the salt, the non-ideal dissolution of HCl in the process solvent, monochlorobenzene (MCB, chlorobenzene), and the partitioning of $HCl_{(solv)}$ to the gas phase. Evaluation of the equilibria present in this reaction has yielded a greater understanding of this difficult reprocessing step.

1.2 Project aims and achievements

To gain insight into the possible conversion of these unwanted amine hydrochloride salts to valuable amine starting material in the solution phase, their solubility and thermal stability had to be understood. In order to accomplish this, the hydrochloride salts of 4,4'-methylene dianiline (MDA) ($C_{13}H_{14}N_2$) and 4-benzylaniline (4-BA) ($C_{13}H_{13}N$) were used as models for the industrial polymeric amine hydrochloride. The aims of this project were:

- To understand the forces controlling the structure and stability of the solid amine hydrochloride salts.

- To understand the solution phase behaviour of these salts, in the process solvent (chlorobenzene) and postulate a mechanism for their conversion to the amine starting material.

In addition to testing the physical properties of these compounds (melting point, thermal gravimetric analysis and solubility in the process solvent), the first objective was achieved through investigation of their solid-state structure by analysis using single crystal X-ray diffraction, which led to calculation of their lattice energies. The crystal structures were also used as a basis for Density Functional Theory (DFT) calculations, which were validated against Inelastic Neutron Scattering (INS) spectra. These calculations were then used to derive a full vibrational assignment of the FTIR spectra of these materials.

The second objective was achieved using the information garnered on the compounds solid state structure, and aided by investigations of their behaviour in the solution phase. These investigations included the effect of temperature on solubility of the hydrochloride salts and the products obtained during reaction under two sets of conditions, culminating in the determination of a kinetic model, which describes the solution phase behaviour of 4-BA.$HCl_{(s)}$ when under these reaction conditions.

1.3 Polyurethanes

Urethanes were first discovered by C A Wurtz (1848) when he coupled a monoisocyanate with a mono alcohol,[3] Equation (3).[2] In 1937 in Germany, O. Bayer reacted 1,4-butanediol

and 1,6-hexamethylene diisocyanate to make the first polyurethane, as competition against the US company Dupont's polymer Nylon. Bayer's polyurethanes were first marketed in Germany under the names Igamid U Plastics and Perlon U synthetic fibres and bristles.[4] During WWII the reaction was very useful to German scientists allowing them to produce adhesives, coatings, drying oils for paints and foams. Since then the polyurethane world market has grown hugely, producing over 9 million tonnes in 2000.[2]

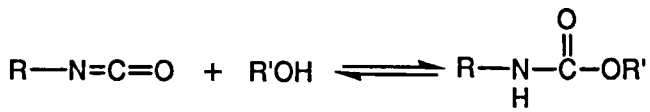

(3)

1.4 Industrial isocyanate synthesis

Methylene diphenyl diisocyanate (MDI) and toluene diisocyanate (TDI) are the major isocyanates used to make polyurethanes.[5] They dominate the global annual isocyanate production of 4.4 million tonnes, having respective shares of 60 and 34 %.[2] The furniture industry mainly uses polyurethanes based on TDI whereas most other applications use MDI polyurethanes.[6] The primary intermediate for MDI is methylene dianiline (MDA) (see Figure 1), also referred to as diamino diphenyl methane (DADPM), more than 2 million tonnes of which was produced in Europe and the USA annually by 2000.[7] Figure 2 shows the reaction scheme for producing MDI from benzene.[2]

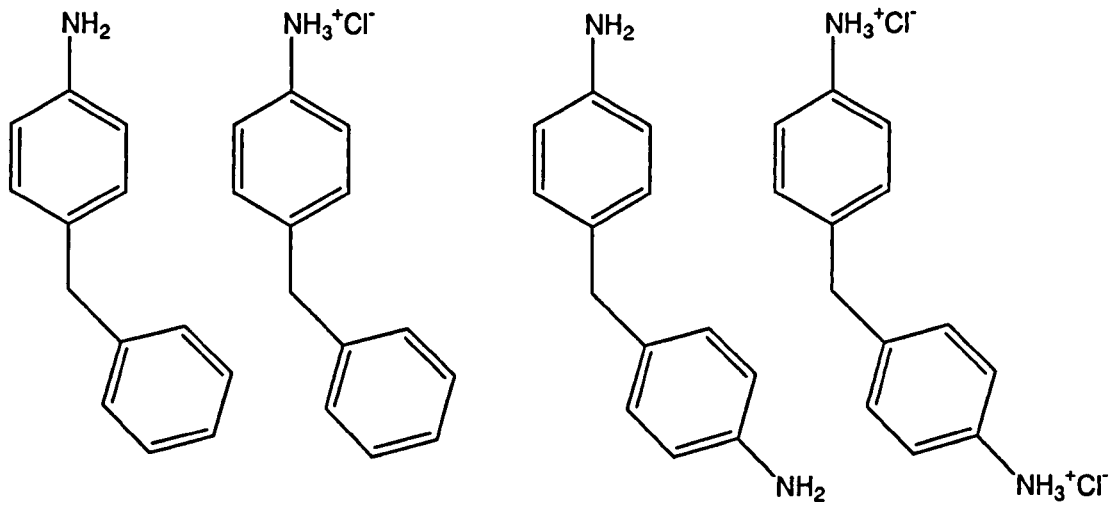

Figure 1 Glossary of chemical formulae of amines and amine hydrochlorides encountered in this project.

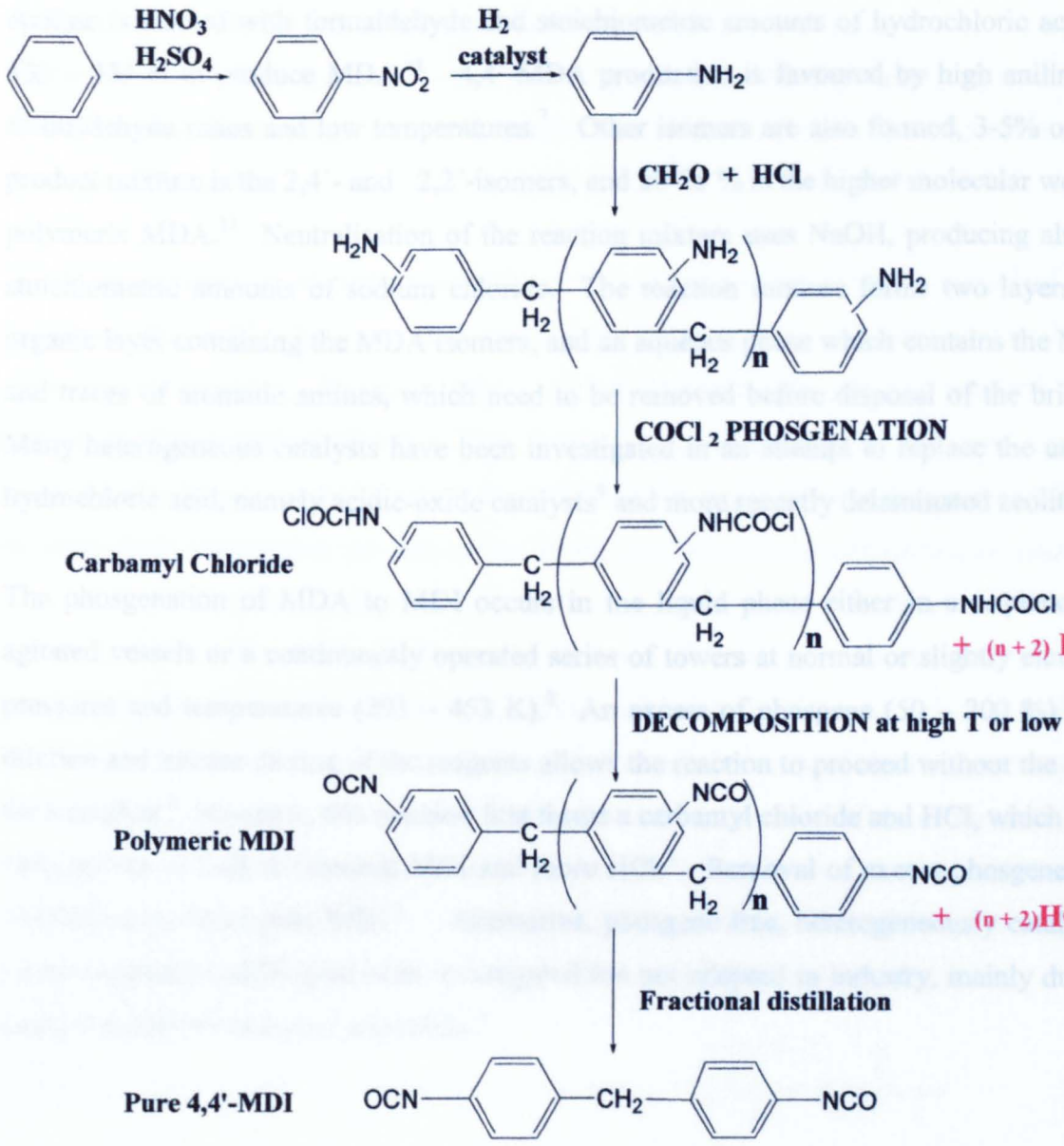

Figure 2 Synthesis of methylene diphenyl diisocyanate (MDI) from benzene.

Where n = 2, 3, 4, 5 or higher with a percentage product distribution of 50 – 80, 10 -20, 5 – 12 and 5 -12 % respectively.

Benzene is first nitrated to mononitrobenzene in a heterogeneous liquid-liquid reaction using sulfuric acid as a catalyst and producing di- and trinitrophenols as the main byproducts (0.1 - 0.5 % of the total weight of mononitrobenzene product).[8] The nitration of benzene is highly exothermic with a heat or reaction of -117 kJ mol^{-1}.[9] An adiabatic process uses this heat to remove water from the reaction mixture, the final temperature reaching 393 – 403 K.[2]

Catalytic hydrogenation of nitrobenzene to aniline is highly exothermic (-443 kJ mol^{-1}) and normally carried out over a solid supported Cu or Ni catalyst in the gas phase.[10] Bayer and Allied use a Ni sulfide catalyst while Lonza and Sumitomo used copper based catalysts.[10] By 1998 80 % of the aniline produced in the US was used in the manufacture of MDI.[10]

Aniline is reacted with formaldehyde and stoichiometric amounts of hydrochloric acid at 333 – 353 K to produce MDA.[11] 4,4′-MDA production is favoured by high aniline to formaldehyde ratios and low temperatures.[7] Other isomers are also formed, 3-5% of the product mixture is the 2,4′- and 2,2′-isomers, and 20-25 % is the higher molecular weight polymeric MDA.[11] Neutralisation of the reaction mixture uses NaOH, producing almost stoichiometric amounts of sodium chloride. The reaction mixture forms two layers, an organic layer containing the MDA isomers, and an aqueous phase which contains the NaCl and traces of aromatic amines, which need to be removed before disposal of the brine.[11] Many heterogeneous catalysts have been investigated in an attempt to replace the use of hydrochloric acid, namely acidic-oxide catalysts[9] and more recently delaminated zeolites.[7]

The phosgenation of MDA to MDI occurs in the liquid phase either in a sequence of agitated vessels or a continuously operated series of towers at normal or slightly elevated pressures and temperatures (293 – 453 K).[9] An excess of phosgene (50 – 200 %) high dilution and intense mixing of the reagents allows the reaction to proceed without the need for a catalyst.[9] However, this reaction first forms a carbamyl chloride and HCl, which then decomposes to form the desired MDI and more HCl.[2] Removal of excess phosgene and distillation produces pure MDI.[2] Alternative, phosgene free, heterogeneously catalysed routes to produce MDI have been investigated but not adopted in industry, mainly due to catalyst instability and poor selectivity.[9]

1.5 Polyurethane market and history of manufacture

Polyurethanes have found many applications in recent years; the furniture industry has the largest demand, accounting for 29 % of the total polyurethane produced globally, followed by the construction and automotive sectors both using 18 %; insulation applications and footwear constitute most of the remainder.[2] As an example of their versatility, the automotive industry puts a variety of polyurethane types to use, flexible foams in car seats and head rests, semi-rigid foams in energy absorption parts, integral skin foams in bumpers, dashboards and steering wheels; polyurethane based coatings can provide enhanced corrosion and impact resistance of lacquers.

The properties of polyurethanes are governed by the type of polyol and isocyanate used. The higher the molecular weight of the polyol, the softer and more elastic is the resulting foam. The ratio of isocyanate to water controls hardness, which is also influenced by the

addition of polymer polyols such as polyacrylonitrile/polystyrene dispersion to the polyol reactant stream.[2] In addition to the key reagents, the blowing agent, catalyst, fire retardants, cross linking agents and surfactants also contribute to the overall properties of the polyurethane.

The blowing agent, until 1950 was CO_2, produced by adding water to the polyol and isocyanate reaction.[2] The isocyanate reacts with water to form CO_2 which expands the polymerising material, Equation (4).[2] Chlorofluorocarbons (CFCs) replaced CO_2 permitting the manufacture of a low density rigid foam which had low thermal conductivity. However, the Montreal Protocol of 1986 negotiated the phase-out of CFCs to limit their destruction of the ozone layer, and so non environmentally harming alternatives were needed. By the late 1990s a continuous flexible foam process was constructed using liquid CO_2.[12] Currently all types of foam are at least partially blown using CO_2, other alternatives being hydrofluorocarbons (HFCs) and solvents such as dichloromethane, acetone and methyl formate.[2] The relative rates of blowing and polymer growth are controlled by the catalyst, which determines the rates of the isocyanate with water, and isocyanate with polyol reactions. The surfactant has two uses; to stabilise the foam until enough polymerisation has occurred for the structure to be self supporting, and to help mix incompatible materials.

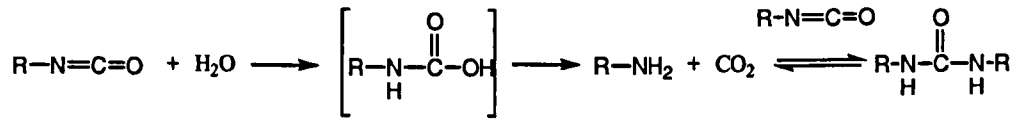

(4)

One defining property of polyurethanes is density, with mattresses and cushions made from flexible foams having density ranging from 10 – 80 kg m^{-3}, insulation material is made from low-density rigid foams, 28 – 50 kg m^{-3} and shoes and dashboards are made from high density flexible foams, and have densities greater than 100 kg m^{-3}.

The global polyurethanes market has grown by approximately 7 % p.a. since 1985,[2] whilst the Chinese market alone is expected to grow 10 % per year until 2015,[13] at which point it will be become the largest polyurethanes market in the world. A new plant operated by BASF, Huntsman and three Chinese partners in Shanghai is expected to produce 240 000 tonnes of methylene diphenyl diisocyanate p.a. together with 160 000 tonnes of toluene diisocyanate.[13]

Polyurethanes have also found medical uses, as catheters and artificial heart-assisting devices, most commonly made from MDI derived polyurethanes.[14] Worry over the

possible degradation to form MDA which has carcinogenic and mutagenic properties, has led to the production of another polyurethane based on 4,4'-methylene dicyclohexyl diisocyanate.[14] The possible adsorption of antibiotics onto polyurethane catheters has also been investigated in an attempt to inhibit bacterial growth, and so lessen the possibility of infections.[15]

1.6 Amine hydrochlorides

The reaction of phosgene with MDA is extremely fast at process conditions (293 - 453 K and slightly elevated pressures)[9] typically occurring in less than one millisecond.[2] However, there are two side reactions which also occur in comparable timeframes; these are the reaction of MDA with HCl to form amine hydrochloride salts and the reaction of MDI with MDA to form ureas. The latter reaction results in the effective loss of two molecules of MDI (Equation (5))[2] but can be minimised by using an excess of phosgene. High pressure phosgene processes also limit the formation of amine hydrochloride salts, which can otherwise be reacted slowly and endothermically[2] with phosgene in a train of continuous stirred tank reactors.[16]

$$\text{R-NCO} + \text{R-NH}_2 \longrightarrow \text{R-NHCONH-R} \qquad (5)$$

Hydrogen chloride and excess phosgene are boiled off after MDI is formed, and separated by absorption of phosgene in a suitable solvent. The large amounts of HCl produced are used in other processes, and make the isocyanate business the world's largest producer of hydrogen chloride gas.[2]

Amine hydrochlorides, as a group of compounds, are useful, especially in the pharmaceutical industry. Approximately half of the compounds used in medicine are administered as salts[17] with over 40 % of these being hydrochlorides.[18] Their common therapeutic use is due to the physiological acceptability of the Cl^- ion and ready availability of hydrochloric acid.[18] However, their bioavailability may not always be as good as other salt forms due to the high concentration of Cl^- ions found in the gastrointestinal fluid which would limit the solubility of these hydrochloride salts.[19]

Amine hydrochloride salts are a major problem in the manufacture of isocyanates, as they cause loss of starting material and costly reprocessing.[2] The more basic the amine is, the greater this problem becomes, as the amine hydrochlorides that are produced are less soluble than their less basic counterparts.[2] Investigation of the hydrochloride salts and their back reaction to form the amine starting material is the focus of this project.

1.7 Background theory

In the following section classical physical chemistry pertinent to this investigation will be briefly introduced.

1.7.1 Equilibria

Chemical reactions move towards a state of dynamic equilibrium, Equation (6) where reactants and products have no further tendency to undergo net change.[20] This position will be where the Gibbs free energy (ΔG) of the system equals zero.[20]

$$A \underset{k_2}{\overset{k_1}{\rightleftharpoons}} B \qquad (6)$$

$$\Delta G = -RT \ln Q$$

$$Q = \text{activities of products / activities of reactants}$$

The equilibrium constant (K) can be calculated from the Gibbs free energy, Equation (7).

$$RT\ln K = -\Delta G \qquad (7)$$

$$K = \text{Activities of products / Activities of reactants}$$

Which can be approximated as:

$$K = \text{Concentration of products / Concentration of reactants}$$

At equilibrium the forward and reverse rates must be equal, so K can also be calculated from their ratio, Equation (8).

$$K = k_1 / k_2 \qquad (8)$$

Le Chatelier's principle states that when equilibrium is disturbed, either by a change in temperature, concentration of a species or pressure, it will adjust to minimise the effect of the change.[21] When the reaction is exothermic in the forward direction, increasing the temperature would favour the endothermic, back reaction. This assumes that the system is closed and no species can escape from within the chemical system.

$$\Delta G = \Delta H - T\Delta S \quad (9)$$

ΔG – Gibb's Free energy, ΔH – the enthalpy change of reaction, T – temperature in K, ΔS – the change in entropy of the system.

1.7.2 Definition of reaction environment

Two types of reaction system were considered during the investigation of the solution phase behaviour of 4-benzylaniline hydrochloride (4-BA.HCl, see Figure 1), which is discussed in Chapter 7; an Open and a Closed system. A boundary separates the system from its surroundings; for example the glass wall of the reaction flask, separating the reaction from the lab. If the boundary does not allow interaction between the system and its surroundings, the system is isolated. The system is described as Open if gases, solvent or material can be transferred between the system and its surroundings, otherwise it is Closed.[21]

1.7.3 Definition of acids and bases

There are three main definitions, each additional one making the concept of acids and bases more general. Svante Arrhenius first proposed the classification of acids and bases in 1884,[22] which was followed by Thomas Lowry and Johannes Brϕnsted who independently devised a new definition in 1923,[22] using proton transfer; this was then superseded by G N Lewis' definition based on electron transfer.

1.7.3.1 Arrhenius Definition

An acid is a compound which ionizes in water to give solvated H^+ ions; a base is a hydroxyl compound which gives hydroxide ions in water. The neutralisation reaction between an acid and a base produces a salt and water, Equation (10).[23]

$$HA(acid) + BOH(base) \rightleftharpoons BA(salt) + H_2O \quad (10)$$

A problem with this definition is that it uses hydroxide ions which may not exist in non-aqueous solutions.[23]

1.7.3.2 Brϕnsted-Lowry Theory

A Brϕnsted-Lowry acid is a proton donor and a base is a proton acceptor. This occurs in all solvents where protons can transfer,[23] however, in the following examples the solvent used is water as there is far more data available in these solutions. The acid (AH) can dissociate to form a proton and its conjugate base (A^-). The base (B) can combine with a proton to form the conjugate acid (BH^+) as shown in Equation (11).[24]

$$AH_{(aq)} + B_{(aq)} \rightleftharpoons A^-_{(aq)} + BH^+_{(aq)} \quad (11)$$

The strength of a Bronsted-Lowry acid depends on the magnitude of the equilibrium constant for the ionization reaction with the solvent, when the solvent acts as the base, called the acid ionization constant (K_a). Water undergoes self ionization, Equation (12), with an equilibrium constant (K_w) given by Equation (13)[25] assuming the concentration of water is constant.

$$H_2O + H_2O \rightleftharpoons H_3O^+ + OH^- \quad (12)$$

$$K_w = [H_3O^+]\,[OH^-]\ mol^2\ L^{-2} \quad (13)$$

K_w has a value of 1.00×10^{-14} at 298 K, which gives a concentration of hydrogen ions in pure water of 1×10^{-7} at 298 K. The strength of an acid is given by the value of the equilibrium constant of its reaction with water, Equation (14).

$$HA_{(aq)} + H_2O_{(l)} \rightleftharpoons H_3O^+_{(aq)} + A^-_{(aq)} \quad (14)$$

In a dilute solution the concentration of water is constant, and K_a is given by Equation (15) the stronger the acid the more negative the pK_a.

$$K_a = [H^+][A^-] / [HA] \text{ mol } L^{-1} \quad , \quad pK_a = -(\log_{10} K_a) \tag{15}$$

The pH scale, Equation (16),[25] was introduced in 1909 by S P Sorensen during his work for Carlsberg Breweries.[25] It depends on the concentration of hydrogen ions; a neutral solution has a concentration of 10^{-7} mol L^{-1} and a pH of 7.

$$pH = -\log [H^+] \tag{16}$$

For bases, the ionization reaction is shown in Equations (17),[22] (18); the corresponding ionization constant, K_b is also shown.

$$A^-_{(aq)} + H_2O_{(l)} \rightleftharpoons HA_{(aq)} + OH^-_{(aq)} \tag{17}$$

$$K_b = ([HA][OH^-]) / [A^-] \quad ; \quad pK_b = -(\log_{10} K_b) \tag{18}$$

The pH of a base can be determined by applying the equilibrium for the dissociation of water, Equation (19).[25]

$$-\log([H_3O^+]) = -\log(10^{-14} / [OH^-]) \tag{19}$$

The relationship between pK_a of an acid and pK_b of its conjugate base is shown in Equation (20). The stronger the acid, the weaker the conjugate base and vice versa. The more negative the pK_a the stronger is the acid, the stronger bases have small pK_b values. Table 1 lists some common acids and bases, ammonia makes a reasonably strong base, but its conjugate acid is weak.

$$pK_w = pK_a + pK_b, \text{ where } pK_w = 14 \text{ at } 298 \text{ K} \tag{20}$$

Acid	HA	A^-	pK_a
Hydrochloric acid	HCl	Cl^-	-6
Hydrofluoric acid	HF	F^-	3.5
Ammonium ion	NH_4^+	NH_3	9
Base	**A^-**	**HA**	**pK_b**
Phosphate ion	PO_4^{3-}	HPO_4^{2-}	1.3
Ammonia	NH_3	NH_4^+	5
Cyanide ion	CN^-	HCN	5

Table 1 Common acids and bases and their ionization constants, when in water.[26]

A problem with the Brϕnsted-Lowry definition is that it is limited to protic solvents.

1.7.3.3 Lewis Definition

This definition does not depend on the type of solvent, or whether hydrogen transfer occurs. An acid is an electron deficient species and will accept an electron pair from other species. H^+, BF_3 and $AlCl_3$ are acids.[23] Bases are electron donors, containing pairs of electrons which can be donated. Cl^-, H_2O, OH^- and NH_3, esters and ketones are bases.[23] The reaction between boron trifluoride and ammonia is classed as a Lewis acid – base reaction, since it does not involve the transfer of protons. Boron trifluoride accepts electrons from the lone pair of ammonia, the Lewis base.[22] The Lewis definition of acids and bases encompases those which can be described as Brϕnsted-Lowry acids and bases but the reverse is not true.

1.7.4 Gas dissolution – ideal and non-ideal solutions

In an ideal solution the solute and solvent obey Raoult's law, *i.e.* the partial pressure of each component (P_A) is proportional to its vapour pressure as a pure liquid (P_A^*), Equation (21).[27] The solution also has to obey Raoult's law throughout the composition range, from a mole fraction of 0 to 1; this is more likely when the solute and solvent are similar, and is true for a mixture of benzene and toluene.[20]

$$P_A = x P_{A^*} \qquad \text{Where x is the mole fraction } x = n_2 / (n_1 + n_2) \tag{21}$$

P_A - partial pressure of the component, solute or solvent, P_{A^*} - vapour pressure of the pure liquid, x – is the mole fraction, n_1 and n_2 are the no. of moles of the solvent and solute, respectively.

The variation of partial pressure of a gas dissolved in a solvent is never ideal over the whole concentration range, but there may be a linear relationship between mole fraction and partial pressure at low concentrations of the dissolved gas.[27] This linear relationship is not Raoult's law; the constant of proportionality is not the vapour pressure of the pure substance but Henry's law constant, Equation (22).[27]

$$P_A = H x \tag{22}$$

P_{A^*} - vapour pressure of the pure liquid, x – is the mole fraction and H – Henry's law constant.

The plot of the vapour pressure of A against its mole fraction (x) is shown in Figure 3, the slope of the tangent to the experimental curve at $x_A = 0$ is the Henry's law constant.[20]

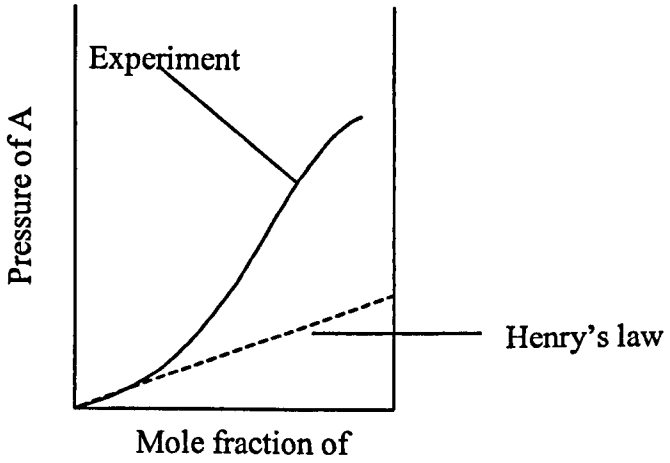

Figure 3 Plot of pressure v.s. mole fraction of a solute obeying Henry's Law.

1.7.5 Solvents

The dissolution of a solid in a solvent is influenced by the type of solvent used and interactions with the solvent molecules; London forces, dipole-dipole interactions or H-bonding.

Solvents can be classed as protic or aprotic, the former are classed as hard solvents which solvate small anions by means of strong H-bonds. The relative permittivity, also known as

the dielectric constant, can be also be used to classify solvents. This is given by Equation (23) and it is the ratio of the capacitance of a capacitor filled with the solvent against the capacitance of a vacuum.[21]

$$\varepsilon_r = \frac{C}{C_0} \qquad (23)$$

C – the capacitance of a capacitor which is filled with the solvent, C_0 – is the capacitance when there is a vacuum between the plates of the capacitor.

The higher the relative permittivity the more separated the ions are in solution, and so are less likely to be found as ion pairs. [28] If the aprotic solvent has a relative permittivity higher than 15 it is classed as dipolar aprotic, *e.g.* dimethylformamide, dimethylsulfoxide and acetone. The relative permittivities of some common solvents are listed in Table 2. The size of the relative permittivity does not account for all trends in solubility; donor strength also plays a part. This is the ability of the solvent to donate a lone pair of electrons to the solute cation.[28]

Solvent	Relative permittivity, ε
Ethanol	24.33
Methanol	32.64
Water	78.36
Benzene	2.27
Monochlorobenzene	5.62
Nitrobenzene	34.82
Dimethylsulfoxide	45

Table 2 Relative permittivities of solvents at 298 K. [28, 29]

Of relevance to this work, high molecular weight amine salts are known to exist as ion-pairs when dissolved in solvents of low dielectric constant, such as chloroform, where the separation of the ion pair is negligible.[30]

1.7.6 Lattice energies

The lattice enthalpy of a substance is the energy needed to form a gas of the ions from the solid compound, Equation (24).[31] The enthalpy of formation of the lattice is the negative of the lattice enthalpy, the energy required at absolute zero to break down a mole of crystal into its ions, and separate them by infinite distance.[32]

$$MX_{(s)} \longrightarrow M^{+}_{(g)} + X^{-}_{(g)} \quad (24)$$

The enthalpy of atomisation (ΔH_{at}) ionization (ΔH_{ion}) electron gain (ΔH_{eg}) formation (ΔH_f) and lattice energy (ΔH_{latt}) of a compound can be illustrated in a Born-Haber cycle. If the energies of all the other steps are known, the lattice energy can be calculated using Hess's law, as the sum of all the other parts should equal the heat of formation from the elements, Equation (25).[33]

$$\Delta H_f = \Delta H_{at} + \Delta H_{ion} + \Delta H_{eg} + \Delta H_{latt} \quad (25)$$

1.7.6.1 Solvation

The solvation of a non-polar compound in a non-polar solvent depends only on dispersive forces; van der Waals forces between the solute and solvent molecules and between the solvent molecules.[33] The driving force of the solvation is the entropy term in the Gibbs Free Energy Equation, Equation (9).

The overall enthalpy of solution for an ionic compound is the sum of the lattice energy and the enthalpy of solvation (Figure 4).[33] The latter depends on the strength and number of interactions between the solvent molecules and the ions. The polarity of the solvent determines the strength of the interactions, and the size of the ion will determine the number of coordinated solvent molecules. When $\Delta H_{solution}$ is negative the free energy of solution will also be negative, as the entropy term will reinforce this, since greater disorder is present in solution compared to the solid lattice. If $\Delta H_{solution}$ is positive, energy must be supplied to the system to dissolve the compound.[33]

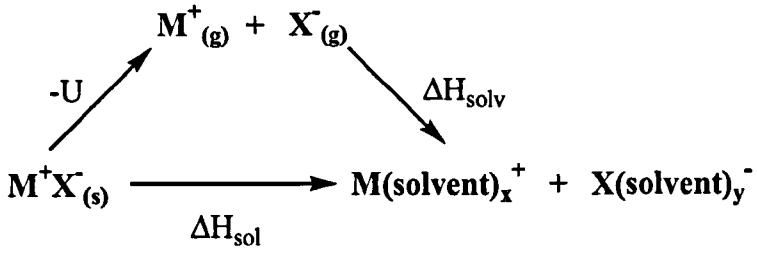

Figure 4 Enthalpy of solution (ΔH_{sol}). Showing the balance between the enthalpy of solvation (ΔH_{solv}) and the lattice energy (-U).

1.7.7 Description of traditional methods for calculating lattice energies

The lattice energy (-U) of molecular crystals are usually between 2.1 and 16.7 kJ mol^{-1}, between 41.8 – 83.7 kJ mol^{-1} for noble gases and between 167.4 – 209.2 kJ mol^{-1} for neutral organic molecules.[32] Ionic solids such as KCl and $MgBr_2$ have lattice energies of 719 and 2421 kJ mol^{-1}.[31]

The lattice energy of ionic solids are traditionally calculated from the Born and Landé equation (Equation (26)).[33] The electrostatic energy component becomes increasingly negative as the distance (r) between the ions increases. There are other interactions, besides those between the ion pair, and these are summed in the Madelung constant (A) which is dependent on the positions of the ions and the geometric characteristics of the lattice.[32] These other interactions in the case of a 1:1 electrolyte are the attractions between cations and the anion nearest neighbours, and the repulsions between similar charged nearest neighbours.

$$U = E_{COUL} + E_R = \frac{A N Z^+ Z^- e^2}{4\pi\varepsilon_0 r_0^2}\left(1 - \frac{1}{n}\right) \qquad (26)$$

U – lattice enthalpy, E_{COUL} – coulombinc energy, E_R – repulsive energy, A - Madelung constant, N – Avogadros number, Z – charge on the cation or the anion, ε_0 – the vacuum permittivity (8.85×10^{-12} C^2 $J^{-1}m^{-1}$), r_0 – equilibrium distance between the ions (distance between the ions corresponding to the minimum of the lattice energy, e – electronic charge, 1.6×10^{-19} C and n – Born exponent.

The attractive energy of the ions becomes infinite at short r distances, but at close distances electrons in the atoms repel each other (E_R). These forces decrease by the 9^{th} – 12^{th} power

of the interatomic distance.[32] E_{COUL} is the attractive coulombic energy which becomes infinite at infinitesimally small r values, and has to be balanced by the repulsive terms. The Born exponent (n) increases with increasing electron density of the ions present. Thus the lattice energy can be calculated from knowledge of the interionic distance and the crystal structures, both of these are determined from single crystal X-ray diffraction (XRD) studies.[33]

To calculate the lattice energy of organic crystals atom-atom potential energy calculations can be used, where the point charges are associated with atoms in the molecule. The interactions between atoms depend on the internuclear distances and the type and charges assigned to the atoms (Equation (27)).[34]

$$E(R_{ij}) = A \exp(-B R_{ij}) - C R_{ij}^{-6} + q_i q_j R_{ij}^{-1} \quad (27)$$

E – atom-atom potential energy, R_{ij} – distance between two atoms *i* and *j* in different molecules, q_i and q_j are the charges on the atoms, A, B and C are parameters that depend on the atom type.

A problem with the atom-atom potential energy calculations is that the intermolecular interactions such as dispersion forces are due to interactions between whole molecules and not between separate atoms.[34]

1.7.7.1 Lattice energies, the Pixel method

The lattice energies of the five compounds studied in this project (4-BA, 4-BA.HCl, MDA, MDA.2HCl and MDA.HCl) were calculated by A Gavezzotti (University of Milan), using his Pixel method.[35] This technique calculates the electrostatic and polarization energies of a molecule from the molecular electron density which is obtained from the crystal structure. Each pixel has a density (ρ_i) a volume (V_i) and a charge (q_i) Equaiton (28).[36]

$$q_i = \rho_i V_i. \quad (28)$$

The electron density contains a few million pixels, in a grid of step 0.08 Å, this is reduced before using it to calculate the lattice energy, by screening out the pixels which have approximately zero electron density. The number of pixels is further reduced by condensing n x n x n pixels into one large pixel, which has a total charge equal to the sum

of all the little n pixels, and is placed at the centre of the n x n x n cube. These two steps reduce the number of pixels to thousands, so that integration is possible. The molecule is therefore represented by a box containing thousands of pixels. The boxes overlap slightly and this corresponds to the repulsion energy between the molecules.[34] Coulombic energy (E_{COUL}), polarization energy (E_{POL}), dispersion energies or the London forces (E_{DISP}) and the repulsive forces (E_{REP}) are calculated for the pixel-pixel interactions in the electron density. The summation of these individual terms is the total lattice energy, Equation (29).[36]

$$E_{TOT} = E_{COUL} + E_{POL} + E_{DISP} + E_{REP} \quad (29)$$

E_{TOT} – total lattice energy, E_{COUL} – coulombic energy between any two molecules, E_{POL} – polarization energy, E_{DISP} – dispersion energy and E_{REP} – the repulsion energy.

An advantage of this method over atom-atom methods is that all the electrical properties are distributed over 1 x 10^4 sites, the pixels, instead of just a few atom positions. This means the intermolecular forces are better predicted. [36] Another advantage of the Pixel method is that the calculation depends on only 4 parameters compared with the 10's of parameters required for the atom-atom type calculations. [34]

1.8 Analytical techniques

The solid state structure of the amines and their hydrochloride salts has been investigated using single crystal X-ray diffraction and vibrational spectroscopy, Inelastic Neutron Scattering (INS) and Fourier Transform Infrared (FTIR). The spectroscopy investigations were accompanied by Density Functional Theory (DFT) calculations, which have allowed the assignment of the vibrational modes. The thermal stability of these compounds has been investigated using thermal gravimetric analysis (TGA) and differential scanning calorimetry (DSC). Solution phase techniques have also been employed; of most use was the development of a pre-saturation pulse program for ^{1}H NMR of monoclorobenzene (chlorobenzene) solutions.

1.8.1 Fourier Transform Infrared Spectroscopy (FTIR)

FTIR spectroscopy has been used in this project as a diagnostic tool for the extent of hydrochlorination of prepared samples of the amine hydrochlorides. It has also been used to investigate the dissolution of the amines and amine hydrochlorides and $HCl_{(g)}$ in chlorobenzene. Two major advances in infrared spectroscopy were the introduction of the Michelson interferometer in 1891, and the application of the Fourier Transform in 1966, which allowed much faster recording of spectra.[37]

Infrared spectroscopy measures molecular vibrations, which cause a change in the electric dipole moment of the molecule.[20] A non-linear molecule will have 3N degrees of freedom, where N is the number of atoms in the molecule. Three of these are translational modes and three are rotation, leaving 3N-6 vibrational modes.[38] However, not all of these will be infrared active, and some may be degenerate. There are different types of vibrational modes: stretches (ν), bends (δ), rocks (ρ), torsions (τ) and wags (ω).

Two techniques were used in this project, Transmission FTIR for liquid phase investigations and attenuated total reflectance for solids.

1.8.1.1 Attenuated total reflectance (ATR)

This technique relies on the IR radiation being internally reflected back off the face of a prism; at a certain angle of incidence (θ) all the radiation will be reflected back and an evanescent wave will travel into the sample which is compressed onto the face of the prism (Figure 5). This radiation is absorbed by the sample, and the resulting totally reflected radiation gives the IR spectrum of the sample, similar to the equivalent transmission spectrum.[39] Obtaining good optical contact between the internal reflection element (IRE) and the sample is a limitation of the technique; but is overcome for solid samples by a pressure clamp which reproducibly applies the same pressure to compact the solid sample onto the IRE. The IRE is often made from ZnSe, Ge or Si, each having a different penetration depth of the evanescent wave. The benefits of this technique are ease of sample preparation and its use in systems that strongly absorb.

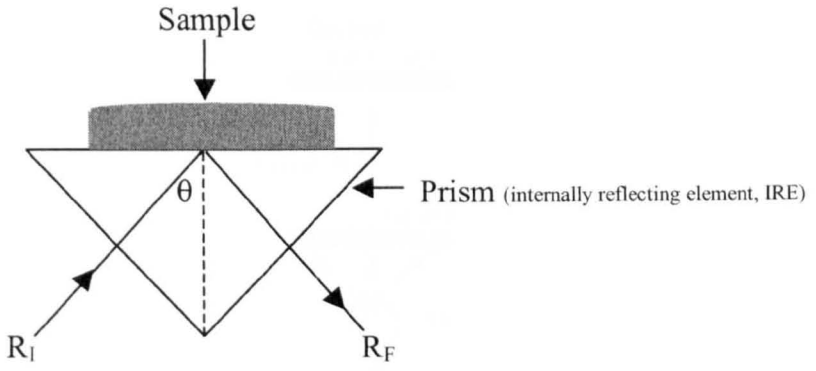

Figure 5 Internal reflection element of an ATR probe.

Showing incident (RI), final radiation (RF) and the angle of incidence (θ). [38]

1.8.2 X-ray diffraction (XRD)

Single crystal X-ray crystallography allows the determination of the structure of a crystal by interpreting the diffraction pattern caused by the scattering of monochromatic X-rays by the electron density in the crystal sample (Figure 6).[40] For the crystal structure to be fully determined the crystal must be completely within the diameter of the X-ray beam, the optimum size of the crystal is a few tenths of a mm.[40] The diffraction pattern contains information on the amplitude of the scattered waves ($|F|$) from the intensity of the diffraction spots, but no information on the phase of the waves (ϕ).[40] The diffraction pattern also has a specific geometry due to direction of the scattered X-rays, which is caused by the lattice and unit cell geometry of the crystal. It also has symmetry in the positions and intensities of the spots throughout the pattern; this is caused by symmetry of the unit cell. Therefore, an analysis of the diffraction pattern yields the geometry and symmetry of the unit cell. Mathematical analysis of the intensities of the diffraction pattern is difficult, and takes a lot of computational time, but gives the full molecular structure through refinement of a predicted model structure.

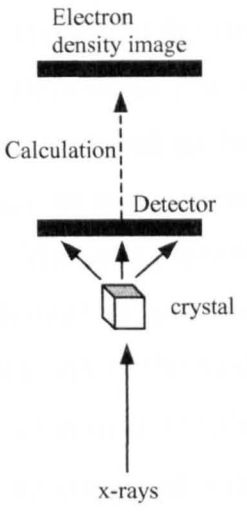

Figure 6 Overview of X-ray diffraction experiment.

The geometry of the unit cell is calculated using Bragg's law, Equation (30),[32] Bragg reflection is shown in Figure 7. The lines in Figure 7 represent parallel planes going through the lattice points in the crystal. The angle of incidence of each beam that reflects off a plane has an equal angle of reflection. Interference effects are caused as each plane is reflecting X-rays. The planes are defined by the indices *hkl* and the space between the planes is d, which is determined by the parameters of the unit cell, a, b and c. The Bragg equation gives the path difference between two rays reflected from adjacent planes.

$$\lambda = 2d_{hkl}\sin\theta \tag{30}$$

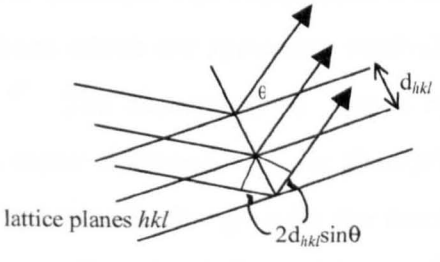

Figure 7 Bragg diffraction by a 3-dimensional crystal structure.

The lines represent a set of parallel lattice planes, viewed edge on.[40]

The difficulty of XRD is the loss of the phase information of the reflected waves. The diffraction pattern is the Fourier Transform of the electron density, the waves have to add together to give positive regions of electron density, which represent atoms, and cancel out negative regions. This restricts the relationships between the phases of the reflections. The Direct Methods approach selects the most intense reflections and works out the likely relationships between their phases. The most probable phases, together with the observed amplitudes are then Fourier transformed to give the electron density; this is the model structure. The forward Fourier transform of the model gives a set of calculated structure factors ($F_c(hkl)$) which have an amplitude ($|F_c(hkl)|$) and a phase ($\phi_c(hkl)$). The calculated amplitudes ($|F_c|$) can be compared with the observed amplitudes from the diffraction pattern ($|F_o|$), Equation (31).[40] For atoms placed at random in the unit cell the R-factor will be 0.83 if it is centrosymmetric or 0.59 if non-centrosymmetric.[41] A good starting model will have an R-factor of less than 0.5 if it is centrosymmetric or less than 0.4 if non-centrosymmetric.[32] An R-factor of 0.02 – 0.07 is achievable for a correct and complete structure which has been determined from good diffraction data.[40]

$$R = \frac{\Sigma \, | \, |F_o| - |F_c| \, |}{\Sigma \, | \, |F_o|} \qquad (31)$$

If the R-factor is large, the model structure can be improved by taking the reverse Fourier transform of the calculated phases and the observed amplitudes. The forward Fourier transform of the new model will then give improved calculated phases and amplitudes. This process can be repeated until the R-factor is low and all the atoms in the structure have been found.

Before refinement of the structure can commence, a data reduction process is performed which averages reflections which are symmetry equivalent, and corrects for absorption of X-rays by the crystal.[40] The absorption of X-rays by the crystal is greater for those containing atoms with many electrons. As the absorption of X-rays also depends on the path length of the X-rays, it will change with the orientation of the crystal in the X-ray beam, which will in turn affect the diffracted X-rays.[40] If the crystal has a needle-like shape, absorption will be greater through the length than through the thin width of the crystal.

Least squares analysis is used to refine the structure. This finds the best fit of the calculated amplitudes with the observed ones, by varying the parameters. These are the positions and vibrations of the atoms; three positional coordinates and one displacement parameter for the vibrations of each atom. Anisotropic displacement allows the atoms to vibrate different amounts in different directions, so giving 9 parameters for each atom.[40] A ratio of observed reflections to parameters between 6 and 20 is required to give reliable parameters;[40] usually this means there are 50 – 100 reflections for each atom.[42] Constraints can be added to H-atoms, keeping their bond lengths fixed and by associating them with the atoms they are bonded to. This is not useful when studying H-bonded molecules, where the position of the H will determine the strength of the interaction. A common reason for poor refinement of the structure is the presence of solvent molecules in the unit cell which have not been accounted for in the model structure.[32] After the refinement, a difference electron density ($\Delta\rho$) map should not contain any large peaks or holes, which would otherwise suggest missing or wrong atoms, *i.e.* if $\Delta\rho \pm 1$ e Å^{-3} the structure is acceptable.[40] A value of $\Delta\rho$, the difference in electron density between the highest peak and lowest trough in the electron density map, of less than 0.3 e Å^{-3} but greater than -0.3 e Å^{-3} was used to determine acceptable refinement of the structures in this project. Providing crystals of sufficient size and quality can be grown, X-ray diffraction provides an excellent description of the molecular structure.

1.8.2.1 H-bonding

After ionic interactions, H-bonds are the strongest intermolecular interactions, affecting the crystal packing to optimise the number of H-bonds.[32] They are very important in nature, *e.g.* controlling DNA base pairing, the structure of water and folding of proteins.[32] A H-bond occurs when a hydrogen atom is bonded to two atoms, D-H---A, where D is the donor and A the acceptor. A special case called a bifurcated H-bond occurs where the hydrogen is shared between three atoms.[43]

H-bonds can be classed by strength which is dependent on their geometry, Table 3.[44] Strong H-bonds (544 – 628 kJ mol^{-1}) have a DHA angle of almost 180 °, allowing maximum interaction between the proton and the acceptor. Strong H-bonds usually lengthen the D-H bond and the proton sits almost half way between the donor and acceptor atoms. Medium strength H-bonds occurring in water, alcohols and amines (8.37 – 33 kJ mol^{-1}) shift the proton towards the centre of the D---A space, and have a more restricted angle than strong H-bonds. Weak bonds have very restricted DHA angles and so can not maximise the interaction between the proton and the acceptor atom.

Strength	Length	H...A (Å)	D...A (Å)	Angle <DHA
Strong	D-H~H...A	1.2 – 1.5	2.2 – 2.5	175 – 180
Moderate	D-H < H...A	1.5 – 2.2	2.5 – 3.2	130 – 180
Weak	D-H < H...A	2.2 – 3.3	3.2 – 4.0	90 - 150

Table 3 Summary of H-bond types.[44]

Weak H-bonding includes X-H---Ph H-bonds, first observed in 1957, where X is nitrogen. There are various geometries of these types of H-bond, all with similar energy. The geometry where the proton points directly at the centre of the aromatic ring are slightly more favourable energetically, but the most common are those where the H points at a carbon of the ring, or where the H is above the centre of the ring but the X-H bond is not perpendicular to the plane of the ring.[43]

H-bond distances (H...A) measured by X-ray diffraction are on average 0.11 Å longer than those measured by neutron diffraction.[44] This is due to the increased scattering power of hydrogen atoms in neutron compared to X-ray diffraction.[44] Since X-rays are scattered by the electrons in an atom, hydrogen has a low X-ray scattering power, whereas the neutron scattering power of hydrogen is high, a half that of C and a third of that of N.[40]

1.8.3 Density Functional Theory (DFT)

DFT is a computational electronic structure method which can be used to optimise the geometry of the chemical structure and then calculate the possible vibrational frequencies of the molecules within the structure.[45] The calculations performed in this project were not isolated molecule calculations but periodic structure calculations, as they were based on the crystal structures obtained from single-crystal XRD. DFT can achieve greater accuracy than Hartree-Fock methods by computing electron correlation, using functions of the electron density, which in turn have been calculated from the coordinates of the molecules, called a functional. DFT methods separate the electron energy into several terms, Equation (32).[45]

$$E = E^{T} + E^{V} + E^{J} + E^{XC} \quad (32)$$

E^T – kinetic energy term, E^V – contains terms for the potential energy of the nuclear-electron attraction and the repulsion between nuclei, E^J – electron-electron repulsion term, E^{XC} – the exchange-correlation term including the remaining part of the electron-electron interaction.

All of the terms except the nuclear-nuclear repulsion term are functions of the electron density. DFT includes the effect of electrons reacting to the motion of another, whereas Hartree-Fock only approximates this effect, and so is less accurate. All the remaining unknown contributions to the electronic energy are included in E^{XC}. The accuracy of the DFT calculation depends on the best approximation achieved for E^{XC}, which is determined by the level of theory used.

To run a calculation, a level of theory is chosen, for example the hybrid functional Becke, Lee, Yang and Parr (BLYP), the localised density approximation (LDA) or the generalised gradient approximation (GGA). LDA is the local density approximation which usually gives good structural information but is unreliable at estimating binding energies.[46] GGA is a generalised gradient approximation of the exchange correlation where the density at one point and how that density is changing, its gradient, is taken into account when calculating E^{XC}. The hybrid functionals are a hybrid of DFT exchange functionals and Hartree-Fock exchange, the most popular is B3LYP.

The basis set is the mathematical representation of the molecular orbitals in a molecule.[45] The more relaxed basis sets allow electrons to occupy larger volumes of space and are necessary for calculating systems which have lone pairs or anions, an example is the 6-31++G(d), which has diffuse functions on the heavy atoms and on the hydrogen atoms. Generally, the more relaxed the basis set, the more computational time is needed.

1.8.4 Inelastic Neutron Scattering, INS, spectroscopy

INS can be used to validate DFT calculations.[47] DFT calculates the vibrational frequencies and atomic displacements. These can be used to predict the INS spectrum, which reflects the amplitude of motion of the associated atoms. The program aCLIMAX[48] can be used to simulate INS spectra from DFT calculations. In this project, INS spectra were acquired using the TOSCA crystal field analyser spectrometer at the ISIS facility, Rutherford Appleton Laboratory.[49] This approach is considered to be a rigorous test as all vibrations are active in INS, whereas IR and Raman spectroscopies are constrained by selection rules

depending on the electronic properties of the molecules.[48] INS is also extremely useful as it has a wide dynamic range of 50 – 4000 cm^{-1} with reasonable resolution. INS is also particularly sensitive to motions involving H atoms, as the inelastic neutron scattering cross section of hydrogen is high, 80 barn, compared with almost all the other elements which have less than 5 barn. INS spectroscopy measures the loss in energy of the neutron when it is scattered by interaction with the nucleus of the atoms in the sample. Energy is transferred from the incident neutrons to the scattering atoms making them vibrate, these vibrations occur at the same frequency as they would when measured by IR or Raman.

The TOSCA spectrometer [49] (Figure 8) calculates the energy loss of the scattered neutrons using time of flight methodology, since the incident neutron energy is defined by the time that the neutrons arrive at the sample. This is possible as the final energy of the scattered neutrons, the distance around the analyser system and the length of the flight path are known. The spectrometer can measure spectra between 0 – 8000 cm^{-1} with good resolution obtained below 2000 cm^{-1}.[50]

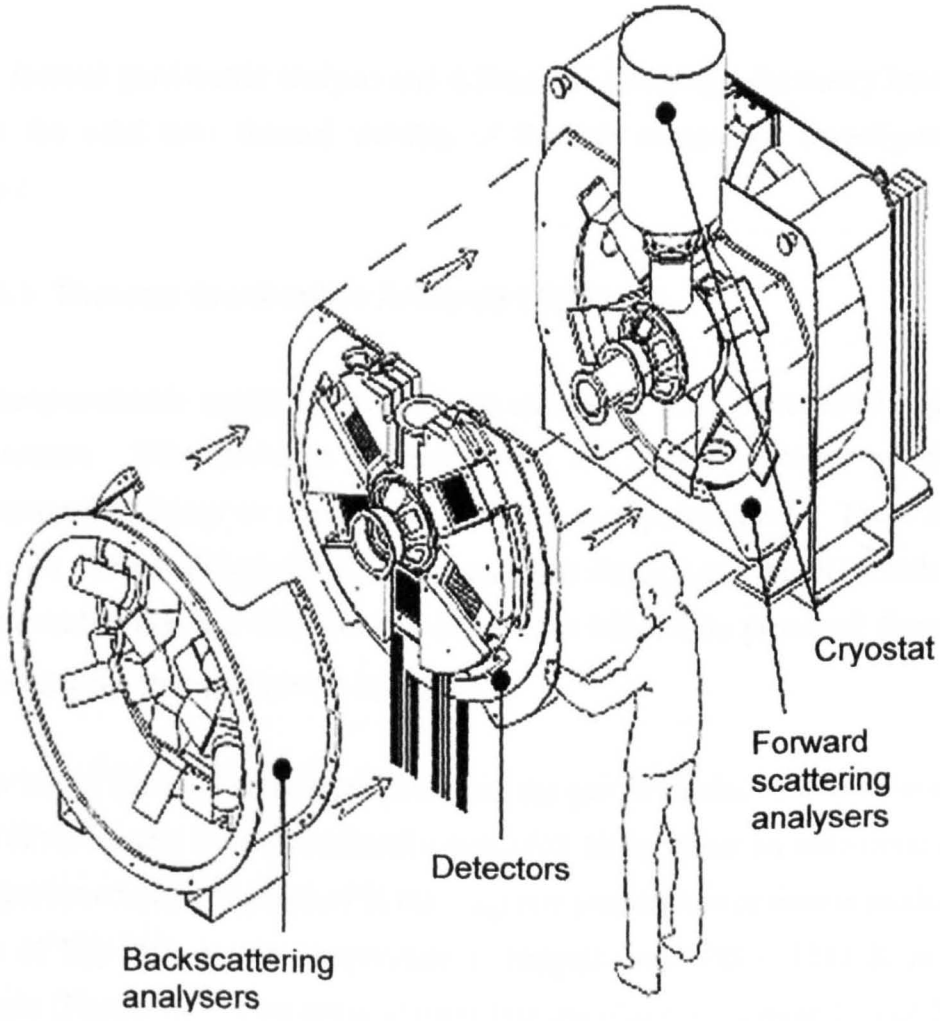

Figure 8 Tosca spectrometer.

A neutron source is needed for INS spectroscopy; the two types are nuclear fission reactors, *e.g.* the 20 MW FRM-II reactor in Munich, or a spallation source, *e.g.* ISIS, Chilton. In the former, thermal neutrons react with ^{235}U to form high energy neutrons, fission products and heat. Approximately 2.5 neutrons are produced from each fission event, one of which is used to maintain the reaction, 0.5 are lost to absorption, and one can leave the reactor core and be used in experiments. Nuclear reactors are continuous neutron sources. A spallation source, however, is a pulse source. It produces hydride ions, which are then accelerated by a linear accelerator then injected through an aluminium oxide foil, which strips both electrons of the H^-, producing protons. These then are accelerated in a synchrotron, producing a 100 ns pulse which is fired at a tungsten target, housed within a beryllium reflector assembly. Each proton that hits the target produces approximately 15 neutrons.[51] The INS spectrometer then analyses the scattered neutrons to yield the vibrational spectrum of the sample.

1.8.5 Thermal analysis

Both thermal gravimetric analysis and differential scanning calorimetry have been used to probe the solid state thermal stability of the five compounds investigated during this project.

1.8.5.1 Thermal Gravimetric Analysis (TGA)

Thermogravimetric analysis measures the change in mass of a sample against time or temperature. TGA provides information on the thermal stability of solid materials, measuring the change in mass during reaction or vaporisation.[52] There are three main parts of a thermobalance, the electrobalance, the furnace and the PC which both controls the thermobalance and acquires the data. The balance is protected from corrosive or oxidising gases by purging with inert gas.

A few mg of the solid sample are placed on the pan of an electrobalance in a furnace. The mass of the sample is then continually measured during either an isothermal experiment or a temperature ramp. A graph of % mass against temperature or time is produced; the TGA curve of $Mg(OH)_2$ as the temperature is ramped from 333 – 1233 K is shown as an example (Figure 9).[52] Two areas of mass loss are observed, a rapid loss of 27 % between 473 and 723 K, followed by slower mass loss up to 1073 K. These two regions are

interpreted as the fast decomposition of the hydroxide to form MgO, which causes loss of most of the water vapour, followed by slower diffusion of water which is adsorbed onto the oxide.

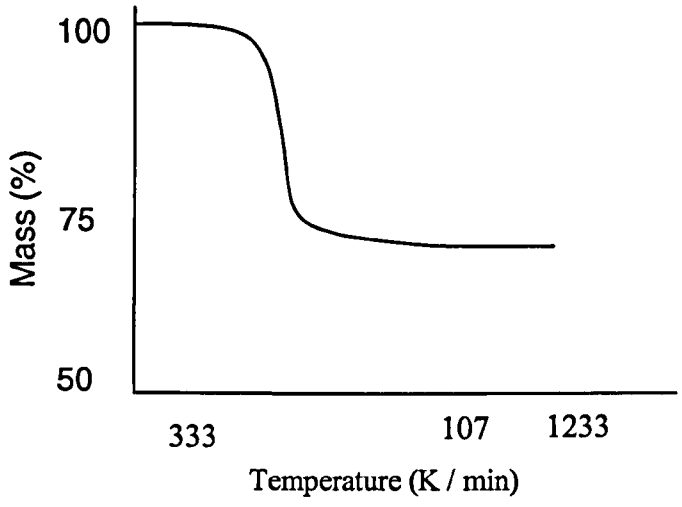

Figure 9 Mass loss of $Mg(OH)_2$ observed during temperature ramp from 333 – 1233 K.

1.8.5.2 Differential scanning calorimetry (DSC)

In this technique the solid sample is placed in the oven in an aluminium pan alongside an empty reference pan. The heat flow, Equation (33),[53] in or out of the sample is measured by taking the difference between the temperatures of the sample and the reference as the temperature of the oven is ramped linearly.

$$dQ/dt = MC_p\,(dT/dt) \qquad (33)$$

dQ/dt – heat flow, M – mass of the sample, C_P – heat capacity of the material, dT/dt – heating rate.

During a melting process, the sample will not change temperature as it is using the energy to change phase, but the reference pan will continue to increase in temperature, and the difference is measured. If there is no phase transition, the heat flow is the heat capacity of the material. Crystallisation is exothermic and so a positive heat flow would be recorded, melting is endothermic and gives a negative heat flow (Figure 10).[52]

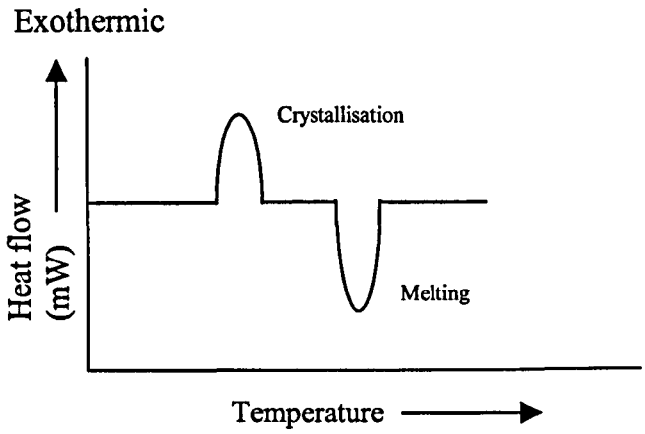

Figure 10 Example of a Differential Scanning Calorimetry trace.

1.8.6 Solution phase ^{1}H NMR spectroscopy

Nuclear magnetic resonance, NMR, was first observed in 1946,[54] but it was not until the introduction of the Fourier Transform in the late 1970s which made some relaxation techniques or double resonance experiments possible.[55] A basic introduction to the topic follows.

1.8.6.1 Background of NMR technique

Some nuclei have a non-zero nuclear spin quantum number (I) and in the presence of a magnetic field they can have 2I + 1 orientations. Protons have a spin of I = ½ which gives them two possible orientations, one of low energy which is aligned with the magnetic field and one of high energy which is opposed to the field.[54] At thermal equilibrium there is a slight excess of those in the lower energy orientation, this is called the bulk magnetization (M) parallel to the applied magnetic field (B_0).[56] When a radiofrequency signal (rf) is applied to the system, the distribution of spin orientations is changed if the signal matches the Larmor frequency, the resonance frequency of the spins,[56] *i.e.* it will tip the spins away from B_0. As soon as M is tilted away from the z-axis, it will start to precess about B_0 (Figure 11).[56]

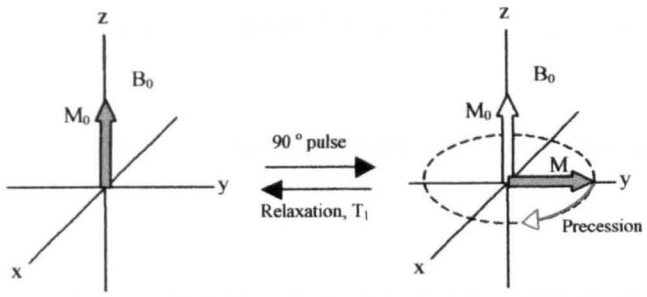

Figure 11 Effect of a 90 ° pulse

A receiver coil measures the signal oriented along the y-axis, and so measures positive, then zero and then negative signal as the spins precess from y to x and then to –y. The frequency of this oscillating signal is the difference between the frequency of the spins and the excitation frequency.[54] The magnetization, M, decays back to thermal equilibrium, M_0, exponentially. The components of M which are parallel and perpendicular to M_0 decay through different process, spin-lattice and spin-spin relaxation (described in Equations (34) and (35)) with time constants T_1 and T_2 respectively.[57]

$$\frac{dM_z}{dt} = -(M_z - M_0)/T_1 \qquad (34)$$

$$\frac{dM_x}{dt} = -M_x/T_2 \quad \text{and} \quad \frac{dM_y}{dt} = -M_y/T_2 \qquad (35)$$

M_0 – the equilibrium magnetization, M_z– component of the magnetization parallel to M_0, M_x, M_y - components of the magnetization perpendicular to M_0, T_1 – spin-lattice relaxation time, T_2 – spin-spin relaxation time.

The spin-lattice (or longitudinal) relaxation occurs by energy transfer from the nuclear spin to the other spins in the system, caused by fluctuating magnetic fields in the sample.[56] Spin-spin relaxation occurs through transfer of spin between excited nuclei.[57]

The oscillating signal is therefore, gradually decaying, and is represented by a cosine function that experiences exponential decay.[54] This signal is called the free induction decay (fid) which is Fourier transformed into the frequency domain and a spectrum is produced.

The chemical shift of a proton is the difference in frequency of the proton resonance to that of an internal standard, usually tetramethyl silane (TMS) Equation (36).[54]

$$\delta = [\ \nu_S\ (Hz)\ -\ \nu_{TMS}\ (Hz)\ ]\ /\ \text{Spectrometer operating frequency} \quad (36)$$

δ – Chemical shift (ppm), ν_S – resonance frequency of the proton in the sample, ν_{TMS} – resonance frequency of TMS.

1.8.6.2 Pre-saturation pulse sequence

The investigation of species present at low concentration in solution by ^1H NMR spectroscopy is a common problem in biological samples. Here, the signal intensity of the residual water protons in a D_2O solution is typically much greater than the intensity of the biological complex being investigated. The intensity of the residual H_2O protons can be reduced by applying a selective 180° pulse which tips only the water protons and adjustment of the delay to a time, whereby the water magnetization has reached zero. This is followed by the application of the normal 90 ° read pulse, which will allow the collection of the solute data with only a small contribution from the water protons.[55]

The kinetic experiments in this project faced a similar problem, where quantitative ^1H NMR with a detection limit of free amine of the order of 1×10^{-2} mmol L^{-1} was required. As the vast majority of the protons in this concentration of amine solution would be due to the aromatic protons of the monochlorobenzene (chlorobenzene) solvent, the dynamic range which can be investigated is limited. Suppression of the chlorobenzene signal was required.

Recent improvements in the pre-saturation pulse sequence technique have enabled the suppression of two solvents, for use on LC-NMR samples.[58] This technique is known as the WET sequence, Water suppression Enhanced through T_1 effects, [59] and can reduce the water signal to the order of 10^{-5}.[60] The modification of this pulse sequence was developed and optimised during this project for application to amine solutions of low concentration in chlorobenzene (see Chapter 2).

1.9 Kinetics

A major focus of this project was to understand the solution phase behaviour and kinetics of low solubility amine hydrochloride salts in chlorobenzene. A brief introduction on chemical kinetics follows.

1.9.1 Types of reaction

Reactions can be closed, where nothing is lost or gained by the reaction, or open, where matter is lost or gained by the system.[61] Reactions are also defined by being heterogeneous or homogeneous, reversible or not and either isothermal or non-isothermal.

The order of reaction defines the dependence of the rate on the concentration of the reactant; the most important categories in this work are zero and first order, Equations (37), (38) and (39).

Zero order with respect to A:

$$-\frac{dA}{dt} = k$$

$$A_0 - A = kt \qquad (37)$$

1st order with respect to A:

$$-\frac{dA}{dt} = kA \qquad (38)$$

$$-\int \frac{dA}{dt} = k\int dt$$

Taken between t_0 where A is $[A]_0$ and t where A is [A]

$$\ln(A_0 / A) = kt \qquad (39)$$

$$A = A_0 e^{-kt}$$

1.9.1.1 Consecutive reactions

Complex reactions can be parallel, where one product simultaneously reacts to form a series of different products, or consecutive, in which the product of the first reaction is the reactant in the next, Equation (40).

$$A \xrightarrow{k_1} B \xrightarrow{k_2} C \qquad (40)$$

1.9.1.1.1 Two 1st order consecutive reactions

Consecutive reactions where both steps are 1st order are described in most text books.[62] The rate equations and the derivation of their integrated rate laws are shown below.

$dA/dt = -k_1A$ $\qquad$ $dB/dt = k_1A - k_2B$ $\qquad$ $dC/dt = k_2B$

$A = A_0 e^{-kt}$ $\qquad$ $dB/dt = k_1A_0 e^{-kt} - k_2B$

If B_0 is assumed to be zero, then the equation for B can be integrated as a linear first order equation, using an integrating factor.

Rewrite with B = y

$$dY/dt = k_1A_0 e^{-kt} - k_2Y$$

This equation is first order and linear as the coefficients $k_1A_0 e^{-kt}$ and k_2 do not depend on Y. A linear first order differential equation is one which has the form: [63]

$$dy/dt + p(t)y = g(t)$$

The integrating factor $I = \exp(\int p(t)dt)$ [63]

The integrating factor is $\exp(\int k_2 dt) = e^{k_2t}$, rewriting the equation for dY/dt gives:

$$e^{k_2t} dY = e^{k_2t}(k_1A_0 e^{-k_1t} - k_2Y)\, dt$$

$$e^{k_2t} dY + (k_2Y e^{k_2t} - k_1A_0 e^{(k_2-k_1)t})\, dt = 0$$

An equation is exact if $\dfrac{dM(y,t)}{dY} = \dfrac{dN(y,t)}{dt}$

$M(y, t) = k_2Y e^{k_2t} - k_1A_0 e^{(k_2-k_1)t}$ $\qquad$ $dM/dy = k_2 e^{k_2t}$

$N(y, t) = e^{k_2t}$ $\qquad$ $dN/dt = k_2 e^{k_2t}$

The solution for exact equations is a function, g, which satisfies

$$dg/dt = M \quad \text{and} \quad dg/dy = N$$

the solution is $g(Y,t) = \text{constant}$

where $N(Y, t)dt + M(Y, t)dY = 0$

$$dg/dt = k_2 Y e^{k_2 t} - k_1 A_0 e^{(k_2-k_1)t} \quad \text{and} \quad dg/dy = e^{k_2 t}$$

$$g = Y e^{k_2 t} + h(y)$$

$$dg/dt = k_2 Y e^{k_2 t} + dh/dt$$

but $$dg/dt = k_2 Y e^{k_2 t} - k_1 A_0 e^{(k_2-k_1)t}$$

so $$dh/dt = - k_1 A_0 e^{(k_2-k_1)t}$$

$$h = \frac{- k_1 A_0 e^{(k_2-k_1)t}}{(k_2 - k_1)} + C$$

$$g = Y e^{k_2 t} \frac{- k_1 A_0 e^{(k_2-k_1)t}}{(k_2 - k_1)} = C$$

$$Y = \left(C + \frac{k_1 A_0 e^{(k_2-k_1)t}}{(k_2 - k_1)} \right) e^{-k_2 t}$$

At $t = 0, Y = 0$ $\quad 0 = C + \frac{k_1 A_0}{(k_2 - k_1)}$ $\quad$ So $C = \frac{k_1 A_0}{(k_2 - k_1)}$

$$Y = \left(- \frac{k_1 A_0}{(k_2 - k_1)} + \frac{k_1 A_0 e^{(k_2-k_1)t}}{(k_2 - k_1)} \right) e^{-k_2 t}$$

$$= \frac{k_1 A_0}{(k_2 - k_1)} (e^{-k_1 t} - e^{-k_2 t})$$

In terms of B $\quad B = \frac{k_1 A_0}{(k_2 - k_1)} (e^{-k_1 t} - e^{-k_2 t})$

For C: $\quad dC/dt = k_2 B$

$$= \frac{k_2 k_1 A_0}{k_2 - k_1} (e^{-k_1 t} - e^{-k_2 t})$$

let C = Y $\quad dY/dt = \frac{k_2 k_1 A_0}{k_2 - k_1} (e^{-k_1 t} - e^{-k_2 t})$

$$Y = \frac{k_2 k_1 A_0}{k_2 - k_1} (-1/k_1 e^{-k_1 t} + 1/k_1 e^{-k_2 t}) + \text{Constant}$$

Y = 0 at t = 0 $\quad 0 = \frac{k_2 k_1 A_0}{k_2 - k_1} (-1/k_1 + 1/k_1) + \text{Constant}$

$$= \frac{k_2 k_1 A_0}{k_2 - k_1} \cdot \frac{-(k_2 - k_1)}{k_1 k_2} + \text{Constant}$$

$$\text{Constant} = A_0$$

$$C = \frac{k_2 k_1 A_0}{k_2 - k_1}\left(\frac{-k_2 e^{-k_1 t} + k_1 e^{-k_2 t}}{k_1 k_2}\right) + A_0$$

$$= A_0\left(1 + \frac{k_2 e^{-k_1 t} + k_1 e^{-k_2 t}}{k_1 - k_2}\right)$$

The three final equations for a first order consecutive process are shown in Equations (41), (42) and (43).[64]

$$A = A_0 e^{-kt} \quad (41)$$

$$B = \frac{k_1 A_0}{(k_2 - k_1)}\left(e^{-k_1 t} - e^{-k_2 t}\right) \quad (42)$$

$$C = A_0\left(1 + \frac{k_2 e^{-k_1 t} + k_1 e^{-k_2 t}}{k_1 - k_2}\right) \quad (43)$$

The magnitude of k_1 and k_2 control the shape of the reaction profile for two 1st order consecutive reactions. For example, the reaction profile where k_2 is significantly smaller than k_1 is shown in Figure 12.[61] This case allows formation of significant quantities of intermediate B before it is consumed by the reaction to produce C.[20] If k_2 was much greater than k_1, the overall rate of formation of the product would depend on the slower, first, step, and very little of intermediate B would be observed.[20]

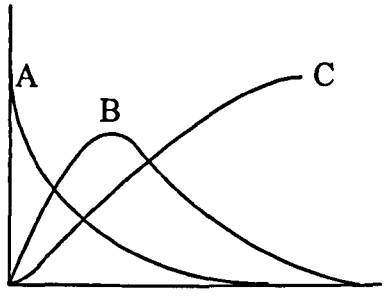

Figure 12 Reaction profile for a 1st order consecutive process.

1.9.1.1.2 1st order followed by 0th order consecutive reactions

Not all consecutive processes are first order. A simpler system exists in the body, when alcohol is absorbed and then oxidised by liver alcohol dehydrogenase in the liver to give acetaldehyde.[62] In this case the first step is 1st order and the second 0th order. The derivations of the integrated rate laws are much simpler, Equation (44). These equations

are true at short times, at longer times the concentration of A and B will tend to zero and the concentration of C will depend on the rate of metabolism of acetaldehyde in the body.[62]

$dA/dt = -k_1A$ $\quad dB/dt = k_1A - k_2B$ $\quad dC/dt = k_2$

$A = A_0 e^{-kt}$ $\quad dB/dt = (k_1A_0 e^{-kt} - k_2)$ $\quad C = k_2t$

$$\int dB = \int (k_1A_0 e^{-kt})dt - \int k_2dt$$

Integrating between B=0 at t = 0 and B = B_t at time t

$$\left[B\right]_0^{B_t} = \left[\frac{-k_1A_0 e^{-kt}}{k_1}\right]_0^t - k_2dt$$

At time 0, only A_0 exists $\quad B = A_0 - A_0 e^{-kt} - k_2t$

The three final equations for 1st followed by 0th order consecutive reactions are Equations (44), (45) and (46). The reaction profile for this type of consecutive reaction is shown in Figure 13.[62]

$$A = A_0 e^{-kt} \quad (44)$$

$$B = A_0 - A_0 e^{-kt} - k_2t \quad (45)$$

$$C = k_2t \quad (46)$$

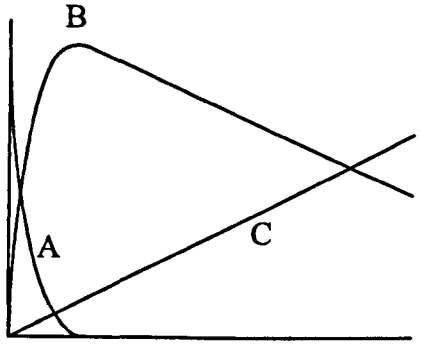

Figure 13 Reaction profile for a 1st then 0th order consecutive process.

The authors of the work described above, on the kinetics of the reactions of alcohol in the body, stated that a literature search of consecutive reactions resulted, most commonly, with 1st order consecutive processes; none mentioned 1st and 0th order consecutive reactions. This is not because zero order reactions are unknown, they are common in gas phase reactions and reactions proceeding at the surface of a catalyst, and are desired in the reaction of controlled release drug delivery systems.[65, 66]

A more complicated case is a consecutive process where the first stage is 0^{th} order but the second stage is 1^{st} order. A search of the chemical literature for this type of system, which was encountered in this project, was unsuccessful. In this type of process, a condition is set at time (t') the concentration of A is zero and B is B_{max}, after time (t') the concentration of B follows a first order decay. The derivation of these rate equations is shown in Chapter 6, and represents the development of a kinetic model that is consistent with the reaction profiles observed for 4-benzylaniline hydrochloride (4-BA.HCl) in chlorobenzene.

1.10 Statistical analysis

A non linear least squares approach was used to analyse the data from the solution investigations of 4-BA.HCl in chlorobenzene, and determine the rate coefficients. A curve drawn through a scattered set of data points is chosen so that the sum of the squares of the vertical distances from the data points to the line is minimised.[67]

R^2, the coefficient of determination (Equation (47))[67] and can be used to compare the goodness of fit of a model with an experimental data set. A value of R^2 of 1 would imply the model predicts the data perfectly, a value of 0.49 would imply just less than half of the variability in the data set can be predicted by the model.[68]

$$R^2 = 1 - SS_{error} \qquad \text{Where } SS_{error} = \Sigma e^2_i \tag{47}$$

R - the coefficient of determination, SS_{error} is the sum of the squares of the deviations, also known as the sum of the squares of the errors about the regression line, e^2_i – is the vertical deviation of the i^{th} data point from the line

Except for the errors quoted with the parameters determined using the non-linear least squares analysis, all errors in this project are quoted as standard deviations (σ) calculated from Equation (48).[68]

$$\sigma = \sqrt{\frac{\Sigma (x_1 - \mu)^2}{n - 1}} \tag{48}$$

σ - the standard deviation, μ - the mean value of the data, x_1 – is a single datum point, (n-1) – degrees of freedom,

Chapter 2

Experimental

2 Experimental

A vacuum line was designed and built for this project (Figure 14) and was used in the purification of chlorobenzene, the initial dissolution of $HCl_{(g)}$ in chlorobenzene experiments and the synthesis of the amine hydrochloride salts. The vacuum line operated satisfactorily holding a good vacuum of 1 x 10^{-5} Torr using an Edwards 5 rotary pump and a mercury diffusion pump. The line was constructed from Pyrex glass. The diffusion pump was protected from contaminants by two liquid nitrogen traps; the rotary pump was then in turn protected from mercury vapour by another liquid nitrogen trap. The two manifolds were fitted with Young's taps and B14 sockets for connection to various pieces of apparatus.

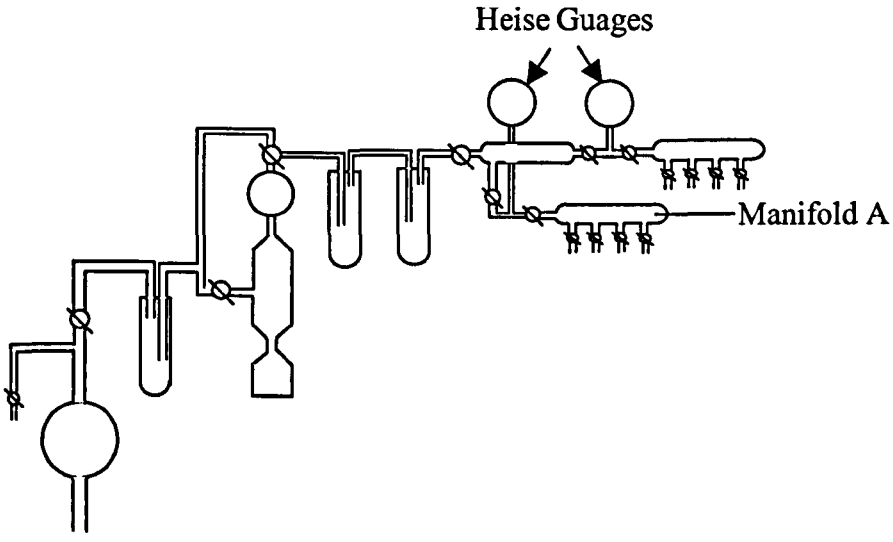

Figure 14 Vacuum line.

The volumes of the manifolds were calibrated using a known pressure and volume of N_2. The resulting pressures in various parts of the line were recorded using the Bourdon tube pressure gauge (Heise), with a precision of ± 1 Torr. The total volume of Manifold A plus the dead space between the Young's tap on the manifold and that on the small vessel plus the volume of the gauge was 0.249 ± 0.002 L. The volume of the small vessel was 0.020 ± 0.001 L.

2.1 Chlorobenzene

Chlorobenzene (Hopkin and Williams, General Purpose Reagent Grade), was purified by distillation over calcium hydride (CaH_2) and stored over 4A molecular sieves.[69] Calcium hydride is a drying agent used for a number of solvents including hydrocarbons, alcohols

and ethers. The distillation of chlorobenzene followed the same procedure as for dichloromethane.[69] The solvent (150 cm^3) was heated to reflux (405 K) in a round bottomed flask containing 8.3 g CaH_2 (Sigma-Aldrich powder, purity: 90 – 95 %). The pure vapour passed along a condenser fitted with a water cooling jacket and was collected over 4 A molecular sieve beads. The initial few millilitres of distillate were discarded as the temperature of the vapour above the solvent had not reached 132 °C, once this temperature was reached; the distillate produced was assumed to be pure chlorobenzene, as impurities would have lowered the boiling point. Care was taken to ensure the distillation did not boil dry, removing the apparatus from the oil bath whilst a small volume of chlorobenzene remained with the CaH_2 in the round bottomed flask. This solution was allowed to cool before disposing of the CaH_2 in a large bucket of ice. This was done slowly in the fume cupboard as heat and $H_{2(g)}$ were evolved.

The molecular sieves are calcium aluminosilcates which have a cage like structure with a pore size of 4 Å. The sieves were activated before use by heating under vacuum at 433 K for approximately 3 h.

The distilled chlorobenzene was degassed on the vacuum line using a freeze thaw pump cycle. A small volume of chlorobenzene (10 ml) was placed in a bulb with a Young's tap and connected to the vacuum line (Figure 14). The chlorobenzene was frozen using liquid N_2, then allowed to warm to room temperature to allow any gases trapped in solution to escape into the vacuum above the solvent. The remaining chlorobenzene was then frozen, and the excluded gases pumped away. This freeze thaw pump cycle was repeated three times, or until no more bubbles could be observed during thawing.

This purification procedure was time consuming taking on average 1.5 d to complete. It was used for experiments on the dissolution of HCl (Section 2.2.3), solubility of amines and amine hydrochlorides in chlorobenzene (Section 2.5.1) and the initial solution phase dissociation of 4-BA.$HCl_{(s)}$ investigations (Section 2.5.2). ^1H NMR was used to determine the purity of the distilled chlorobenzene, as discussed in Chapter 3, Section 3.1.

2.2 Hydrogen chloride (HCl)

2.2.1 Preparation of anhydrous HCl

Anhydrous $HCl_{(g)}$ can be made from the reaction of concentrated HCl with concentrated sulfuric acid (H_2SO_4), Equation (49).[70]

$$Cl^- + H_2SO_4 \rightarrow HCl + [HSO_4]^- \quad (49)$$

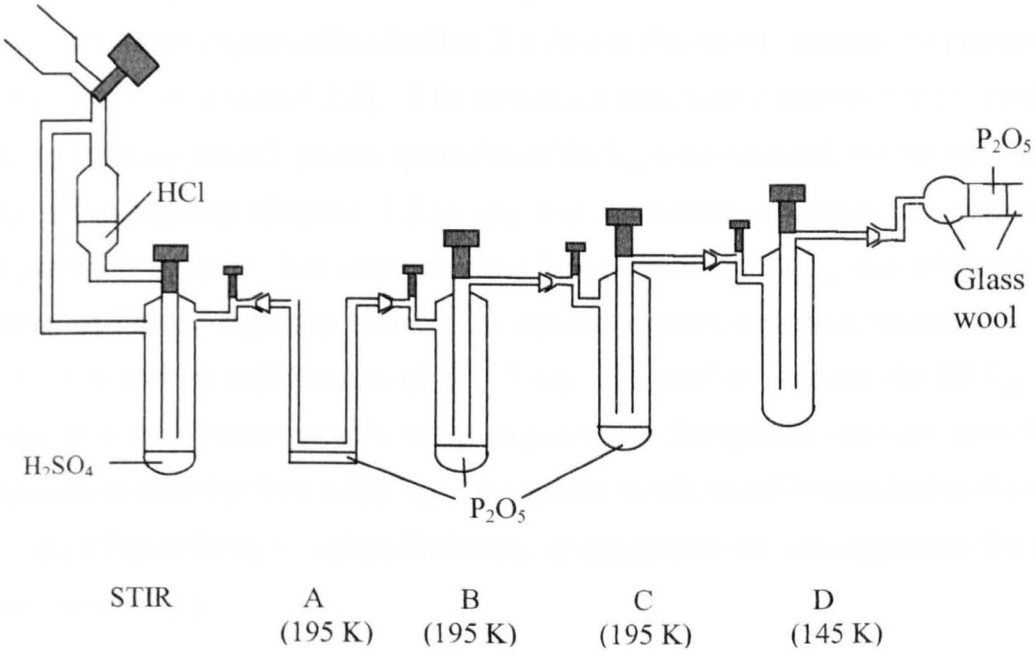

Figure 15 Apparatus used to prepare anhydrous HCl.

Before reaction, the four cooling baths were prepared. Those at 203 K were prepared by mixing dichloromethane (Fisher Scientific, Analytical Reagent Grade) with CO_2 pellets, both solvent and pellets were added until the desired temperature was reached. The bath at 145 K was prepared using isopentane (BDH, General Purpose Reagent Grade, purity: 95.0 %) and liquid N_2. This bath took much longer to prepare, and used a large volume of isopentane (1.5 L), although most evaporated during preparation. This bath was ready when the resulting material had the consistency of toffee.

The apparatus shown above (Figure 15) consisted of a reaction vessel with a dropping funnel and a pressure-equilibrating arm. Traps A to D were attached to the vessel using standard joint silicone grease (ACC Silicones). Traps A, B and C contained a small amount of drying agent (phosphorus pentoxide, P_2O_5, Fisher Chemicals) and were cooled to 195 K using the dry ice slush baths. The collection vessel (D) also contained P_2O_5 and

was cooled to 145 K using the isopentane – liquid N_2 slush bath. The drying tube attached to collection vessel D contained P_2O_5 to limit access of moisture from the air.

Concentrated HCl (8 cm^3) was added four drops at a time to concentrated sulfuric acid (10 cm^3) The HCl generated was distilled through traps A, B and C, to trap out water, and collected in trap D. This was then attached to the vacuum line where the HCl was degassed and vacuum distilled into a pressure vessel, a metal bomb. The Monel metal bomb contained P_2O_5 and the HCl was stored here until required.

The above procedure was used to prepare $HCl_{(g)}$ for the dissolution of HCl in chlorobenzene experiments (Section 2.2.2) and the initial attempts to prepare the amine hydrochlorides (Section 2.3). This procedure took approximately 1 d to complete and as the project continued, greater quantities of $HCl_{(g)}$ were required; for the dissolution of HCl in chlorobenzene (Section 2.2.3) and the continuing syntheses of batches of amine hydrochloride salts. For convenience a lecture bottle of $HCl_{(g)}$ was obtained from Linde Gas. A Praxair regulator, suitable for corrosive gases, with an inlet pressure range of 0 – 280 bar and an outlet range of 0 – 7 bar was used to regulate the $HCl_{(g)}$. A Whitey stainless steel bonnet needle valve connected to Swagelock stainless steel fittings, was used to control the flow of $HCl_{(g)}$. The lecture bottle could be attached to the vacuum line using a Cajun fitting to a glass B14 cone, or attached to the flow apparatus described below in Section 2.2.3.

2.2.2 HCl dissolution in chlorobenzene using the vacuum line

A measured volume of chlorobenzene (5 cm^3) was degassed using a repeated freeze, thaw, pump cycle. The manifold above the vessel was then charged with a pressure of $HCl_{(g)}$ (400 Torr). The Young's tap to the vessel was opened to the vacuum manifold, allowing contact of $HCl_{(g)}$ with chlorobenzene. The decrease in pressure of the manifold was monitored, and when no further decrease was observed, the vessel was isolated. Excess HCl was trapped in another vessel, already attached to the manifold, using liquid N_2, the manifold was then evacuated. This vessel was removed from the vacuum line and placed in a cold but empty liquid N_2 Dewar flask in the fume cupboard to allow the HCl to heat up slowly and evaporate.

The HCl-chlorobenzene solution was removed from the vacuum line, and the solution transferred to a liquid phase FTIR cell using the apparatus shown in Figure 16. A syringe filled with N_2 was used to push the HCl-chlorobenzene solution through a syringe into the IR cell. FTIR was used to analyse the solutions (see Chapter 3). This experimental set up was designed to minimise the loss of $HCl_{(g)}$ from the solution. Unfortunately this vacuum line technique for the dissolution of HCl in chlorobenzene did not produce an HCl-chlorobenzene solution.

Blank experiments using N_2 in place of HCl in the vacuum manifold established the pressure drop described above was due solely to the increase in volume on opening the manifold to the reaction vessel. This pressure drop was approximately 24 Torr, which was of a similar magnitude to the pressure drops observed during these HCl experiments. This is consistent with the spectroscopic measurements, in that no dissolution of HCl in chlorobenzene was detectable during these procedures.

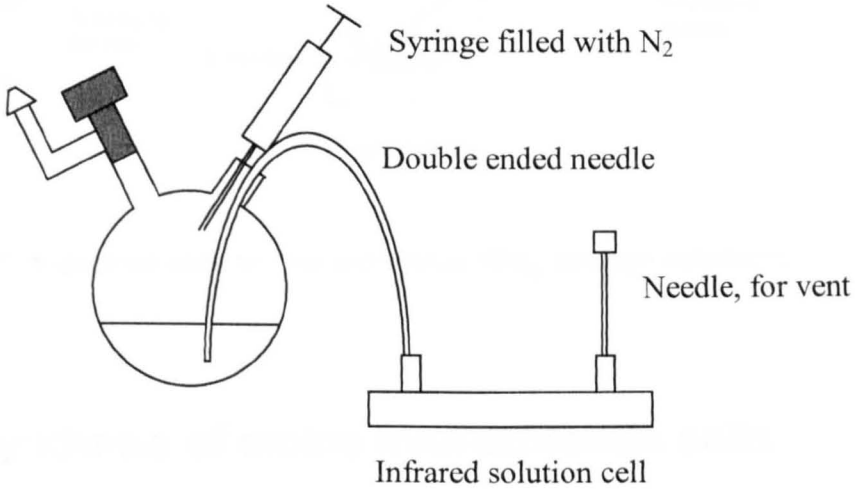

Figure 16 Apparatus for transfer of HCl- chlorobenzene solution to the liquid phase FTIR cell.

2.2.3 Flow HCl apparatus

As the vacuum line HCl dissolution experiments were unsuccessful, a more vigorous technique was designed, where $HCl_{(g)}$ was bubbled through a stirred volume of chlorobenzene.

Bubbling $HCl_{(g)}$ through chlorobenzene (50 cm^3) was achieved using the apparatus shown in Figure 17. This consisted of a small manifold with two B14 cones fitted to accept N_2 and $HCl_{(g)}$ lines. A silicone oil bubbler sandwiched between two empty Dreschel bottles allowed observation of gas flow and prevented suck back of solution or oil into the gas lines if a blockage occurred. The gas was admitted to the reactant solution through a glass sinter and the vessel stirred using a standard magnetic stirrer hotplate, which provided a good vortex. A rubber septum was fitted to allow sampling of the solution during reaction. Another Dreschel bottle and oil bath followed the round bottomed reaction vessel. Excess HCl was neutralised using a $NaOH_{(aq)}$ trap. This technique was successful in producing solutions of HCl in chlorobenzene (see Chapter 3 Section 3.2.3).

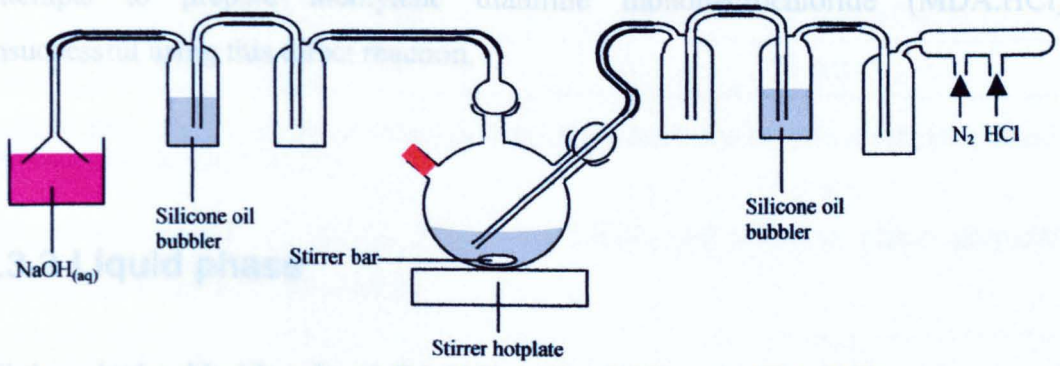

Figure 17 Apparatus used to flow anhydrous $HCl_{(g)}$ through solutions.

2.3 Synthesis of amine hydrochloride salts

Two methods have been used to synthesise the solid amine hydrochloride salts. The first was direct reaction between $HCl_{(g)}$ and solid amine in the vacuum manifold, using an excess of $HCl_{(g)}$. This reaction was to investigate the reaction of the solid amines with gaseous HCl.

The second synthesis; the bubbling of $HCl_{(g)}$ through a stirred solution of amine in chlorobenzene, was to asses the solution phase reaction of these amines (solvated amine + solvated HCl), which was more relevant to the solution phase industrial process.

2.3.1 Direct reaction between $HCl_{(g)}$ and solid amine

Both 4-benzylaniline hydrochloride (4-BA.HCl) and methylene dianiline dihydrochloride (MDA.2HCl) salts could be made by reaction of the solid amine with $HCl_{(g)}$ using the vacuum manifold. A sample of the solid amine (~0.1 g), either 4-benzylaniline (4-BA, 98 %, Alfa-Aesar) or 4,4'-methylene dianiline (MDA, 97 %, Sigma-Aldrich), was placed in a small vessel attached to the vacuum line. The manifold was charged with an excess of $HCl_{(g)}$, which was then released into the small vessel containing the solid amine. Reaction was deemed complete when the observed pressure drop was less than 1 Torr in 30 min, equivalent to 2 % of the total HCl required for complete hydrochlorination.

Attempts to prepare methylene dianiline monohydrochloride (MDA.HCl) were unsuccessful using this direct reaction.

2.3.2 Liquid phase

All three hydrochloride salts (4-BA.HCl, MDA.2HCl and MDA.HCl) were prepared using the HCl flow apparatus (Figure 17). Low concentration solutions (less than 0.05 mol L^{-1}) of 4-BA or MDA in chlorobenzene were degassed by bubbling through with N_2 for approximately 5 min prior to reaction. HCl was then bubbled slowly (less than 50 cm^3 min^{-1}) through the solution for approximately 20 min. The regulator on the HCl lecture bottle was set to 0.5 bar and the flow of gas was controlled by visual inspection of the bubbles formed in the silicone oil bubbler (Figure 17) and adjustment of the Whitey valve attached to the HCl regulator. 4-BA.HCl and MDA.2HCl were prepared using an excess of $HCl_{(g)}$.

In the case of MDA.2HCl, completion of reaction was assumed when a pale yellow solid had formed. Observation of solid formation in the reaction to form 4-BA.HCl was not easy as a brown opaque solution was formed at the onset of reaction.

Once reaction was complete (observation of solid MDA.2HCl, or after 20 min in the case of 4-BA.HCl) the $HCl_{(g)}$ flow was switched off and the solution and apparatus purged through with N_2 for 10 min to remove excess $HCl_{(g)}$. The solutions were filtered using a Büchner funnel and Whatman cellulose Grade 1 filter papers.

2.3.3 Direct gas – solid vs. solution phase reaction: MDA.2HCl

All salts made were analysed by ^{1}H NMR in DMSO, FTIR spectroscopy and elemental analysis. The results from selected elemental analysis of MDA.2HCl syntheses are shown in Table 4. The ^{1}H NMR and FTIR spectra are discussed in Chapter 3.

Sample	Elemental Analysis (%)				Result
	C	H	Cl	N	
Required	78.9	7.1	0	14.2	MDA
	66.5	6.4	15.1	11.9	MDA.HCl
	57.6	5.9	26.2	10.3	MDA.2HCl
Solution phase	57.7	5.9	26.2	10.2	MDA.2HCl
Direct reaction	57.5	5.9	25.9	10.2	MDA.2HCl

Table 4 Elemental Analysis of direct and solution reactions to form methylene dianiline dihydrochloride (MDA.2HCl).

The direct reaction of $HCl_{(g)}$ with solid MDA and solution phase preparations of MDA.2HCl were both successful.

2.3.4 Direct gas-solid vs. solution phase: 4-BA.HCl

4-BA.HCl was also prepared successfully using both the gas-solid route and the solution phase process. All samples were characterised using ^{1}H NMR and FTIR spectroscopy and elemental analysis, Table 5. The reaction using the sparge apparatus was observed to be less rapid than that of MDA with HCl.

Sample	Elemental Analysis (%)				Result
	C	H	Cl	N	
Required	85.2	7.1	0	7.7	4-BA
	71.1	6.4	16.2	6.4	4-BA.HCl
Solution Phase	71.0	6.4	16.2	6.4	4-BA.HCl
Direct reaction 1	70.95	6.4	16.1	6.4	
Direct reaction 2	70.9	6.4	16.4	6.4	

Table 5 Elemental Analysis of direct and solution reactions to form 4-benzylaniline hydrochloride (4-BA.HCl).

2.3.5 Development of method to make monohydrochloride (MDA.HCl)

The reactions between 4-BA and MDA with HCl in solution were known by the industrialists to produce 4-BA.HCl and MDA.2HCl respectively. There was no evidence for the formation of the intermediate in the MDA series (MDA.HCl). For mechanistic reasons, it was considered beneficial to investigate if this potential intermediate could be prepared. Attempts at preparing methylene dianiline monohydrochloride (MDA.HCl) using the direct reaction of HCl(g) with MDA(s) on the vacuum line were not successful and produced only mixtures, as determined by elemental analysis, Table 6. It is possible that only the surface particles of MDA react with $HCl_{(g)}$ and form MDA.2HCl and that only a small amount of $HCl_{(g)}$ penetrates the surface of the sample. Therefore most of the solid MDA remains unreacted. The successful preparation of MDA.HCl, Solution phase 1, was unintentional though fortuitous and was the result of a limited supply of $HCl_{(g)}$ that occurred due to a partial blockage in the HCl feed line. This opportune result indicated firstly that MDA.HCl could be prepared but also which preparation route might work.

Sample	Elemental Analysis (%)				Result
	C	H	Cl	N	
Required	78.9	7.1	0	14.2	MDA
	66.5	6.4	15.1	11.9	MDA.HCl
	57.6	5.9	26.2	10.3	MDA.2HCl
Solution phase 1	66.7	6.5	15.3	11.9	MDA.HCl
Solution phase 2 #1	56.4	5.7	28.2	9.2	Mixture
Solution phase 2 #2	56.2	5.8	25.7	9.6	Mixture
Direct reaction 1	73.1	6.9	15.7	13.0	Mixture
Direct reaction 2	68.8	6.6	12.1	12.2	MDA.HCl (Cl is low)
Direct reaction 3	56.5	5.9	24.9	10.1	MDA.2HCl (Cl is low)

Table 6 Elemental Analysis of direct and solution phase reactions to form methylene dianiline monohydrochloride (MDA.HCl).

Duplicate elemental analyses of the resultant mixture from solution phase reaction 2 were obtained and show the approximate reproducibility of this analytical technique.

To prepare MDA.HCl *via* the solution phase reaction, a high degree of mixing and a stoichiometiric amount of HCl was required. A large bulb (>1 L) fitted with a bypass

(Figure 18) was attached to the vacuum line and a stoichiometric amount of $HCl_{(g)}$ (233 Torr, 2.97 x 10^{-3} mol) was distilled into it using an iso-pentane / liquid nitrogen slush bath. The bulb was then topped up to 760 Torr with $N_{2(g)}$, removed from the vacuum manifold and attached to the flow apparatus (Figure 17). Nitrogen gas was then passed through the bypass on the bulb into the solution of MDA (0.589 g, 2.97 x 10^{-3} mol) in chlorobenzene (50 cm^3) to degass the solution for 10 min. The iso-pentane / liquid nitrogen slush bath was used to maintain the HCl as a solid during this time. The two stopcocks on the bulb were then switched to allow $N_{2(g)}$ to flow through the bulb and into solution, the overpressure of $N_{2(g)}$ already in the bulb prevented suck back of the MDA solution. Gradual warming of the HCl under a continual flow of nitrogen then allowed the slow release of a dilute stream of HCl into the reaction solution, ensuring efficient mixing.

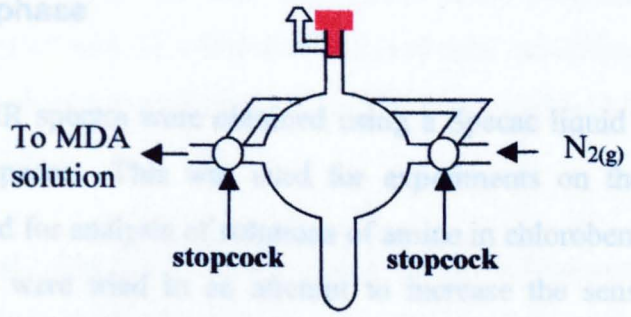

Figure 18 Apparatus for preparation of a stoichiometric amount of $HCl_{(g)}$.

Sample	Elemental Analysis (%)				Result
	C	H	Cl	N	
Required	78.9	7.1	0	14.2	MDA
	66.5	6.4	15.1	11.9	MDA.HCl
	57.6	5.9	26.2	10.3	MDA.2HCl
Solution phase 1	66.7	6.5	15.3	11.9	MDA.HCl
NEW METHOD	66.6	6.4	15.2	11.8	MDA.HCl

Table 7 Elemental Analysis of solution preparations of methylene dianiline monohyrodhcloride (MDA.HCl).

Dispersion of MDA by dissolution in chlorobenzene and slow release of an aliquot of $HCl_{(g)}$ into the solution allowed the repeatable preparation of MDA.HCl. The elemental analysis of a sample of MDA.HCl made using this new method is consistent with the expected percentage elemental distribution for the monhydrochloride salt (Table 7).

2.4 Analytical techniques used

2.4.1 FTIR spectroscopy

The FTIR spectra of the five compounds investigated in this project (4-BA, MDA, 4-BA.HCl, MDA.HCl and MDA.2HCl) were obtained using a Nicolet Avatar 360 FTIR spectrometer. This spectrometer used a triglycine sulfate (TGS) detector, and had a measured signal to noise ratio of 25.1 where the signal measured was the band at 3400 cm^{-1} in the MDA spectrum using 32 scans. The noise was measured over the region of 2600 – 2300 cm^{-1}. FTIR spectroscopy of solutions of HCl, 4-BA and MDA in chlorobenzene were also obtained using this spectrometer.

2.4.1.1 Liquid phase

Liquid phase FTIR spectra were obtained using a Specac liquid cell with CaF_2 windows and a 0.1 mm spacer. This was used for experiments on the dissolution of HCl in chlorobenzene and for analysis of solutions of amine in chlorobenzene. Thicker spacers of 0.2 and 0.5 mm were tried in an attempt to increase the sensitivity to free amine in chlorobenzene solutions, but this was not successful. The strong absorbance of chlorobenzene below 1700 cm^{-1} dominated the FTIR spectrum and so the detection limit of free amine in solution was poor, only 0.06 mol L^{-1}.

2.4.1.2 Solid state

A Pike attenuated total reflectance (ATR) accessory (MIRacle ATR accessory with diamond/ZnSe lense and high pressure clamp) was attached to the Nicolet spectrometer for analysis of solids; 4-BA, MDA, 4-BA.CHl, MDA.HCl and MDA.2HCl. This technique had a calculated signal to noise ratio of 62.3, where the signal measured was the band at 2825 cm^{-1} in the MDA spectrum using 256 scans, and the noise was measured over the region of 2050 – 1950 cm^{-1}. The transmission at 1000 cm^{-1} was 33 % when no sample was present. For each spectrum obtained, 256 scans of the spectrometer were preformed. This spectrometer set up provided an easy method for analysis of the solid samples.

2.4.2 Single crystal x-ray diffraction (XRD)

2.4.2.1 Crystal preparation

Single crystals of each of the five compounds were obtained using a variety of solvents.

- Crystals of 4-BA and MDA were prepared by dissolving a few mg of each in a very small volume of anhydrous chlorobenzene (a few drops) (Aldrich, purity: 99.8 %, < 0.005 % water), producing saturated solutions. No heating was required to dissolve the amines. The solutions were left to crystallise by evaporation of the excess solvent over a number of days.
- Crystals of 4-BA.HCl and MDA.HCl were prepared by dissolving a few milligrams of each in a few drops of methanol (analytical reagent grade, purity ≥ 99.8 %). Again the solutions were left to crystallise in the fume cupboard over a number of days.
- Crystals of MDA.2HCl were prepared using a diffusion technique (Figure 19). A few milligrams of MDA.2HCl were dissolved in a small volume of methanol (Analytical reagent grade, purity ≥ 99.8 %) in a small sample vial. The vial was placed in a larger beaker which was filled with chlorobenzene, in which MDA.2HCl is insoluble. The crystals were formed upon diffusion of chlorobenzene into the methanol solution.

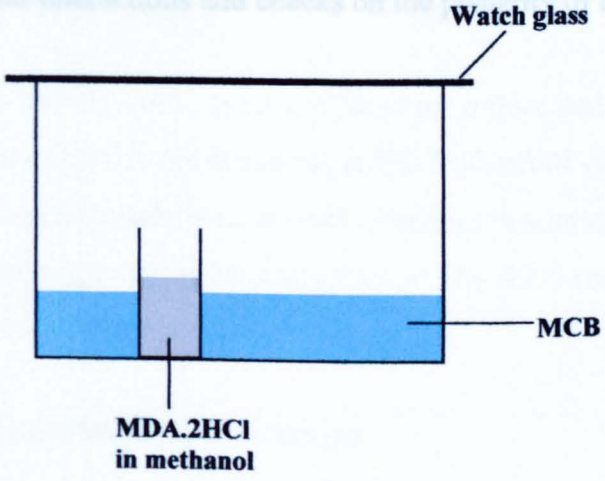

Figure 19 Experimental set up for vapour-diffusion crystallisation procedure.

2.4.2.2 Diffractometer

The crystallographic measurements were determined using a Nonius Kappa CCD diffractometer with a Mo-K_α radiation, λ = 0.71073 Å at 150 K. The output of the diffractometer was a list of reflections with positions and intensities; these were used to determine the crystal structure.

2.4.2.3 Programmes used for refinement and visualisation.

Determination of the crystal structures was carried out using WinGX and ShelX 97 software.[71, 72, 73] WinGX is a windows system which incorporates crystal structure refinement programs such as ShelX 97 and also validation software such as PLATON.[74] All structures were validated using the PLATON software, which checks the crystallographic information file (CIF) and issues a set of alerts. There are ten groups of tests that the software performs, Table 8. Test 2 checks that the anisotropic displacement parameters along the bond of two atoms bonded together are equal, which is true for correctly identified atoms, this is known as the Hirschfeld rigid bond test.[75] Bond angles and lengths are checked against standard averages, *i.e.* the incorrect assignment of the hybridisation of a carbon atom could be due to a missing H atom from the structure. The distances between atoms are also checked, if two atoms are separated by less than the sum of their van der Waals radii there is likely to be a missed interaction, such as a H-bond or one of the atoms is in the wrong position.

The PLATON software also produced a list of atom coordinates, bond lengths, bond angles, intermolecular interactions and checks on the planarity of aromatic rings.[74]

Test	Description
0	Data completeness, consistency and quality
1	Checks unit cell and space group symmetry
2	(an)isotropic displacement parameters
3	Intramolecular issues
4	Intermolecular issues
5	Coordination issues
6	Solvent accessible voids
7	Bonds and their associated standard uncertainties
8	Validation software problems
9	Problems with reflection data

Table 8 PLATON validation software tests.

2.4.3 Lattice energies

The lattice energies were calculated by A. Gavezzotti at the University of Milan, using his Pixel[36] method. The crystallographic information files obtained at Glasgow were used to calculated the electron density using MP2 level of theory and the 6-31G** basis set.

2.4.4 Inelastic Neutron Scattering (INS) spectroscopy

Inelastic Neutron Scattering (INS) spectra of the two amines and their hydrochloride salts were obtained on the TOSCA spectrometer at the Rutherford Appleton Laboratory, July 2005. The TOSCA spectrometer is an Inelastic Neutron Scattering spectrometer optimised for vibrational spectroscopy within the energy range 30 – 4000 cm^{-1} (0 – 500 meV), but the best spectra are obtained below 2000 cm^{-1} (250 meV).

2.4.4.1 TOSCA, experimental procedure

Spectra were recorded at 20 K using the 24 position sample-changer.[50] The size of the beam at the sample is 40 x 40 mm, and so the samples were folded into an aluminium foil packet of this size. The packets contained 1 - 3 g of sample and were flattened to 1 mm in

thickness, ensuring the sample was evenly distributed in the sachet, after which all sachets were loaded into position on the sample changer. The first sample loaded was pre-cooled in liquid nitrogen before the sample changer was lowered by crane into the spectrometer well. This reduced the time required for cooling the sample before the spectrum was recorded. The Ray-of-Light program[50] was used to control the webcam situated at the top of the sample changer. This allowed confirmation of rotation of the sample changer before the next sample spectrum was started, as the webcam can see the number of the sample which is 12 positions away from the sample in the beam. The output of the TOSCA automatic analysis program was used directly to produce the INS spectra.[50]

2.4.5 DFT

Periodic Density Functional Theory (DFT) calculations were performed for each compound, using the Dmol^3 software [76] and inputs from the crystallographic information already obtained. Using the vibrations calculated by the DFT calculations, the program auntieCLIMAX (a-CLIMAX)[48] was used to predict the INS spectra. This allowed validation of the DFT calculations by comparison with the spectra obtained on TOSCA. The DFT calculations were then used to assign the vibrational spectra through the visualisation software of Dmol^3. This was a lengthy process; the DFT calculations produced a list of vibrational frequencies for each compound and each in turn was viewed using the visualisation software. The assignment of each vibration was then made, most of the vibrational modes were not isolated vibrations but coupled to others in the molecule, *e.g.* the δ(N-H) of 4-BA observed at 1509 cm^{-1} was coupled to the ν(N-C) mode and also the ν(C-C) ring stretching mode.

2.4.6 Thermal Gravimetric Analysis (TGA)

TGA analysis of the hydrochloride salts was performed at Glasgow and at Huntsman, Everberg, Belgium.

2.4.6.1 Glasgow

TGA experiments were performed in Glasgow on a Q500 TA Instruments Thermogravimetric Analyzer. All samples were run under a flow of N_2 of 10 cm^3 min^{-1}. The isothermal measurements were ramped to temperature at a rate of 5 K min^{-1}. The 4-BA.HCl sample was ramped to 473 K at a rate of 1 K min^{-1}.

2.4.6.2 Huntsman

TGA analysis of MDA.2HCl and 4-BA.HCl were performed on a Mettler Toledo Instrument, followed by ATR-FTIR analysis of the residual material using a Specac Golden Gate ATR element attached to a Bruker FTIR spectrometer.

2.4.6.3 Melting point

The melting points of each of the five compounds,(4-BA, MDA, 4-BA.HCl, MDA.HCl, MDA.2HCl) were determined using a manual melting point apparatus (Stuart Scientific, SMP1) which consisted of an electrically powered heating block, a magnifying eyepiece and a mercury-in-glass thermometer.[77] A glass capillary, sealed at one end, was filled with a small amount of sample to a depth of 1 - 2 mm, and placed in the heating block of the apparatus. The approximate melting point range was determined using a fast temperature ramp. A more precise melting point was then established on a fresh sample, using a slower temperature ramp of ~ 2 K min^{-1}. The sample was viewed as it melted, through the magnifying glass fitted to the apparatus, and the temperature recorded using the mercury thermometer. Decomposition occurred on the samples of MDA.2HCl, as observed by the blackening of the sample before melting. Melting points were obtained for the other compounds, when the samples became clear liquids.

2.4.6.4 Differential Scanning Calorimetry (DSC)

The DSC Q100 instrument was used for the differential scanning calorimetry measurements. It is a heat-flux DSC instrument, where the sample pan and reference pan are heated in the same furnace and the temperature difference between the two pans is measured.

A few mg of sample were placed in an aluminium pan and fitted with a lid; this assembly was then pressed using the Thermal Analysis sample press. The sample and reference pan

were then placed in the furnace, and the temperature programmed to ramp for each compound as listed in Table 9.

Compound	Ramp (K min^{-1})	Final temperature (K)
4-BA	2	48
MDA	5	150
4-BA.HCl	10	300
MDA.2HCl	10	500

Table 9 DSC experiments, ramp and final temperatures.

2.4.7 Proton nuclear magnetic resonance spectroscopy (^{1}H NMR)

2.4.7.1 Product speciation

^{1}H NMR spectra were recorded on a Bruker Avance 400 MHz spectrometer fitted with a Quattro Nucleus Probe (QNP) able to investigate four nuclei; ^{1}H, ^{19}F, ^{31}P and ^{13}C.

The hydrochloride salts were insoluble in chloroform ($CDCl_3$) and very insoluble in chlorobenzene, so anhydrous dimethyl sulfoxide-d_6 (DMSO), (Aldrich, 99.9 atom % D, < 50 ppm water) was used for initial ^{1}H NMR experiments, see Chapter 3 Section 3.3.4. These experiments were performed to check that full conversion from amine to amine hydrochloride had been achieved in the solution phase or direct gas-solid syntheses. As an example the ^{1}H NMR spectrum of MDA.2HCl is shown in Figure 20, showing the assignments of the NH_3^+, CH_2 and aromatic protons. The latter are fully assigned and discussed in Chapter 3, Section 3.3.4.

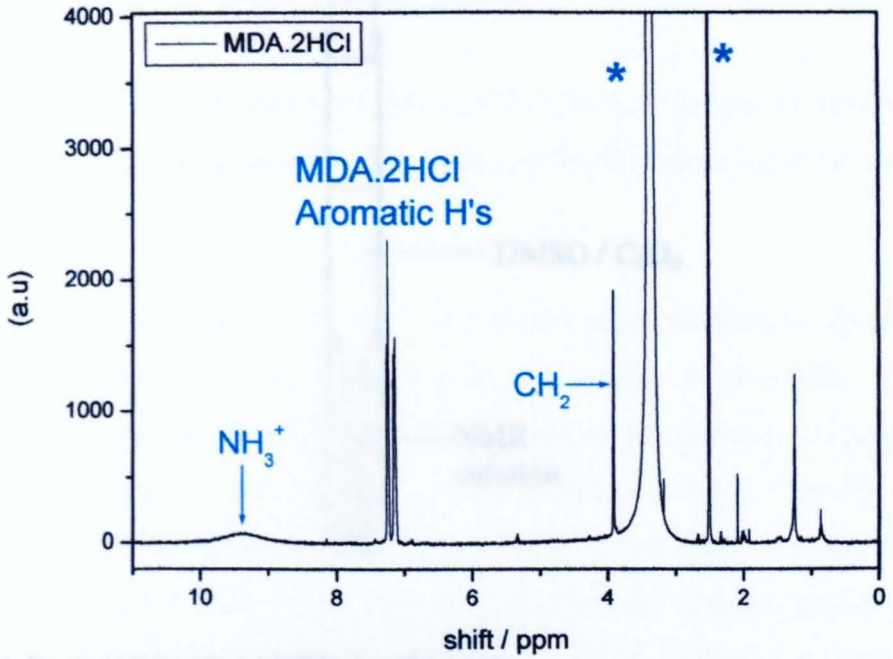

Figure 20 ^{1}H NMR spectrum of MDA.2HCl in DMSO.

*** - solvent signals at 2.5 ppm (DMSO methylene signal) and 3.5 ppm (water in DMSO)**

The investigations of the dissociation of HCl in chlorobenzene (Chapter 3, Section 3.2.3), the preliminary solution phase investigations of the dissociation of 4-BA.HCl$_{(s)}$ (Chapter 6, Section 6.1), and the kinetic experiments on 4-BA.HCl$_{(s)}$ (Chapter 6, Section 6.3) were performed in chlorobenzene, the industrial process solvent. Normally a non-deuterated solvent sample will be diluted with $CDCl_3$ to provide a deuterium signal for the NMR spectrometer lock. However, it was found during initial ^{1}H NMR studies in this project that small levels of impurities present in $CDCl_3$ had a proton resonance coinciding with the region of interest (2 – 6 ppm) which covered the methylene and amine signals of 4-BA and 4-BA.HCl.

A Wilmad NMR capillary tube containing the deuterated solvent (Figure 21) was used to analyse the chlorobenzene solution samples, allowing the deuterated solution to remain separated from the sample solutions. The deuterated solvent was either dimethyl sulfoxide-d_6 (DMSO), used during the preliminary dissociation experiments, or d_6-benzene (C_6D_6), used during the kinetic experiments. The latter was preferred as its most prominent signals did not interfere with those of the species being investigated, namely the region between 2 and 6 ppm. This region contains the NH_2, and CH_2 proton resonances of 4-BA, as shown in Figure 22. In the case of solutions of 4-BA.HCl in chlorobenzene this region contains the CH_2 resonance of 4-BA.HCl.

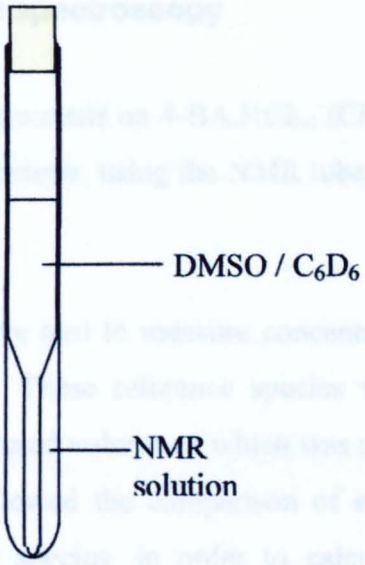

Figure 21 Deuterated solvent NMR capillary tube.

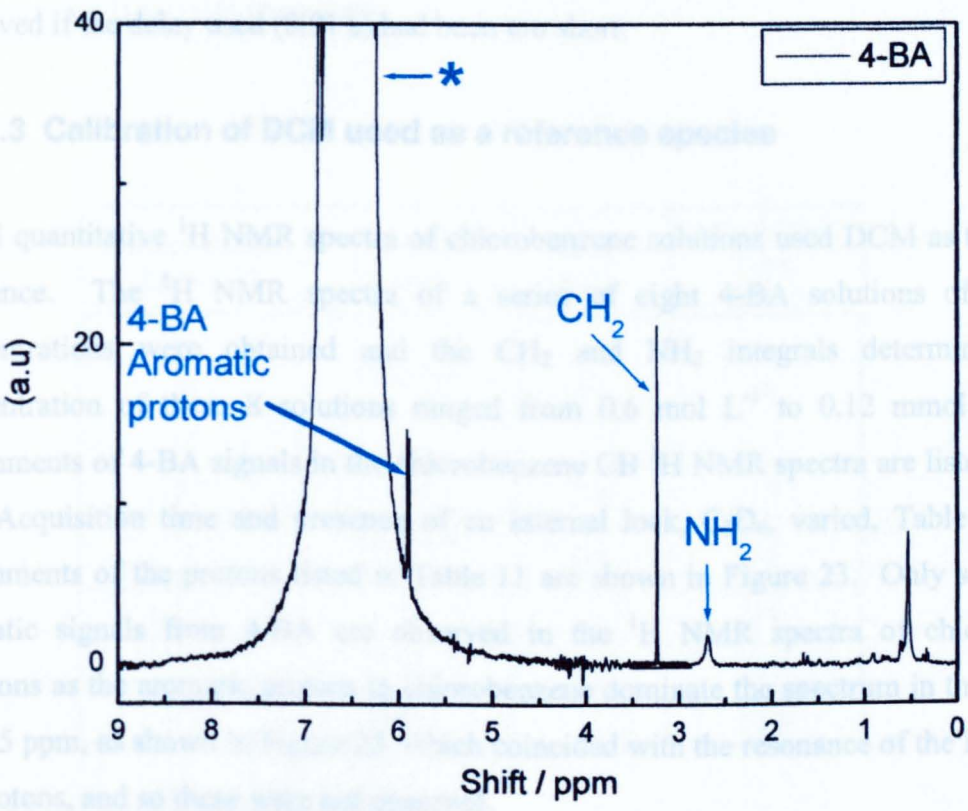

Figure 22 ^{1}H NMR spectrum of 4-BA in chlorobenzene

Using the deuterated solvent NMR capillary tube. * - represents the aromatic proton signal of the chlorobenzene solvent

2.4.7.2 Quantitative ^{1}H NMR spectroscopy

The quantitative ^{1}H NMR measurements on 4-BA.HCl$_{(s)}$ (Chapter 6) were performed on a Bruker Avance 400 MHz spectrometer, using the NMR tube arrangement shown in Figure 21.

To use ^{1}H NMR as a quantitative tool to measure concentrations of species in solution, internal references were used. These reference species were liquids, cyclohexane or dichloromethane (DCM), a measured volume of which was added to the inserts containing the deuterated solvent. This allowed the comparison of signal intensity of the species investigated with the reference species, in order to calculate concentrations. It also avoided any unwanted interaction of the reference material with the species in question. A plot of the CH_2 and NH_2 integrals, referenced to DCM, against the delay (D1) ranging from 0.01 – 3 s showed no change in the integral values. This confirms that the delay used during these experiments was long enough to allow full relaxation of the spins before the next pulse was applied. An increase in the integrals with increasing delay would have been observed if the delay used (0.01 s) had been too short.

2.4.7.3 Calibration of DCM used as a reference species

Initial quantitative ^{1}H NMR spectra of chlorobenzene solutions used DCM as the internal reference. The ^{1}H NMR spectra of a series of eight 4-BA solutions of measured concentrations were obtained and the CH_2 and NH_2 integrals determined. The concentration of these 8 solutions ranged from 0.6 mol L^{-1} to 0.12 mmol L^{-1}. The assignments of 4-BA signals in the chlorobenzene CB ^{1}H NMR spectra are listed in Table 10. Acquisition time and presence of an internal lock, C_6D_6, varied, Table 11. The assignments of the protons listed in Table 11 are shown in Figure 23. Only some of the aromatic signals from 4-BA are observed in the ^{1}H NMR spectra of chlorobenzene solutions as the aromatic protons in chlorobenzene dominate the spectrum in the region of 6 – 7.5 ppm, as shown in Figure 22, which coincided with the resonance of the H_X, H_Y and H_Z protons, and so these were not observed.

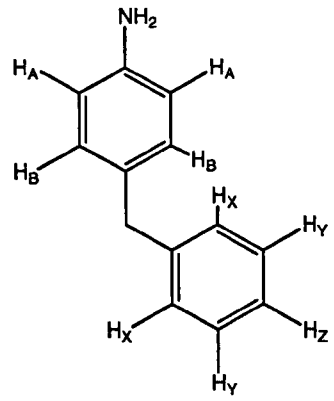

Figure 23 Assignment of protons in the ^{1}H NMR spectra of 4-BA as used in Table 10.

Assignment		H_B	CH_2	NH_2	Water in chlorobenzene	C_6D_6 impurities
δ value (ppm)	Unlocked	6.1	3.4	2.9	0.7	-
	Locked	6.3	3.7	3.15	1.0	0 & 0.4

Table 10 Assignments of the protons of 4-benzylaniline (Figure 23) in the ^{1}H NMR spectra of solutions of 4-BA in chlorobenzene.

Concentration (mmol L^{-1})	Condition (Scans)	Insert C_6D_6	Acquisition time (min)
600	Unlocked 16	No	2
60			
6			
5.2	128	Yes	15
3	Unlocked 128	No	15
1.3	128	Yes	15
0.6	256		60
0.12	8000		8.5 h

Table 11 4-BA solutions ^{1}H NMR conditions.

The integrals of the CH_2 and NH_2 signals scaled proportionally with the concentration of the 4-BA solutions (Figure 24).

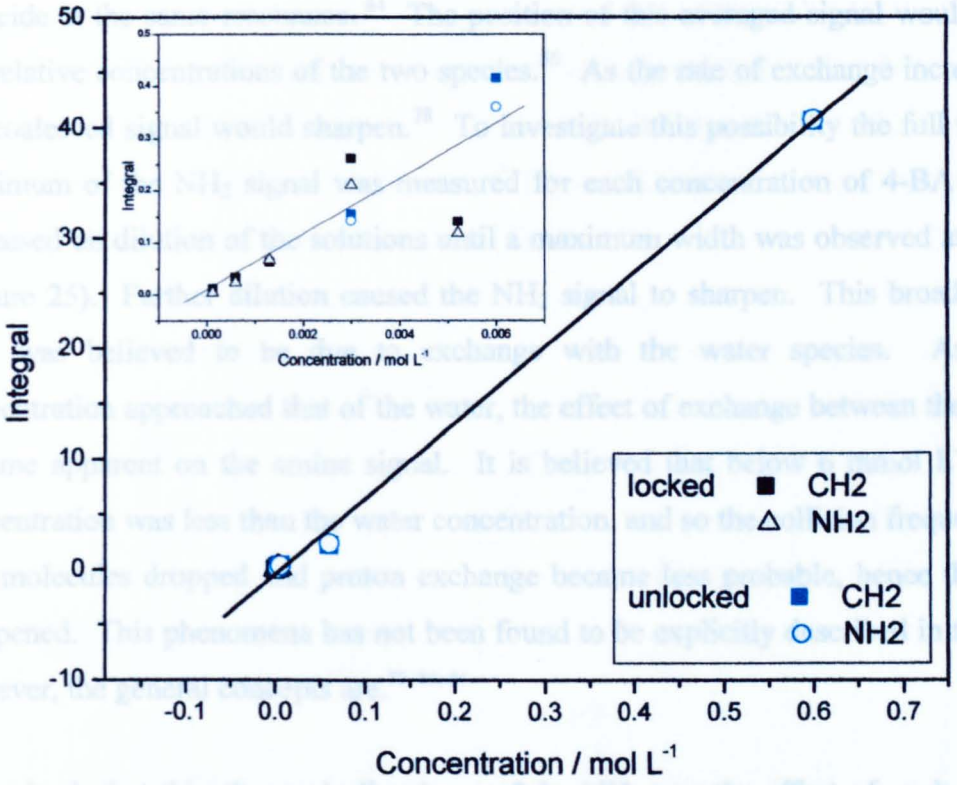

Figure 24 Plot of the integrals of the CH_2 and NH_2 signals of 4-benzylaniline (4-BA) as a function of concentration of 4-BA in chlorobenzene.

(Straight lines are drawn using all data, from both locked and unlocked ^{1}H NMR spectra)

It is possible that the NH_2 protons of 4-BA exchanged with another species present in chlorobenzene. However, as both the NH_2 and CH_2 signals integrated almost equally, the NH_2 appeared not to lose substantial population during this exchange process. This indicated that the exchange process, if it occurs, was slow.

As the concentration of 4-BA was decreased the line shape of the NH_2 signal changed, indicating that there may be an exchange process occurring. This exchange process was thought to occur between the protons of the NH_2 and those of a signal observed at ~1 ppm in the locked spectra and 0.7 ppm in the unlocked spectra (Table 10). This species was assigned to residual water, which was not removed from chlorobenzene *via* the distillation procedure outlined in Section 2.1.

If an exchange process occurred between two nuclei the line shape of the ^{1}H NMR signals of each nucleus would be affected. As the rate of exchange of the protons between the two species increased the line-shapes of the two signals would broaden.[78] If the exchange process was sufficiently fast, the rate of exchange would be greater than the frequency difference between the proton resonance frequencies of the two signals, both signals would

coincide at the same resonance.[54] The position of this averaged signal would depend on the relative concentrations of the two species.[55] As the rate of exchange increased further the coalesced signal would sharpen.[78] To investigate this possibility the full width at half maximum of the NH_2 signal was measured for each concentration of 4-BA solution. It increased on dilution of the solutions until a maximum width was observed at 6 mmol L^{-1} (Figure 25). Further dilution caused the NH_2 signal to sharpen. This broadening of the NH_2 was believed to be due to exchange with the water species. As the amine concentration approached that of the water, the effect of exchange between the two species became apparent on the amine signal. It is believed that below 6 mmol L^{-1}, the amine concentration was less than the water concentration, and so the collision frequency of these two molecules dropped and proton exchange became less probable, hence the NH_2 peak sharpened. This phenomena has not been found to be explicitly described in the literature, however, the general concepts are.[79, 80, 81]

As a check that this change in lineshape of the NH_2 was the effect of exchange, the full widths at half maxima were measured for the CH_2 and the 'water' signals. Neither appeared to change on dilution (Figure 25). The approximate concentration of water in distilled chlorobenzene is discussed in Chapter 3 Section 3.2.6.

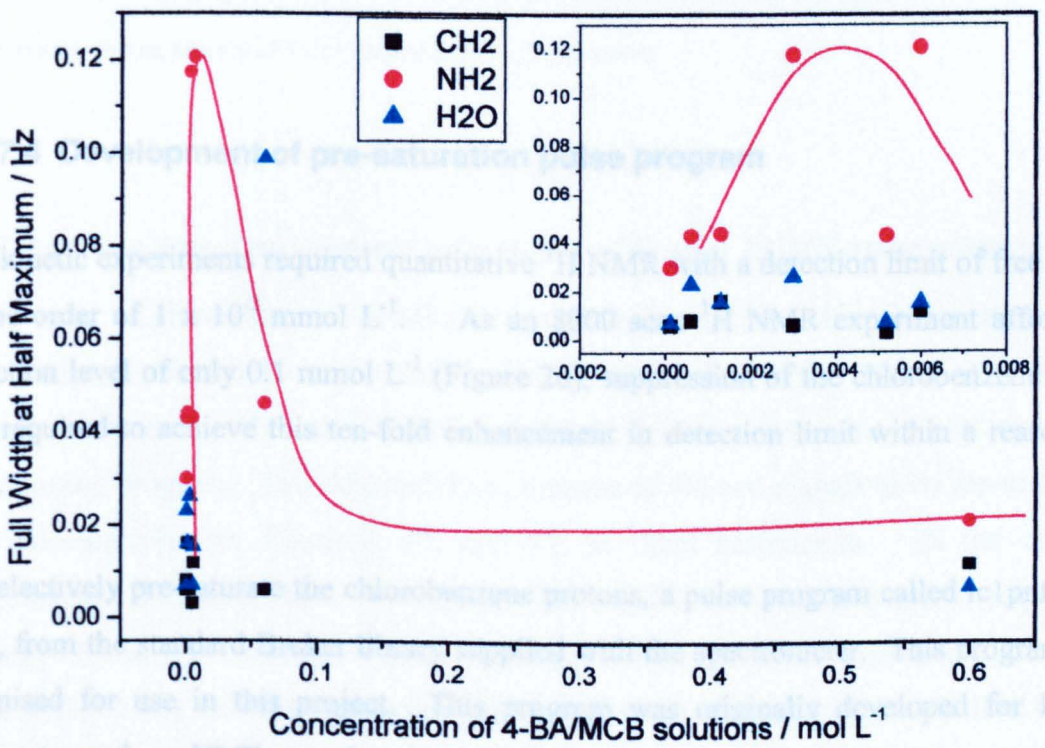

Figure 25 Full width at half maxima (FWHM) of the ^{1}H NMR signals of the NH_2 and CH_2 of 4-BA and the water of chlorobenzene, as a function of concentration of solutions of 4-BA in chlorobenzene.

(Lines are shown as a guide to the eye)

The limit of detection for the equilibrium between 4-BA.HCl and 4-BA in chlorobenzene using ^{1}H NMR depended on the ability to observe the NH_2 signal at low concentration. This has been investigated using low concentration 4-BA solutions. The NH_2 signal was observed at concentrations as dilute as ~ 0.1 mmol L^{-1}, when the spectrum was recorded over 8000 scans taking approximately 8 h (Figure 26).

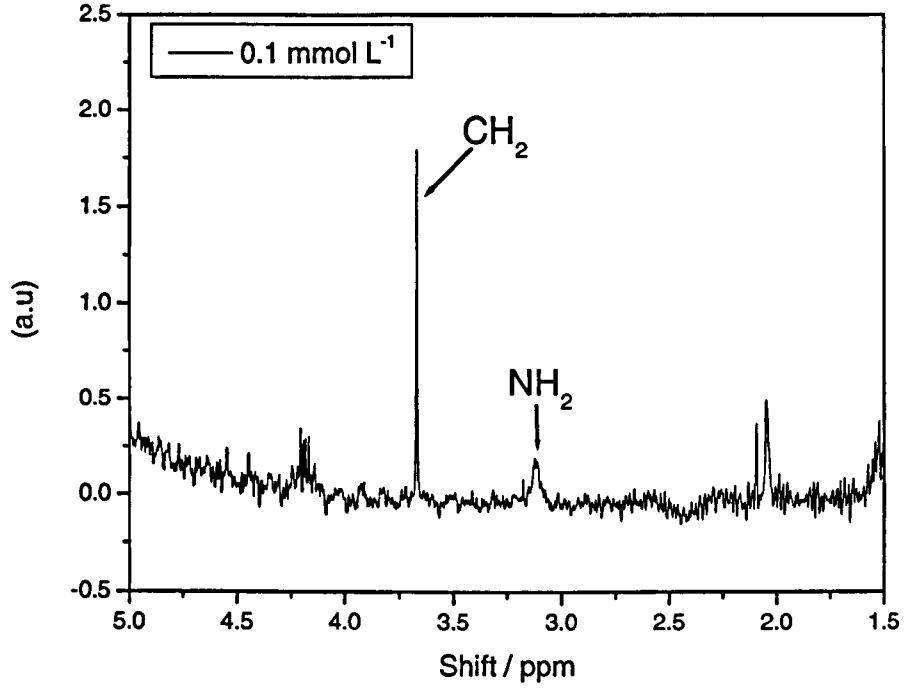

Figure 26 ^{1}H NMR spectrum of 0.1 mmolL^{-1} 4-BA solution, over 8000 scans.

2.4.7.4 Development of pre-saturation pulse program

The kinetic experiments required quantitative ^{1}H NMR with a detection limit of free amine of the order of 1 x 10^{-2} mmol L^{-1}. As an 8000 scan ^{1}H NMR experiment afforded a detection level of only 0.1 mmol L^{-1} (Figure 26), suppression of the chlorobenzene signal was required to achieve this ten-fold enhancement in detection limit within a reasonable time.

To selectively pre-saturate the chlorobenzene protons, a pulse program called lc1pnf2 was used, from the standard Bruker library supplied with the spectrometer. This program was optimised for use in this project. This program was originally developed for Liquid Chromatography - NMR samples, a combined technique where Liquid Chromatography separates a solution containing a mixture of species, and then the ^{1}H NMR spectrum of each fraction is obtained. These fractions of the solutions are very dilute, and contain large quantities of the LC elutents, water and acetonitrile. Pre-saturating these two different

solvent signals allowed the ^{1}H NMR spectra of these very dilute solutions to be obtained. The lc1pnf2 program was adapted and optimised during this project to saturate the two most intense chlorobenzene signals to enable measurement of very dilute amine solutions. The two signals to be pre-saturated are shown in Figure 27.

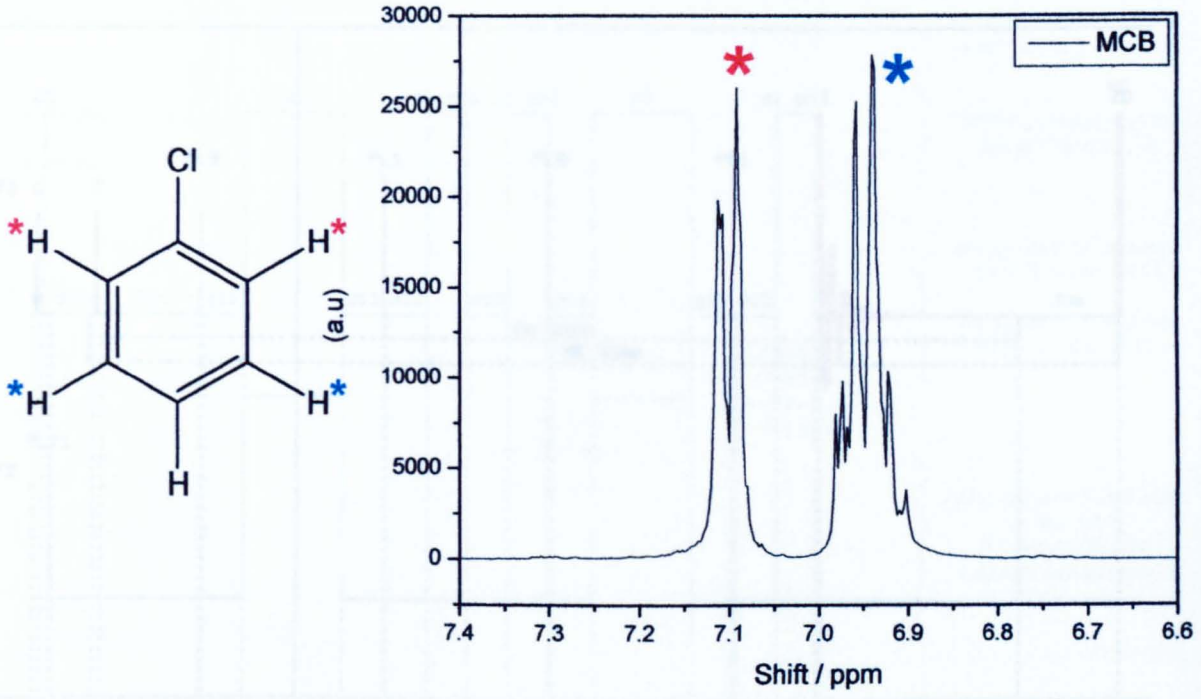

Figure 27 ^{1}H NMR spectrum of chlorobenzene.

*** - aromatic proton signals of chlorobenzene to be suppressed.**

2.4.7.4.1 Pre-saturation protocol-adaptation of Bruker LCMS pulse program

In the case of chlorobenzene solutions, pre-saturation of two chlorobenzene aromatic protons signals allowed the improvement of the detection limit of free amine. The original program performed a 16 scan ^{1}H NMR spectrum of the solution prior to performing the presaturation program. This detected the resonance of the two signals to be pre-saturated, and automatically set Channels F1 and F2 to these resonances. In the case of chlorobenzene solutions, these two channels (F1 and F2) were set with offset frequencies (O1 and O2) of 7.092 and 6.939 ppm. Through a series of NMR experiments on a low concentrated 4-BA solution, the power levels of the two channels were optimised to give the best pre-saturation of the chlorobenzene signals (60 d.b.). The length of the pulse (d1) was also optimised; changing it from the default 2.4 to 3 s, which ensured the solute protons were fully suppressed (flipped to 180 ° from the equilibrium postion, -z axis shown in Figure 11) before the read pulse was applied.

Before each sequence of pre-saturation NMR experiments, the spectrum of chlorobenzene was obtained to check the frequencies of the chlorobenzene signals.

The pre-saturation pulse sequence (lc1pnf2) shown in Figure 28 and listed in Table 12, was adapted changing the parameters listed in Table 13.

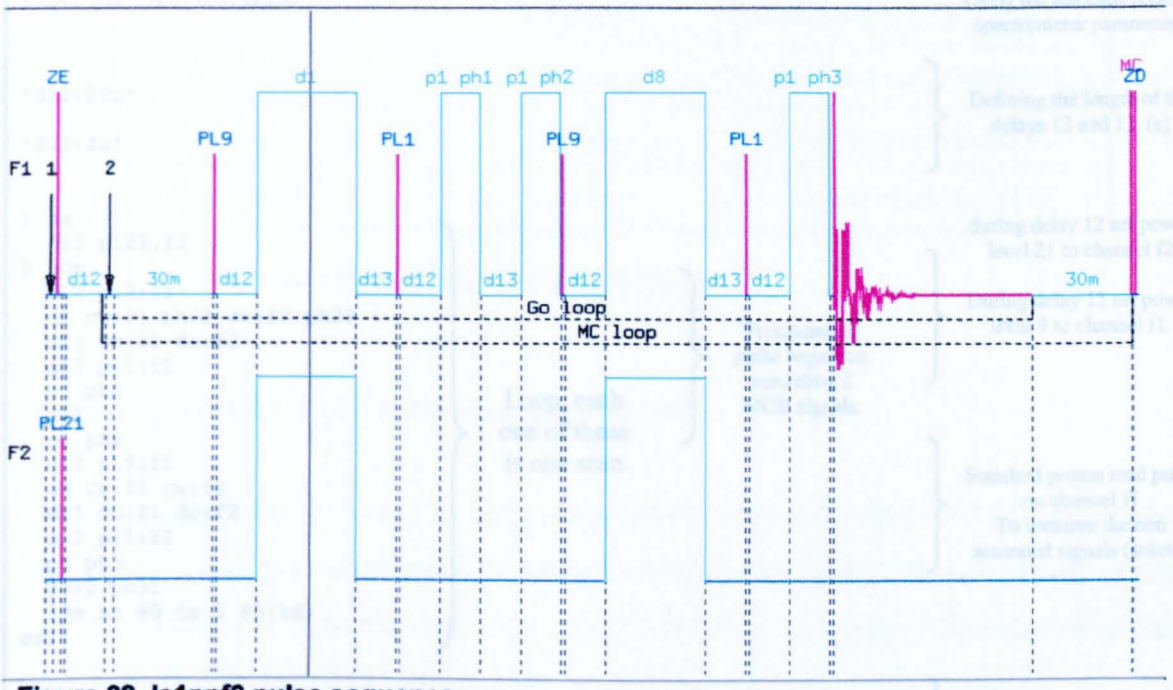

Figure 28 lc1pnf2 pulse sequence.

Showing presaturation pulses applied to channels F1 and F2 and the delay (d1).

Pre-saturation pulse program	Comment
;lc1pnf2 ;avance-version (02/05/31) ;1D version of noesyprtp using double presaturation during relaxation ; delay and mixing time ;presaturation using f1 and f2 - channel	lines starting with ; are comments, descriptions or literature references
prosol relations=<lcnmr>	
#include <Avance.incl>	Using the standard Avance spectrometer parameters
"d12=20u" "d13=4u"	Defining the length of the delays 12 and 13. (s)

1 ze
  d12 pl21:f2
2 30m
  d12 pl9:f1
  d1 cw:f1 ph29 cw:f2 ph29
  d13 do:f1 do:f2
  d12 pl1:f1
  p1 ph1
  d13
  p1 ph2
  d12 pl9:f1
  d8 cw:f1 cw:f2
  d13 do:f1 do:f2
  d12 pl1:f1
  p1 ph3
  go=2 ph31
  30m mc #0 to 2 F0(zd)
exit
 	
Loop, each one of these is one scan
 	
Presaturation pulse sequence, saturating 2 MCB signals.
	during delay 12 set power level 21 to channel f2
	
	During delay 12 set power level 9 to channel f1.
	
	Standard proton read pulse on channel f1
	To measure the non saturated signals (solute)

ph1=0 2 ph2=0 0 0 0 0 0 0 0 2 2 2 2 2 2 2 2 ph3=0 0 2 2 1 1 3 3 ph29=0 ph31=0 2 2 0 1 3 3 1 2 0 0 2 3 1 1 3	Defining the phase of the pulses, set to 90 ° intervals.
;pl1 : f1 channel - power level for pulse (default) ;pl9 : f1 channel - power level for presaturation ;pl21: f2 channel - power level for presaturation ;p1 : f1 channel - 90 degree high power pulse ;d1 : relaxation delay; 1-5 * T1 [ca. 1-2sec] ;d8 : mixing time [ca. 80 msec] ;d12: delay for power switching [20 usec] ;d13: short delay [4 usec] ;NS: 8 * n, total number of scans: NS * TD0 ;DS: 4	Explanations The power levels, pl9, pl21, are set the data acquisition folder, with the channel frequencies, f1 and f2. The delay d1 was also changed to 3 s.
;$Id: lc1pnf2,v 1.8 2002/06/12 09:05:01 ber Exp $	

Table 12 Presaturation pulse program lc1pnf2.

Showing the pulses on channels F1 and F2, the read pulse on channel F1 and the definition of the delays and pulses.

Parameter	Value	Comment
Pulse program	Lcpnf2	Bruker library
Experiment Parameters	LC1D12	Bruker library
No. of scans	1000	30 minutes
d1	3 s	Length of presaturation pulse
O1P	6.939 ppm	Offset frequency of Channel F1
O2P	7.092 ppm	Offset frequency of Channel F2
Pl 9	60 d.b.	Power level of channel F1
Pl 21	60 d.b.	Power level of channel F2

Table 13 Pre-saturation pulse sequence parameters.

^{1}H NMR protocol for pre-saturation experiments

The parameters listed in Table 13 were amended for each individual ^{1}H NMR experiment. This meant the experiments were performed manually; each sample was loaded, rotated, locked on C_6D_6 and shimmed manually. The following list explains the steps taken using the xwinnmr software (Bruker) to run the adapted pre-saturation pulse program.

- edc – edit current. Creates a new data set, change the name of the existing file, and the new NMR will be saved under the new file name.
- rpar LC1D12 – read parameters. (Reads the standard parameters set)
- getprosol – get probe and solvent. (Gets the probe and solvent parameters)
- eda – edit data acquisition. (Edit the fields required, pl9, pl21, d1, no. of scans, O1 and O2)
- rga – lets the spectrometer calculate the receiver gain.

Processing data after acquisition:

- ft – Fourier Transforms the FID
- apk – automatic phase correction.

- abs – baseline smoothing

Each ^{1}H NMR experiment took approximately ½ h, a substantial improvement on the 8 h experiments previously required.

The improvement in the ^{1}H NMR spectrum of a 3 mmol L^{-1} solution of 4-BA using the pre-saturation pulse sequence, compared with an ^{1}H NMR experiment without pre-saturation is shown in Figure 29. The chlorobenzene signal is not fully suppressed as some of the spins have precessed back during the delay between the presaturation pulse (P1 and P2) and the application of the 90 ° read pulse, and so is observed in Figure 29 (b).

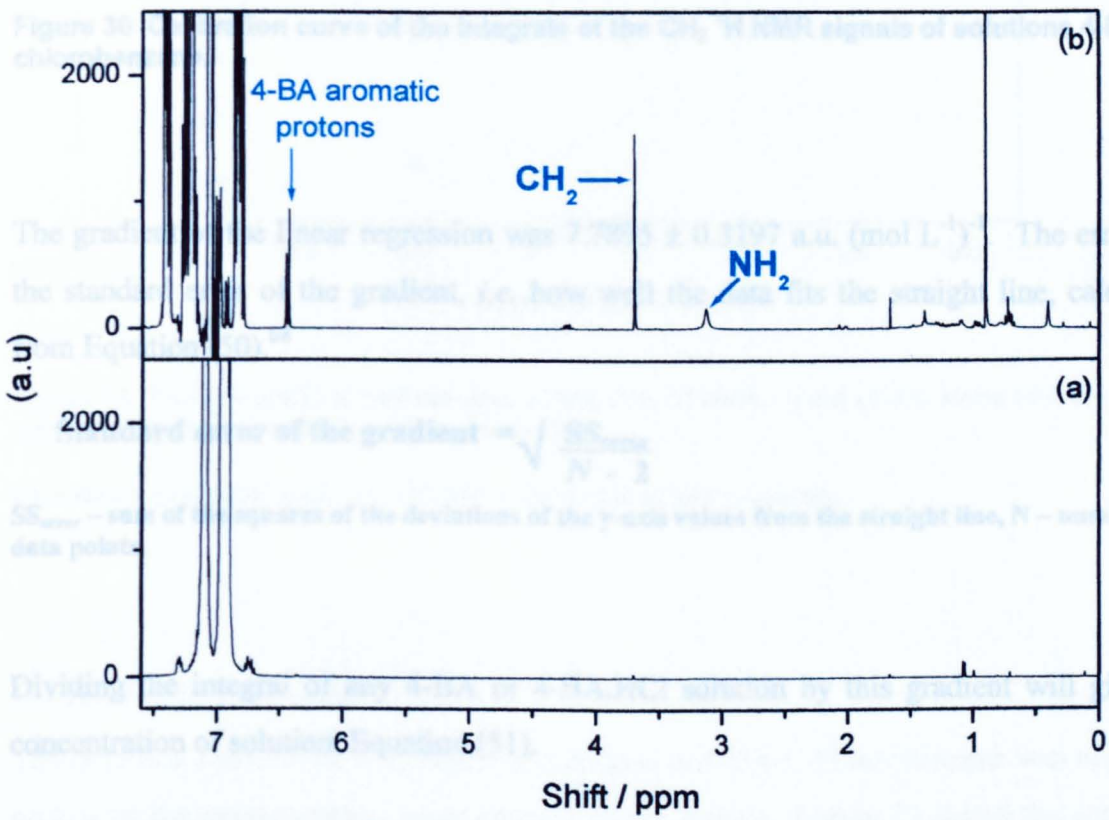

Figure 29 Comparison of a ^{1}H NMR spectrum of a solution of 4-BA in chlorobenzene (3 mmol L^{-1}) (a) without and (b) with the pre-saturation pulse sequence.

2.4.7.4.2 Calibration

Solutions of 4-BA in chlorobenzene were prepared between 0.05 and 3 mmol L^{-1}. The integral of the CH_2 signals showed a linear relationship with concentration (Figure 30).

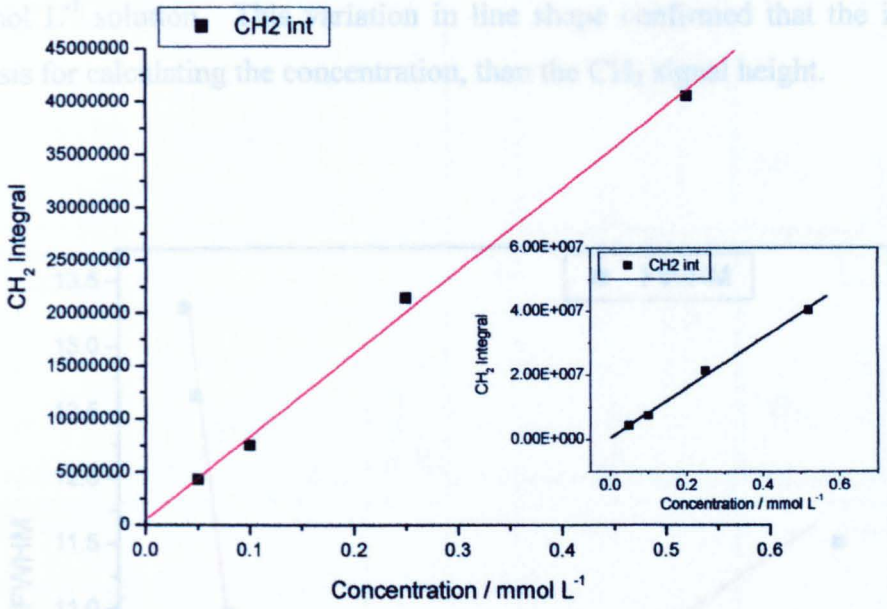

Figure 30 Calibration curve of the integrals of the CH_2 ^1H NMR signals of solutions 4-BA in chlorobenzene.

The gradient of the linear regression was 7.7895 ± 0.3197 a.u. (mol L^{-1})$^{-1}$. The error was the standard error of the gradient, *i.e.* how well the data fits the straight line, calculated from Equation (50).[68]

$$\text{Standard error of the gradient} = \sqrt{\frac{SS_{error}}{N - 2}} \quad (50)$$

SS_{error} – sum of the squares of the deviations of the y-axis values from the straight line, N – number of data points.

Dividing the integral of any 4-BA or 4-BA.HCl solution by this gradient will give the concentration of solution, Equation (51).

$$\text{Concentration} = \int CH_2 / 7.7895 \quad (51)$$

Periodic checks of this concentration factor were performed by obtaining the ^1H NMR spectrum of a 3 mmol L^{-1} standard solution of 4-BA in chlorobenzene.

The line shape of the CH_2 signal varied with concentration (Figure 31). At low concentrations (0.05 mmol L^{-1}) it was at its widest, and it narrowed at higher concentrations (0.5 mmol L^{-1}). However, this relationship was not consistent, as the full width at half height of the CH_2 signal of a 3 mmol L^{-1} solution was comparable to that of a

0.25 mmol L^{-1} solution. This variation in line shape confirmed that the integral was a better basis for calculating the concentration, than the CH_2 signal height.

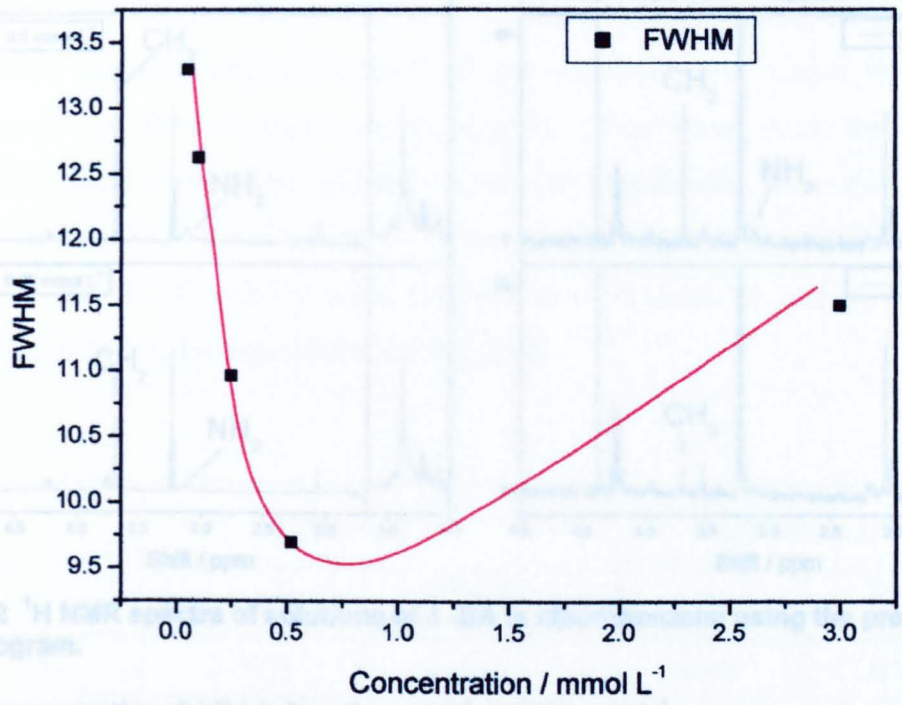

Figure 31 The full width at half maxima of the CH_2 ^1H NMR signal of solutions of 4-BA in chlorobenzene as a function of concentration.

Line shown as a guide to the eye, FWHM – Full width at half maximum

2.4.7.4.3 Detection limit

The detection limit of the NH_2 signal in solutions of 4-BA in chlorobenzene was improved greatly by the pre-saturation of the chlorobenzene signals. Figure 32 shows the spectra of all the 4-BA solutions used for the calibration of the presaturation pulse sequence. Spectrum (a) in Figure 33 shows the minimum concentration of 4-BA solutions in chlorobenzene (0.05 mmol L^{-1}), by observation of the NH_2 and CH_2 signals. Spectrum (b) in Figure 33 establishes that it was not possible to observe either signal in a solution of 4-BA in chlorobenzene of 0.01 mmol L^{-1}. Therefore the improved detection limit was greater than 0.01 mmol L^{-1}.

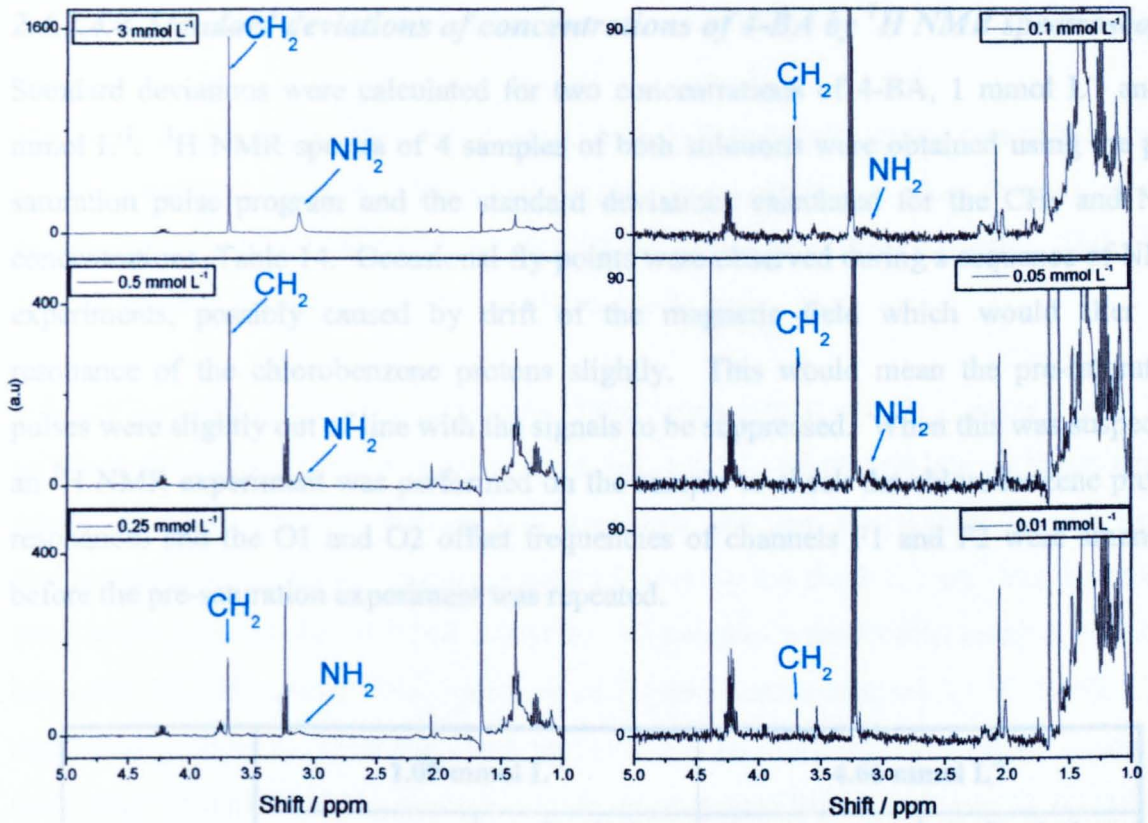

Figure 32 ^{1}H NMR spectra of solutions of 4 -BA in chlorobenzene using the presaturation pulse program.

Range in concentration of 4-BA is from 3 mmol L^{-1} to 0.01 mmol L^{-1}.

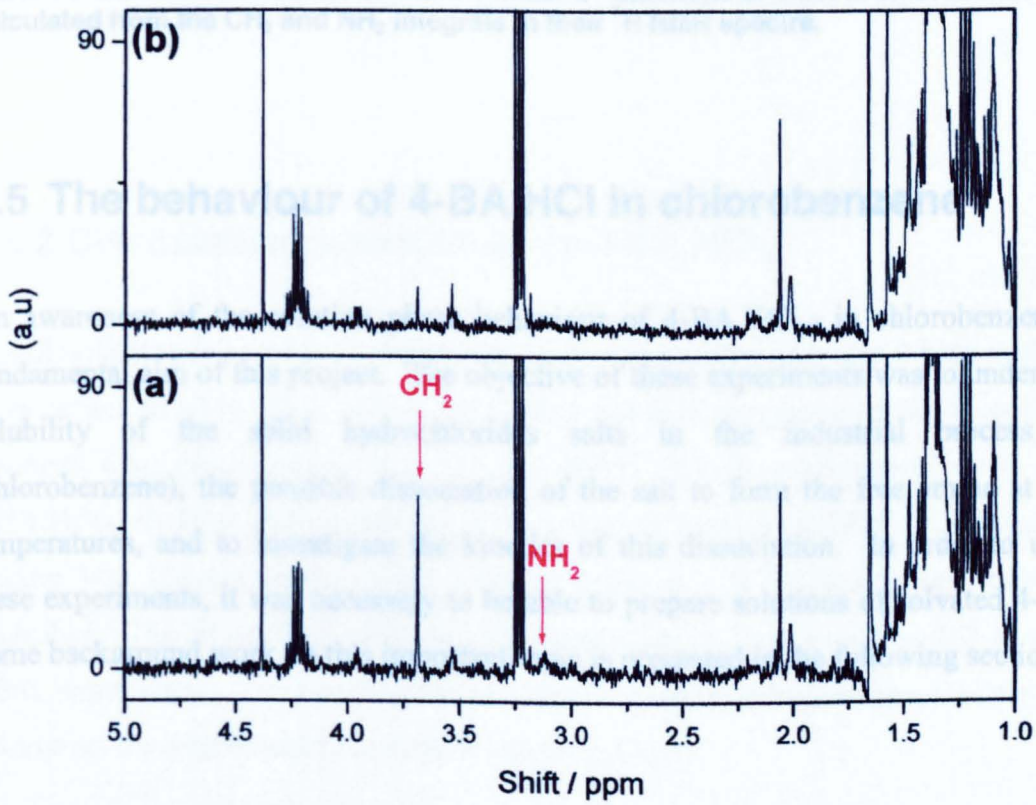

Figure 33 ^{1}H NMR spectra of two solutions of 4-BA in chlorobenzene (a) 0.05 mmol L^{-1} and (b) 0.01 mmol L^{-1}.

Showing the detection limit of the NH_2 ^{1}H NMR signal of < 0.05 mmol L^{-1}.

2.4.7.4.4 Standard deviations of concentrations of 4-BA by ^{1}H NMR spectroscopy

Standard deviations were calculated for two concentrations of 4-BA, 1 mmol L^{-1} and 4 mmol L^{-1}. ^{1}H NMR spectra of 4 samples of both solutions were obtained using the pre-saturation pulse program and the standard deviations calculated for the CH_2 and NH_2 concentrations, Table 14. Occasional fly-points were observed during a sequence of NMR experiments, possibly caused by drift of the magnetic field which would alter the resonance of the chlorobenzene protons slightly. This would mean the pre-saturation pulses were slightly out of line with the signals to be suppressed. When this was suspected an ^{1}H NMR experiment was performed on the sample to check the chlorobenzene proton resonances and the O1 and O2 offset frequencies of channels F1 and F2 were amended before the pre-saturation experiment was repeated.

	1.07 mmol L^{-1}		4.66 mmol L^{-1}	
	Mean (mmol L^{-1})	Standard Deviation	Mean (mmol L^{-1})	Standard Deviation
CH_2	0.7936	0.02184	3.55418	0.22975
NH_2	1.02797	0.01004	3.71228	0.28217

Table 14 Standard deviations of 1 and 4 mmol L^{-1} solutions of 4-BA in chlorobenze calculated from the CH_2 and NH_2 integrals in their ^{1}H NMR spectra.

2.5 The behaviour of 4-BA.HCl in chlorobenzene

An awareness of the solution phase behaviour of 4-BA.$HCl_{(s)}$ in chlorobenzene was a fundamental aim of this project. The objective of these experiments was to understand the solubility of the solid hydrochlorides salts in the industrial process solvent (chlorobenzene), the possible dissociation of the salt to form the free amine at different temperatures, and to investigate the kinetics of this dissociation. In order to undertake these experiments, it was necessary to be able to prepare solutions of solvated 4-BA.HCl. Some background work on this important topic is presented in the following sections.

2.5.1 Solubility determinations

The initial investigation of the solubility of 4-BA.HCl in chlorobenzene was carried out in a 6-place Radley's carousel. This system had six identical 25 cm^3 baffled flasks heated by an aluminium hotplate controlled by an ETS-D4 Fuzzy logic thermocouple. Each flask was subjected to identical heating and stirring conditions.

4-BA.$HCl_{(s)}$ (0.02 g) and chlorobenzene (15 cm^3) were placed in each of the 6 flasks. The solutions were stirred using a crossbar stirrer bar, with the stirrer hotplate set to position 9, where the most vigorous stirring was achieved, and the temperature on the Fuzzy thermocouple set to 303 K. Samples were taken every day for 5 d, 1 cm^3 was required to have ample solution for ^1H NMR analysis. All samples were filtered using a Whatman inorganic Anotop syringe filter (porosity of 0.2μm) before analysis by ^1H NMR. The concentration from six solutions which had been treated to essentially identical conditions were then obtained and the average concentration determined by integration of the CH_2 signal in the ^1H NMR spectra, as described in Section 2.4.7.4.2.

This reaction was repeated at room temperature, 293 K, 323 and 333 K. The room temperature experiment was monitored for 5 d and the 323 and 333 K experiments for 6 and 3 h respectively.

2.5.2 Dissociation experiments on 4-BA.$HCl_{(s)}$

The dissociation experiments of 4-BA.$HCl_{(s)}$ were performed in a round bottom flask, with a condenser attached *via* a ground glass joint and silicone grease (ACC Silicones). The reactions were carried out at 323, 347 and 403 K. Distilled chlorobenzene (5 cm^3) and 4-BA.$HCl_{(s)}$ (0.03 g) were heated using a silicone oil bath and an IKA RCT basic hotplate (Figure 34). The temperature was controlled using an ETS-D4 Fuzzy logic thermocouple controller. The Fuzzy logic thermocouple controller was set to 408 – 413 K to for the reflux experiment. The range in temperature is quoted as the temperature was adjusted throughout the experiment to maintain reflux conditions.

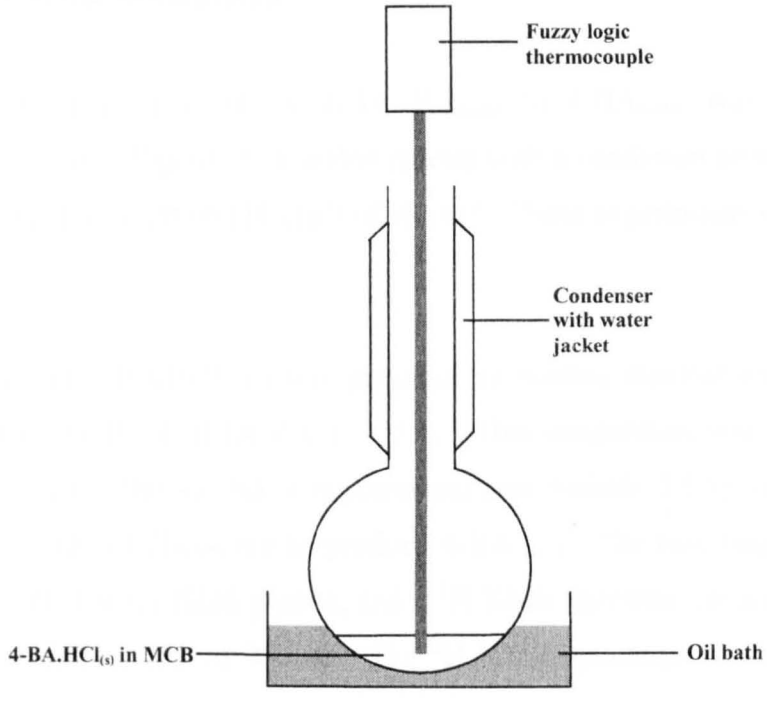

Figure 34 Apparatus for the experiments on the dissociation of 4-BA.HCl$_{(s)}$ in chlorobenzene.

One sample was taken from each reaction at the times shown in Table 15, and filtered through a cotton-wool-filled pipette. The samples were analysed using ^{1}H NMR and the concentrations of 4-BA$_{(solv)}$ and 4-BA.HCl$_{(solv)}$ were determined by integration of the CH_2 and NH_2 proton resonances. These experiments were performed prior to optimisation of the pre-saturation pulse program (see Section 2.4.7.4) and so the detection limit of free amine, 4-BA$_{(solv)}$ was 0.1 mmol L^{-1}. The sample taken from the reflux experiment was filtered and then cooled for 30 min before analysis by ^{1}H NMR.

Temperature (K)	Mass of 4-BA.HCl$_{(s)}$ (g)	Duration (h)
323	0.03	4
347	0.03	4
403 (Reflux)	0.03	¼

Table 15 Experimental conditions for the experiments on the dissociation of 4-BA.HCl$_{(s)}$ in chlorobenzene.

2.5.3 Filtered solutions

The solution phase reaction of 4-BA.HCl$_{(solv)}$ to 4-BA$_{(solv)}$ was performed using the apparatus shown in Figure 35, a sealed reactor with a condenser attached and a head space above the reaction solution (10 cm^3) of 98 cm^3. These experiments were performed at 333 and 353 K.

The solution of 4-BA.HCl$_{(solv)}$ was prepared by heating distilled chlorobenzene (10 cm^3) with 4-BA.HCl$_{(s)}$ (0.04 g) for 4 h at 323 K. This temperature was chosen as it had been established during the solubility experiments (see Section 2.5.1) that at this temperature 4-BA.HCl$_{(s)}$ did not dissociate to produce 4-BA$_{(solv)}$. The resulting solution was filtered through a cotton wool filled pipette, and a ^{1}H NMR spectrum obtained, before reacting at higher temperature, 333 or 353 K. The ^{1}H NMR spectrum was used to check that no 4-BA$_{(solv)}$ was present.

The filtered solutions were heated to either 333 K or 353 K in the apparatus shown in Figure 34. Samples were taken periodically over 24 h for the 333 K experiment and 6 h for the 353 K experiment.

After discussion with the industrial sponsors of this project, a repeat of the 353 K experiment was performed using Whatman Inorganic Anotop syringe filters with a porosity of 0.2 μm to filter the pretreated solution. These results showed markedly different results, (see Chapter 6, Section 6.1.2).

2.5.4 Dissociation of MDA.2HCl experiment at reflux

The dissociation of MDA.2HCl was investigated on one occasion only, to determine the possibility of the investigation of the solution phase kinetics of this material. The majority of the solution investigations concentrated on 4-BA.HCl as this was partially solutble in the process solvent. In our hands MDA.2HCl was insoluble in chlorobenzene.

Distilled chlorobenzene (5 cm^3) with MDA.2HCl (0.083g) were refluxed for 15 min using the same apparatus as the dissociation experiments on 4-BA.HCl (Figure 34). The thermocouple was set to 405 K. The MDA.2HCl was first analysed by elemental analysis to determine that it was the completely hydrochlorinated material, containing no MDA

impurity. The solution was cooled and a sample filtered before analysis by ^{1}H NMR spectroscopy.

The results obtained from this experiment (see Chapter 3) although interesting, indicated that it would be a difficult and lengthy process to derive a complete reaction scheme and associated kinetic data for this essentially insoluble system (MDA.2HCl in chlorobenzene).

2.5.5 Dissociation of 4-BA.HCl$_{(solv)}$ kinetic experiments

The kinetic experiments described in Chapter 6, Section 6.2) represent the investigation of the dissociation of 4-BA.HCl$_{(s)}$ at 373 K under closed and open conditions. Closed conditions were obtained by performing the reaction in a sealed vessel, where the partitioning of HCl$_{(solv)}$ to the gas phase was limited. Open conditions were obtained by performing the reaction in the same apparatus as the closed experiments, except using unsealed vessels, so the partitioning of HCl$_{(solv)}$ to the gas phase was not limited.

For ease of reaction set up, anhydrous chlorobenzene was purchased from Aldrich (purity 99.8 %, < 0.005 % water). This greatly increased the time available for kinetic experiments performed in the last few months of the project, as the time taken for the purification protocol of chlorobenzene was 1-1.5 days (see Section 2.1). A comparison of the ^{1}H NMR spectra of distilled and Aldrich chlorobenzene is shown in Chapter 3 Figure 37. The impurities observed in this Aldrich chlorobenzene were did not interfere with the measurement of the CH_2 and NH_2 ^{1}H NMR signal intensities used to measure the concentrations of species observed in the kinetic experiments.

An experimental set up was required where the dissociation of 4-BA.HCl$_{(s)}$ in chlorobenzene could be observed over a period of approximately 24 h. The reactor also needed to have a small head space above the solution, so that the two reaction conditions could be distinguished. A large head space above a solution would have approximated to an open system. The experiments required sampling the reaction mixture at least 12 times during reaction, taking 1 cm^3 of solution for each sample. Different reactor configurations were tested, a simple round bottomed flask and condenser arrangement (Figure 34) fitted with a rubber septum at the top for the closed experiments was not a viable option. The head space above the solution in this arrangement would have been large, and so the loss of HCl$_{(solv)}$ to the gas phase would not have been limited. The apparatus shown in Figure

35 was commissioned from the glassblower incorporating a condenser, ensuring no leakage of gas from joints. The vessel had a small head space of 98 cm^3.

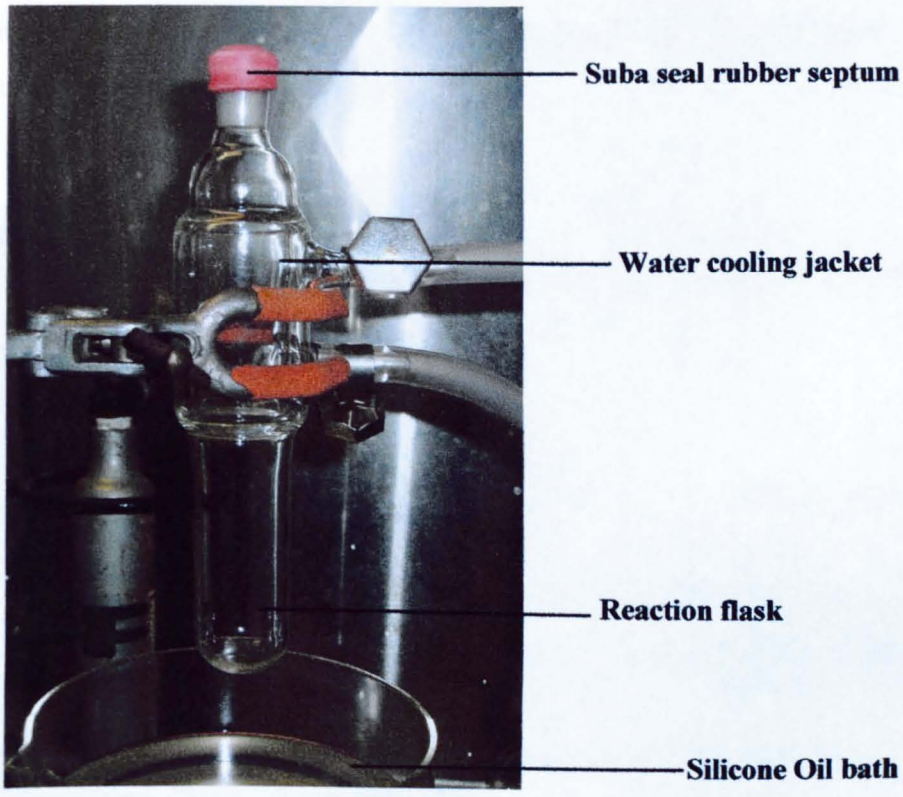

Figure 35 Apparatus built at Glasgow used for the kinetic experiments.

Single pot experiments were deemed undesirable, as a systematic increase in concentration of products would have been observed if the volume of reaction solution was small compared with the size required to be taken for each sample. It would therefore have been necessary for the reaction volume to be approximately 100 cm^3 to allow the sampled volume of 12 cm^3 to be taken. This would have required a much larger reactor, and a much larger head space to allow for the resulting vapour pressure of the 100 cm^3 of chlorobenzene and the $HCl_{(g)}$ produced during reaction, without over-pressurisation of the glass reactor.

The Radleys carousel 6 reaction station (Radleys Discovery Technologies) was a preferred option, having a smaller head-space above solution of 75 cm^3 and improved stirring ability. The carousel housed 6 reaction vessels, treating each under the same mixing and temperature conditions. Each flask had baffles and contained a cross-shaped stirrer bar, which gave superior mixing than the configuration shown in Figure 35. The

polytetrafluoroethylene (PTFE) caps with nitrile o-rings and full glass interior of the reaction vessels ensured no degradation of the vessel occurred from the presence of $HCl_{(g)}$. The PTFE caps and grease-free Rodaviss ground glass joints which connected the reaction pot and condenser tubes resulted in gas tight seals. Both the closed and open kinetic experiments were performed using the Radley's carousel and each vessel sampled only twice during reaction. The condenser arrangement, allowed cooling of all 6 vessels at the same height above reaction solution.

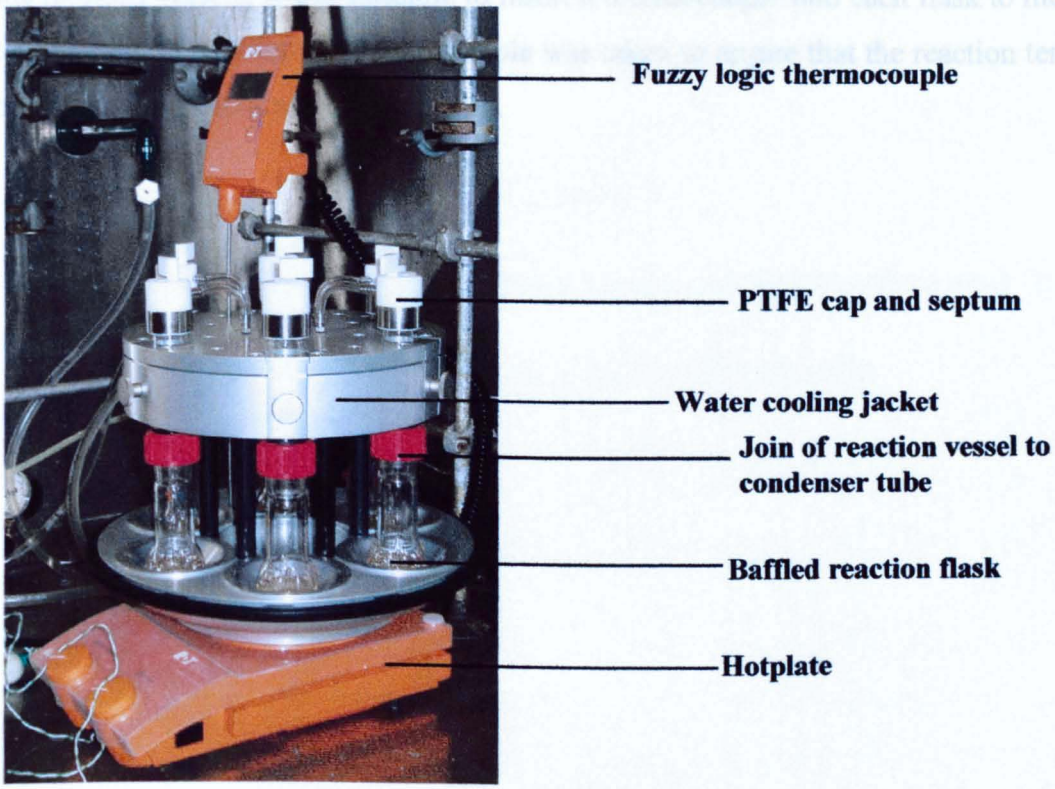

Figure 36 Radley's carousel 6 reaction station.

2.5.5.1 Closed experiments

Chlorobenzene (15 cm^3) with 4-BA.HCl (approximately 0.03 g), in each of the six carousel flasks, was heated to 373 K for 25 h. The flasks were sealed reaction vessels, and samples taken with a long stainless steel needle through a PTFE septum. All samples were filtered using a Whatman inorganic Anotop syringe filter before analysis by ^1H NMR. These ^1H NMR experiments were performed using the pre-saturation pulse program having a detection limit of 4-BA of 0.01 mmol L^{-1}.

2.5.5.2 Open experiments

The open experiments were performed using exactly the same reactor configuration as the closed experiments, except no septa were fitted to the reaction vessels. There was no hindrance for the partitioning of $HCl_{(solv)}$ to the gas phase. Chlorobenzene (15 cm^3) with 4-BA.HCl (0.02 g) in each of the six carousel flasks was heated to 373 K for 24 h. Twelve samples were taken periodically throughout the reaction and filtered using Whatman inorganic Anotop syringe filters before analysis by ^1H NMR. As no stoppers were fitted to the reaction vessels, it was possible to insert a thermocouple into each flask to measure the temperature of solution after each sample was taken to ensure that the reaction temperature of 373 K was maintained over the 24 h.

Chapter 3

Dissolution of HCl in monochlorbenzene characterisation and thermal stability of amine hydrochloride salts

3 Dissolution of HCl in chlorobenzene, characterisation and thermal stability of amine hydrochloride salts.

This chapter describes and discusses the purification of chlorobenzene, the dissolution of HCl, the amines (methylene dianiline and 4-benzylaniline) and the hydrochloride salts (4-benzyl aniline hydrochloride and methylenedianiline dihydrochloride) in chlorobenzene. The investigation of the physical properties of the hydrochloride salts, their melting points and thermal stability are also discussed.

3.1 Distillation of monochlorobenzene (chlorobenzene)

Chlorobenzene is the solvent used in the industrial synthesis of methylene diisocyanate. Consequently, the solution phase kinetic investigations in this project were performed in chlorobenzene, and so the purification of chlorobenzene and the subsequent dissolution of HCl, the amines and the amine hydrochlorides were investigated. It would have been easier to conduct solution based experiments in an alternative solvent; one which would solubilise MDA.2HCl *e.g.* methanol. However, the crucial solvent-solute interactions would have little relevance to the industrial process. Throughout all this work, and despite the low solubility of amine hydrochlorides, chlorobenzene was selected for the majority of the solution investigations.

The distillation of chlorobenzene over CaH_2 and storing over activated 4 Å molecular sieves removed an unknown impurity. Comparison of the ^1H NMR spectrum of this solvent with anhydrous chlorobenzene purchased from Sigma-Aldrich (Figure 37) shows the loss of a ^1H NMR resonance at 1.2 ppm, the origins of this signal are unknown.

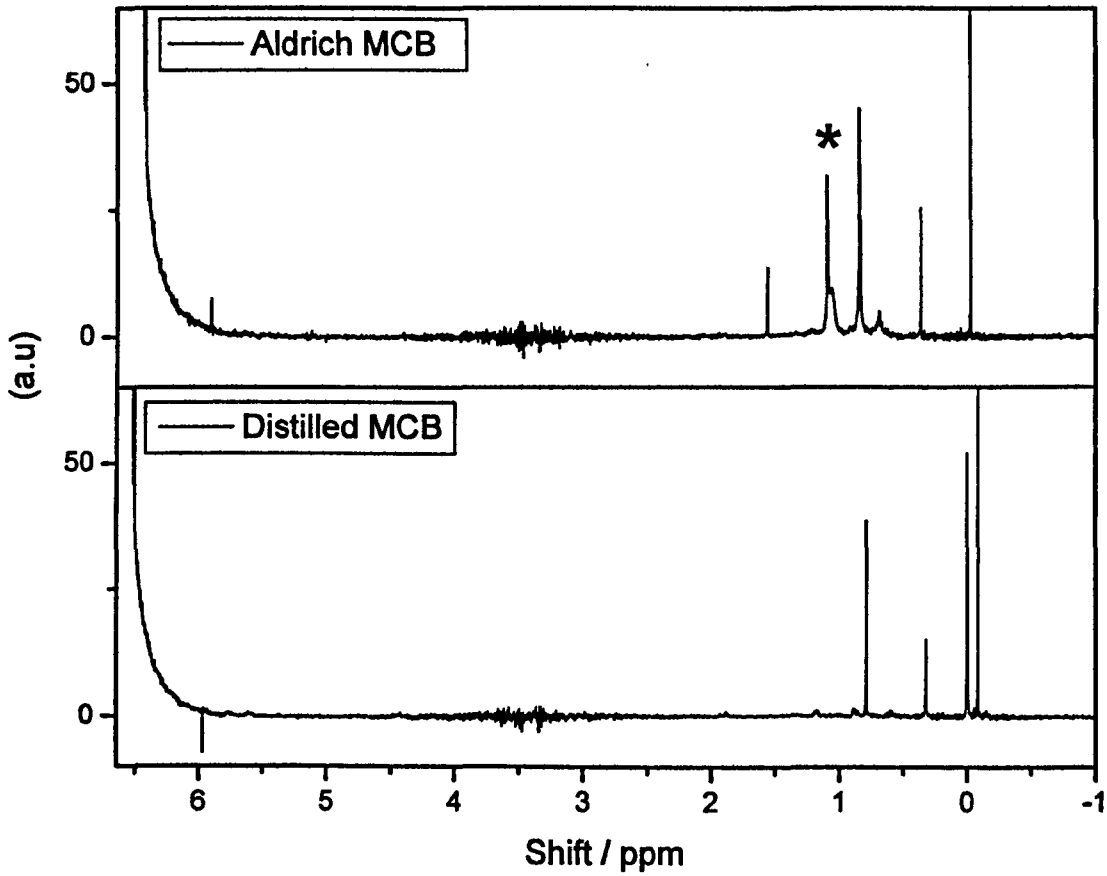

Figure 37 ^{1}H NMR spectra of distilled and Sigma-Aldrich anhydrous chlorobenzene.

*** - impurity in chlorobenzene**

3.1.1 Addition of water to MBC

Using purified chlorobenzene, small volumes of water were added in an attempt to find the resonance of the water protons when water molecules were dissolved in the solvent, as shown in Figure 38. This was important, to establish if there was a species present in the solvent which exchanged with the NH_2 and NH_3 protons of 4-benzylaniline (4-BA) and 4-benzylaniline hydrochloride (4-BA.HCl) respectively, when dissolved in chlorobenzene. It was believed that this exchange process was broadening the amine proton signals, as discussed in Chapter 2.

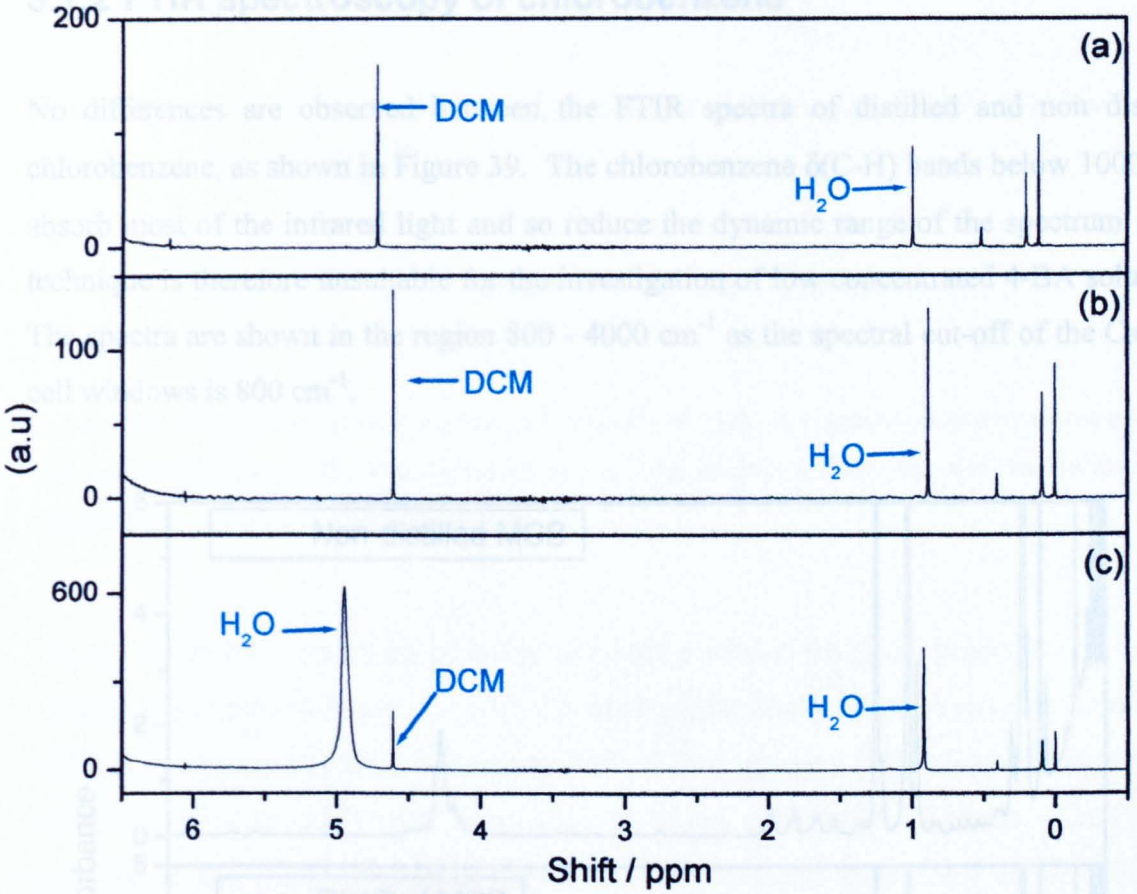

Figure 38 ^{1}H NMR spectra of (a) distilled chlorobenzene, (b) addition of 0.19 mol L^{-1} (c) addition of a further 0.36 mol L^{-1} of water to distilled chlorobenzene.

Dichloromethane (DCM, 0.02 molL^{1}) was used in 3 of the spectra as an internal reference for the concentrations of species present.

The signal at 0.9 ppm increases in intensity on addition of water to distilled chlorobenzene, Figure 38. By comparison with the internal reference (DCM, 0.02 mol L^{-1}) the concentration of this signal was calculated to increase from 0.017 mol L^{-1} in distilled chlorobenzene to 0.023 and 0.051 mol L^{-1} in spectra (b) and (c) respectively. Addition of 0.55 mol L^{-1} water (spectrum (c)) results in a turbid solution where individual bubbles of water are observed; the ^{1}H NMR spectrum of this solution shows peak shapes representative of a badly mixed system, as signified by the broad resonance at 4.9 ppm. The saturation concentration of water in chlorobenzene is therefore 0.051 mol L^{-1}.

The concentration of water in distilled chlorobenzene is 0.017 mol L^{-1}. This value is in agreement with the literature which states a concentration range of 0.15 – 0.02 mol L^{-1} between 288 and 298 K.[82]

3.1.2 FTIR spectroscopy of chlorobenzene

No differences are observed between the FTIR spectra of distilled and non distilled chlorobenzene, as shown in Figure 39. The chlorobenzene δ(C-H) bands below 1000 cm^{-1} absorb most of the infrared light and so reduce the dynamic range of the spectrum. This technique is therefore unsuitable for the investigation of low concentrated 4-BA solutions. The spectra are shown in the region 800 - 4000 cm^{-1} as the spectral cut-off of the CaF_2 IR cell windows is 800 cm^{-1}.

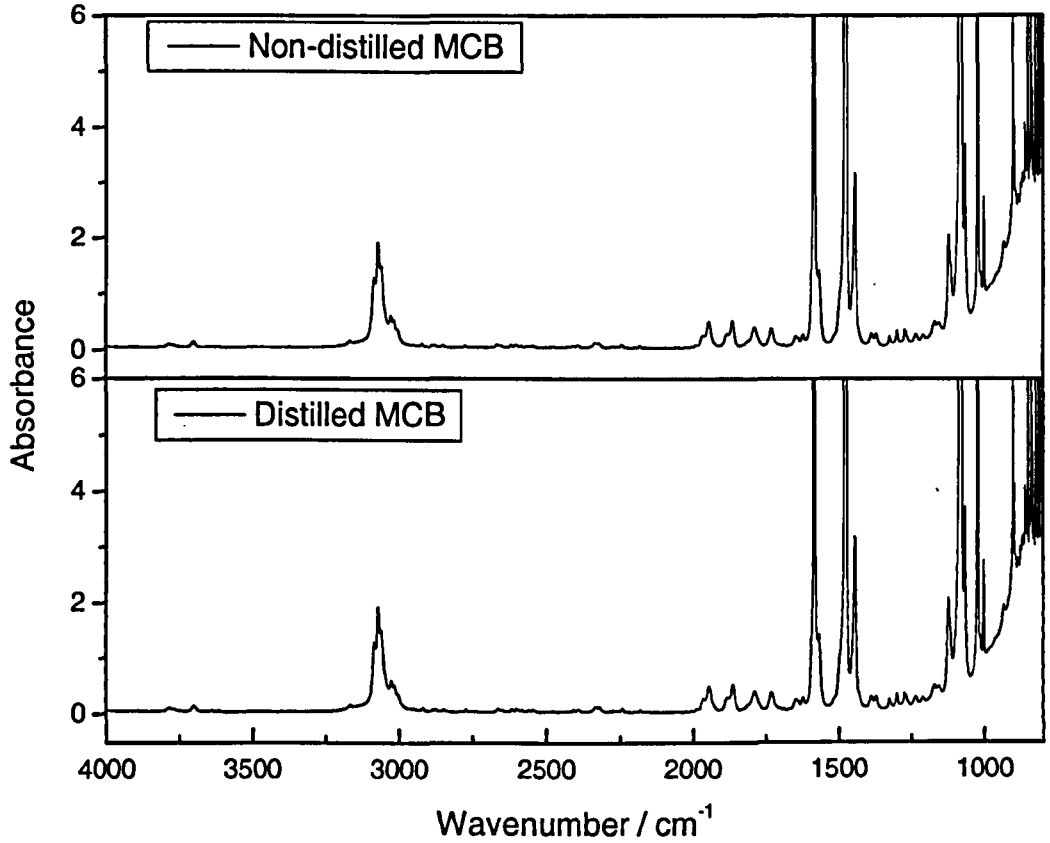

Figure 39 FTIR spectrum of distilled and non distilled chlorobenzene.

3.2 Dissolution of HCl in chlorobenzene

As the primary reagent in the reactions studied in this work, the behaviour of HCl in the industrial solvent was of great interest. FTIR spectroscopy was used as the primary method for the detection of $HCl_{(solv)}$.

3.2.1 Gas phase FTIR

The compound HCl is an anharmonic oscillator with a potential energy function as described by Equation (52).[20]

$$V = hcD_e[1-e^{-a(r-r_e)}]^2 \qquad \text{where} \qquad a = (\mu\omega^2/(2hcD_e))^{1/2} \tag{52}$$

V- potential energy, h – Plank's constant, c – velocity of light, D_e – minimum energy of the potential well, assumed here to be the dissociation energy, r_e – equilibrium distance between the two atoms, μ – reduced mass, ω - the vibrational frequency,

The gas phase FTIR spectrum of anhydrous HCl produced using the procedure outlined in Chapter 2 is shown in Figure 40, with the band profile centre point observed at 2886 cm^{-1}, which is in agreement with the literature. [83, 84] This frequency differs from the equilibrium wavenumber value of 2990 cm^{-1} since HCl is a strong anharmonic oscillator. The P and R branches of the rotational fine structure are observed and stem from the fact that the rotation of the molecule is accelerated or retarded as the molecule vibrates. The R branch, shown on the left of the spectrum, represents the rotational transitions of $J + 1 \leftarrow J$. The P branch, shown on the right, at lower wavenumbers, show the rotational transitions of lower energy, $J - 1 \leftarrow J$.[21]

The effects due to ^{35}Cl and ^{37}Cl isotopes are clearly observed with a ratio of 3:1, which agrees with their natural abundance of 75.53 and 24.47 % respectively.[54] The $H^{37}Cl$ band is displaced slightly towards lower wavenumbers, in agreement with the literature.[85] The absorbances of the rotational bands and their intensities, for the ^{35}Cl isotope are listed in Table 16.

R branch absorbances (cm^{-1})		Intensity (a.u)	P branch Absorbances (cm^{-1})		Intensity (a.u)
R(0)	2903.9	0.367	P(1)	2864.8	0.368
R(1)	2925.5	0.528	P(2)	2843.3	0.492
R(2)	2944.6	0.573	P(3)	2821.3	0.546
R(3)	2963.0	0.560	P(4)	2798.6	0.513
R(4)	2980.7	0.457	P(5)	2775.5	0.421
R(5)	2997.7	0.362	P(6)	2751.8	0.309
R(6)	3014.1	0.256			

Table 16 R and P branch assignments for $H^{35}Cl$FTIR gas phase spectrum.

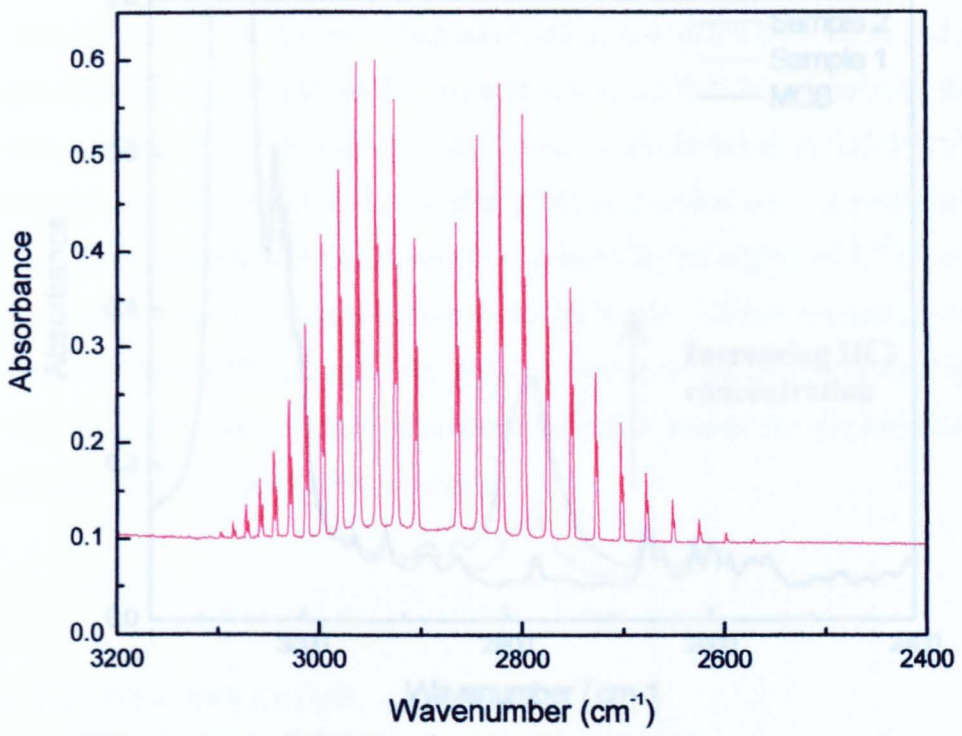

Figure 40 Gas phase FTIR spectrum of HCl.

3.2.2 Dissolution of HCl – using the vacuum line

Containing a known pressure of $HCl_{(g)}$, 300 Torr, in the manifold above a stirred volume of chlorobenzene, did not enable the dissolution of HCl, as indicated by the FTIR spectrum of the solution. The spectrum of this solution did not show any bands attributable to $HCl_{(solv)}$, merely the spectrum of chlorobenzene. This implied that the pressure of HCl above the chlorobenzene was not great enough to force the gas into solution. This experiment was repeated twice, using 600 Torr of $HCl_{(g)}$ above the solvent. These experiments also afforded the FTIR spectra of chlorobenzene. This was an unexpected result and indicated that chlorobenzene has a low affinity for HCl.

3.2.3 Dissolution of HCl – bubbling through chlorobenzene

Bubbling HCl through chlorobenzene, using the apparatus described in Chapter 2 did produce a band at 2780cm^{-1} in the FTIR spectrum. Further bubbling of HCl through the same solution increased the absorbance of this band, as shown in Figure 41.

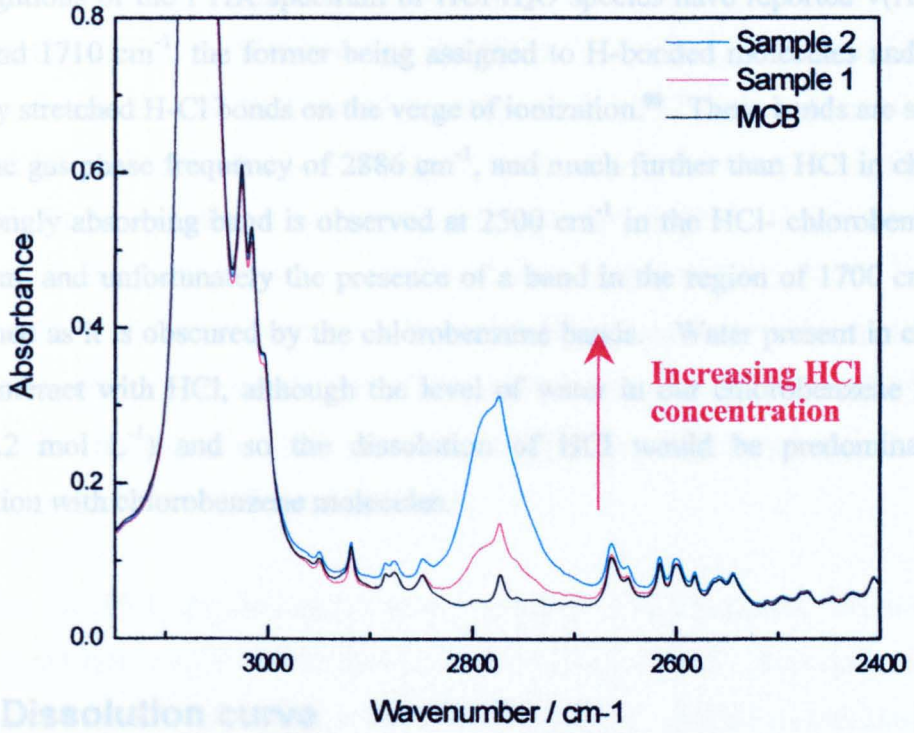

Figure 41 FTIR spectrum of HCl dissolved in chlorobenzene.

3.2.3.1 Shift in frequency of gas phase to liquid phase

The difference in observed vibrational frequency from the gas phase to HCl dissolved in chlorobenzene is substantial, 106 cm^{-1}, and is comparable to the shift from gas phase to liquid phase HCl of 100 cm^{-1}.[86] Leberknight and Ord also note a shift of similar magnitude of 103 cm^{-1} wavenumbers when HCl is dissolved in chlorobenzene, and similarly a shift of 133 cm^{-1} when HCl is dissolved in benzene.[87] This shift is reported to be the result of a decrease in the force constant of the H-Cl bond.[87] West reported that the HCl band shifts to smaller wavenumber on dissolution in varying solvents, with the trend of increasing shift with increasing dielectric constant of the solvent.[86] Williams shows similar trends with a 10 cm^{-1} shift for dissolution in benzene, a shift of only 40 cm^{-1} for dissolution in chlorobenzene, and 170 cm^{-1} for dissolution in nitrobenzene.[88] This effect was attributed to a combination of complex formation between HCl and the solvent molecules and an increase in the dipole moment of HCl.[88] The difference between the observed ν(H-Cl) wavenumber in this project and Williams value may be due to the differing levels of water in the chlorobenzene used; our system is believed to be anhydrous.

Investigations of the FTIR spectrum of HCl-H_2O species have reported ν(H-Cl) bands at 2500 and 1710 cm^{-1}, the former being assigned to H-bonded molecules and the latter, to strongly stretched H-Cl bonds on the verge of ionization.[89] These bands are shifted greatly from the gas phase frequency of 2886 cm^{-1}, and much further than HCl in chlorobenzene. No strongly absorbing band is observed at 2500 cm^{-1} in the HCl- chlorobenzene solution spectrum, and unfortunately the presence of a band in the region of 1700 cm^{-1} cannot be confirmed as it is obscured by the chlorobenzene bands. Water present in chlorobenzene could interact with HCl, although the level of water in our chlorobenzene is small (less than 0.2 mol L^{-1}) and so the dissolution of HCl would be predominantly through interaction with chlorobenzene molecules.

3.2.4 Dissolution curve

Successful saturation of chlorobenzene with HCl was achieved using the sparge apparatus. Repeated experiments show a dissolution of $HCl_{(g)}$ taking approximately 30 minutes to reach saturation, a rate of 3 mmol L^{-1} min^{-1}. This was determined by measuring the area under the band at 2780 cm^{-1} of samples taken at various times during the experiment (Figure 42).

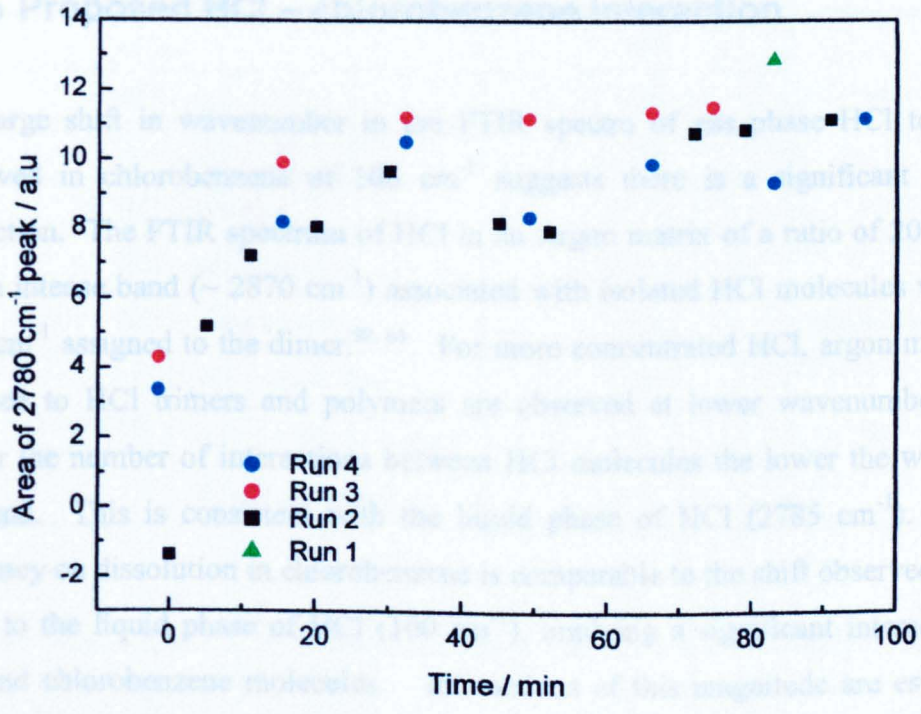

Figure 42 Change in area of 2780 cm^{-1} band as HCl dissolves in chlorobenzene.

Back titration of a sample of this saturated solution, against $NaOH_{(aq)}$ gave the concentration of HCl in chlorobenzene as 0.099 ± 0.038 mol L^{-1}. Fogg and Gerrard report the mole fraction for HCl in chlorobenzene to be 0.0319.[27] The difference in these two values is believed to be due to differing amounts of water present during the experiment. The mole fraction of HCl in water is much greater than in chlorobenzene, with a value of 0.259, which in 50 ml of water would give a concentration of 2.54 mol L^{-1}.[27] It is possible that the presence of small quantities of water in chlorobenzene would increase the capacity of HCl solvation in chlorobenzene. Given the procedures outlined in Chapter 2 Section 2.1, the chlorobenzene used in this work is thought to be anhydrous and probably has water levels lower than those in the earlier studies.

Solvation of HCl in monosubstituted benzenes, chlorobenzene, bromobenzene and iodobenzene has been found to deviate from Raoult's law;[90] the dissolution of HCl in substituted aromatic solvents is non-ideal. Dissolution of HCl in the halobenzenes has been reported as having increasing solubility in the order iodo-, bromo-, chloro-, fluoro-, benzene itself and toluene.[91] A stronger interaction between HCl and benzene, than HCl with chlorobenzene is consistent with HCl having a smaller shift in wavenumber from the gas phase when in chlorobenzene than when in benzene.

3.2.5 Proposed HCl – chlorobenzene interaction

The large shift in wavenumber in the FTIR spectra of gas phase HCl to that of HCl dissolved in chlorobenzene of 106 cm^{-1} suggests there is a significant solute-solvent interaction. The FTIR spectrum of HCl in an Argon matrix of a ratio of 2000:1 (Ar:HCl) has an intense band (~ 2870 cm^{-1}) associated with isolated HCl molecules with a band at 2818 cm^{-1} assigned to the dimer.[92, 93] For more concentrated HCl, argon matrices, bands assigned to HCl trimers and polymers are observed at lower wavenumbers.[92, 93] The greater the number of interactions between HCl molecules the lower the wavenumber of the band. This is consistent with the liquid phase of HCl (2785 cm^{-1}). The shift in frequency on dissolution in chlorobenzene is comparable to the shift observed from the gas phase to the liquid phase of HCl (100 cm^{-1}), implying a significant interaction between HCl and chlorobenzene molecules. Interactions of this magnitude are established, *e.g.* studies of mixtures of HCl with *trans*-2-butene; 2-methylpropene and *cis*-2-butene dissolved in liquefied argon were found to form 1:1 complexes with strongly absorbing IR bands at 2685, 2678 and 2679 cm^{-1} respectively, Table 17.[94] These complexes are reported

to be H-bonded dimers where the proton of HCl points directly towards the middle of the C=C double bond for *cis* and *trans*-2- butene and towards the $=CH_2$ region of 2-methylpropene.[94] A similar structure is also reported in the gas phase between HCl and ethyne and between HCl and cyclopropane, in the latter case the H-bond is directed towards the centre of one edge of the cyclopropane ring, with HCl lying along the C_2 axis.[95] Finally, and of most relevance here, the structure of a HCl-benzene complex has been studied using microwave spectroscopy and has C_{6v} symmetry where the H-Cl unit is coaxial with the C_6 rotational axis of the benzene ring and all the delocalised π electrons have an equal share in the H-bonding interaction.[96] We propose that in the case of chlorobenzene the structure is similar; the HCl pointing towards the ring, perpendicular to the C_2 rotational axis of chlorobenzene (Figure 43). This interaction would increase the effective mass of the HCl and so cause a decrease in the observed vibrational frequency from the gas phase molecule. The shift in vibrational frequency of a molecule (HX) on formation of a hydrogen bond with an acceptor (A), increases with increasing strength of the H-bond. For HCl the expected shift in frequency is ~ 700 cm^{-1} on formation of a strong H-bond, 300 - 700 cm^{-1} on formation of a moderate strength H-bond and < 300 cm^{-1} on formation of a weak H-bond.[44] This criteria classes the interaction of HCl with chlorobenzene as a weak H-bonding interaction.

Species		Wavenumber (cm^{-1})	Reference
$HCl_{(g)}$		2886	84
$HCl_{(liquid)}$		2785	
$HCl_{(solid)}$		2768	
HCl in benzene		2753	87
HCl in chlorobenzene		2783	
HCl in chlorobenzene		2780	this project
1:1 complex in Argon	HCl - *trans*-2-butene	2685	94
	HCl - 2-methylpropene	2678	
	HCl - *cis*-2-butene	2679	

Table 17 Wavenumber of ν(H-Cl) bands of pure HCl and HCl dissolved in different solvents.

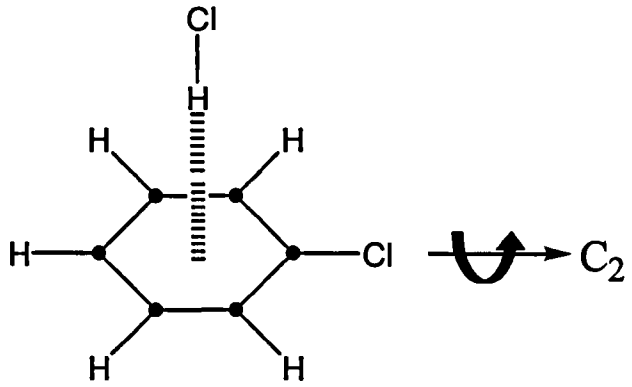

Figure 43 Proposed structure of HCl-chlorobenzene complex.

3.2.6 ^{1}H NMR of HCl in chlorobenzene

The ^{1}H NMR spectrum of a saturated solution of HCl in chlorobenzene has a signal at 0.45 ppm (Figure 44) which is assigned to $HCl_{(solv)}$. The ^{1}H NMR resonance of HCl has been reported to shift downfield on increasing pressure, from -0.33 ppm at 1 atm,[83] to 0.15 ppm at 5 - 20 atm to its liquid phase resonance at 3.2 ppm at 187 K.[97] The proton signal of HCl is also reported to shift downfield to 0.07 ppm on formation of a H-bond with $(CH_3)_2O$, when measured in the gas phase. [83]

Using dichloromethane (DCM, 0.1 mol L^{-1}), as an internal reference, the $HCl_{(solv)}$ concentration was calculated to be twice the HCl saturation concentration determined via titration. This discrepancy is thought to arise due to the exchange of $HCl_{(solv)}$ with residual water in the solvent. The water resonance observed at 0.9 ppm in the spectrum of distilled chlorobenzene is not observed in Figure 44. The water resonance may coincide with, and broaden, the HCl resonance. As a check that the signal observed at 0.45 ppm was due to $HCl_{(solv)}$, the solution was diluted by a half using distilled chlorobenzene (Figure 44). The signal decreased in intensity by less than a half, (18.9 %) therefore the signal was believed to be due to both $HCl_{(solv)}$ and water. The concentration of residual water in chlorobenzene was calculated as being 0.014 mol L^{-1}, which is comparable to the concentration of water calculated for distilled chlorobenzene (see Section 3.1.1). The concentration of HCl in chlorobenzene present in Figure 44 (b) was calculated to be 0.031 mol L^{-1}, comparable with the concentration determined via titration. This concentration of HCl in chlorobenzene can now be stipulated as 0.031 mol L^{-1} with a residual water content of

0.014 mol L^{-1}. At this stage, it is not known exactly how this small quantity of water interacts with the solvated HCl molecules. It is expected that higher concentrations of water would aid the dissolution of higher concentrations of HCl in chlorobenzene.

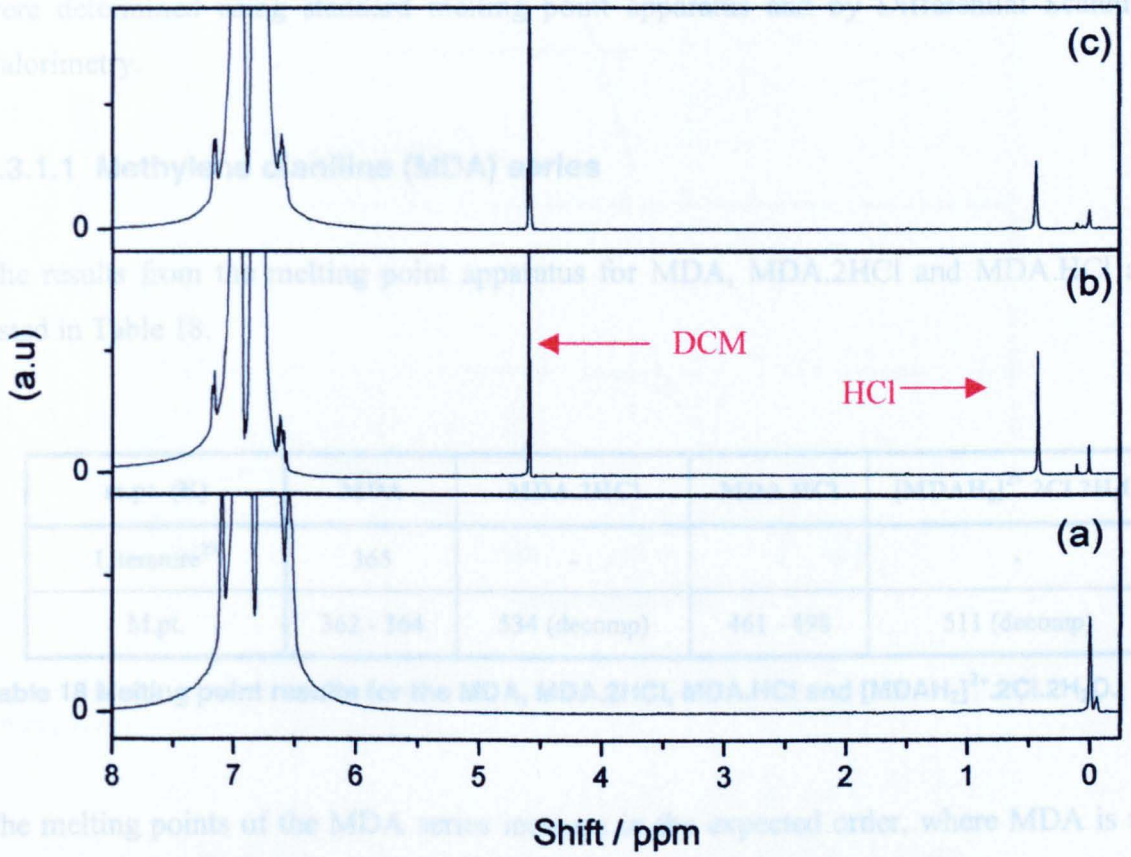

Figure 44 ^{1}H NMR spectra of (a) distilled chlorobenzene, (b) HCl dissolved in chlorobenzene and (c) the solution used for spectrum (b) diluted by a factor of a half, which was expected to reduce the intensity of the HCl signal (at 0.45 ppm) by a factor of a half.

3.3 Characterisation of amines and amine hydrochloride salts

A series of characterisation experiments were performed on the amines, 4-benzylaniline and methylene dianiline (4-BA and MDA) and the hydrochloride salts, 4-benzylaniline hydrochloride, methyelene dianiline dihydrochloride and methylene dianiline monohydrochloride (4-BA.HCl, MDA.2HCl and MDA.HCl). The amine hydrochloride salts were prepared by the direct reaction of $HCl_{(g)}$ with solid amine and *via* the solution phase reaction as described in Chapter 2, Section 2.3.2. These investigations include the determination of their melting points, differential scanning calorimetry measurements and FTIR spectroscopy. The solubility in chlorobenzene was also determined and their ^{1}H NMR spectra obtained when dissolved in dimethyl sulfoxide (DMSO).

3.3.1 Melting points and Differential Scanning Calorimetry (DSC) of amines and amine hydrochloride salts

The melting points or dissociation temperatures of the amines and their hydrochloride salts were determined using standard melting point apparatus and by Differential Scanning Calorimetry.

3.3.1.1 Methylene dianiline (MDA) series

The results from the melting point apparatus for MDA, MDA.2HCl and MDA.HCl are listed in Table 18.

m.pt. (K)	MDA	MDA.2HCl	MDA.HCl	$[MDAH_2]^{2+}.2Cl.2H_2O$
Literature[29]	365	-	-	-
M.pt.	362 - 364	534 (decomp)	461 - 498	511 (decomp)

Table 18 Melting point results for the MDA, MDA.2HCl, MDA.HCl and $[MDAH_2]^{2+}.2Cl.2H_2O$.

The melting points of the MDA series increase in the expected order, where MDA is the least tightly bound solid, followed by MDA.HCl and then MDA.2HCl. Interestingly, the recrystallised MDA.HCl, which will be discussed in Chapter 4, is more stable thermally than polycrystalline MDA.HCl and only slightly less stable thermally than MDA.2HCl. The melting points for MDA and MDA.2HCl determined by DSC (Figure 45) were 361 and 534 K respectively. For MDA, the melting point is obtained from the DSC trace from the point where the two red lines cross; the tangent to the melting endotherm crosses the horizontal. The different shape of the DSC trace of MDA.2HCl signifies a crystallisation after melting, which is consistent with a compound which can convert to a structure which is more stable thermally, after it has melted.[52] In the case of MDA.2HCl it is suggested that after melting, the structure rearranges to a more stable form, possibly through partial dissociation of HCl, forming MDA.HCl. These temperatures are far above the reaction temperature encountered in the industrial process and so this transformation of MDA.2HCl is believed to have little relevance to the industrial process under investigation in this work.

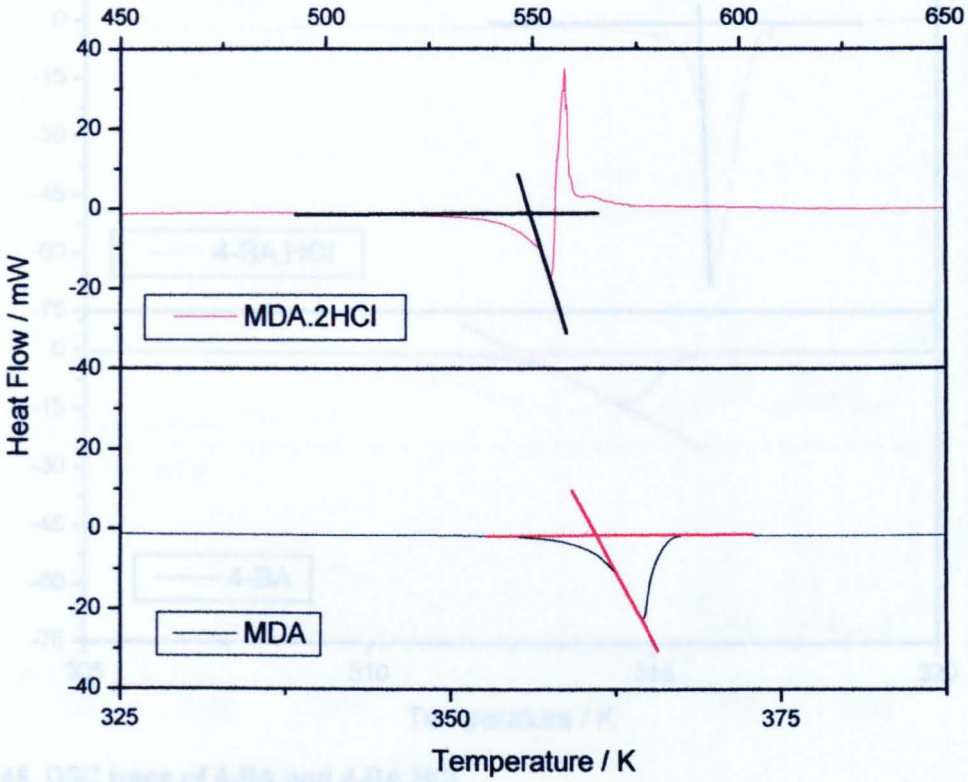

Figure 45 DSC trace of MDA and MDA.2HCl showing melting points at 361 and 534 K respectively.

3.3.1.2 4-Benzylaniline (4-BA) series

The melting points of 4-BA and 4-BA.HCl determined by DSC (Figure 46) and the standard melting point apparatus are listed in Table 19.

m.pt. (K)		Comment
4-BA	4-BA.HCl	
308 – 311	-	Literature [29]
313	453	M.pt.
313	498	DSC

Table 19 Melting points and DSC results for 4-BA and 4-BA.HCl.

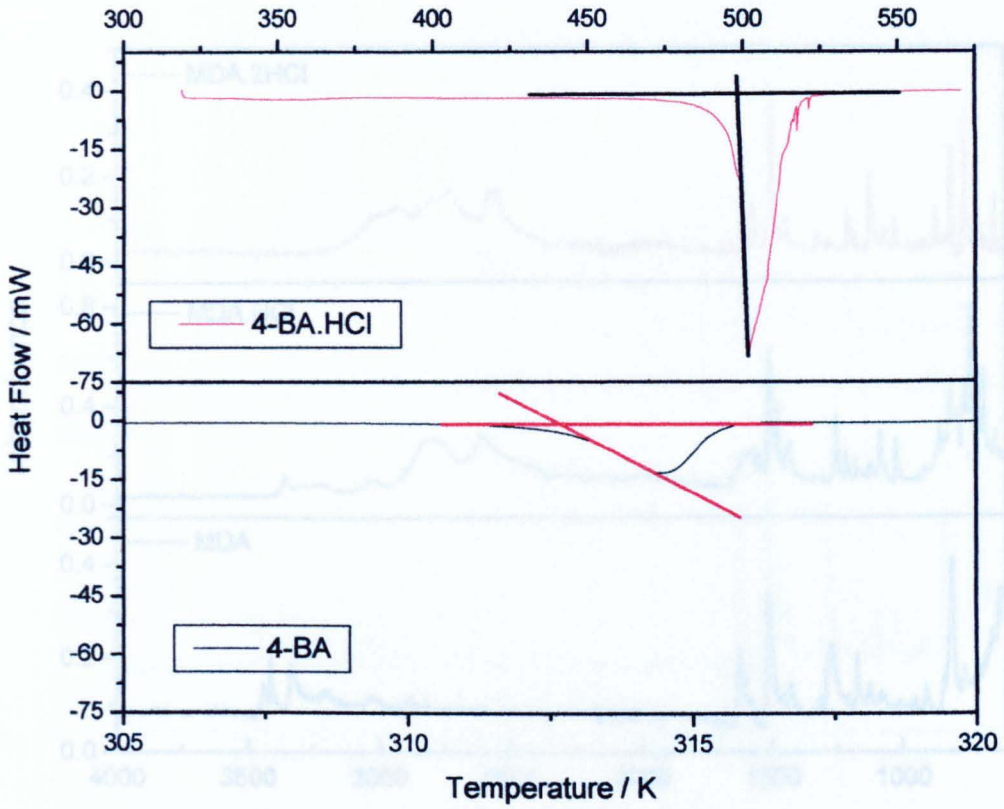

Figure 46 DSC trace of 4-BA and 4-BA.HCl.

The melting point of 4-BA derived from the DSC matches exactly with the standard melting point technique, both being slightly higher than the literature value.[29]

3.3.2 FTIR spectroscopy as a simple diagnostic tool

The FTIR spectra of MDA, MDA.HCl and MDA.2HCl (Figure 47) were obtained using the Attenuated Total Reflectance (ATR) accessory. Comparison of the spectra shows the dramatic shift in wavenumbers of the ν(N-H) band, from 3400 cm^{-1} for the NH_2 group of the free amine, to 2740 cm^{-1} for the NH_3^+ group of MDA.2HCl. The assignments of these bands are with reference to the literature,[98] the characteristic band of an aryl-NH_2 species occurring at 3390 cm^{-1} and that of the aryl primary amine salt having an ν(N-H) below 3000 cm^{-1}.[98] The FTIR spectrum of MDA.HCl appears to be a combination of the spectral features observed in the spectra of MDA and MDA.2HCl, having both bands associated with NH_2 and NH_3 species. This is consistent with the assumed structure of MDA.HCl, having both a protonated amine group (NH_3^+) and a non-protonated amine (NH_2) group.

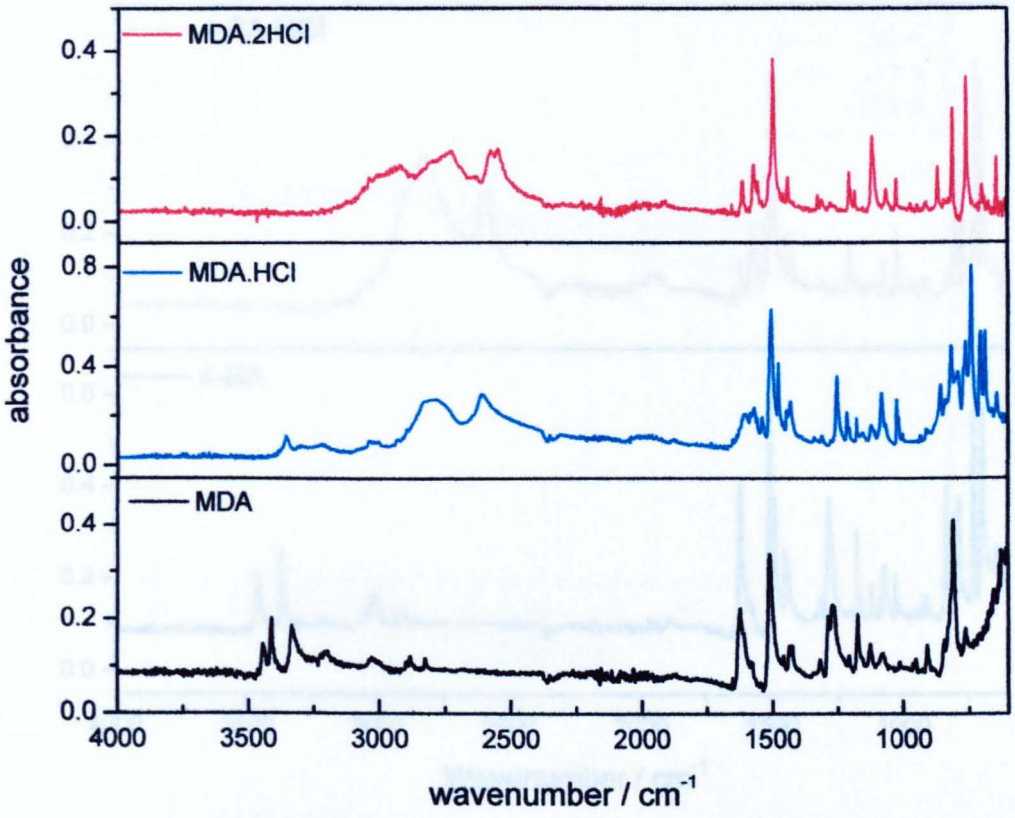

Figure 47 FTIR spectra of MDA, MDA.HCl and MDA.2HCl, using the ATR accessory.

The ATR-FTIR spectra of 4-BA and 4-BA.HCl are shown in Figure 48. Similar characteristic features are observed in the 4000 – 2000 cm^{-1} region as in the MDA series, (Figure 47). The two bands at 3500 and 3390 cm^{-1} are assigned as the asymmetric and symmetric ν(N-H) of the NH_2 group, which is consistent with the literature.[98] The band centred at 2830 cm^{-1} in the spectrum of 4-BA.HCl is assigned as the ν(N-H) of the NH_3 group, similar to that of MDA.2HCl.

The full vibrational assignments of the FTIR spectra of 4-BA, 4-BA.HCl, MDA, MDA.HCl and MDA.2HCl are presented and discussed in Chapter 5.

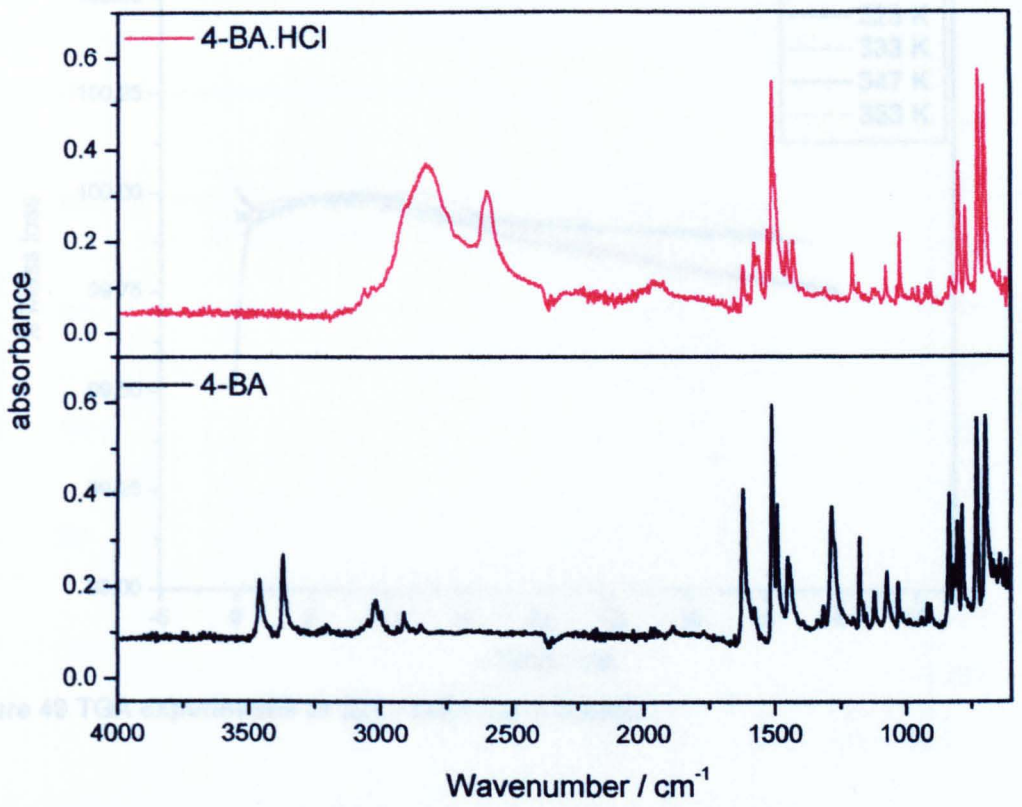

Figure 48 FTIR spectra of 4-BA and 4-BA.HCl, using the ATR accessory.

3.3.3 Thermal Gravimetric Analysis (TGA)

Thermal gravimetric analysis was performed on 4-BA.HCl and MDA.2HCl, to determine the possible solid phase dissociation of these hydrochloride salts. These results have key implications to the solution phase investigations, as outlined in Chapter 6.

3.3.3.1 4-BA.HCl

A mass loss of 17 % from a sample of 4-BA.HCl would be consistent with the dissociation of 4-BA.HCl, losing one mole of HCl, to form 4-BA, Equation (53).

$$\text{4-BA.HCl} \xrightarrow{17\ \%} \text{4-BA} + \text{HCl} \qquad (53)$$

No mass loss is observed at temperatures below 323 K, and only minor mass loss (<0.25 % in 35 min) is observed at 333, 347 and 353 K (Figure 49).

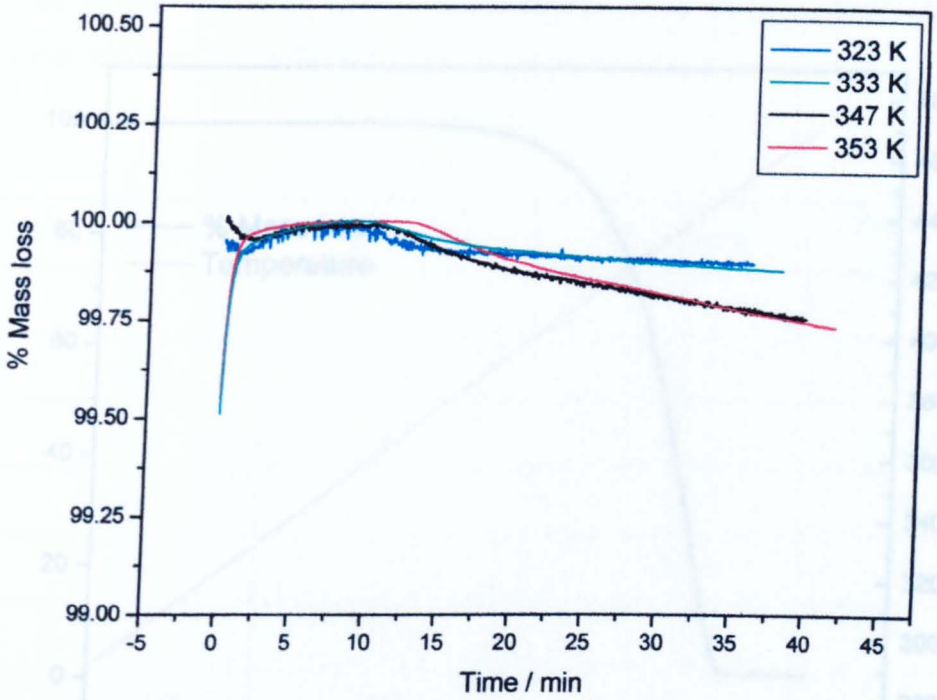

Figure 49 TGA experiments at 323 - 353 K on 4-BA.HCl.

A temperature ramp experiment which increased the temperature in a ramp of 1 K min^{-1} to a final temperature of 473 K shows mass loss starts at approximately 403 K (Figure 50) and is complete within 48 min.

An isothermal experiment at 403 K results in a mass loss of 20 % in 5 ½ h (Figure 51). This mass loss is greater than expected for the dissociation of 4-BA.HCl to form 4-BA, and appears to be continual, *i.e.* it does not plateau. This loss of mass is assumed to be the loss of complete 4-BA.HCl units, which would be expected to continue until 100 % mass loss is reached. However, these TGA experiments are ambiguous as discussed in Section 3.3.3.2.)

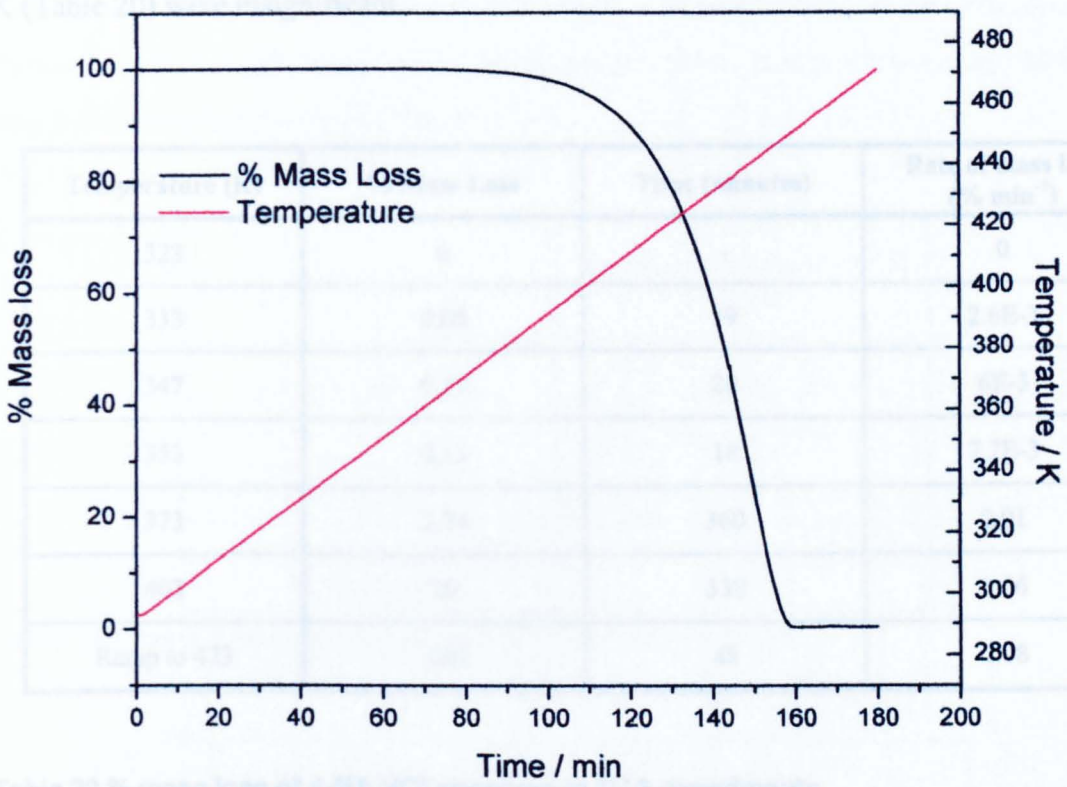

Figure 50 TGA experiment on 4-BA.HCl, temperature ramp to 473 K.

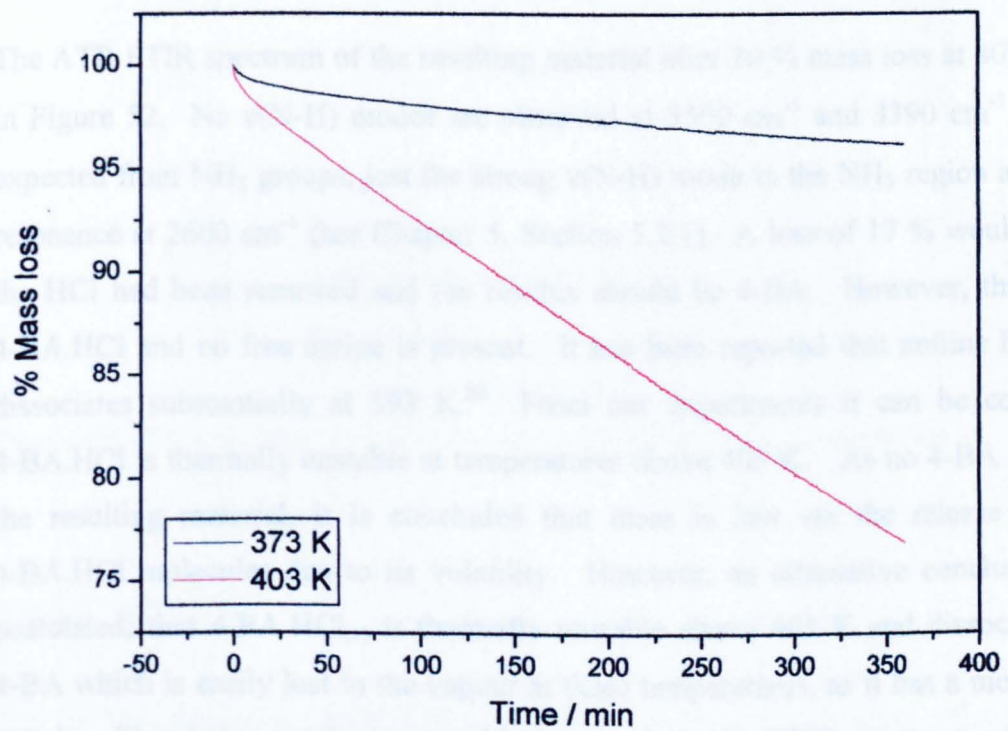

Figure 51 TGA experiments on 4-BA.HCl at 373 and 403 K.

The rate of mass lost during the TGA experiments on 4-BA.HCl at temperatures below 373 K (Table 20) were insignificant.

Temperature (K)	% Mass Loss	Time (minutes)	Rate of mass loss (% min^{-1})
323	0	-	0
333	0.05	19	2.6E-3
347	0.12	20	6E-3
353	0.13	18	7.2E-3
373	3.74	360	0.01
403	20	330	0.06
Ramp to 473	100	48	2.08

Table 20 % mass loss of 4-BA.HCl observed in TGA experiments.

3.3.3.2 ATR-FTIR analysis of 4-BA.HCl sample after TGA at 403 K

The ATR FTIR spectrum of the resulting material after 20 % mass loss at 403 K is shown in Figure 52. No ν(N-H) modes are observed at 3500 cm^{-1} and 3390 cm^{-1} as would be expected from NH_2 groups, just the strong ν(N-H) mode in the NH_3 region and the Fermi resonance at 2600 cm^{-1} (see Chapter 5, Section 5.2.1). A loss of 17 % would indicate all the HCl had been removed and the residue should be 4-BA. However, this material is 4-BA.HCl and no free amine is present. It has been reported that aniline hydrochloride dissociates substantially at 393 K.[99] From our experiments it can be concluded that 4-BA.HCl is thermally unstable at temperatures above 403 K. As no 4-BA is detected in the resulting material, it is concluded that mass is lost via the release of complete 4-BA.HCl molecules due to its volatility. However, an alternative conclusion must be postulated; that 4-BA.$HCl_{(s)}$ is thermally unstable above 403 K and dissociates to form 4-BA which is easily lost to the vapour at these temperatures, as it has a melting point of 313 K. This latter conclusion would also result in the FTIR spectrum of the residual 4-BA.$HCl_{(s)}$ as shown in Figure 52.

Above 373 K 4-BA.HCl appears to have a finite vapour pressure that results in a modest loss of amine hydrochloride molecular units. Similar amine hydrochlorides, aniline hydrochloride and 4,4'-MDA.2HCl, are reported to have vapour pressures at 403 K of 5.69 and 2.86 Torr respectively (Table 21).

Compound	Vapour pressure at 403 K (Torr)
Aniline hydrochloride	5.69
2,4-toluenediamine dihyrochloride	6.05
4,4'-methylenedianiline dihyrochloride	2.86

Table 21 Vapour pressures of amine hydrochlorides at 403 K.[99]

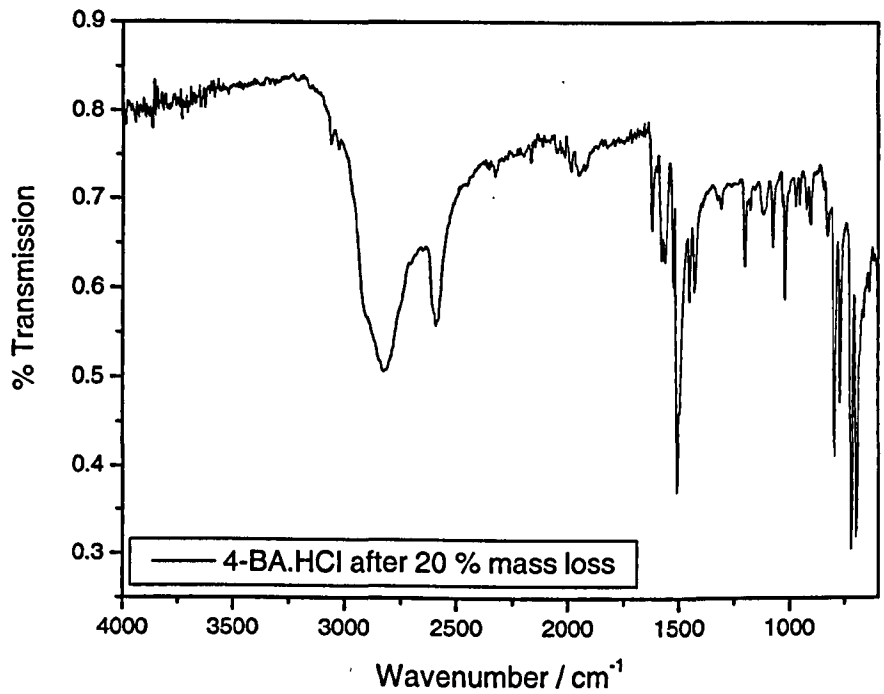

Figure 52 FTIR spectrum of 4-BA.HCl material after 20 % mass loss at 403 K.

3.3.3.3 MDA.2HCl

The thermal stability of MDA.2HCl is a more complicated case than 4-BA.HCl. A mass loss of 13% would be consistent with the loss of one mole of HCl, resulting in MDA.HCl. A further loss of 16 % would be consistent with the further loss of HCl to form MDA, Equation (54). The total mass loss expected for the dissociation of 2 moles of HCl from MDA.2HCl would be 27 %.

$$MDA.2HCl \xrightarrow{13\ \%} MDA.HCl \xrightarrow{16\ \%} MDA \quad (54)$$

A temperature ramp experiment which increased the temperature in a ramp of 5 K min^{-1} to a final temperature of 573 K (Figure 53) shows an initial period of slow mass loss, 5.5 % in 28 minutes, until the temperature reaches 438 K; followed by a period of rapid mass loss, 79 % in 15 minutes. Slow mass loss is observed after 517 K.

The initial period of mass loss could be the loss of residual chlorobenzene solvent. The percentage mass loss of 79 % is greater than expected for the loss of HCl to form MDA or MDA.2HCl. There are two possibilities to explain this large loss of mass, either it is the loss of complete MDA.2HCl units, due to the substantial vapour pressure of 10.1 Torr at 433 K,[99] or it is caused by the dissociation of MDA.2HCl and the subsequent loss of MDA.HCl units or MDA.

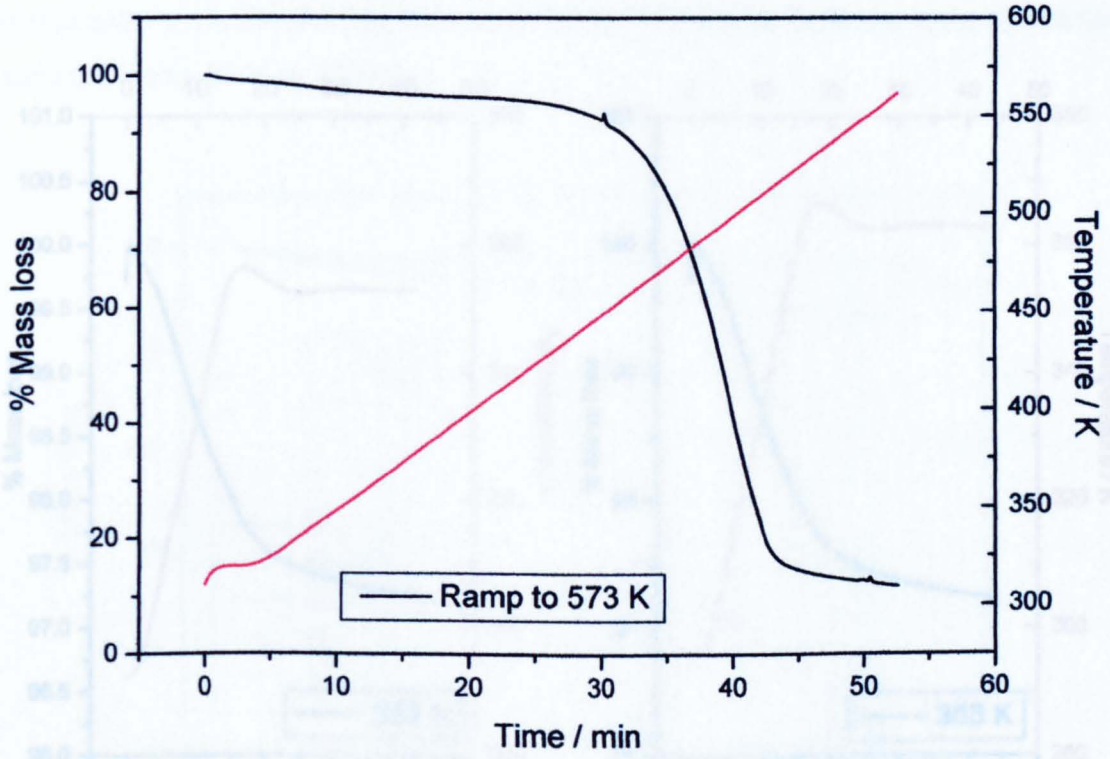

Figure 53 TGA ramp on MDA.2HCl to 573 K.

Mass loss commences at 438 K, 35 K above the process temperature, which is consistent with MDA.2HCl being stable during the industrial process.

Isothermal TGA experiments were also performed on MDA.2HCl at 353, 363, 383, 403, 413, 438 and 473 K, as outlined in Table 22. Overall a small loss in mass is observed during TGA experiments on MDA.2HCl at 353 and 363 K (Figure 54). This mass loss is split into two regions, a mass loss of 2.3 % observed during the temperature ramp of each experiment; followed by a region of smaller mass loss during the isothermal period of the experiments, losing only 0.4 and 0.3 % during the 353 and 363 K experiments respectively. The regions of mass loss observed during both experiments are less than expected for the loss of one mole of HCl from MDA.2HCl (Equation (54)). The initial region of mass loss could be due to loss of residual chlorobenzene solvent, and the second, once the experimental temperature had been reached, could be due to the gradual and small loss of MDA.2HCl units, due to the low vapour pressure of the material at these temperatures.

For isothermal experiments above 383 K a more significant mass loss is observed; these results are shown in Figure 55 and listed in Table 22. The initial temperature ramp period for the 403 K isothermal experiment is not shown in Figure 55.

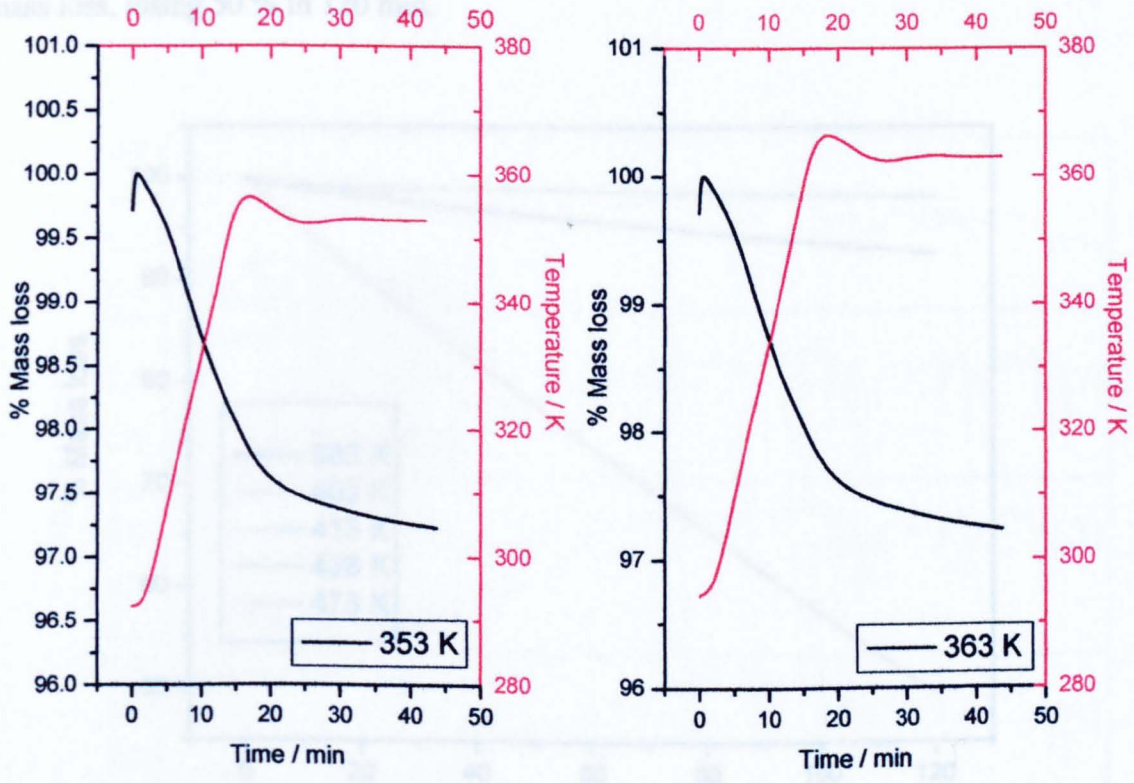

Figure 54 TGA experiments on MDA.2HCl at 363 and 353 K.

TGA Experiment (K)	Rate of mass loss (% min^{-1})		Total mass loss (%)
	Initial	Isothermal	
353	0.14	0.02	3.0
363	0.12	0.01	2.8
383	-	0.07	0.7
403	0.11	0.06	4.3
413	-	0.02	1.8
438	-	0.05	6.5
473	-	0.42	50

Table 22 Comparison of TGA results for MDA.2HCl.

The initial loss in mass during the temperature ramp, is similar for 353, 363 and 403 K experiments, this mass loss is thought to be evaporation of residual chlorobenzene solvent molecules from the MDA.2HCl sample. The total mass losses observed for all experiments are similar, barring the one at 473 K. This latter experiment shows substantial mass loss, losing 50 % in 120 min.

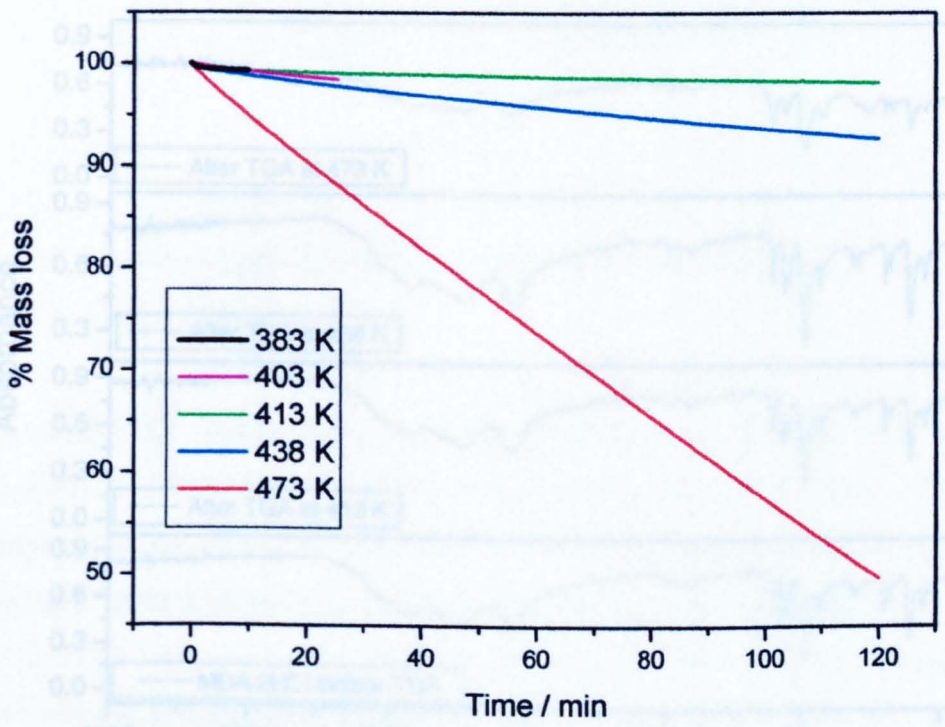

Figure 55 TGA experiments on MDA.2HCl at 383, 403, 413 and 438 K.

3.3.3.4 ATR-FTIR analysis of MDA.2HCl samples after TGA experiments

The resulting samples after TGA experiments at 413 and 438 K show no evidence of free amine; no ν(N-H) originating from NH_2 are observed at 3500 cm^{-1} and 3390 cm^{-1}. Only the strong ν(N-H) in the NH_3 region and the Fermi resonance at 2600 cm^{-1} (see Chapter 5, Section 5.2.2) are observed, indicating this is pure MDA.2HCl. Like the 4-BA.HCl investigation, this is inconclusive for amine hydrochloride dissociation. The absence of free amine in the FTIR spectrum could be the result of evaporation of MDA produced by dissociation of the hydrochloride salt; or if no dissociation occurs, release of complete MDA.2HCl molecules. For MDA.2HCl there is another possible route resulting in mass loss; the partial dissociation of MDA.2HCl to form MDA.HCl. This process appears to occur at 473 K, as the resulting FTIR spectrum shows a band at 3333 cm^{-1} indicative of an NH_2 group, and a reduction in intensity of the ν(N-H) NH_3 bands between 3240 and 2610 cm^{-1}, this spectrum closely resembles that of MDA.HCl (Figure 47). This spectrum is recorded after 50 % mass loss, which is greater than the 13 % mass loss expected for the conversion to MDA.HCl. Therefore it is expected that MDA.HCl once formed has a substantial vapour pressure, or dissociates further and MDA formed is lost from the system.

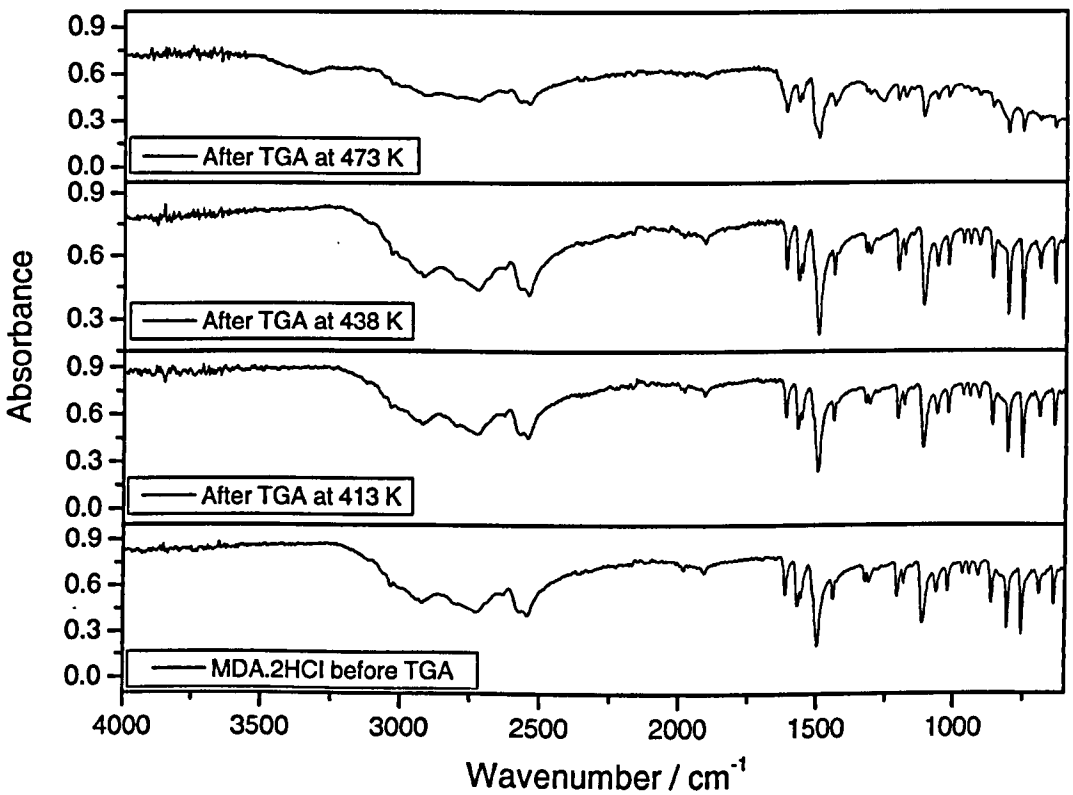

Figure 56 ATR FTIR of samples after TGA experiments.

Compared with the temperature ramp experiment on 4-BA.HCl, MDA.2HCl mass loss is initiated 30 K higher than 4-BA.HCl.

3.3.3.5 TGA summary

4-BA.HCl and MDA.2HCl are thermally unstable at temperatures well below their melting points of 501 and 533 K respectively.

Analysis by ATR-FTIR showed that at temperatures above 473 K MDA.2HCl will partially dissociate to form MDA.HCl (Figure 57) which then loses mass itself. The contribution of the dissociation of MDA.2HCl to MDA.HCl to the industrial process is likely to be very limited, as the industrial process operates at a much lower temperature, at approximately 403 K.

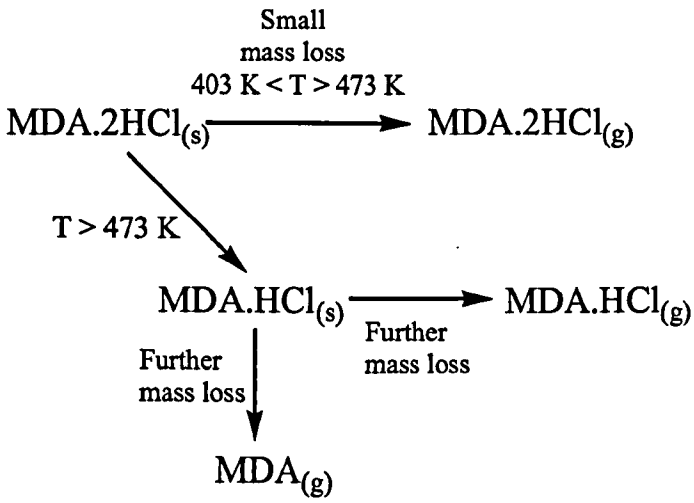

Figure 57 Scheme describing the thermal stability of MDA.2HCl.

Using ATR-FTIR spectroscopy, analysis of resulting samples after TGA experiments on 4-BA.HCl, at 403 K showed no evidence for the formation of free amine. The loss of mass at temperatures above 373 K, could proceed via the loss of complete 4-BA.HCl units or the dissociation of to form $4\text{-BA}_{(s)}$, followed by vapourisation of 4-BA (Figure 58). In light of the TGA-FTIR experiment on MDA.2HCl (Figure 56) the residual sample of a TGA experiment can contain compounds which have a melting point lower than the temperature at which the TGA experiment was performed. In the case of MDA.2HCl the products observed in the FTIR spectrum (Figure 56) could have been either MDA.HCl or a mixture of MDA and MDA.2HCl. MDA and MDA.HCl both have melting points lower than the temperature of the TGA experiment (473 K), which implies for the case of 4-BA.HCl that

if 4-BA was produced to any significant extent, then it should be observed in the FTIR analysis. These results influence the understanding of the experiments on the solution phase dissociation of 4-BA.$HCl_{(s)}$ which are discussed in Chapter 6.

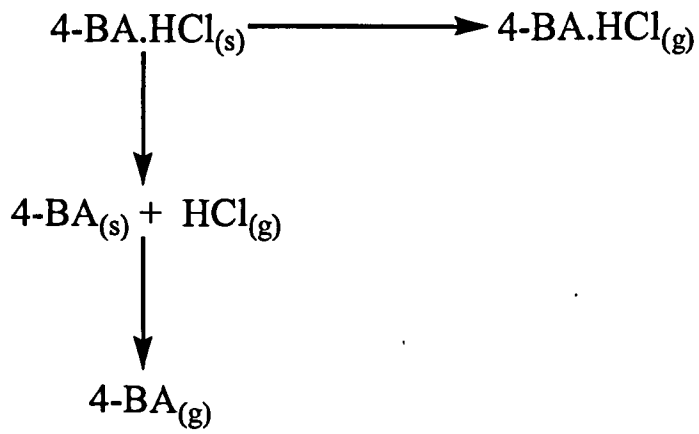

Figure 58 Scheme describing the thermal stability of 4-BA.$HCl_{(s)}$.

A more definitive TGA experiment would be to measure the outlet gas stream using either mass spectroscopy or gas phase FTIR, to determine the products formed via the thermal treatment of 4-BA.$HCl_{(s)}$.

3.3.4 ^{1}H NMR of amine hydrochlorides in DMSO and methanol

Examination of samples via ^{1}H NMR was a useful and quick confirmation of the extent of hydrochlorination of the preparations of these compounds.

Both aromatic rings of the MDA series of compounds are *para*-substituted aromatics. The system has two H_A, two $H_{A'}$, two H_B and two $H_{B'}$ protons as designated in Figure 59. The symmetry present in MDA results in a second order spin-coupling system. It is called second order as the frequency separation of the multiplets from the H_A and H_B protons is of a similar magnitude to the coupling constant between them. This means the spectra have line intensities and line positions which are not as would be predicted if the two sets of protons were isolated from each other. The letters A and B are chosen as the protons have comparable chemical shifts, and the spin coupling system is called an $[AA'BB']_2$ system.[97] Using X as a label for one of the protons would signify the chemical shifts were far apart as in the AA'XX' system of dioxane.[55] The prime is used, A', to differentiate between nuclei which are chemically equivalent but which are not magnetically equivalent.[100] The two pairs of protons H_A and H_B have the same chemical shift but different coupling

constants, J(AB), J(AA'), J(AB') and J(BB').[55] This spin coupling system results in the spectra shown in Figure 59.

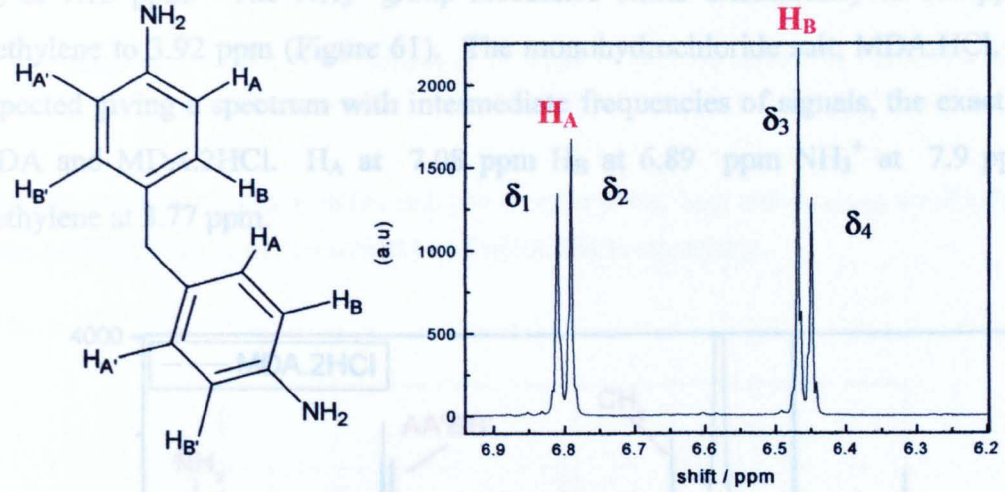

Figure 59 Example ^{1}H NMR spectrum of the aromatic AA'BB' spin system of MDA in DMSO.

The most intense lines in the spectra have the appearance of a simple AB spin coupling system, and the approximate chemical shift of the AA'BB' spin system, δ_{AB}, can be calculated using Equation (55).[55] The ^{1}H NMR resonances, δ_1, δ_2, δ_3 and δ_4, using the δ scale in ppm, are shown in Figure 59.

$$\delta_A = \delta_1 - (\delta_1 - \delta_2) \qquad \delta_B = \delta_3 - (\delta_3 - \delta_4) \qquad \delta_{AB} = \delta_2 - \tfrac{1}{2}\nu_{AB} \tag{55}$$

$$\text{where} \quad \nu_{AB} = \sqrt{(\delta_1 - \delta_4)(\delta_2 - \delta_3)}$$

δ_A and δ_B are the midpoints of the H_A and H_B multiplets as shown in Figure 59, ν_{AB} – the midpoint of the chlorobenzene multiplet.

3.3.4.1 MDA series in DMSO

For MDA the H_A is observed at 6.81 ppm and H_B at 6.47 ppm, as calculated in Equation (55). The methylene protons, H_C, resonate as a singlet at 3.56 ppm and the NH_2 proton has a broad resonance at 4.8 ppm. The DMSO solvent signals are a quintet at 2.52 ppm and a water signal at 3.4 ppm.

The aromatic and methylene protons of MDA shift to lower frequency upon reaction of HCl with one and then the other amine groups (Figure 60). On hydrochlorination of both amine groups, the AA'BB' spin system signals occur at lower frequency, H_A at 7.25 ppm H_B at 7.15 ppm. The NH_3^+ group resonance shifts dramatically to 9.3 ppm and the methylene to 3.92 ppm (Figure 61). The monohydrochloride salt, MDA.HCl, behaves as expected giving a spectrum with intermediate frequencies of signals, the exact average of MDA and MDA.2HCl. H_A at 7.08 ppm H_B at 6.89 ppm NH_3^+ at 7.9 ppm and the methylene at 3.77 ppm.

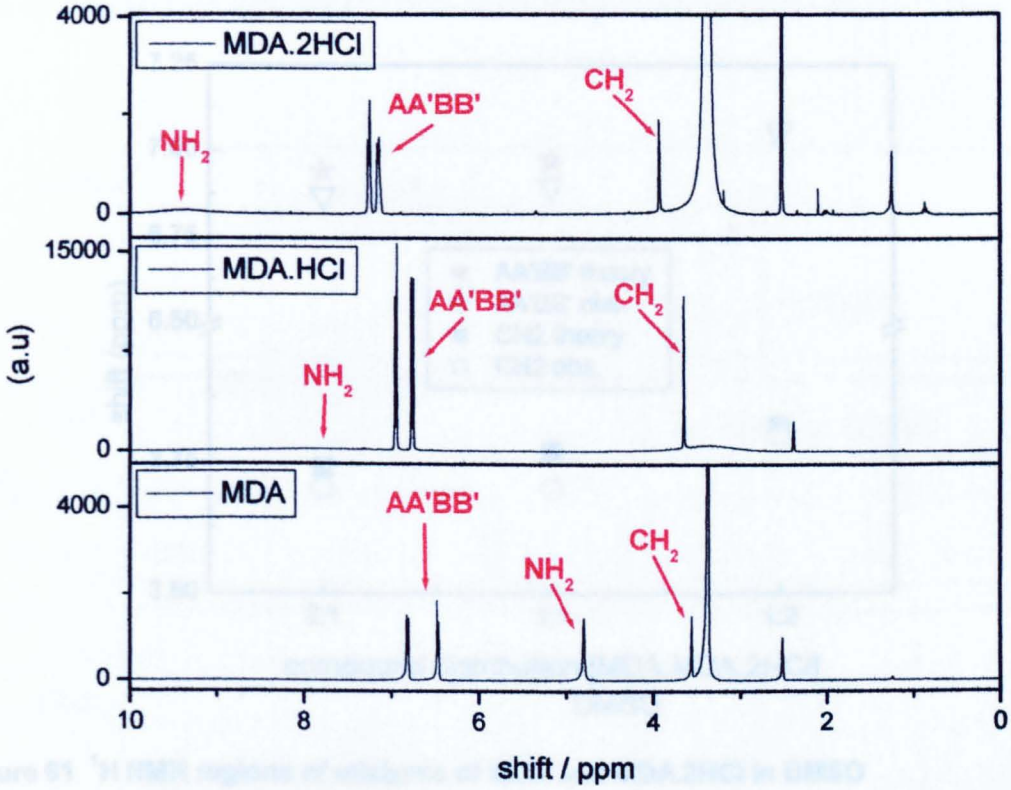

Figure 60 ^{1}H NMR spectra of MDA, MDA.HCl and MDA.2HCl in DMSO.

Samples containing MDA.2HCl, and unreacted amine, resulting from incomplete hyrdrochlorination (see Chapter 2, Section 2.3.3) can be distinguished from pure compounds (MDA or MDA.2HCl) using the AA'BB' and methylene group resonances. This has been tested with mixtures of MDA.2HCl and MDA as shown in Figure 61. However, MDA.HCl is in fact indistinguishable from a 50:50 mixture of these compounds.

The theoretical chemical shifts of the AA'BB' and methylene resonances were calculated for mixtures of MDA:MDA.2HCl of the ratio of 2:1, 1:1 and 1:2. Equimolar solutions of MDA and MDA.2HCl in DMSO were prepared and then mixed to these ratios, by volume. For example the 2:1 mixture of MDA:MDA.2HCl solution was prepared by mixing 0.5

cm^3 of a 0.03 mmol L^{-1} MDA solution with 0.25 cm^3 of a 0.03 mmol L^{-1} solution of MDA.2HCl. The theoretical chemical shifts of, for example, the AA'BB' group resonance were calculated using Equation (56).

$$\delta = (x_{MDA}\,\delta_{MDA} + x_{MDA.2HCl}\,\delta_{MDA.2HCl}) \; ; \; x_{MDA} = [MDA] / ([MDA] + [MDA.2HCl]) \quad (56)$$

Where x_A and x_B are the mole ratios of A and B respectively, δ_{MDA} and $\delta_{MDA.2HCl}$ are the chemical shifts of the AA'BB' group resonance of MDA and MDA.2HCl respectively.

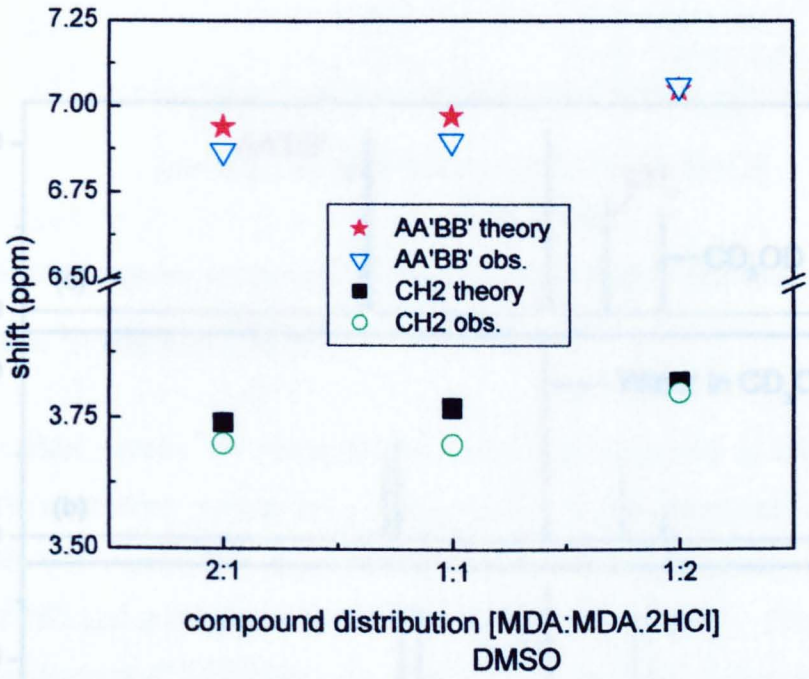

Figure 61 ^{1}H NMR regions of mixtures of MDA and MDA.2HCl in DMSO

The calculated chemical shifts match well with the observed shifts of the prepared solutions. As the concentration of MDA.2HCl increased in the mixed solutions the methylene and AA'BB' group resonances increased to lower frequency. This scale can be used to estimate the distribution of MDA and MDA.2HCl in a mixed solution, *i.e.* the mixture of products obtained *via* the direct reaction of MDA with $HCl_{(g)}$ which produced mixtures of MDA and MDA.2HCl, the extent of hydrochlorination could be analysed by dissolving the mixture in DMSO and obtaining the ^{1}H NMR spectrum.

The shift in frequency of the amine protons is not precisely diagnostic, as these signals are broad due to proton exchange with water present in the solvent.

3.3.4.2 MDA series in MeOH-d_4

The ^{1}H NMR spectra of MDA, MDA.2HCl and MDA.HCl dissolved in deuterated methanol (CD_3OD) are shown in Figure 62. The AA'BB' and methylene group resonances shift to lower frequency on hydrochlorination, in a similar manner to the DMSO solutions. An average spectrum is obtained when solutions of mixtures of MDA and MDA.2HCl in CD_3OD are used, the positions of the aromatic and methylene shifts depending on the proportion of MDA and MDA.2HCl present (Figure 63). Unlike the solutions of MDA and MDA.2HCl in DMSO, no NH_2 or NH_3 signals are observed caused by exchange of the NH_2 or NH_3 protons with the OD deuterium atoms from methanol-d_4.

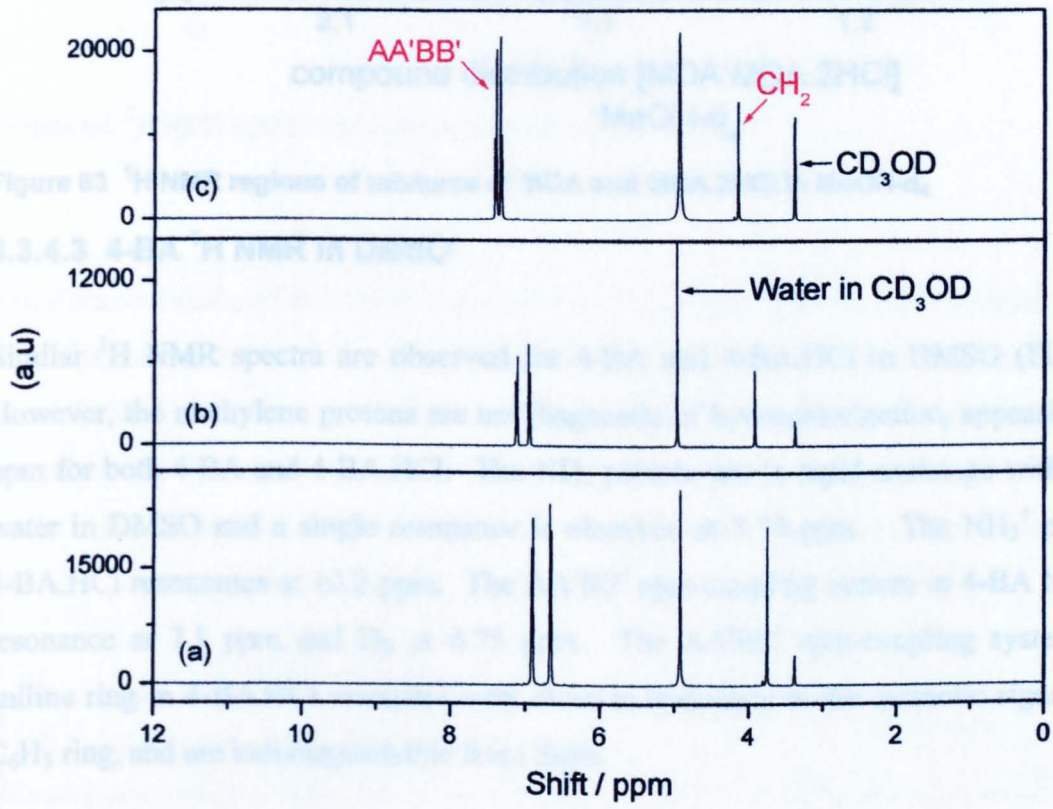

Figure 62 ^{1}H NMR spectra of (a) MDA, (b) MDA.HCl and (c) MDA.2HCl in MeOH-d_4.

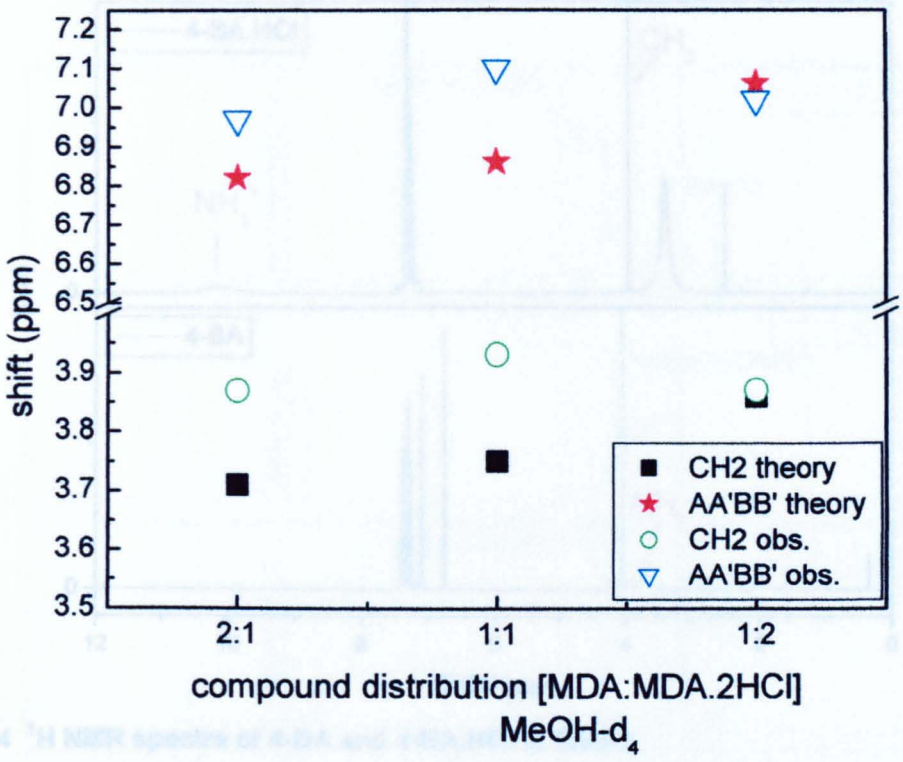

Figure 63 ^{1}H NMR regions of mixtures of MDA and MDA.2HCl in MeOH-d_4

3.3.4.3 4-BA ^{1}H NMR in DMSO

Similar ^{1}H NMR spectra are observed for 4-BA and 4-BA.HCl in DMSO (Figure 64). However, the methylene protons are not diagnostic of hydrochlorination, appearing at ~ 4 ppm for both 4-BA and 4-BA.HCl. The NH_2 protons are in rapid exchange with residual water in DMSO and a single resonance is observed at 3.74 ppm. The NH_3^+ protons in 4-BA.HCl resonantes at 10.2 ppm. The AA'BB' spin-coupling system in 4-BA has an H_A resonance at 7.1 ppm and H_B at 6.75 ppm. The AA'BB' spin-coupling system of the aniline ring in 4-BA.HCl resonates very close in frequency to the aromatic signals of the C_6H_5 ring, and are indistinguishable from them.

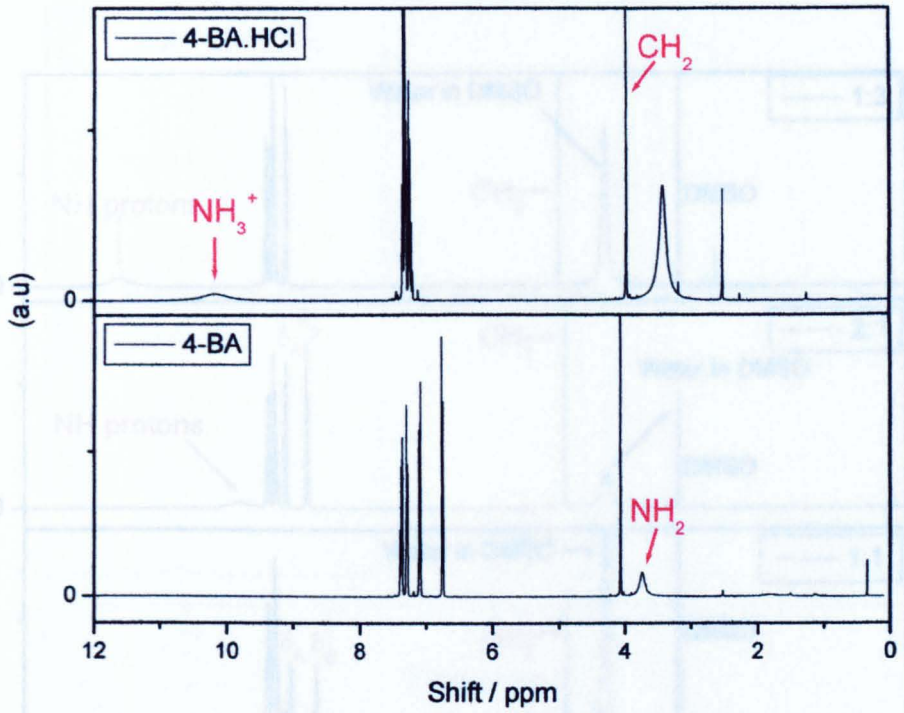

Figure 64 ^{1}H NMR spectra of 4-BA and 4-BA.HCl in DMSO.

The chemical shifts of the methylene, amine and aromatic regions of mixtures of 4-BA and 4-BA.HCl are listed in Table 23. These mixtures of 4-BA and 4-BA.HCl show the same trend as those of MDA and MDA.2HCl; the amine and aromatic signals shift to lower frequency on hydrochlorination (Figure 65). The shift in frequency of the methylene protons is not sufficient to be diagnostic of hydrochlorination, but the amine and the aromatic protons do shift in frequency substantially.

4-BA:4-BA.HCl	CH_2	Amine	Aromatic	
			δ_A	δ_B
1:3	3.94	8.95	-	-
2:1	3.89	7.56	7.04	6.80
1:1	3.86	-	6.98	6.69

Table 23 ^{1}H NMR shifts of mixtures of 4-BA and 4-BA.HCl (ppm)

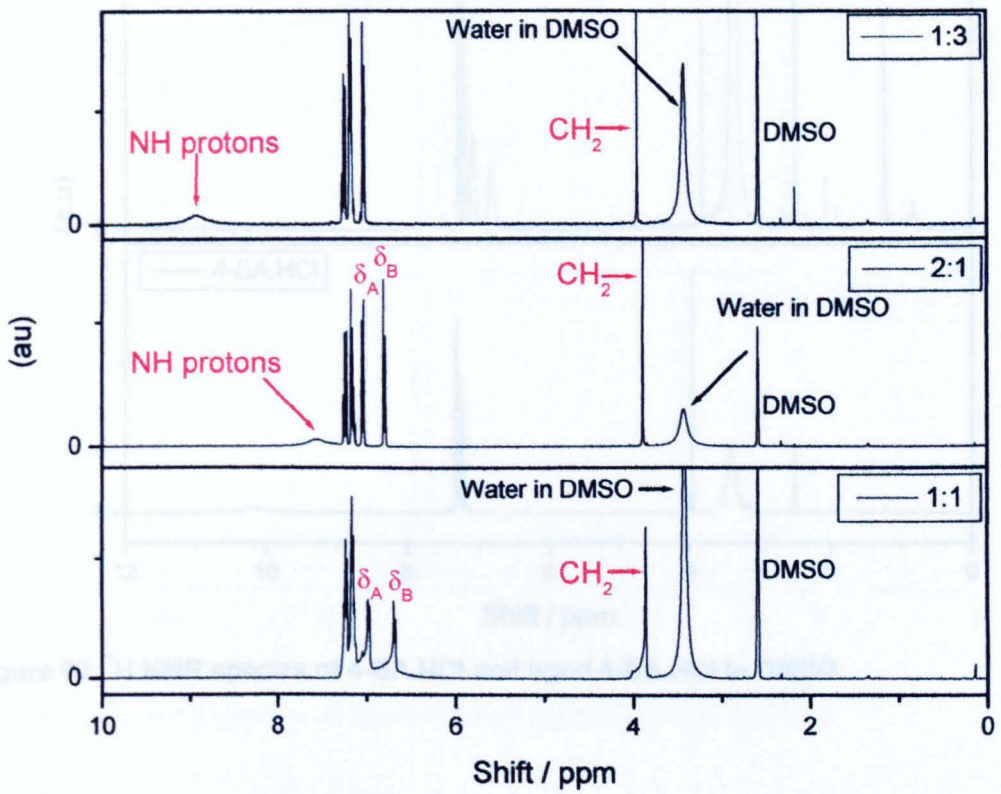

Figure 65 ^{1}H NMR spectra of mixtures of 4-BA and 4-BA.HCl in DMSO.

3.3.5 Ageing of samples

Samples of 4-BA.HCl and MDA.HCl are not stable over long periods of time; storing in a desiccator for more than two weeks results in some decomposition of the samples. 4-BA.HCl appears to lose HCl and the resulting ^{1}H NMR spectrum is consistent with a mixture of 4-BA and 4BA.HCl (Figure 66). The methylene signal shifts upfield from 3.98 ppm to 3.72 ppm, the amine protons from 10.2 ppm to 7.7 ppm and the AA'BB' is distinguishable from the other aromatic protons, and are observed at approximately 6.94 and 6.69 ppm.

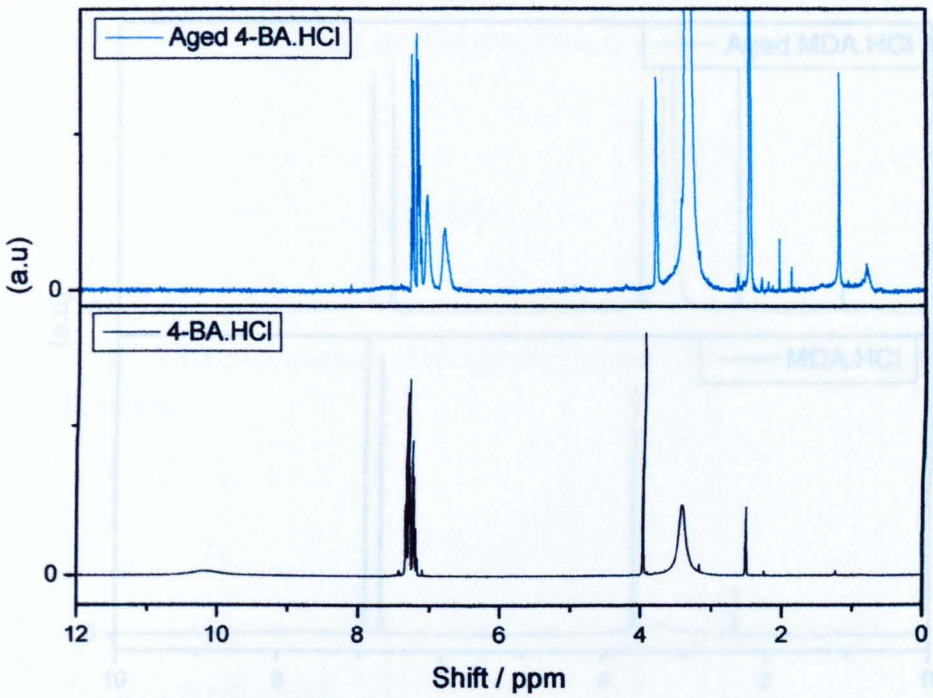

Figure 66 ^{1}H NMR spectra of 4-BA.HCl and aged 4-BA.HCl in DMSO.

A similar situation occurs with MDA.HCl (Figure 67) which on ageing appears to lose HCl and give a spectrum consistent with that of a mixture of MDA and MDA.HCl with signals lying to higher frequency than those of MDA and to lower frequency of those of MDA.HCl. The methylene resonance appears at 3.57 ppm, the amine at 7.2 ppm and the aromatic H_A and H_B protons at 6.87 and 6.62 ppm respectively.

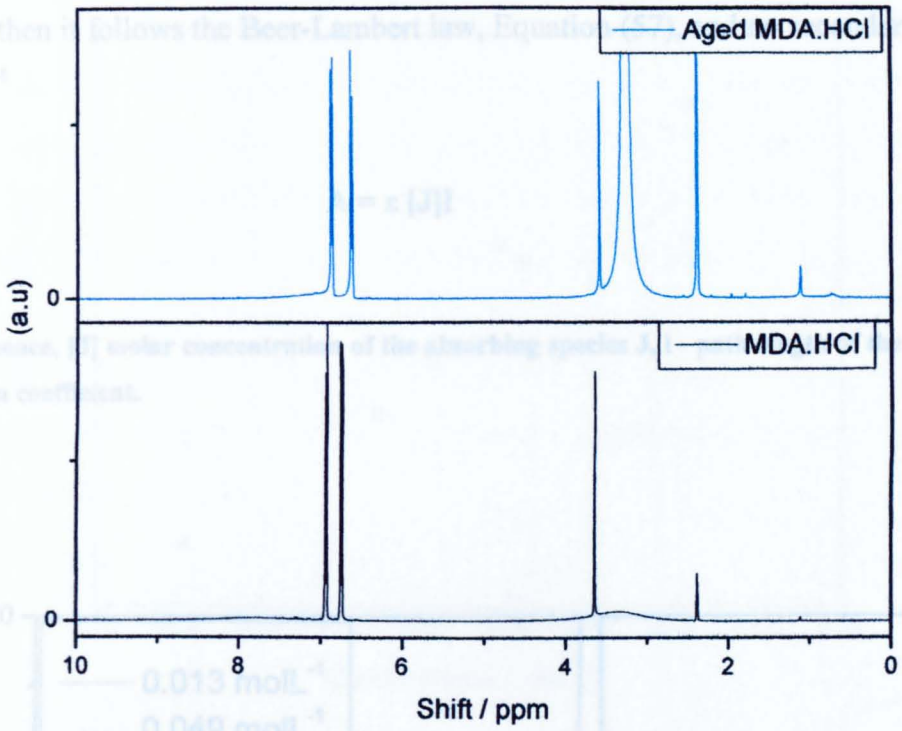

Figure 67 ^{1}H NMR spectra of MDA.HCl and aged MDA.HCl in DMSO.

The change in ^{1}H NMR spectra of the samples indicates they are not stable over long periods of time. The spectra are consistent with dehydrochlorination, as the spectra appear to show the samples are returning to their free amine forms (4-BA, MDA). All subsequent samples of the hydrochloride salts which were prepared, were kept for a maximum of two weeks, and fresh samples were made for all kinetic experiments.

3.3.6 Dissolution of amines and amine hydrochlorides in chlorobenzene

FTIR and ^{1}H NMR spectroscopy were used to investigate the dissolution of MDA, 4-BA, 4-BA.HCl and MDA.2HCl in the industrial process solvent (chlorobenzene).

3.3.6.1 Dissolution of MDA in chlorobenzene

The saturation concentration of MDA in chlorobenzene is approximately 0.138 ± 0.007 mol L^{-1}. The FTIR spectra of solutions of varying concentration were recorded (Figure 68) and the area under the ν(N-H) mode at 3400 cm^{-1} was measured for each and the

concentration curve determined (Figure 69). If the initial part of the concentration curve is linear then it follows the Beer-Lambert law, Equation (57), and no secondary species are present.[94]

$$A = \varepsilon [J] l \quad (57)$$

A- absorbance, [J] molar concentration of the absorbing species J, l - path length of the cell, ε – molar absorption coefficient.

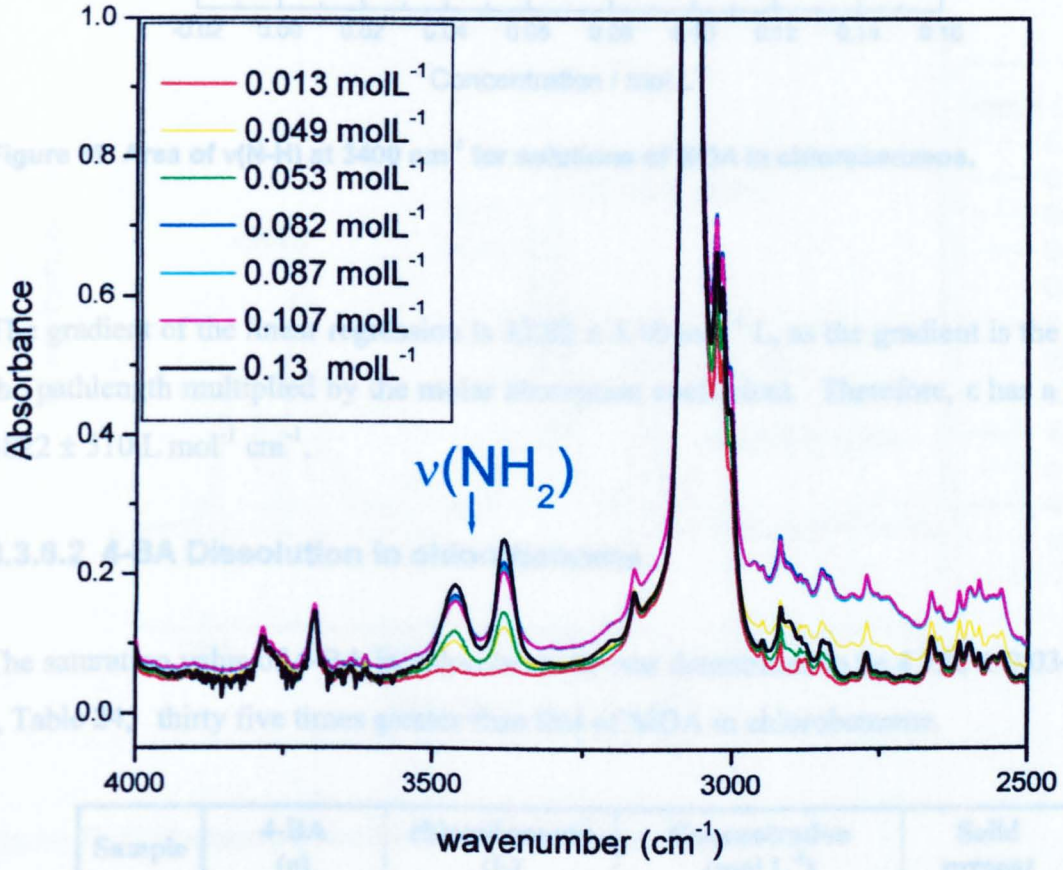

Figure 68 FTIR spectra of solutions of MDA in chlorobenzene.

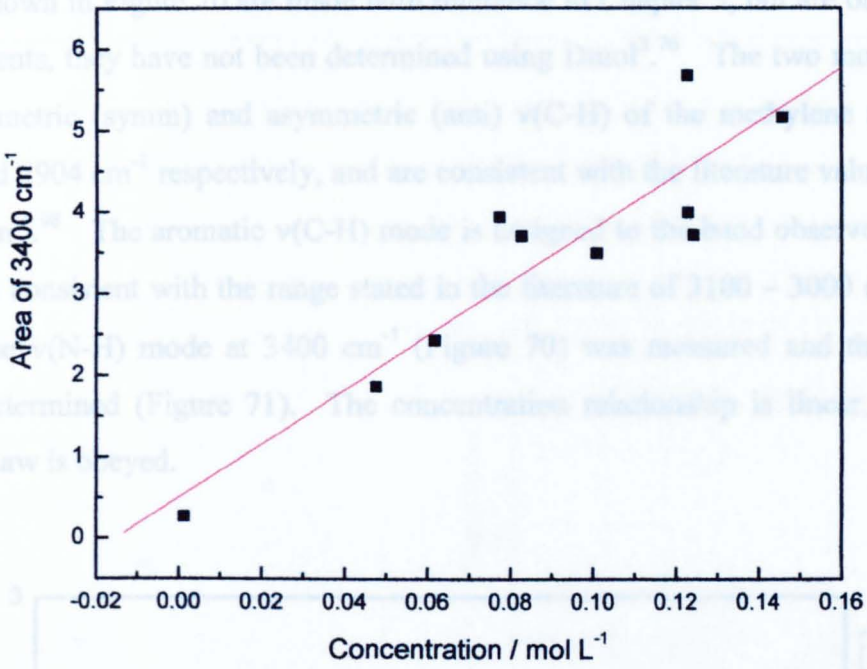

Figure 69 Area of ν(N-H) at 3400 cm^{-1} for solutions of MDA in chlorobenzene.

The gradient of the linear regression is 32.82 ± 5.10 mol^{-1} L, as the gradient is the value of the pathlength multiplied by the molar absorption coefficient. Therefore, ε has a value of 3822 ± 510 L mol^{-1} cm^{-1}.

3.3.6.2 4-BA Dissolution in chlorobenzene

The saturation value of 4-BA in chlorobenzene was determined to be 4.722 ± 0.034 mol L^{-1}, Table 24, thirty five times greater than that of MDA in chlorobenzene.

Sample	4-BA (g)	chlorobenzene (L)	Concentration (mol L^{-1})	Solid present
1	0.8605	1.0 x 10^{-3}	4.7	NO
2	0.1705	0.2 x 10^{-3}	4.66	NO
3	0.7774	0.2 x 10^{-3}	4.85	YES
4	0.1729	0.2 x 10^{-3}	4.72	YES
5	0.1712	0.2 x 10^{-3}	4.68	NO

Table 24 Saturation values of 4-BA in chlorobenzene.

The FTIR spectra of a series of 4-BA solutions were recorded, the assignments of the bands shown in Figure 70 are made with reference to Chapter 5, but are only approximate assignments, they have not been determined using Dmol^3.[76] The two modes assigned as the symmetric (symm) and asymmetric (anti) ν(C-H) of the methylene are observed at 2844 and 2904 cm^{-1} respectively, and are consistent with the literature values of 2853 and 2926 cm^{-1}.[98] The aromatic ν(C-H) mode is assigned to the band observed at 3030 cm^{-1}, which is consistent with the range stated in the literature of 3100 – 3000 cm^{-1}.[98] The area under the ν(N-H) mode at 3400 cm^{-1} (Figure 70) was measured and the concentration curve determined (Figure 71). The concentration relationship is linear, as expected if Beer's Law is obeyed.

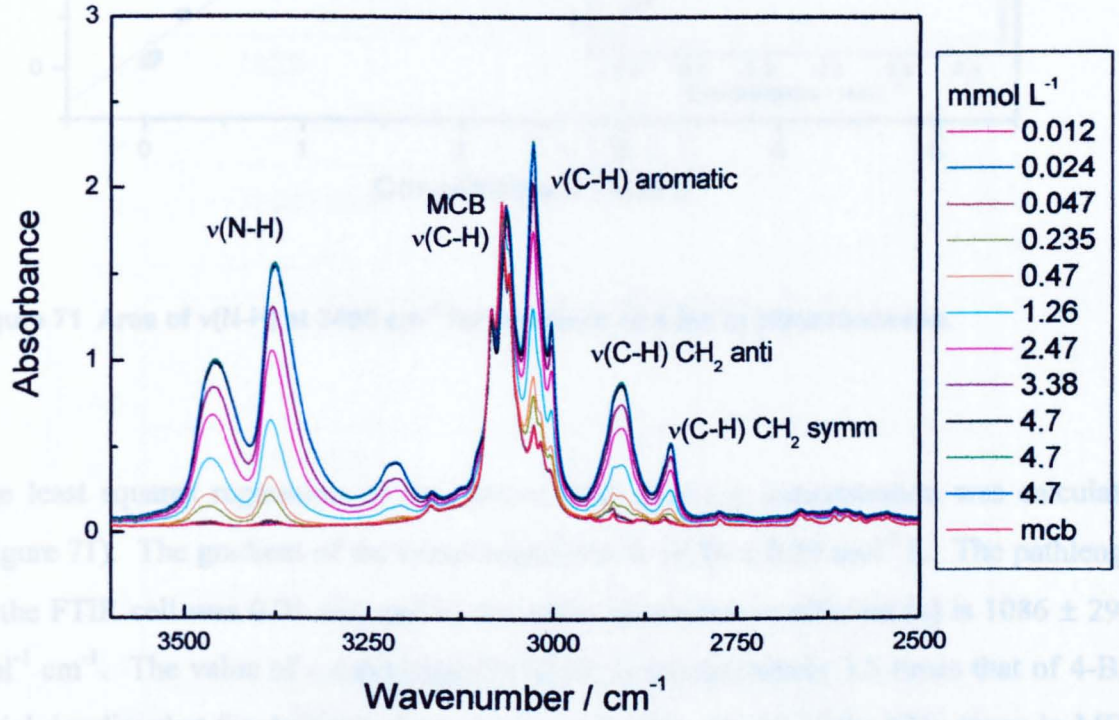

Figure 70 FTIR spectra of solutions of 4-BA in chlorobenzene.

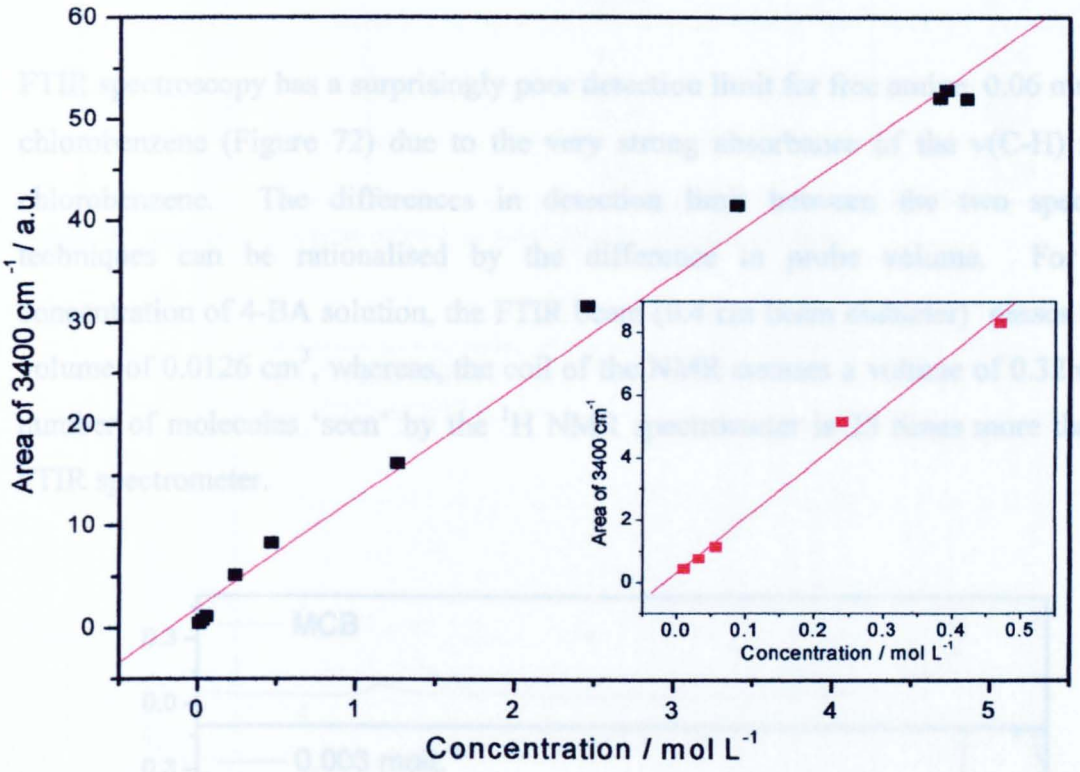

Figure 71 Area of ν(N-H) at 3400 cm^{-1} for solutions of 4-BA in chlorobenzene.

The least squares regression of the plot of peak area v.s. concentration was calculated (Figure 71). The gradient of the linear regression is 10.86 ± 0.29 mol^{-1} L. The pathlength of the FTIR cell was 0.01 cm, and so the molar absorption coefficient (ε) is 1086 ± 29 L mol^{-1} cm^{-1}. The value of ε calculated for MDA is approximately 3.5 times that of 4-BA, which implies that the dynamic dipole moment for the ν(N-H) of the NH_2 group in MDA is greater than that in 4-BA.

3.3.6.3 Detection limit of amine by ^{1}H NMR compared with by FTIR spectroscopy

^{1}H NMR spectroscopy using the solvent suppression pulse program, outlined in Chapter 2, was found to be more sensitive than FTIR spectroscopy by a factor of 6. ^{1}H NMR spectroscopy also provided information on the total solvated products *via* the CH_2 signal which represents both 4-BA.HCl$_{(solv)}$ and 4-BA$_{(solv)}$ and *via* the NH_2 signal, the concentration of 4-BA$_{(sov)}$. The detection limit of the solvent suppression ^{1}H NMR

spectroscopy for free amine dissolved in chlorobenzene is 0.01 mmol L^{-1}, (see Chapter 2, Figure 33).

FTIR spectroscopy has a surprisingly poor detection limit for free amine, 0.06 mmol L^{-1} in chlorobenzene (Figure 72) due to the very strong absorbance of the ν(C-H) modes of chlorobenzene. The differences in detection limit between the two spectroscopic techniques can be rationalised by the difference in probe volume. For a given concentration of 4-BA solution, the FTIR beam (0.4 cm beam diameter) passes through a volume of 0.0126 cm^3, whereas, the coil of the NMR encases a volume of 0.32 cm^3. The number of molecules 'seen' by the ^1H NMR spectrometer is 25 times more than by the FTIR spectrometer.

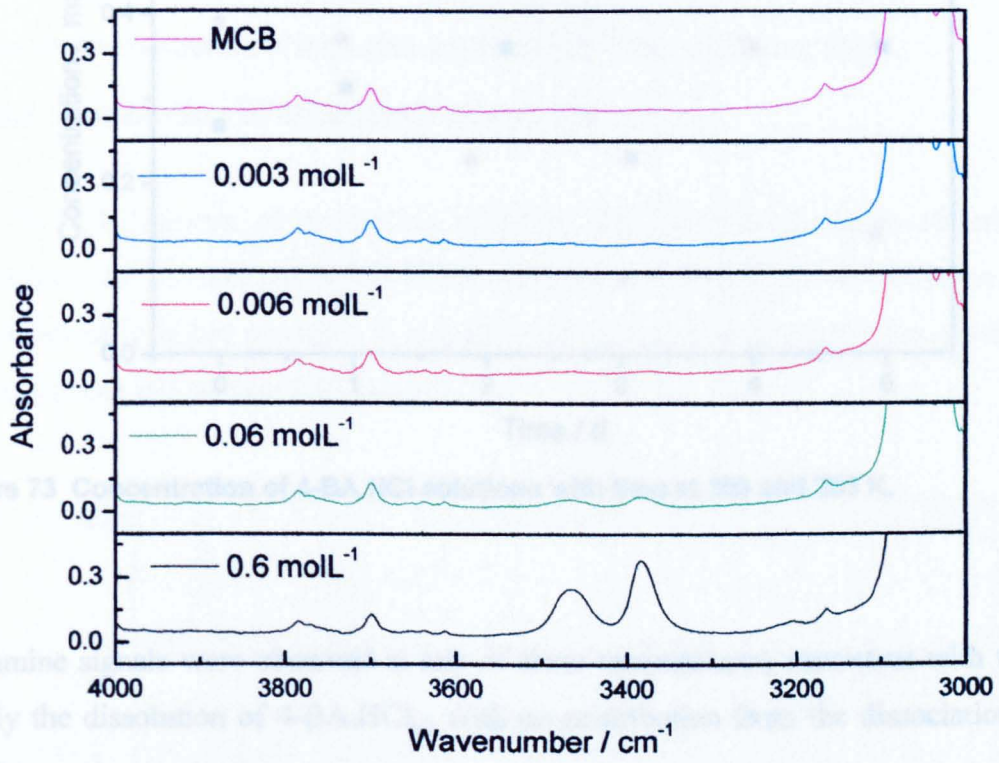

Figure 72 FTIR spectra of 4-BA solutions

3.3.6.4 Dissolution of 4-BA.HCl in chlorobenzene

The concentration of 4-BA.$HCl_{(solv)}$ in chlorobenzene was determined at three temperatures, 293, 303, 323 K (Figure 73 and Figure 74). The solutions were stirred and six samples were taken over a period of 5 days for the 293 and 303 K experiments, and over 6 and 3 hours at 323 and 333 K respectively. The samples were analysed by ^1H NMR and the concentrations determined, Table 25.

Temperature (K)	Mean concentration (mmol L^{-1})	Standard deviation
293	0.26	0.13
303	0.33	0.10
323	0.12	0.03
333	0.52	0.19

Table 25 Average concentrations of 4-BA.HCl in chlorobenzene.

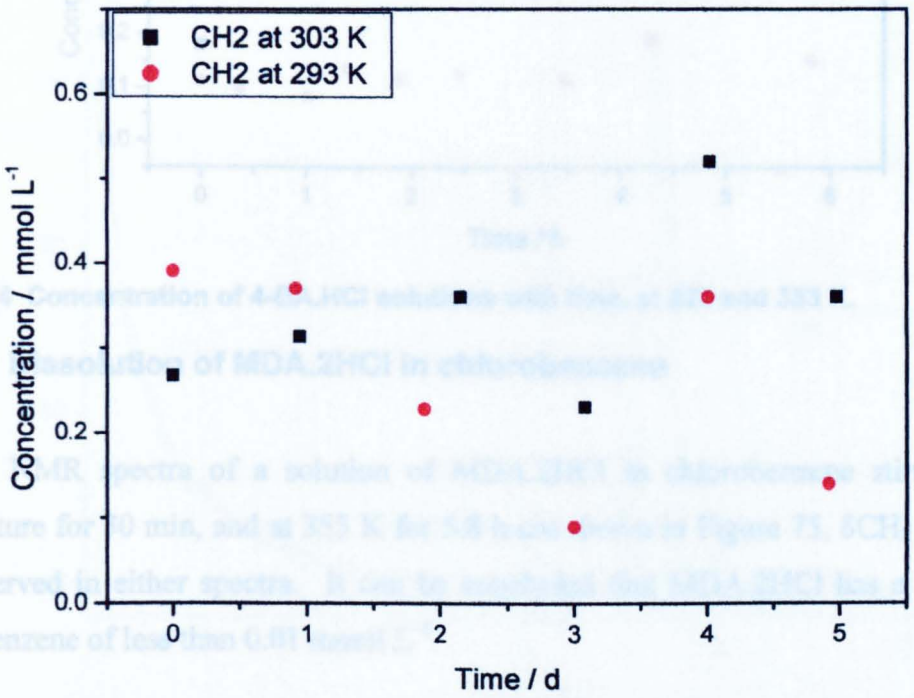

Figure 73 Concentration of 4-BA.HCl solutions with time at 293 and 303 K.

No amine signals were observed at any of these temperatures, consistent with this being purely the dissolution of 4-BA.$HCl_{(s)}$ with no contribution from the dissociation to form 4-$BA_{(solv)}$.

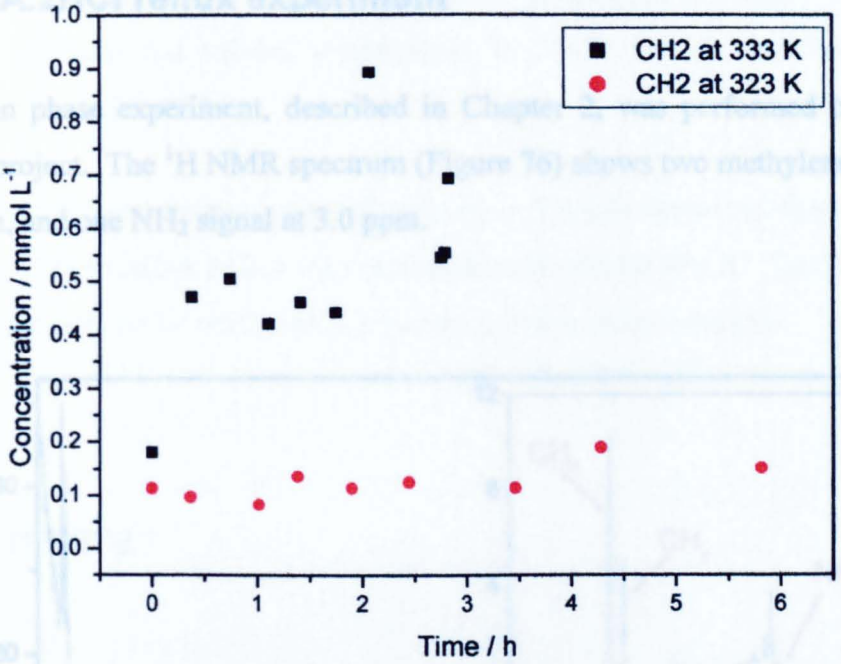

Figure 74 Concentration of 4-BA.HCl solutions with time, at 323 and 333 K.

3.3.6.5 Dissolution of MDA.2HCl in chlorobenzene

The ^{1}H NMR spectra of a solution of MDA.2HCl in chlorobenzene stirred at room temperature for 30 min, and at 355 K for 5.8 h are shown in Figure 75, δCH_2 or δNH_2 are not observed in either spectra. It can be concluded that MDA.2HCl has a solubility in chlorobenzene of less than 0.01 mmol L^{-1}.

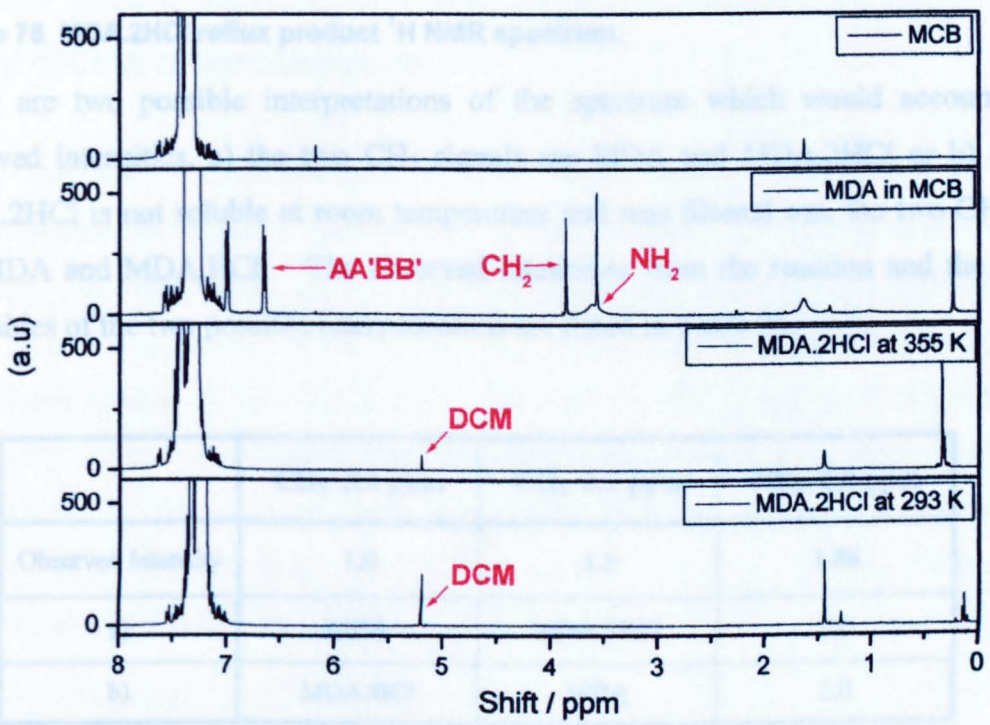

Figure 75 ^{1}H NMR spectra of MDA and MDA.2HCl in chlorobenzene.

3.3.7 MDA.2HCl reflux experiment

One solution phase experiment, described in Chapter 2, was performed on MDA.2HCl during this project. The ^{1}H NMR spectrum (Figure 76) shows two methylene signals at 3.4 and 3.1 ppm, and one NH_2 signal at 3.0 ppm.

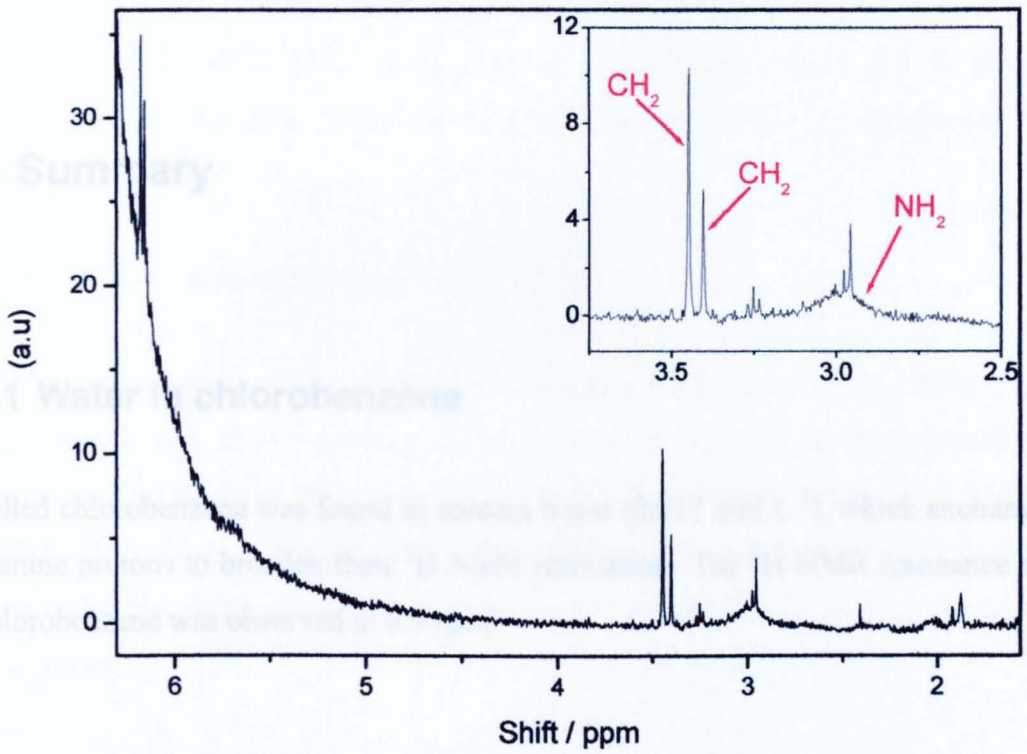

Figure 76 MDA.2HCl reflux product ^{1}H NMR spectrum.

There are two possible interpretations of the spectrum which would account for the observed intensities, a) the two CH_2 signals are MDA and MDA.2HCl or b) assuming MDA.2HCl is not soluble at room temperature and was filtered out, the two CH_2 signals are MDA and MDA.HCl. The observed intensities from the reaction and the expected intensities of the two possible interpretations are listed in Table 26.

	CH_2 3.4 ppm	CH_2 3.1 ppm	NH_2 3.0 ppm
Observed Intensity	1.0	1.5	1.88
a)	MDA	MDA.2HCl	2.0
b)	MDA.HCl	MDA	2.0

Table 26 ^{1}H NMR intensities of MDA.2HCl reflux experiment.

At this time it is impossible to determine which assignment is correct. Further work is needed to calibrate the solvent suppression ^{1}H NMR for all three products, MDA, MDA.2HCl and MDA.HCl.

The TGA results (previously described in Section 3.3.3.4) show that thermal dissociation of the solid to form MDA.HCl occurs at temperatures above 473 K. Therefore, the results of this experiment can be attributed to a purely solution phase reaction.

3.4 Summary

3.4.1 Water in chlorobenzene

Distilled chlorobenzene was found to contain water (0.017 mol L^{-1}), which exchanges with the amine protons to broaden their ^{1}H NMR resonance. The ^{1}H NMR resonance of water in chlorobenzene was observed at 0.9 ppm.

3.4.2 HCl in chlorobenzene

HCl dissolves in chlorobenzene, as a non-ideal solute. Dissolution of $HCl_{(g)}$ in chlorobenzene is not easy, requiring 30 min to saturate a solution by bubbling the gas through, an overpressure of HCl above chlorobenzene does not allow dissolution of the gas. The FTIR frequency shifts dramatically from the gas phase to the dissolved state, in agreement with some of the literature. This shift in vibrational band and the ^{1}H NMR frequency are consistent with a solute-solvent complex, where the hydrogen of the HCl is interacting with the aromatic ring of the solvent molecule. The concentration of HCl in MCB was determined from ^{1}H NMR to be 0.031 mol L^{-1} with a associated water concentration of 0.014 mol L^{-1}.

3.4.3 Amines and amine hydrochlorides

3.4.3.1 Thermal stability

4-BA.HCl and MDA.2HCl are thermally unstable at temperatures well below their melting points of 501 and 533 K respectively.

4-BA.HCl loses substantial mass at temperatures above 403 K through loss of complete 4-BA.HCl units. MDA.2HCl loses mass at temperatures above 373 K through the vapourisation of complete MDA.2HCl units, but above 473 K dissociates to form MDA.HCl.

3.4.3.2 ^{1}H NMR spectroscopy

^{1}H NMR spectroscopy of the MDA series of compounds dissolved in DMSO, show the CH_2, aromatic and amine protons are diagnostic of the extent of hydrochlorination. However, 1:1 mixtures of MDA and MDA.2HCl were indistinguishable from MDA.HCl. ^{1}H NMR spectroscopy of 4-BA and 4-BA.HCl solutions in DMSO show that the CH_2 signals are do not change upon hydrochlorination, however, the amine and aromatic signals are diagnostic.

^{1}H NMR spectroscopy is a useful tool to check sample integrity. Samples were found to age over a two week period. The ^{1}H NMR spectrum of an aged sample has signals which have shifted to lower frequency consistent with the loss of HCl.

3.4.3.3 Solubility of amines and amine hydrochlorides in MBC

Compound	Saturation concentration in chlorobenzene (mol L^{-1})	Temperature (K)
4-BA	4.722 ± 0.034	298
MDA	0.138 ± 0.007	298
4-BA.HCl	$0.31 \times 10^{-3} \pm 0.11 \times 10^{-3}$	Below 333
MDA.2HCl	$< 0.01 \times 10^{-3}$	Below 355

Table 27 Summary of saturation concentrations of 4-BA, MDA, 4-BA.HCl and MDA.2HCl in chlorobenzene.

Chapter 4

Crystal Structures and Lattice Energies

4 Crystal Structures and Lattice Energies

The crystal structures of 4-benzylaniline (4-BA), methylene dianiline (MDA), 4-benzylaniline hydrochloride (4-BA.HCl), methylene dianiline dihydrochloride (MDA.2HCl) and a basic hydrochloride of methylene dianiline (3MDA.2HCl.H_2O) have been determined. The preparation of the crystals was described in Chapter 2. The results of each crystal structure determination have been used to calculate the lattice energy of each compound. In the case of the basic salt, formally 3MDA.2HCl.H_2O but in fact $[MDAH_2]^{2+}.2Cl^-.2MDA.H_2O$, this calculation is considered to be an approximation.

4.1 Crystallography

The five crystal structures were obtained at Glasgow using a Nonius Kappa CCD diffractometer equipped with an Oxford Cryostream cryostat. Refinement was carried out using WinGX and SHELXL97 software (see Chapter 2). Table 28 summarises the crystallographic data and structure refinements for each of the five compounds. Hydrogen atom positions were refined only for those hydrogen atoms attached to nitrogen and also, in the case of the basic salt 3MDA.2HCl.H_2O, to the water oxygen atom. The determination of these crystal structures was performed with the help and guidance of Dr K.W. Muir.[101]

A search of the Cambridge Structural Database, Version 5.28 of November 2006,[102, 103] for molecular fragments similar to Figure 77 found 64 compounds containing this motif. The structure of MDA at room temperature has been previously published;[104] comparison of our MDA structure with the published data is discussed below. One compound found which contained molecules of MDA H-bonded to Cl^- ions was tris(4,4'-diaminodiphenylmethane)-sodium chloride.[105, 106] In this compound one proton of each amine was reported to be weakly H-bonded to a Cl^- ion, resulting in each Cl^- being H-bonded to six different MDA molecules. Similarly, each Na^+ ion was reported to be coordinated to six different MDA molecules through an interaction with the lone pairs of the nearest N atom. The majority of the search results were large, multi-ringed compounds where the nitrogen atoms of the MDA motif were secondary amines, as in the case of bis(4-(2-pyridylmethylamino)phenyl)methane,[107] and not of direct relevance to this work.

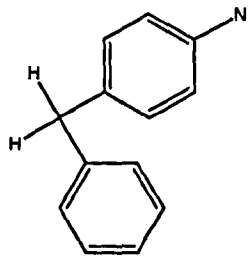

Figure 77 Molecular fragment sought in the CSD.

Identification code	4-BA	MDA	4-BA.HCl	MDA.2HCl	3MDA.2HCl. H_2O
Empirical formula	$C_{13}H_{13}N$	$C_{13}H_{14}N_2$	$C_{13}H_{14}ClN$	$C_{13}H_{16}Cl_2N_2$	$C_{39}H_{46}Cl_2N_6O$
Formula weight	183.24	198.26	219.70	271.18	685.72
Temperature /K	150	150	120	150	120
Crystal system	Monoclinic	Orthorhombic	Monoclinic	Monoclinic	Monoclinic
Space group	$P2_1/c$	$P2_12_12_1$	$P2_1/n$	$P2/n$	$C2$
a /Å	9.5107(5)	5.9003(5)	5.5504(2)	6.0828(9)	25.6208(5)
b /Å	11.0673(6)	9.5998(10)	22.0930(8)	4.5346(9)	5.7067(2)
c /Å	10.0425(6)	19.1346(15)	9.7906(4)	24.586(5)	13.7826(5)
β /°	108.888(2)	90	106.436(1)	90.694(12)	118.962(1)
V /Å^3	1000.1(1)	1083.8(2)	1151.51(8)	678.1(2)	1763.1(1)
Z	4	4	4	2	2
ρ(calc) /g cm^{-3}	1.217	1.215	1.267	1.328	1.292
μ /mm^{-1}	0.071	0.073	0.297	0.459	0.225
F(000)	392	424	464	284	728
Crystal size /mm	0.65 x 0.57 x 0.28	0.40 x 0.15 x 0.08	0.53 x 0.25 x 0.10	0.50 x 0.30 x 0.05	0.56 x 0.25 x 0.20
θmax /°	27.5	27.5	27.2	25.1	30.5
Index ranges	-11≤h≤12 -12≤k≤14 -13≤l≤9	-7≤h≤7 -12≤k≤8 -24≤l≤19	-7≤h≤6 -24≤k≤28 -12≤l≤10	-7≤h≤7 -5≤k≤5 -29≤l≤29	-36≤h≤36 -8≤k≤8 -19≤l≤19
No measured	11276	6216	12278	7360	15531
No unique, Rint	2265, 0.106	1427, 0.080	2504, 0.048	1194, 0.104	5192, 0.047
No observed [I>2σ(I)]	1739	924	1964	776	4851
Completeness to θmax %	98.7	97.4	97.5	98.0	98.6
Absorption correction	None	Empirical	Empirical	Empirical	Empirical
Tmax, Tmin	-	1.066, 0.918	0.971 and 0.715	1, 0.626	0.956, 0.745
Data / Parameters	2265 / 135	1427 / 152	2504 / 148	1194 / 90	5192 / 250
Goodness-of-fit on F^2	1.075	1.055	1.011	1.085	1.031
R1, wR2 [I>2σ(I)]	0.058, 0.127	0.059, 0.098	0.036, 0.076	0.071, 0.120	0.037, 0.082
R1, wR2 (all data)	0.081, 0.139	0.114, 0.110	0.055, 0.082	0.125, 0.136	0.042, 0.083
Δρ(max), Δρ(min) /eÅ^{-3}	0.30, -0.23	0.16, -0.18	0.29, -0.23	0.37 -0.45	0.30, -0.23

Table 28 Crystal data and structure refinements.

4.1.1 4-Benzylaniline (4-BA)

4-Benzylaniline (4-BA) (Figure 78) formed monoclinic crystals in space group $P2_1/c$, Table 28.

The atom numbering shown for 4-BA is consistent with that used for the other structures: each carbon atom in the n = 1 or 2 aromatic rings is numbered sequentially Cn1 – Cn6 starting at the CH_2-substituted atom; for example, C21 denotes the aromatic carbon of ring 2 bonded to the methylene carbon, C1.

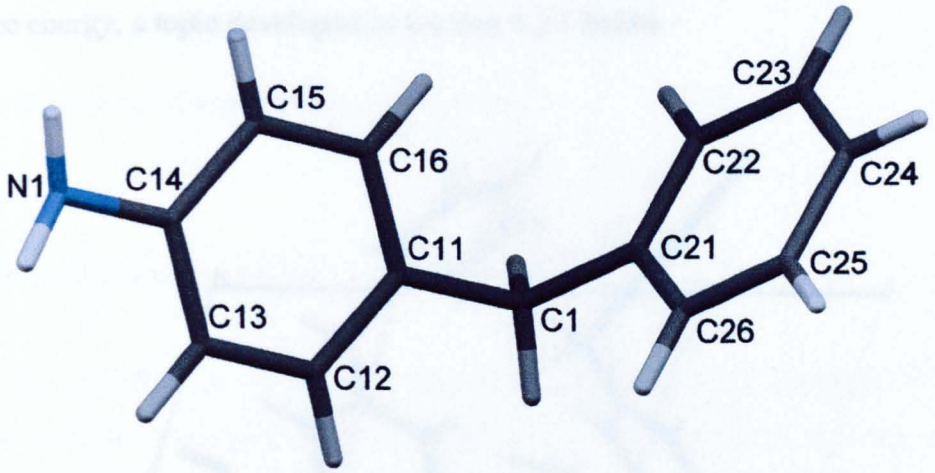

Figure 78 4-BA.

4.1.1.1 Structure refinement

For this crystal the ratio of unique reflections to refined parameters is 16.8 and there are over 83.8 reflections per atom. As discussed in Chapter 1, a ratio of reflections to parameters of 6 - 20 is expected to give reliable parameters for each atom[40] and 50 – 100 or more reflections per atom are ample for precise structure determinations.[42] The crystal structure has an R-factor of 0.058, indicating an acceptable structure refinement, and function values in the final difference electron density synthesis, $\Delta\rho$, are insignificant, lying between -0.23 and 0.30 e $Å^{-3}$ (Table 28).[40] No absorption correction was required as the crystal contained no heavy atoms such as Cl which would absorb X-rays more strongly than carbon, hydrogen or nitrogen atoms.[40]

4.1.1.2 Crystal packing and intermolecular bonding

The unit cell (Figure 79) contains four complete 4-BA molecules. No conventional H-bonds were detected in this crystal structure using the PLATON validation software.[74] This program checks for atoms closer than the sum of their van der Waals radii, which would indicate a significant intermolecular interaction. The shortest Cg…Cg (centroid…centroid) contact between aromatic rings of the stacked molecules is 4.84 Å, rather longer than the optimum π-π stacking distance between rings of 3 – 4 Å.[108] The shortest C-H…Cg and N-H…Cg distances are 2.80 and 3.01(3) Å (see Table 35 below). The significance of such contacts is best considered in the light of their contribution to the total lattice energy, a topic developed in Section 4.2.1 below.

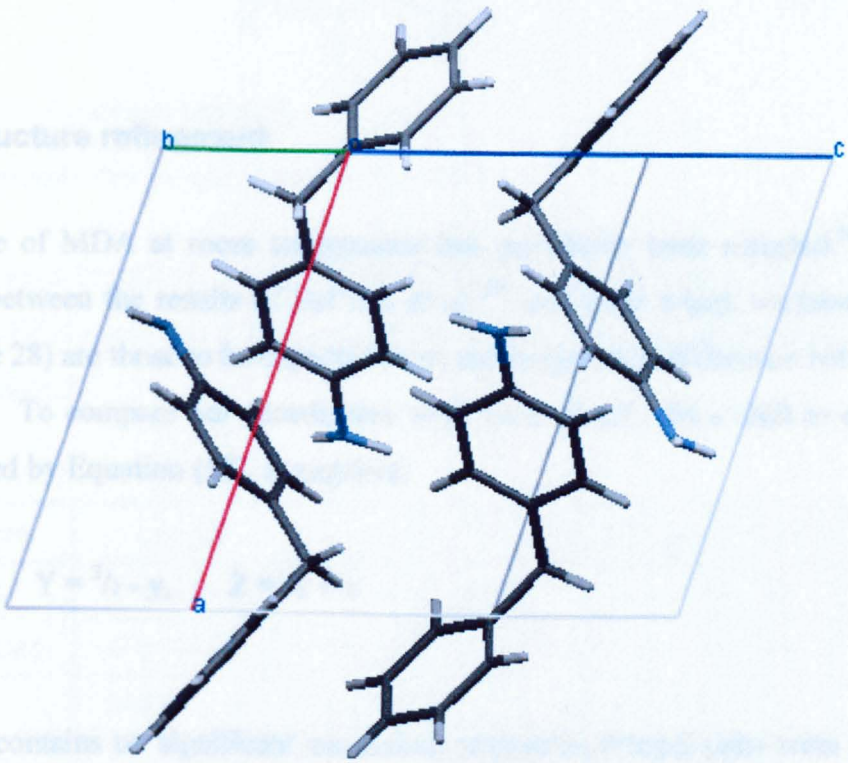

Figure 79 Contents of the 4-benzylaniline unit cell.

4.1.2 MDA

Methylene dianiline (MDA) was found to have a different type of crystal structure from 4-benzylaniline (4-BA) with stronger intermolecular interactions. Four symmetrically identical MDA molecules occupy an orthorhombic cell in the non-centrosymmetric space

group $P2_12_12_1$. This is the only non-monoclinic crystal in this series of compounds. The labelling of the atoms is similar to that of 4-BA and is shown in Figure 80.

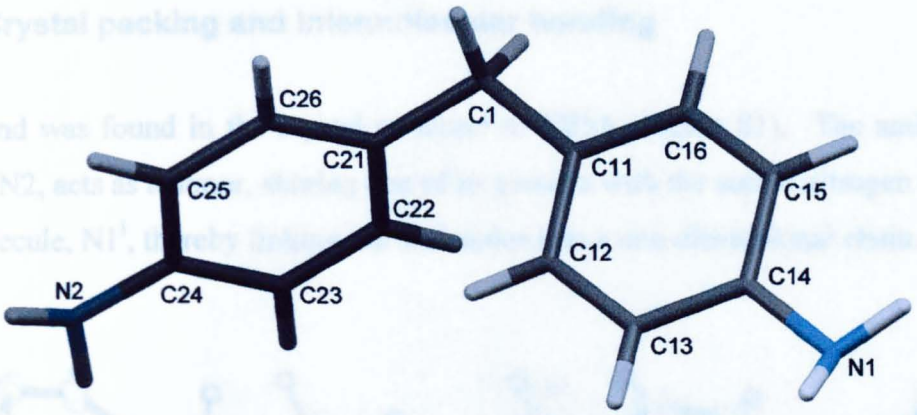

Figure 80 MDA molecule showing labelled atoms.

4.1.2.1 Structure refinement

The structure of MDA at room temperature has previously been reported.[104] The slight differences between the results of Bel'skii *et al.*[104] and those which we have obtained at 150 K (Table 28) are those to be expected from the temperature difference between the two experiments. To compare our coordinates with those of ref. 104 a shift to an equivalent origin, defined by Equation (58), is required.

$$X = \tfrac{1}{2} - x, \qquad Y = \tfrac{3}{2} - y, \qquad Z = \tfrac{1}{2} + z \tag{58}$$

Since MDA contains no significant anomalous scatterers, Friedel pairs were averaged. In consequence, the analysis has a ratio of unique reflections to refined parameters of only 9.4 and just under 50 reflections per atom. In spite of the crystal containing no heavy atoms which would significantly absorb X-rays, an empirical absorption correction was carried out. This was performed as the crystal was plate-like in shape, and the extent of absorption of X-rays would be greater through the length of the crystal, producing weaker reflections, than through the thin width of the crystal.[40] Extreme function values in the final difference electron density synthesis, $\Delta\rho$, are about half those of 4-BA, having values between -0.18 and 0.16 e $Å^{-3}$ (Table 28). Non-centrosymmetric space groups tend to give rise to flatter final difference maps, at least partly because of minor errors in the phases which are not

restricted, as in the centrosymmetric case, to values of 0 or 180°. The refined structure of MDA, however, has an acceptable R-factor of 0.059.

4.1.2.2 Crystal packing and intermolecular bonding

One H-bond was found in the crystal structure of MDA (Figure 81). The amine of one molecule, N2, acts as a donor, sharing one of its protons with the amine nitrogen of another MDA molecule, $N1^{i}$, thereby linking the molecules into a one-dimensional chain.

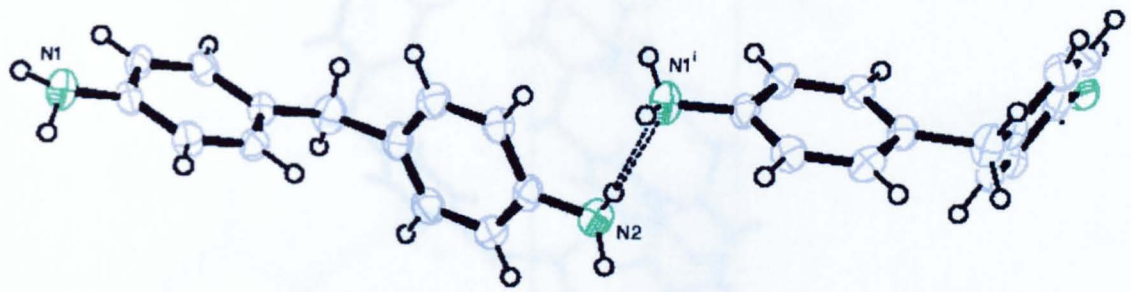

Figure 81 MDA showing H-bonding,

Drawn with thermal ellipsoids with probabilities of 50%.

The H-bond has a length, H...A, of 2.29(4) Å, a D...A distance of 3.172(5) Å and a DHA angle of 165(3)° making this a moderate-to-weak interaction using the criteria of Jeffrey [44] outlined in Table 29.

Strength	Length	H...A (Å)	D...A (Å)	Angle <DHA
Strong	D-H~H...A	1.2 – 1.5	2.2 – 2.5	175 – 180
Moderate	D-H < H...A	1.5 – 2.2	2.5 – 3.2	130 – 180
Weak	D-H < H...A	2.2 – 3.3	3.2 – 4.0	90 - 150

Table 29 Summary of H-bond types. Donor (D) and acceptor (A) atoms are either N or O.44

As shown in Figure 82 the unit cell contains four complete MDA molecules and the H-bonding forms one-dimensional chains of MDA molecules. Due to misalignment of the aromatic rings of adjacent chains the shortest Cg...Cg distance indicative of π-π stacking is 5.0 Å. There are also significant X-H...Cg interactions (see Table 34). The contributions which these interactions make to the lattice energy are presented in the discussion of Table 38 (see below).

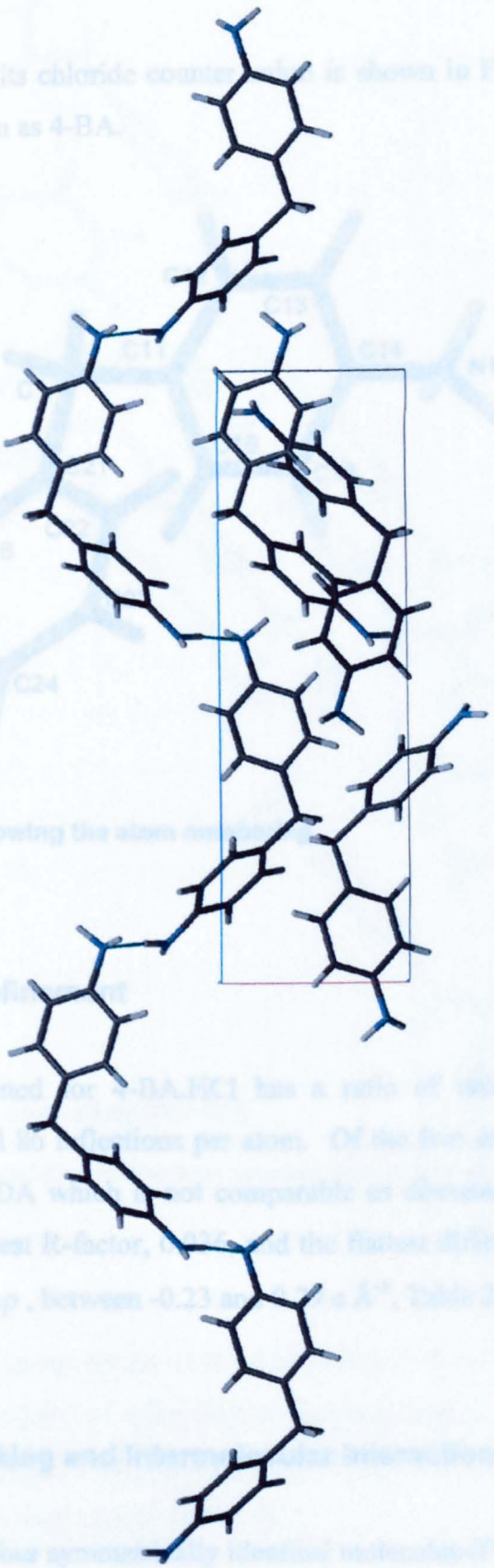

Figure 82 MDA unit cell viewed along the crystallographic b-axis.

4.1.3 4-BA.HCl

The 4-BA cation with its chloride counter anion is shown in Figure 83. Atom labelling follows the same system as 4-BA.

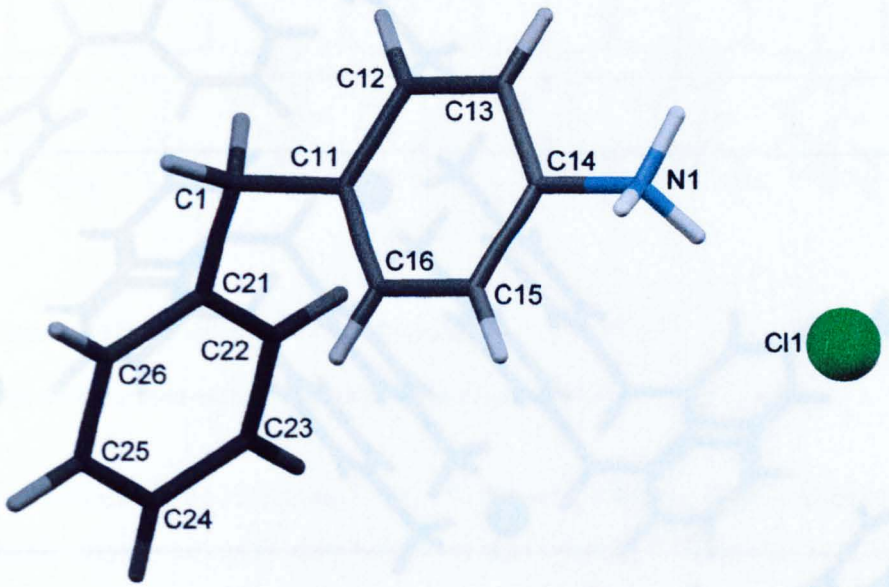

Figure 83 4-BA.HCl showing the atom numbering.

4.1.3.1 Structure refinement

The structure determined for 4-BA.HCl has a ratio of unique reflections to refined parameters of 16.9 and 86 reflections per atom. Of the five structures determined in this project, apart from MDA which is not comparable as discussed above (Section 4.1.2.1), 4-BA.HCl has the lowest R-factor, 0.036, and the flattest difference electron density map with function values, $\Delta\rho$, between -0.23 and 0.29 e $Å^{-3}$, Table 28.

4.1.3.2 Crystal packing and intermolecular interactions

The unit cell contains four symmetrically identical molecules (Figure 84).

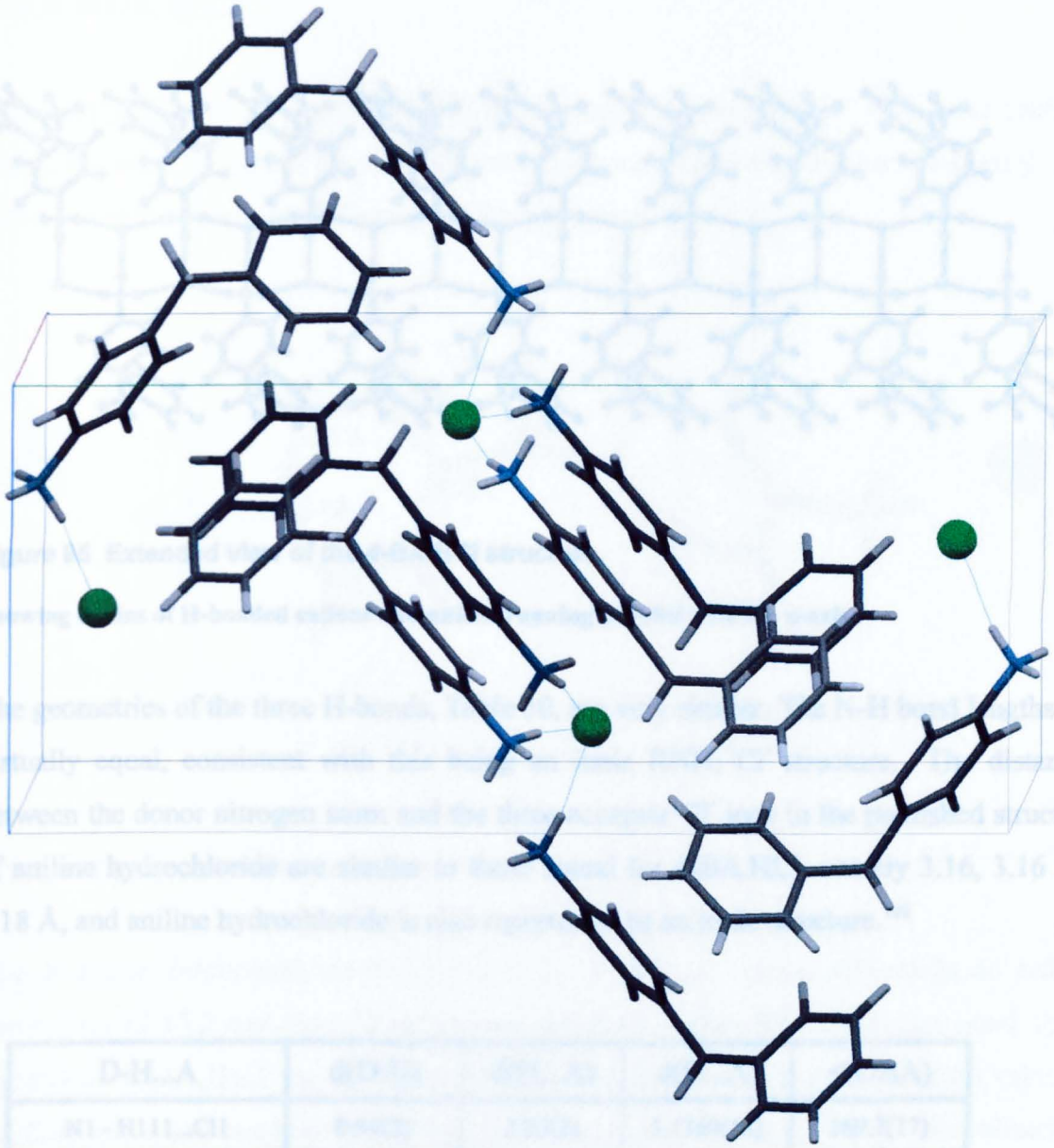

Figure 84 A view of the unit cell of 4-BA.HCl.

Illustrating the hydrogen-bonding interactions between the amines and chloride counter-ions.

Each N-H of the NH_3^+ group forms an H-bond with a different Cl^- anion, forming a ladder structure, which holds chains of 4-BA.HCl molecules together. This results in channels of ionic, hydrophilic, regions running through the structure, with channels of hydrophobic character on either side, as shown in Figure 85.

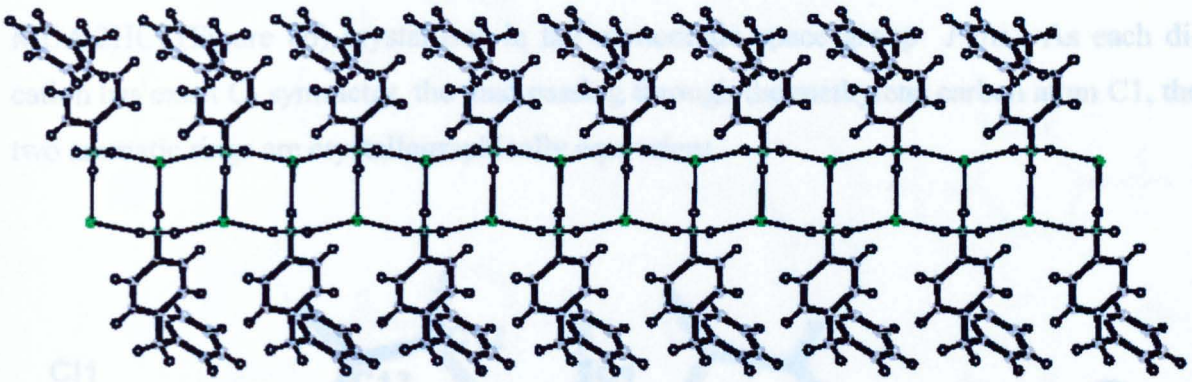

Figure 85 Extended view of the 4-BA.HCl structure.

Showing chains of H-bonded cations and anions running parallel with the a-axis.

The geometries of the three H-bonds, Table 30, are very similar. The N-H bond lengths are virtually equal, consistent with this being an ionic $RNH_3^+Cl^-$ structure. The distances between the donor nitrogen atom and the three acceptor Cl^- ions in the published structure of aniline hydrochloride are similar to those found for 4-BA.HCl, namely 3.16, 3.16 and 3.18 Å, and aniline hydrochloride is also reported to be an ionic structure.[109]

D-H...A	d(D-H)	d(H...A)	d(D...A)	<(DHA)
N1 - H111...Cl1	0.94(2)	2.20(2)	3.1369(15)	169.7(17)
N1 - H113...Cl1^{i}	0.93(2)	2.24(2)	3.1603(15)	168.6(16)
N1 - H112...Cl1^{ii}	0.90(2)	2.29(2)	3.1571(15)	163.1(16)

Table 30 Summary of H-bonding in 4-BA.HCl, (Å & °). Symmetry code: (i) –x+1, -y, -z+1; (ii) -x+2, -y, -z+1.

The shortest Cg...Cg distance between aromatic rings is 3.99 Å, implying that π-π stacking makes a significant contribution to lattice stabilisation. There are also important X-H...Cg interactions which are presented in Table 35 (Section 4.1.6). The relative importance of dispersion and electrostatic contributions to the lattice energy is considered in Section 4.2.2.

4.1.4 MDA.2HCl

MDA.2HCl (Figure 86) crystallises in the monoclinic space group *P2/n*. As each di-cation has exact C_2 symmetry, the diad passing through the methylene carbon atom C1, the two aromatic rings are crystallographically equivalent.

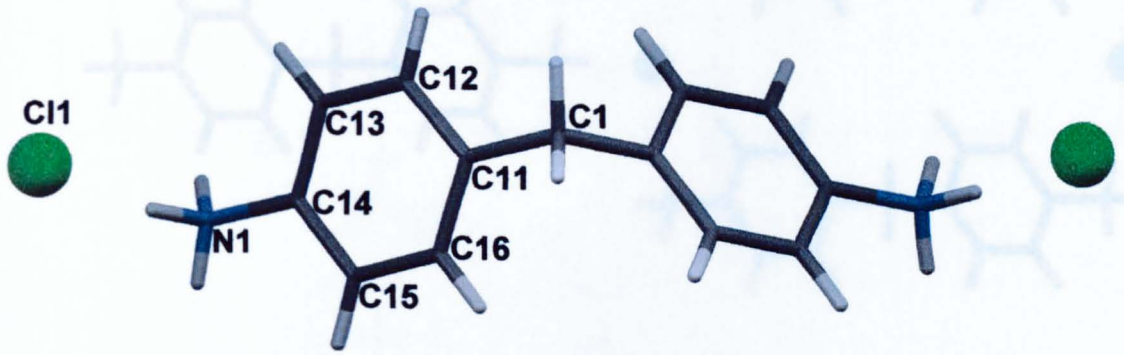

Figure 86 MDA.2HCl.

4.1.4.1 Structure refinement

The structure determined for MDA.2HCl has a ratio of unique reflections to refined parameters of 13.3 and over 72 reflections per atom (Table 28). Obtaining good single crystals for MDA.2HCl was difficult and, with an R-factor of 0.071 and function values in the final difference electron density synthesis between -0.45 and 0.37 e $Å^{-3}$, the refinement is the least satisfactory of the five compounds analysed.

4.1.4.2 Crystal packing and intermolecular interactions

The unit cell contains two $MDAH_2^{2+}$ di-cations and four chloride anions (Figure 87). As there is a Cg...Cg distance between stacked rings of 4.85 Å, π-π interactions are significant in this structure; the optimum distance between rings for this type of interaction is 3 – 4 Å.[108] There are no short X-H...Cg interactions (Table 34) and hydrogen bonding makes a larger contribution than dispersion effects to the lattice energy (see Table 40 below).

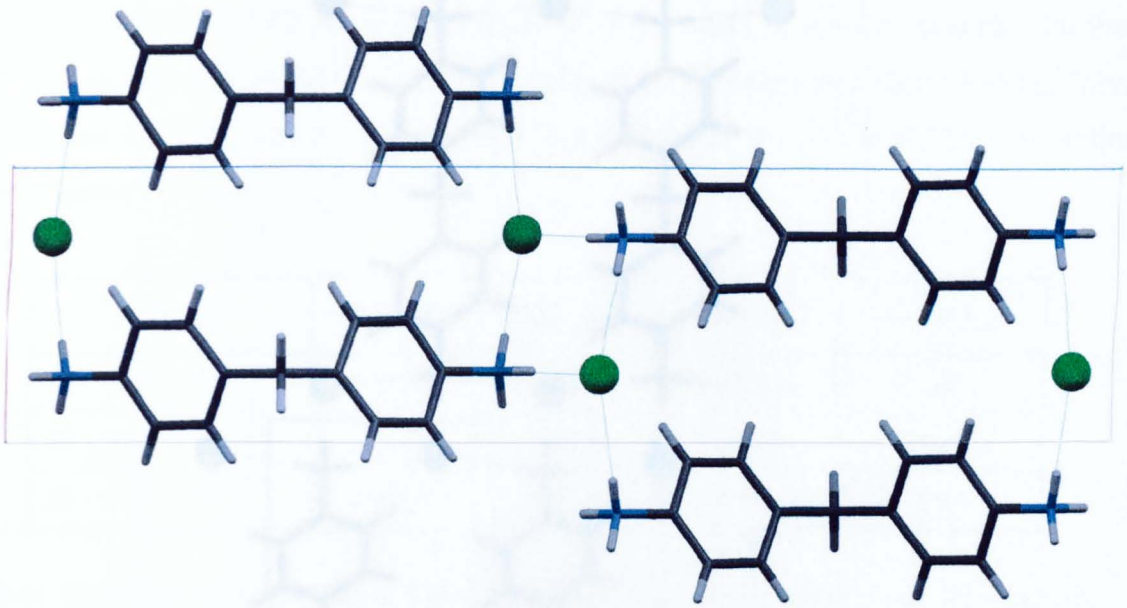

Figure 87 MDA.2HCl packing diagram.

Illustrating the chloride H-bonded ladder, viewed along the short crystallographic *b*-axis of 4.5 Å.

H-bonding thus plays an important role in this structure (Figure 87). Each N-H bond of the cation donates a proton to a different Cl^- anion, resulting in ladders of H-bonds at both ends of the MDA cations and the production of a coordination framework. The extended H-bonding structure is more clearly shown in Figure 88. A summary of these interactions is given in Table 31.

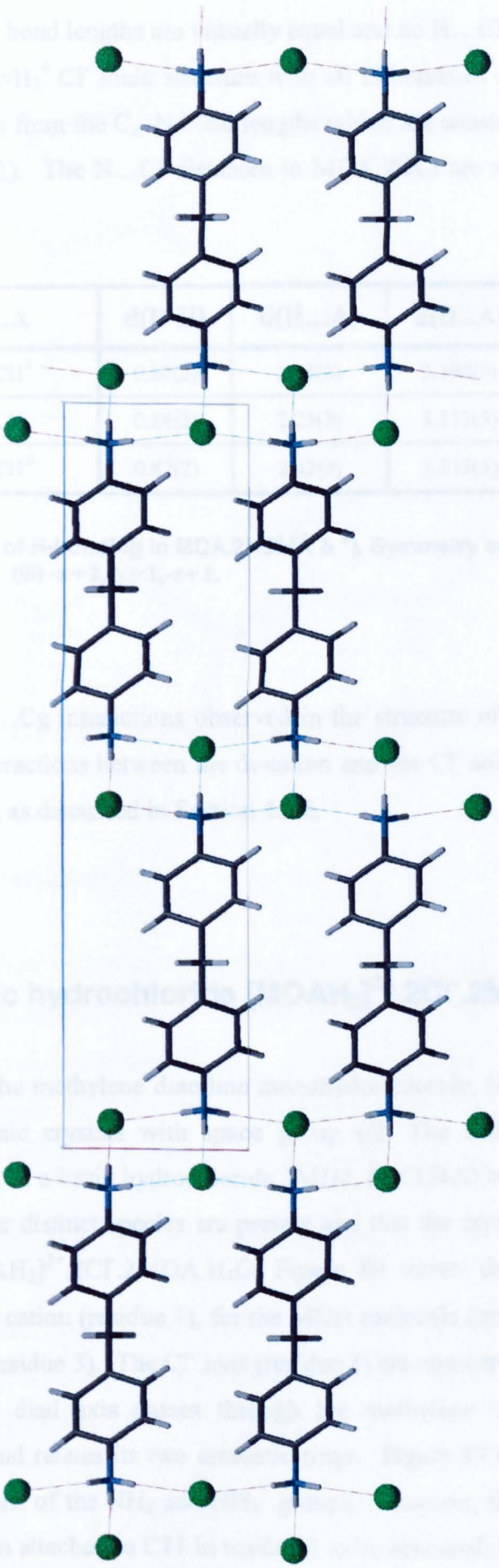

Figure 88 Extended view of H-bonding in MDA.2HCl.

Since all three N-H bond lengths are virtually equal and no H...Cl distance is exceptionally short, this is an $RNH_3^+ Cl^-$ ionic structure with all H-bonds of similar strength. Further confirmation comes from the C_{ar}-N bond lengths which are consistent with a C-NH_3^+ bond (see Section 4.1.6.1). The N...Cl distances in MDA.2HCl are similar to those of aniline hydrochloride.[109]

D-H...A	d(D-H)	d(H...A)	d(D...A)	<(DHA)
N1 - H1N...Cl1^{ii}	0.87(2)	2.35(2)	3.190(5)	164(5)
N1 - H2N...Cl1	0.88(2)	2.25(2)	3.113(5)	165(5)
N1 - H3N...Cl1^{iii}	0.87(2)	2.42(3)	3.233(5)	156(6)

Table 31 Summary of H-bonding in MDA.2HCl (Å & °). Symmetry code: (i) -x+3/2,y,-z+1/2; (ii) -x+1,-y+1,-z+1; (iii) -x+2,-y+1,-z+1.

There are no X-H...Cg interactions observed in the structure of MDA.2HCl, as listed in Table 35. The interactions between the di-cation and the Cl^- anions play a crucial role in lattice stabilisation, as discussed in Section 4.2.2.

4.1.5 The basic hydrochloride $[MDAH_2]^{2+}.2Cl^-.2MDA.H_2O$

Crystallisation of the methylene dianiline monohydrochloride, MDA.HCl, from methanol produced monoclinic crystals with space group *C*2. The composition of the crystals corresponds to that of a basic hydrochloride 3MDA.2HCl.H_2O but the diffraction analysis establishes that four distinct species are present and that the crystal is best represented by the formula $[MDAH_2]^{2+}.2Cl^-.2MDA.H_2O$. Figure 89 shows the atom labelling for the diprotonated MDA cation (residue 1), for the MDA molecule (residue 2) and for the water of crystallisation (residue 3). The Cl^- ions (residue 4) are numbered as shown in Figure 91. A crystallographic diad axis passes through the methylene carbon atom C21 of the $MDAH_2^{2+}$ cation and relates its two aromatic rings. Figure 89 is designed to show most clearly the hydrogens of the NH_2 and NH_3^+ groups. However, this has caused the second methylene hydrogen attached to C11 in residue 1 to be obscured; this hydrogen is visible in Figure 91.

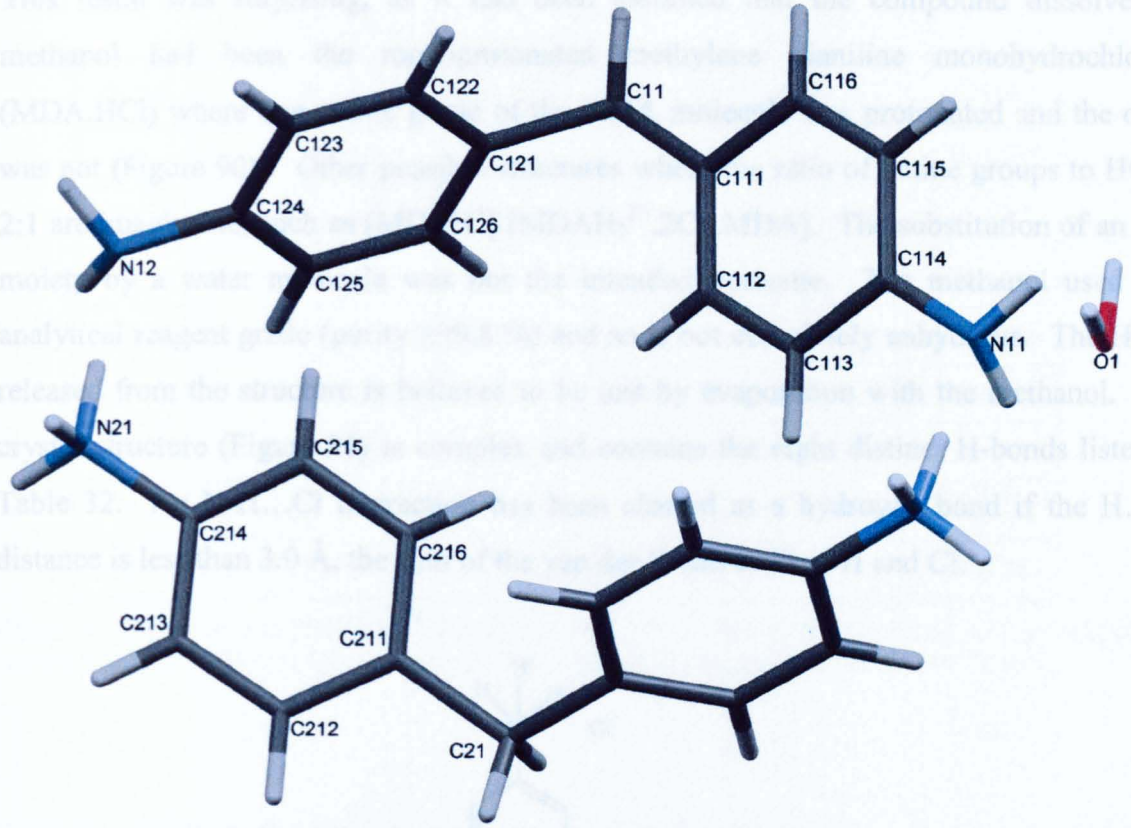

Figure 89 $[MDAH2]^{2+}.2Cl^{-}.2MDA.H_2O$ showing atom numbering.

4.1.5.1 Structure refinement

A satisfactory structure refinement was obtained, with an R-factor of 0.037 and function values in the final difference electron density synthesis, $\Delta\rho$, between -0.23 and 0.30 e $Å^{-3}$. The crystal permitted collection of data to high resolution, θ(Mo-Kα) $\leq$ 30.5°. In consequence, the ratio of the number of unique reflections to parameters is 20.8, substantially higher than for the other four structures determined.

4.1.5.2 Crystal packing and intermolecular interactions

For each di-protonated MDA cation in the unit cell there are two molecules of MDA, one molecule of water and two Cl^- ions. This corresponds to the reaction between MDA.HCl and water shown in Equation (59).

$$3MDA.HCl_{(s)} + H_2O \longrightarrow [MDA.2HCl + 2MDA + H_2O]_{(s)} + HCl_{(g)} \quad (59)$$

This result was surprising, as it had been assumed that the compound dissolved in methanol had been the monoprotonated methylene dianiline monohydrochloride (MDA.HCl) where one amine group of the MDA molecule was protonated and the other was not (Figure 90). Other possible structures where the ratio of amine groups to HCl is 2:1 are imaginable, such as $[MDAH^+].[MDAH_2^{2+}.2Cl^-.MDA]$. The substitution of an HCl moiety by a water molecule was not the intended outcome. The methanol used was analytical reagent grade (purity ≥99.8 %) and so is not completely anhydrous. The $HCl_{(g)}$ released from the structure is believed to be lost by evaporation with the methanol. The crystal structure (Figure 91) is complex and contains the eight distinct H-bonds listed in Table 32. An N-H...Cl interaction has been classed as a hydrogen bond if the H...Cl distance is less than 3.0 Å, the sum of the van der Waals radii of H and Cl.

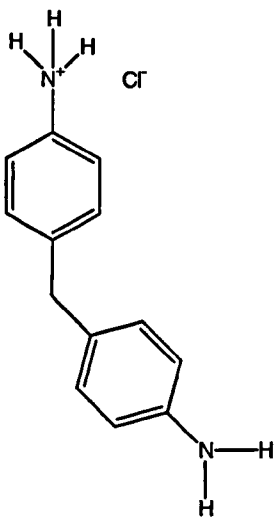

Figure 90 Proposed structure of methylene dianiline monohydrochloride (MDA.HCl).

Bond	D-H...A	d(D-H)	d(H...A)	d(D...A)	<(DHA)
1	N11 - H1B...Cl1^{ii}	0.91(2)	2.48(2)	3.3875(14)	170.2(18)
2	N12 - H1C...Cl1^{iii}	0.85(2)	2.59(2)	3.3729(14)	153.0(17)
3	N12 - H1D...Cl1^{iv}	0.88(2)	2.85(2)	3.6865(15)	157.8(15)
4	N21 - H2A...N12^{i}	0.88(2)	2.19(2)	2.9962(18)	154.0(20)
5	N21 - H2A...O1	0.88(2)	2.36(2)	2.8029(16)	111.4(17)
6	N21 - H2B...N11	0.96(2)	1.94(2)	2.8687(19)	160.9(19)
7	N21 - H2C...Cl1^{v}	0.90(2)	2.43(2)	3.1960(14)	143.3(18)
8	O1 - H1W...Cl1^{ii}	0.91(2)	2.21(2)	3.1183(11)	177.0(20)

Table 32 H-Bonding in $[MDAH_2]^{2+}.2Cl^-.2MDA.H_2O$ (Å °). Symmetry code: (i) -x+1,y,-z+2; (ii) -x+1/2,y-1/2,-z+1; (iii) -x+1/2,y+1/2,-z+2; (iv) - x+1/2,y-1/2,-z+2; (v) -x+1/2,y+1/2,-z+1.

Crystallographic diad axes pass through not only the methylene carbon atom of the di-cation, C21, but also through O1, the oxygen atom of the water molecule. Each NH_3^+ of the di-cation forms four hydrogen bonds, two of these are to neutral amine nitrogen atoms N12^i and N11, bonds 4 and 6 (Table 32) one to Cl1^v, bond 7, and one to the water O, bond 5. Bonds 4 and 5 make up a bifurcated H-bond system, also termed a three-centred H-bond, where one hydrogen atom is H-bonded to two different acceptor atoms.[110] With reference to Table 29 (Section 4.1.2.2 above) the constrained bond angle N-H...O of 111°, of bond 5, classes it as a weak H-bond.

H-bond	H...Cl (Å)	
	Min	Max
$N^+(H_2)H...Cl^-$	2.12	2.15
$N(H)H...Cl^-$	2.14	2.35
$O_wH...Cl^-$	2.13	2.40

Table 33 Average H-bond lengths to chloride anion acceptors. [44]

The two neutral amines each form an N-H...Cl H-bond, bonds 1 and 2, with lengths of 2.48 and 2.59 Å respectively, which are slightly longer than the reported range of H-bond

lengths (Table 33). The N12 atom forms a second but even longer interaction with $Cl1^{iv}$, bond 3, of 2.85 Å. The N11 atom is also H-bonded to a second Cl^- anion but this bond is not listed in Table 32 as it has a length of 3.05 Å, just greater than the sum of the van der Waals radii of H and Cl. A neutron study of bis(2-amino-2-methyl-3-butanone-oximato) nickel(II) chloride monohydrate reports NH...Cl^- bond lengths of 2.301 and 2.445 Å and bond angles of 161.9 and 174.0°.[111] Given the overestimation of the H...A distance of a H-bond determined by X-ray diffraction, with those determined by neutron diffraction (see Section 1.8.2.1) the values reported for nickel(II) chloride monohydrate are very simial to those determined for $[MDAH_2]^{2+}.2Cl^-.2MDA.H_2O$. The water oxygen accepts a H-bond from the NH_3^+ and donates one H-bond to $Cl1^{ii}$, which is also bonded to the neutral amine. This H-bond, bond 8, is of similar length to those reported in the literature (Table 33).[44]

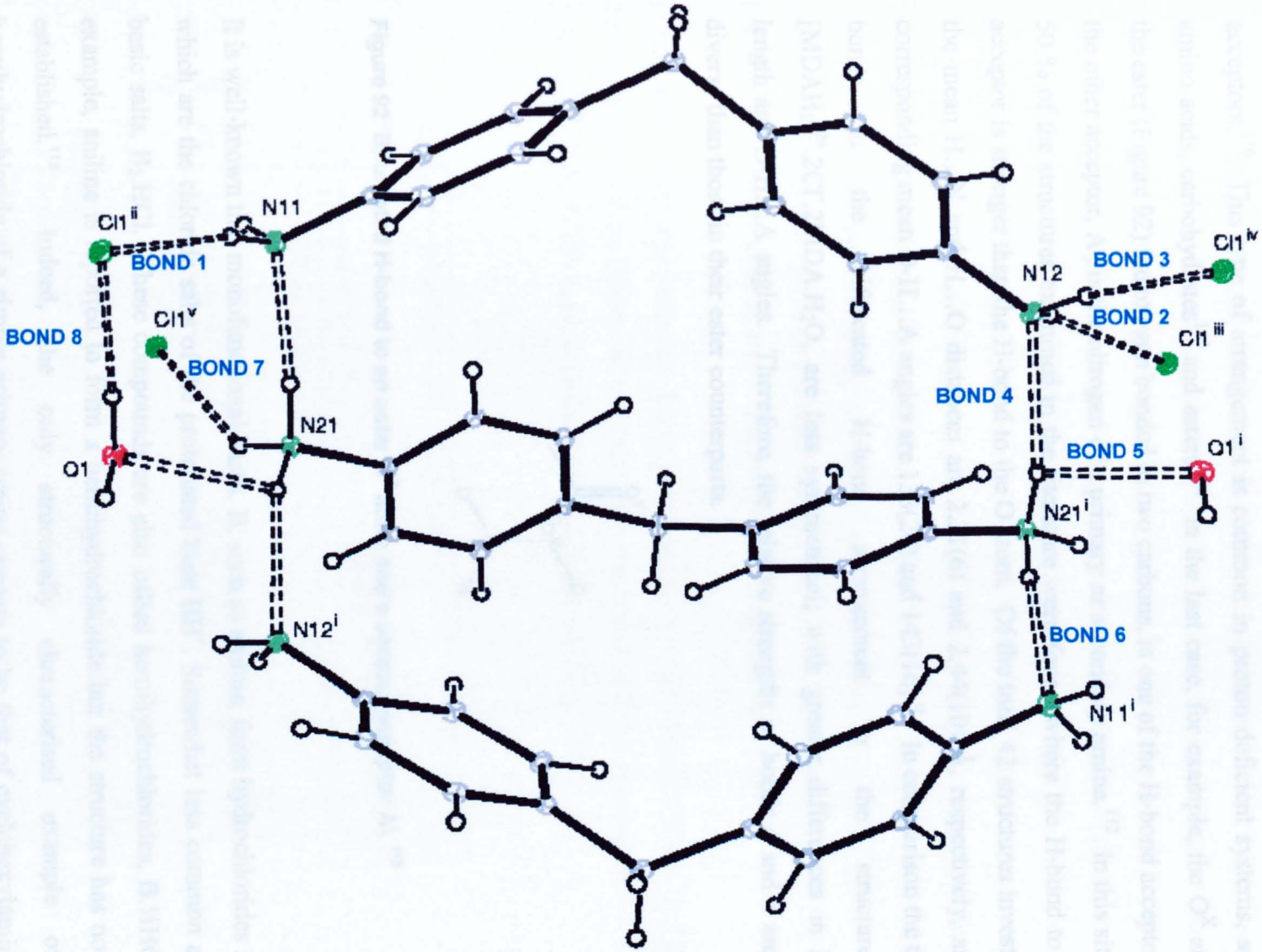

Figure 91 Structure of $[MDAH_2]^{2+}.2Cl^-.2MDA.H_2O$ showing hydrogen bonds numbered as in Table 5.

The bifurcated H-bond found in the structure of $[MDAH_2]^{2+}.2Cl^-.2MDA.H_2O$ is also known as a three-centred H-bond, where one hydrogen atom donates to two different acceptors.[110] This type of arrangement is common in proton deficient systems, such as amino acids, carbohydrates[110] and esters.[112] In the last case, for example, the O^X atom of the ester (Figure 92) the oxygen bonded to two carbons, is one of the H-bond acceptors and the other acceptor, A', is the nitrogen of a primary or secondary amine.[112] In this situation 50 % of the structures examined in the literature were found where the H-bond to the N acceptor is stronger than the H-bond to the O atom. Of the total 42 structures investigated the mean H...N and H...O distances are 2.31(6) and 2.44(10) Å, respectively, and the corresponding mean D-H...A angles are 138(20) and 143(16) °. In comparison the two H-bonds in the bifurcated H-bond arrangement in the structure of $[MDAH_2]^{2+}.2Cl^-.2MDA.H_2O$, are less symmetrical; with greater differences in H....A length and D-H...A angles. Therefore, the relative strengths of bonds 4 and 5 are more diverse than those in their ester counterparts.

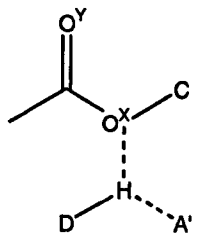

Figure 92 Bifurcated H-bond to an ester O^X atom and a second acceptor A'. [112]

It is well-known that monofunctional bases, B, such as aniline, form hydrochlorides B.HCl which are the chloride salts of the protonated base BH^+. Somewhat less common are the basic salts, B_2.HCl. These compounds are also called hemihydrochlorides, B.½HCl; for example, aniline is reported to form a hemihydrochloride but the structure has not been established.[113] Indeed, the only structurally characterised example of the hemihydrochloride of a simple primary amine appears to be that of cyclohexylamine: the structure contains equal numbers of neutral cycohexylamine molecules and cycohexylammonium chloride cation/anion pairs.[114] More complex possibilities arise for difunctional bases like MDA. The as yet unknown structure of diamino diphenylmethane monohydrochloride, MDA.HCl, could be simply the chloride salt of the monoprotonated base, i.e. $MDAH^+.Cl^-$. Alternatively, it could be $MDAH_2^{2+}.2Cl^-.MDA$. In either case N-H...N hydrogen bonding between protonated and unprotonated amine functions is feasible.

The dramatic change from diamino diphenylmethane monohydrochloride, MDA.HCl, to the resulting structure upon crystallisation, $[MDAH_2]^{2+}.2Cl^-.2MDA.H_2O$, was investigated using FTIR. Figure 93 compares the spectrum of a sample of MDA.HCl which had also been characterised by ^1H NMR, and elemental analysis with that obtained from the $[MDAH_2]^{2+}.2Cl^-.2MDA.H_2O$ crystals. The spectra are different, which means the compound originally believed to be the monoprotonated base, diamino diphenylmethane monohydrochloride (MDA.HCl) has changed on crystallisation. The MDA.HCl starting material has ν(N-H) of NH_2 at 3400 cm^{-1} and ν(N-H) of NH_3^+ at 2600 cm^{-1}, consistent with it having both NH_2 and NH_3^+ functional groups. The IR spectrum for the $[MDAH_2]^{2+}.2Cl^-.2MDA.H_2O$ crystals shows a flattened ν(N-H) for NH_3^+ which can be explained by extensive H-bonding which restricts the vibration of the NH_3^+ group. The ν(N-H) of NH_2 is also partially restricted due to some of the H atoms of the NH_2 groups being involved in H-bonding, and so smearing of this signal is also observed.

In the presence of water, diamino diphenylmethane monohydrochloride, MDA.HCl forms the observed structure (Figure 89). Water is incorporated into the structure and it forms $[MDAH_2]^{2+}.2Cl^-.2MDA.H_2O$, with the loss of HCl, see Equation (59).

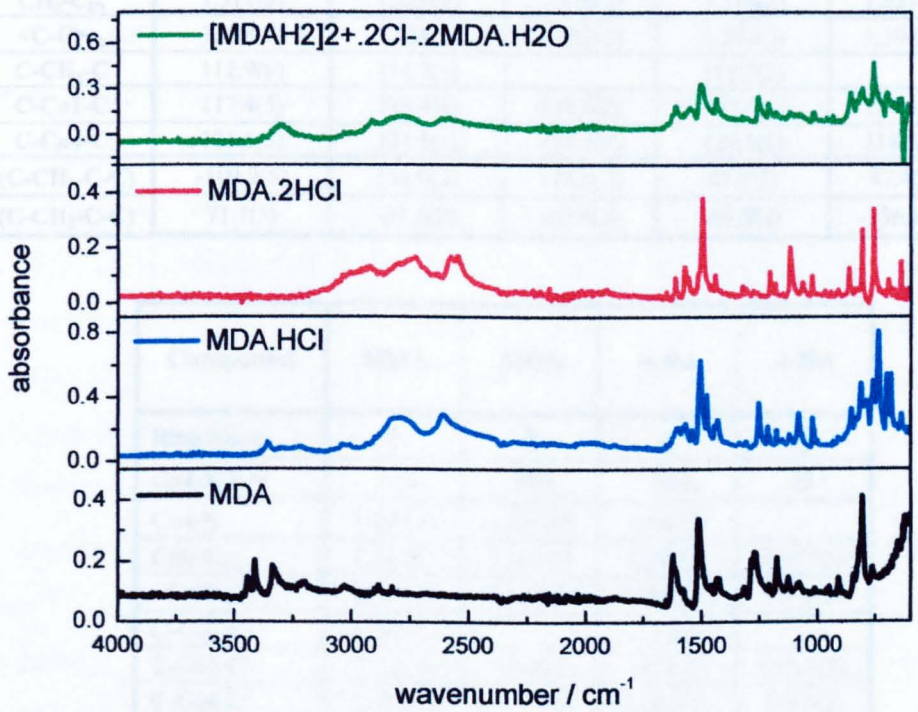

Figure 93 ATR FTIR spectra of the MDA series of compounds.

4.1.6 Other structural features

4.1.6.1 N-C bond lengths

Protonation of the amine nitrogen atoms in the three hydrochloride salts is accompanied by lengthening of the C_{ar}-N bonds, listed for each of the five compounds in Table 34a. The average C-N bond length is 1.468(3) Å for the hydrochloride salts and 1.407(7) Å for the free amines (Table 34b). These values correlate well with mean C_{ar}-N bond lengths from the International Tables for Crystallography of 1.394 and 1.465 Å for pyramidal three-coordinate and for four-coordinate nitrogen atoms, respectively.[115] To take specific examples, *p*-bromoanilinium chloride,[116] *p*-chloroanilinium chloride[117] and *p*-fluoroaniline hydrochloride[118] have C_{ar}-N bond lengths of 1.463(6), 1.464(2) and 1.464(2) Å, respectively, in agreement with the values for MDA.2HCl and 4-BA.HCl.

Compound	MDA.2HCl	4-BA.HCl	4-BA.HCl	$[MDAH_2]^{2+}.2Cl^-.2MDA.H_2O$		
Ring No. *n*	1	1	2	1	2	3
C*n*4-X X =	NH_3^+	NH_3^+	H	NH_2	NH_2	NH_3^+
C*n*4-N	1.472(6)	1.470(2)	-	1.420(2)	1.423(2)	1.463(2)
CH_2-C_{Ph}	1.511(6)	1.521(2)	1.510(2)	1.514(2)	1.521(2)	1.516(2)
$<C\text{-}C>_{Ph}$	1.378(7)	1.388(3)	1.387(2)	1.393(2)	1.394(2)	1.390(2)
C-CH_2-C	112.9(6)	114.7(1)		115.7(2)		114.4(2)
C-C*n*1-C	117.4(5)	118.4(1)	118.6(2)	117.4(1)	117.3(1)	119.0(1)
C-C*n*4-C	121.6(5)	121.5(1)	119.7(2)	119.1(1)	118.8(1)	121.5(1)
τ(C-CH_2-C-C)	-109.2(5)	151.0(2)	114.2(2)	81.9(2)	47.4(2)	-142.3(1)
τ(C-CH_2-C-C)	71.7(5)	-31.3(2)	-65.6(2)	-98.5(2)	-136.5(2)	38.0(1)

Compound	MDA	MDA	4-BA	4-BA
Ring No. *n*	1	2	1	2
C*n*4-X X =	NH_2	NH_2	NH_2	H
C*n*4-N	1.409(4)	1.397(4)	1.388(2)	-
CH_2-C_{Ph}	1.523(4)	1.512(4)	1.511(2)	1.521(2)
$<C\text{-}C>_{Ph}$	1.388(2)	1.395(2)	1.391(2)	1.392(2)
C-CH_2-C	115.6(2)		112.4(1)	
C-C*n*1-C	117.2(2)	117.1(3)	117.2(2)	118.1(2)
C-C*n*4-C	118.4(2)	117.4(3)	118.1(2)	119.5(2)
τ(C-CH_2-C-C)	162.8(3)	112.5(3)	-104.2(2)	-126.2(2)
τ(C-CH_2-C-C)	-17.8(5)	-66.7(4)	74.3(2)	53.4(2)

Table 34 a Selected individual bond lengths and angles (Å & °)

τ - dihedral angle, τ(C_A – C_B – C_C – C_D), the angle between the directions of BA and CD when viewed down BC, as depicted in Figure 94 [119]

Mean distance or angle (Å or °)	
CH_2-C_{Ph}	1.516(2)
<C-C>$_{Ph}$	1.390(2)
C-CH_2-C	114.3(6)
C_{ar}-C*n*1-C_{ar}	117.8(2)
C_{ar}-C*n*4-C_{ar} (NH_3^+)	121.5(1)
C_{ar}-C*n*4-C_{ar} (NH_2)	118.4(3)
C-NH_3^+	1.468(3)
C-NH_2	1.407(7)

Table 34 b Mean bond lengths and angles for all compounds (Å & °)

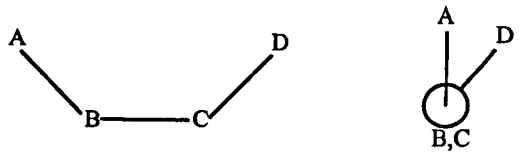

Figure 94 Guide to Table 34: Description of torsion angle $\tau(C_A - C_B - C_C - C_D)$.

4.1.6.2 Bond angles

The *Cn*2-C*n*4-C*n*6 endocyclic bond angle centred on the ring carbon atom attached to amine nitrogen also changes systematically when the amine is protonated. An average value of 121.5(1)° is observed for the protonated amine rings, i.e. both rings in MDA.2HCl (Figure 86) ring 1 of 4-BA.HCl (Figure 83) and ring 2 (denoted C21X in Figure 89) in $[MDAH_2]^{2+}.2Cl^-.2MDA.H_2O$. An average value of 118.4(3)° is observed for the unprotonated amine rings in MDA (Figure 80) ring 1 in 4-BA (Figure 78) and rings 1 and 2 in $[MDAH_2]^{2+}.2Cl^-.2MDA.H_2O$ (denoted C11X and C12X respectively in Figure 89). This change in bond angle on protonation of the amine is expected and presumably reflects the differing group electronegativities.[120] To take specific examples, the corresponding bond angles for *p*-halo anilinium cations are 121.5(5)° both for *p*-bromoanilinium chloride[116] and *p*-chloroanilinium chloride[117] and 121.8° for *p*-fluoroaniline hydrochloride.[118] In contrast, the corresponding angle reported for *p*-chloroaniline is 118.8(2).[117] In a similar fashion, the mean C-C*n*1-C angle of 117.8° in these compounds (Table 34 b) reflects the ability of CH_2 to release electrons into the aromatic ring.

4.1.6.3 X-H→ π ring interactions

A recent survey of the Cambridge Structural Database has found there are 6 possible forms of X-H→ π ring interactions.[121] Table 35 presents the X-H→ π ring interactions found in 4-BA, MDA, 4-BA.HCl and $[MDAH_2]^{2+}.2Cl^-.2MDA.H_2O$ (there are none in MDA.2HCl). A guide to the terms used in Table 35 is shown in Figure 95. The term *residue* refers to the different discrete molecules or ions involved in the interactions. In the case of 4-BA and MDA there is only one residue, an amine molecule. In the case of 4-BA.HCl residue 1 is the Cl^- ion, and residue 2 the protonated 4-BA cation. $[MDAH_2]^{2+}.2Cl^-.2MDA.H_2O$ is more complicated, having four residues: as previously explained, residue 1 is the di-cation, residue 2 the non-protonated MDA molecule, residue 3 the water molecule and residue 4 the Cl^- ion.

Comparison of Table 35 with the description of the six types of interactions described in the literature[121] shows that most of the C-H→ π ring interactions present in these four compounds are of type III, which was the most common geometry found for sp^2 C-H→ π ring interactions.[121] These interactions have a geometry where the H atom is directly above the centre of the ring but the C-H bond points towards a ring carbon atom. An exception to this is 4-BA which has type I interactions, where the C-H bonds point directly at the ring centre, called the classical 'T-shaped' bond,[121] and the C-H bond is perpendicular to the plane of the ring. Another exception is the N-H→ π ring interaction in MDA which is of type II: the proton is attracted to the ring centre but the N atom is not directly above the centre of the ring; 12 % of the N-H→ π ring interactions found in the literature[121] were of this type. Most N-H to ring interactions in the literature are directed at a ring C-C bond, whereas in MDA and 4-BA the N-H→ π ring interactions are directed towards the ring centre.

	X–H(I)	Res(I) →Cg(J)	[ARU(J)]	H..Cg	H-Perp	γ	α	X..Cg	Type[12] I
4-BA	C1 - H1A	[1] → Cg(2)	[4554.01]	2.80	2.76	10.1	155.7	3.723(2)	I
	C23 - H23	[1] → Cg(1)	[2545.01]	2.81	2.78	7.7	144.6	3.623(2)	III
	N1 - H112	[1] → Cg(2)	[4655.01]	3.01(3)	2.68	27.1	135(2)	3.702(2)	III
MDA	C25 - H25	[1] → Cg(1)	[4755.01]	3.03	2.97	12.0	139.3	3.802(3)	III
	N1 - H111	[1] → Cg(1)	[3555.01]	2.88(4)	2.82	12.4	166(2)	3.770(3)	II
	N1 - H112	[1] →Cg(2)	[2654.01]	2.73(4)	2.54	21.5	141(3)	3.545(3)	III
4-BA.HCl	C25 – H25	[2] → Cg(1)	[4554.02]	3.21	3.05	17.9	123.8	3.818(2)	III
MDA.2HCl									
$[MDAH_2]^{2+}$. 2Cl⁻.2MDA. H_2O	C113-H113	[2] → Cg(1)	[4556.02]	2.79	2.75	9.8	134.2	3.516(2)	III
	C115-H115	[2] → Cg(3)	[1545.01]	2.83	2.74	14.2	128.6	3.500(2)	III
	C122-H122	[2] → Cg(2)	[4547.02]	2.83	2.79	9.0	129.5	3.507(2)	III
	C125-H125	[2] → Cg(3)	[2657.01]	3.18	2.96	21.1	138.8	3.942(2)	III
	C212-H212	[1] → Cg(2)	[2667.02]	2.97	2.66	26.3	134.4	3.695(2)	III
	C215-H215	[1] → Cg(1)	[1555.02]	3.02	2.73	25.5	146.6	3.852(2)	III

Table 35 Analysis of X-H...Cg (π-Ring) interactions (using the criteria: H..Cg < 3.4 Å, γ < 30.0 °)
Res(I) – residue I, Cg(I) – ring centre of gravity, X-H...Cg – angle XHCg (deg), X...Cg – distance between X and Cg, H...Cg – distance between H and Cg, ARU – symmetry code.

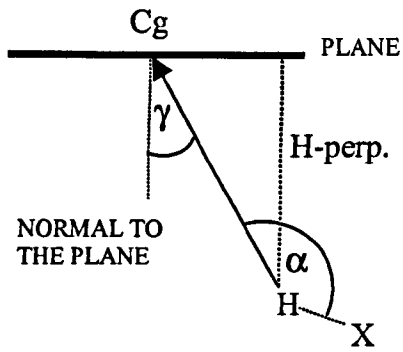

Figure 95 Guide to Table 35.

4.1.7 Correlation of crystallographic studies with solubility

Analysis of the structures of amines and their corresponding hydrochloride salts using single crystal X-ray diffraction allows a qualitative understanding of their physical properties.

4.1.7.1 Comparison of the amines: 4-BA and MDA

The solubility of a compound is not directly related to the lattice energy but is a balance between the lattice energy and the enthalpy of solvation, the latter depending on the strength and number of interactions between the solute and solvent molecules. By comparing the extent of intermolecular interactions present in the two amine structures, a 'common-sense' rationalisation of the differing solubility limits in the process solvent (chlorobenzene) is obtained. The H-bonding interaction present in MDA could explain the limited solubility of only 0.13 mol L^{-1}, when compared with 4-BA which shows no H-bonding, and has a much enhanced solubility of 4.72 mol L^{-1}, as reported in Chapter 3.

4.1.7.2 Comparison of the amine hydrochlorides: 4-BA.HCl and MDA.2HCl

The H-bonded nets of MDA.2HCl will contribute to the lattice energy and could explain the very limited solubility of this compound in chlorobenzene, less than 0.01 mmol L^{-1}, (see Chapter 3). In contrast the 4-BA.HCl structure cannot cross-link and so chains of H-bonded molecules are formed. The hydrophobic regions present in the 4-BA.HCl structure are made up of the aromatic rings of 4-BA cations, ring 2 (Figure 83) and could interact with chlorobenzene molecules, explaining the greater solubility of 4-BA.HCl's (4.7 mmol L^{-1}).

4.2 Lattice energies

The results of the crystal structure analyses were sent to Prof. A. Gavezzotti (University of Milan) who used the atomic coordinates of the non-hydrogen atoms obtained from the crystallography studies, plus normalised hydrogen atom positions, to calculate the lattice energy of each compound. These calculations were performed using the Pixel method,[122] where the valence molecular charge density is calculated using the MP2/6-31G** wave function. And the total Pixel energy is the summation of all the energy contributions, Equation (60). This method of calculating the lattice energy is a novel technique which provides the energetic values of individual interactions *e.g* H-bonding and π-π interactions, of which the geometries are observed in the crystal structures. This method has been developed only in the last few years [35, 36] and provides a molecule-molecule quantification of the energy contributions to the lattice.

$$E_{Pixel} = E_{coulombic} + E_{polarisation} + E_{dispersion} + E_{repulsion} \quad (60)$$

4.2.1 Amines: 4-BA and MDA

Both classical and Pixel methods were used to calculate the lattice energy of the amine molecules. The individual contributions calculated by the Pixel method are listed for both amines in Table 36 and, the most significant base pair interactions are depicted in Table 37 and Figure 96 for 4-BA and in Table 38 and Figure 97 for MDA. In both cases there is only one molecular species in the crystal, so the heat of sublimation, ΔH_{sub}, is equal to the negative of the lattice energy, Equation (61).

$$\Delta H_{sub} = - E_{latt} \quad (61)$$

kJ mol^{-1}	E_{coul}	E_{pol}	E_{disp}	E_{rep}	$E_{total\ Pixel}$	$E_{(UNI+EHT)}$
4-BA	-41	-21	-132	86	-108	**-108**
MDA	-74	-33	-134	110	-130	**-127**

Table 36 Lattice energies calculated for MDA and 4-BA.

As previously noted (Section 4.1.1.2) there are no H-bonds in solid 4-BA and the overall lattice energy is therefore dominated by dispersion, through the C-H and N-H→ π ring and π-π stacking interactions (Table 37). The permanent polarisation of the NH_2 and the aromatic CH groups also gives a significant coulombic energy contribution to the overall lattice energy of -108 kJ mol^{-1}.

Molecular Pair	kJ mol^{-1}				
	E_{coul}	E_{pol}	E_{disp}	E_{rep}	E_{tot}
π- π stacking x, ½-y, ½+z	-9	-4	-33	16	**-23**
C-H→ π ring -x, ½+y, ½-z	-7	-3	-24	16	**-18**
N-H→ π ring 1-x, ½+y, ½-z	-9	-6	-17	17	**-16**

Table 37 Individual base pair interactions in 4-BA.

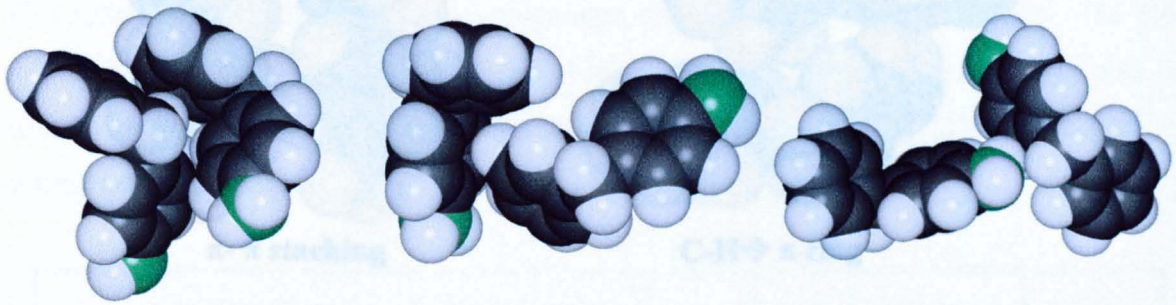

Figure 96 Views of the important individual base pair interactions in 4-BA

The H-bond in MDA has a high coulombic-polarisation energy and a small dispersion contribution, shown in Table 38. The C-H→ π ring interaction is the dominant contribution to the overall lattice energy of -130 kJ mol^{-1}.

Comparing the two amines, the most significant interaction which differentiates them is the H-bond present in MDA. This bond contributes 22 kJ mol^{-1} and the enhanced C-H→ π ring interactions contribute an extra 12 kJ mol^{-1}, giving MDA a greater overall lattice energy.

Molecular Pair	kJ mol^{-1}				
	E_{coul}	E_{pol}	E_{disp}	E_{rep}	E_{tot}
π- π stacking 1-x, y, z	-8	-2	-24	11	**-23**
C-H→ π ring -x, ½+y, ½-z	-12	-5	-31	18	**-31**
N-H→ π ring x-½, ^{3}/$_{2}$-y, 1-z	-11	-5	-21	18	**-19**
H-bond -½-x, 1-y, ½+z	-26	-9	-26	25	**-22**

Table 38 Base pair interactions for individual intermolecular bonds in MDA.

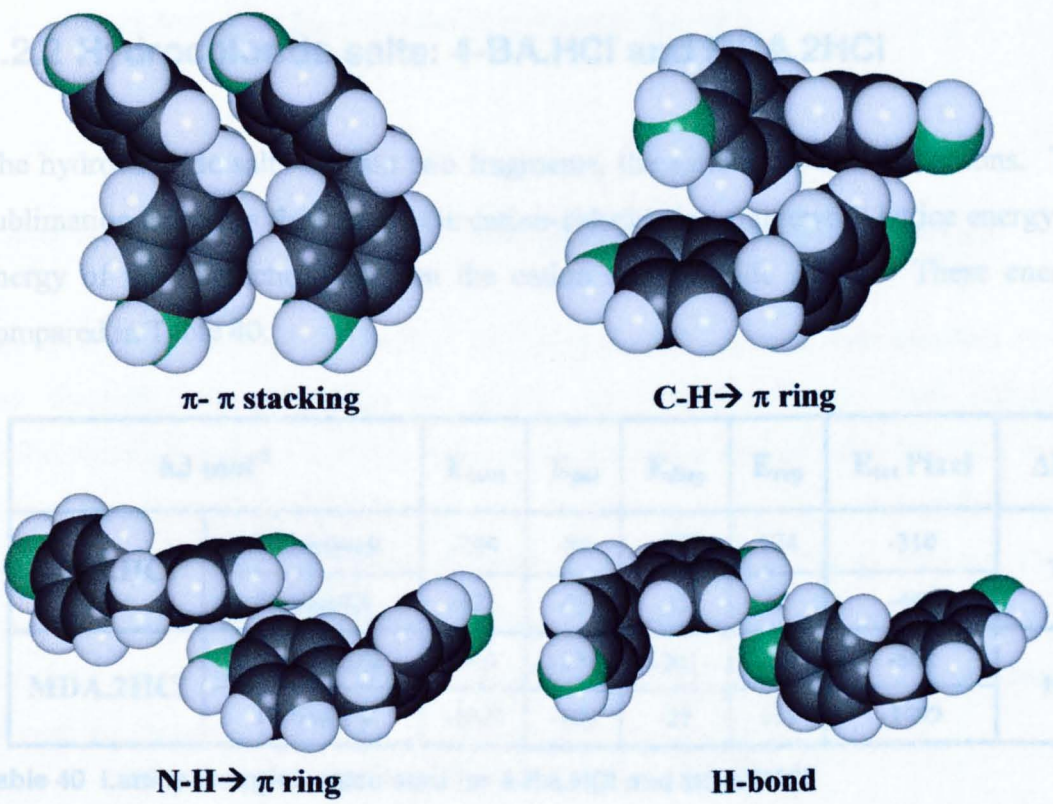

Figure 97 Base pair interactions for individual intermolecular bonds in MDA.

Summation of the atom-atom potential energies, or Unified functions, E_{UNI}, and the coulombic interaction energy calculated from Extended Huckel Theory calculations, E_{EHT}, is another method for calculating the overall lattice energy (see Chapter 1, Section 1.7.7).[123] Comparing the two methods of calculating the lattice energy it is noted that both

calculations give almost identical answers for these non-ionic molecules (Table 36). Since there is only one species in each of the crystals of 4-BA and MDA these lattice energies can be approximated to heats of sublimation, ΔH_{sub}. These ΔH_{sub} values reflect the higher melting point of MDA than 4-BA, and the much lower solubility of MDA than 4-BA in chlorobenzene, 0.13 mmol L^{-1} and 5 mol L^{-1} respectively (Table 39).

	ΔE_{sub} (kJ mol^{-1})	m.pt (K)		Solubility in chlorobenzene (mol L^{-1} at RT)
		Experimental	DSC	
4-BA	108	313	313	5
MDA	130	362 – 364	361	0.13

Table 39 Physical properties of 4-BA and MDA, melting point (m.pt), solubility in chlorobenzene and enthalpy of sublimation (ΔE_{sub}).

4.2.2 Hydrochloride salts: 4-BA.HCl and MDA.2HCl

The hydrochloride salts contain two fragments, the cation and chloride anions. The total sublimation energy is the sum of the cation-chloride ion framework lattice energy plus the energy of the interaction between the cation and chloride anions. These energies are compared in Table 40.

kJ mol^{-1}		E_{coul}	E_{pol}	E_{disp}	E_{rep}	E_{tot} Pixel	ΔE_{sub}
4-BA.HCl	Framework	-244	-84	-157	174	-310	759
	Cation/Cl	-421	-76	-12	60	-449	
MDA.2HCl	Framework	-465	-176	-201	279	-562	1661
	Cation/Cl	-1027	-160	-27	115	-1099	

Table 40 Lattice energies calculated for 4-BA.HCl and MDA.2HCl.

The overall lattice energy of 4-BA.HCl of -759 kJ mol^{-1} has a substantial contribution from the ionic interactions of -449 kJ mol^{-1}. This contribution exceeds the lattice energy of the framework, which indicates that the ionic terms dominate the overall lattice energy. However, the coulombic, polarisation and dispersive terms from the framework contribute significantly to the overall lattice energy. As a consistency check that the magnitude of the

ionic interaction is not overestimated, the overall lattice energy can be compared with that of NaCl which has a value of 766 kJ mol^{-1}.[29]

MDA.2HCl has over twice the ΔE_{sub} of 4-BA.HCl due to its increased H-bonding, giving it much larger coulombic and polarisation terms. This much greater ΔE_{sub} is consistent with MDA.2HCl's higher melting point and undetectably low solubility in chlorobenzene (Table 41).

	ΔE_{sub} (kJ mol^{-1})	m.pt (K)		Solubility in chlorobenzene (mmol l^{-1} at RT)
		Experimental	DSC	
4-BA.HCl	759	453	498	1.2
MDA.2HCl	1661	534	550	< 0.01

Table 41 Comparison of the physical properties of MDA.2HCl and 4-BA.HCl.

M.pt – melting point (K), ΔE_{sub} – enthalpy of sublimation (kJ mol^{-1}).

4.2.3 Estimate of $[MDAH_2]^{2+}.2Cl^{-}.2MDA.H_2O$ lattice energy

The crystal structure of $[MDAH_2]^{2+}.2Cl^{-}.2MDA.H_2O$ contains four residues in the ratio one dication: two molecules of MDA: one water molecule: two chloride ions. Unfortunately it was not possible to calculate the lattice energy using the Pixel method for such a complex structural arrangement. However, using $E_{(UNI)}$ parameters, and $E_{(ESP)}$ calculations an approximation for $[MDAH_2]^{2+}.2Cl^{-}.2MDA.H_2O$ was obtained (Table 42). $E_{(UNI)}$ parameters for water were obtained using those for alcohols, and the $E_{(ESP)}$ was calculated using the atomic point charges for MDA and MDA.2HCl plus standard atomic charges for water.

	$E_{(UNI)} + E_{(EHT)}$	$E_{(PIXEL)}$
4-BA.HCl	671	759
MDA.2HCl	1422	1661
$[MDAH_2]^{2+}.2Cl^{-}.2MDA.H_2O$	1331	-

Table 42 Estimated lattice energies (kJ mol^{-1}) for MDA.HCl, MDA.2HCl and 4-BA.HCl.

Listing values obtained from Pixel (Pixel) and atom-atom type calculations ($E_{(UNI)} + E_{(EHT)}$).

The classical approach gives broadly comparable values of heats of sublimation for 4-BA.HCl and MDA.2HCl to those calculated using the Pixel method. Although the heat of sublimation calculated for $[MDAH_2]^{2+}.2Cl^-.2MDA.H_2O$ is only an approximation, it does show that it is less than MDA.2HCl but greater than 4-BA.HCl, consistent with its melting point of 461 – 498 K which is intermediate between that of 4-BA.HCl and MDA.2HCl.

4.2.4 Summary of lattice energies

Comparison of the lattice energies of the free amines and their corresponding hydrochloride salts, allows a rationalisation of the ease of the reaction of the amine with HCl to form the very stable hydrochloride salts. 4-BA.HCl has a heat of sublimation over seven times that of 4-BA (Table 43). This large increase in lattice energy also consistent with the vast difference in solubility between the two related compounds, with 4-BA having a saturation limit, in chlorobenzene at room temperature, of approximately 5000 times greater than 4-BA.HCl. The situation is similar for MDA and MDA.2HCl, where the heat of sublimation of the latter is over 12 times that of MDA (Table 43). The solubility differences are also reflective of this large difference in lattice energies, where MDA has a solubility of greater than 13000 times that of MDA.2HCl.

Compound	ΔE_{sub} (Pixel, kJ mol^{-1})
4-BA	108
4-BA.HCl	759
MDA	130
MDA.2HCl	1661

Table 43 Comparison of lattice energies of 4-BA, 4-BA.HCl, MDA and MDA.2HCl.

Chapter 5

Vibrational Spectroscopy

5 Vibrational Spectroscopy

Methylene dianiline (MDA), 4-benzylaniline (4-BA) and their respective hydrochloride salts, methylene dianiline dihyrochloride (MDA.2HCl), 4-benzylaniline hydrochloride (4-BA.HCl) and methylene dianiline monohydrochloride (MDA.HCl) have been investigated in the solid phase using vibrational spectroscopy and density functional theory calculations. Inelastic Neutron Scattering (INS) accompanied by Density Functional Theory (DFT) calculations facilitated the assignment of the FTIR spectra.

5.1 Inelastic neutron scattering spectroscopy (INS) and Density functional theory calculations (DFT)

Using the atomic coordinates obtained from the crystallography, periodic DFT calculations were performed for each of the five compounds using the Dmol^3 software.[76] The calculated atomic displacements in the *ab initio* output were used to predict the inelastic neutron scattering, INS, spectra using the ACLIMAX software package.[48] These spectra were compared with those obtained using the TOSCA spectrometer at the Rutherford Appleton Laboratory in July '05.[50]

INS additionally allows access to the vibrational modes below the cut-off for the ATR FTIR spectrum at 600 cm^{-1}. The N-H torsional, τ, mode, τ(NH), on a related compound, 1,2-diaminoethane, has previously been reported to shift substantially upon hydrochlorination. Marques *et al.* state that the $\tau(NH_2)$ modes of 1,2-diaminoethane are observed at 178 and 206 cm^{-1} [51] and calculated at 282 and 321 cm^{-1} [124], these *ab initio* calculations were carried out using Gaussian 98W program for the gas phase isolated molecules. Factor group slitting[51] accounts for the loss of degeneracy in the torsional mode in the solid compound, and so two modes are observed. This is due to interaction of adjacent molecules in the solid, isolated gas phase molecules would have degenerate τ(NH) modes. The N-H torsional mode is shifted to higher wavenumber on formation of the hydrochloride salt, observed at 468 and 489 cm^{-1} [51] and calculated at 469 cm^{-1} [125] respectively.

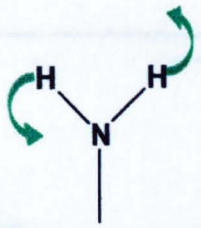

Figure 98 Depiction of the N-H torsional mode, $\tau(NH_2)$.

5.1.1 4-BA and 4-BA.HCl

Good agreement between the calculated and the experimental spectra is observed for 4-BA and 4-BA.HCl, Figure 99 and Figure 100. Using the visualisation tool in the Dmol[3] software, the $\tau(NH_2)$ mode of 4-BA is assigned to the band at 463 cm^{-1}, and the corresponding $\tau(NH_3^+)$ modes of 4BA.HCl to the bands at 495 and 522 cm^{-1}. These shifts of 32 and 59 cm^{-1} are noticeably less than those reported in the literature of approximately 290 and 283 cm^{-1}, for the experimental INS spectra.[51] This difference is attributed to the added complications of the 4-BA.HCl structure compared with that of 1,2-diaminoethane which is relatively simple; H-bonding and coupling to other vibrational modes could play a part. For example the band at 522 cm^{-1} in the INS of 1,2-diaminoethane has been assigned to an $\tau(NH_2)$ H-bonded mode.

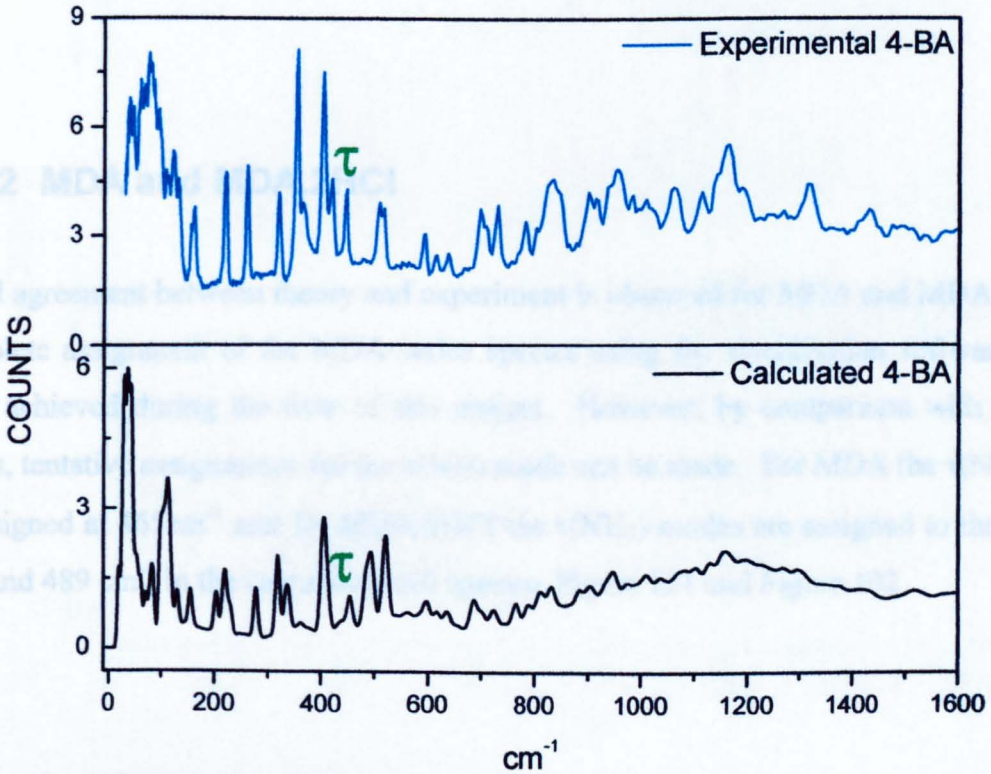

Figure 99 Calculated and experimental INS spectra of 4-BA.

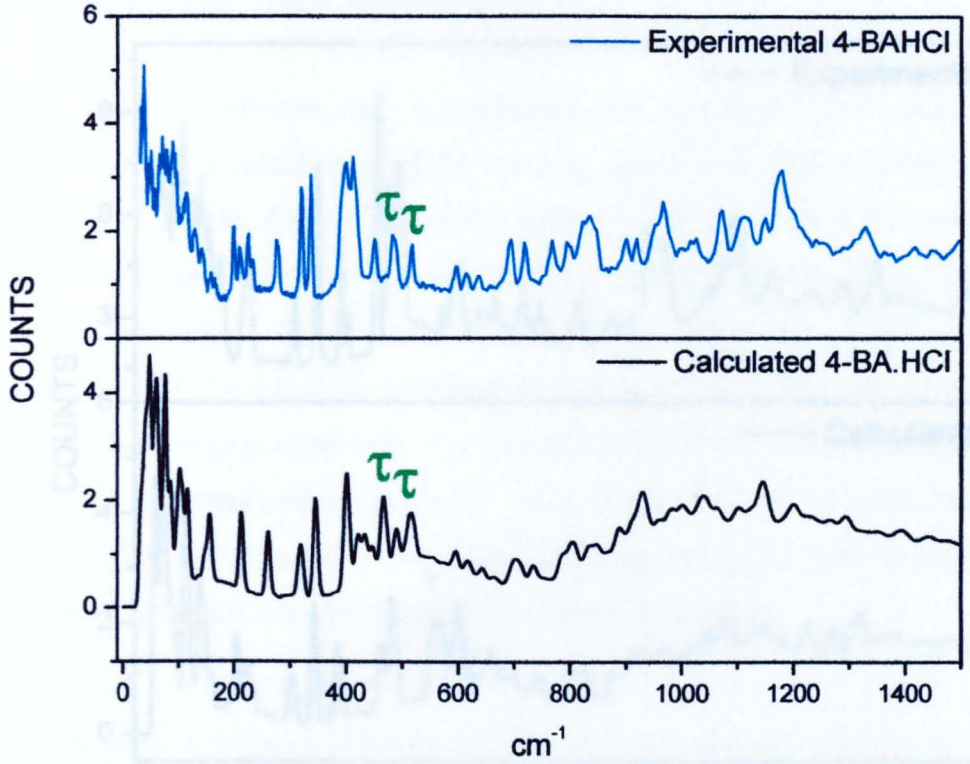

Figure 100 Calculated and experimental INS spectra of 4-BA.HCl.

Other assignments for 4-BA and 4-BA.HCl are the CH_2 rock at 342 cm^{-1} and the N-H, NH_2 or NH_3, in plane bend at 400 cm^{-1}. Both these bands appear at the same frequencies in both spectra.

5.1.2 MDA and MDA.2HCl

Good agreement between theory and experiment is observed for MDA and MDA.2HCl. A complete assignment of the MDA series spectra using the visualisation software has not been achieved during the time of this project. However, by comparison with the 4-BA series, tentative assignments for the τ(NH) mode can be made. For MDA the τ(NH_2) mode is assigned at 465cm^{-1} and for MDA.2HCl the τ(NH_3) modes are assigned to the bands at 454 and 489 cm^{-1} in the calculated INS spectra, Figure 101 and Figure 102.

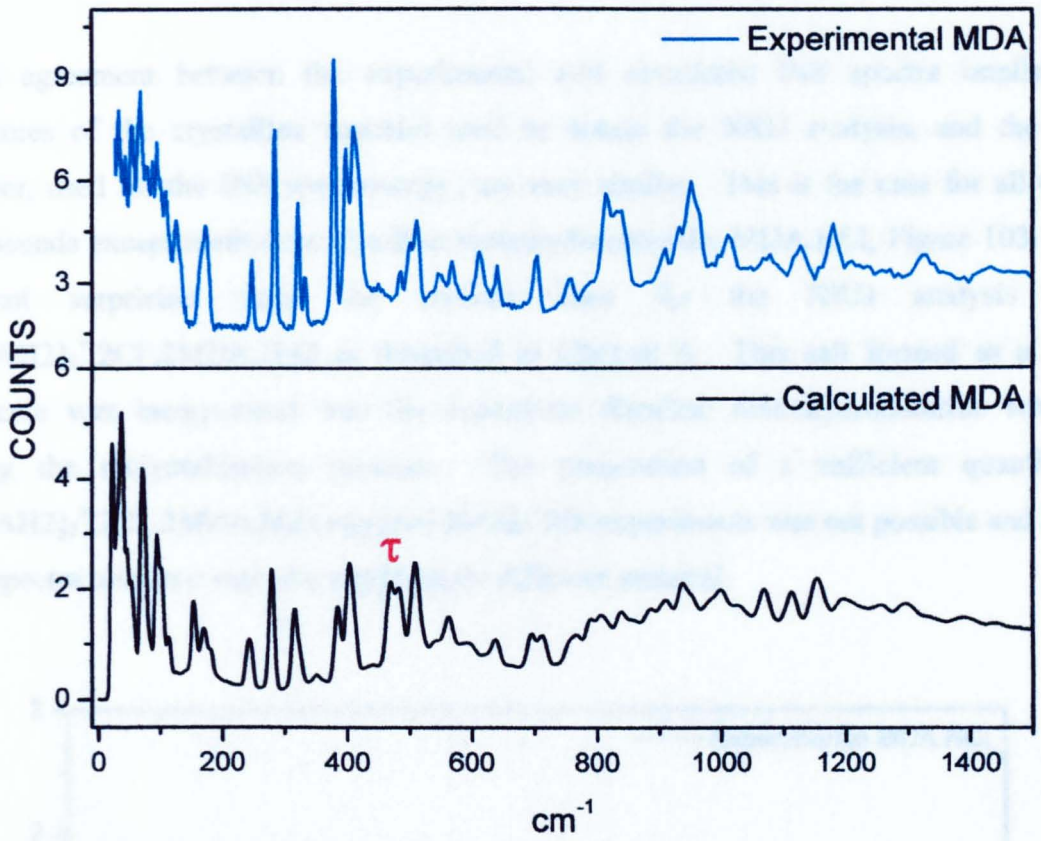

Figure 101 Calculated and experimental INS spectra of MDA.

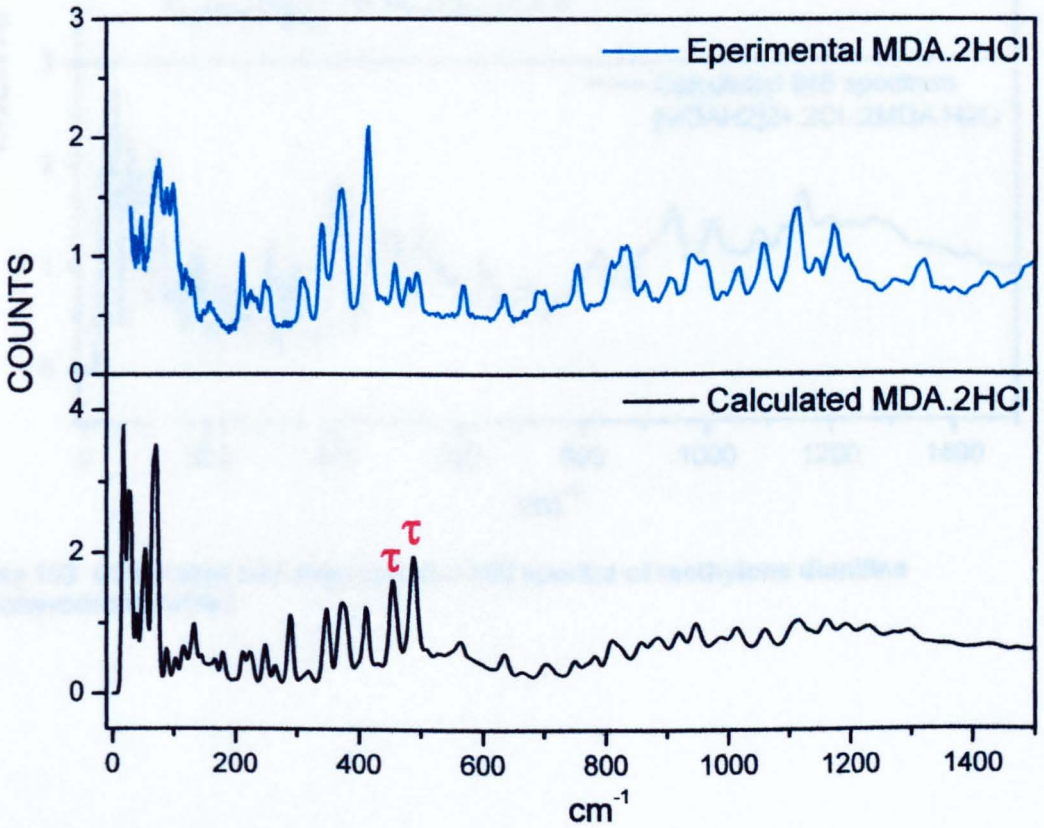

Figure 102 Calculated and experimental INS spectra of MDA.2HCl.

5.1.3 $[MDAH2]_2^+.2Cl^-.2MDA.H_2O$

Good agreement between the experimental and calculated INS spectra implies the structures of the crystalline material used to obtain the XRD analysis, and the solid powder, used for the INS spectroscopy, are very similar. This is the case for all of the compounds except methylene dianiline monohydrochloride, MDA.HCl, Figure 103. This is not surprising since the crystals used for the XRD analysis were $[MDAH2]_2^+.2Cl^-.2MDA.H_2O$ as described in Chapter 4. This salt formed as a water molecule was incorporated into the methylene dianiline monohydrochloride structure during the recrystallisation process. The preparation of a sufficient quantity of $[MDAH2]_2^+.2Cl^-.2MDA.H_2O$ required for the INS experiments was not possible and so the INS spectra obtained was of a significantly different material.

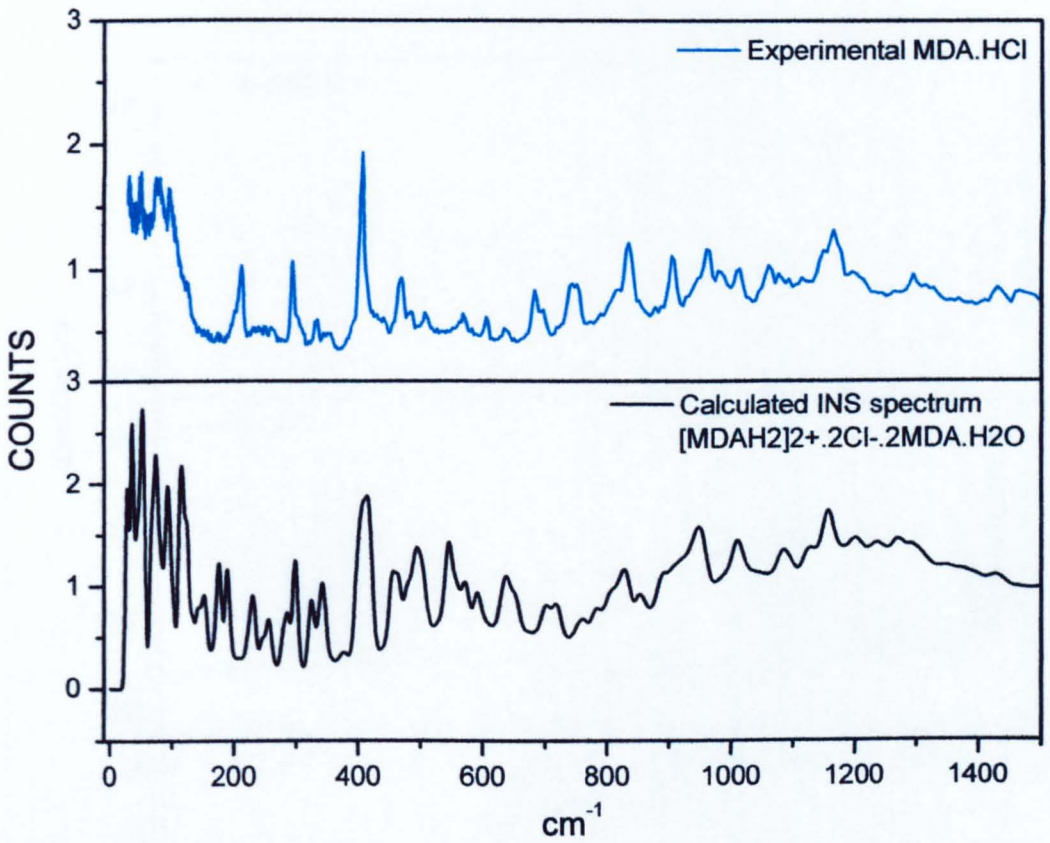

Figure 103 Calculated and experimental INS spectra of methylene dianiline monohyrodrochloride.

5.1.4 Summary of INS spectra

Good agreement between the calculated and experimentally obtained INS spectra for all but MDA.HCl, is confirmation that the H-bonding observed by XRD in the crystalline material must be of a similar nature to the intermolecular bonding in the powdered form.[47] XRD gives structural information on the crystal which has long range order, whereas INS spectroscopy gives information on the local interactions *i.e* the change in vibrational motion of the molecules with formation of H-bonds; MDA compared to MDA.2HCl. The good agreement between calculated and experimental INS implies the local environment of for example the N atom in MDA powder is similar to that of the N atoms in crystalline MDA.

5.2 FTIR

The good agreement obtained between the calculated and experimentally obtained INS spectra, allows the use of the visualisation tool in the Dmol^3 software to assign the FTIR spectra of 4-BA, 4-BA.HCl, MDA and MDA.2HCl.

5.2.1 4-BA and 4-BA.HCl

The assignments for the 4-BA and 4-BA.HCl spectra, Figure 104 are listed in Table 44 and Table 45 respectively.

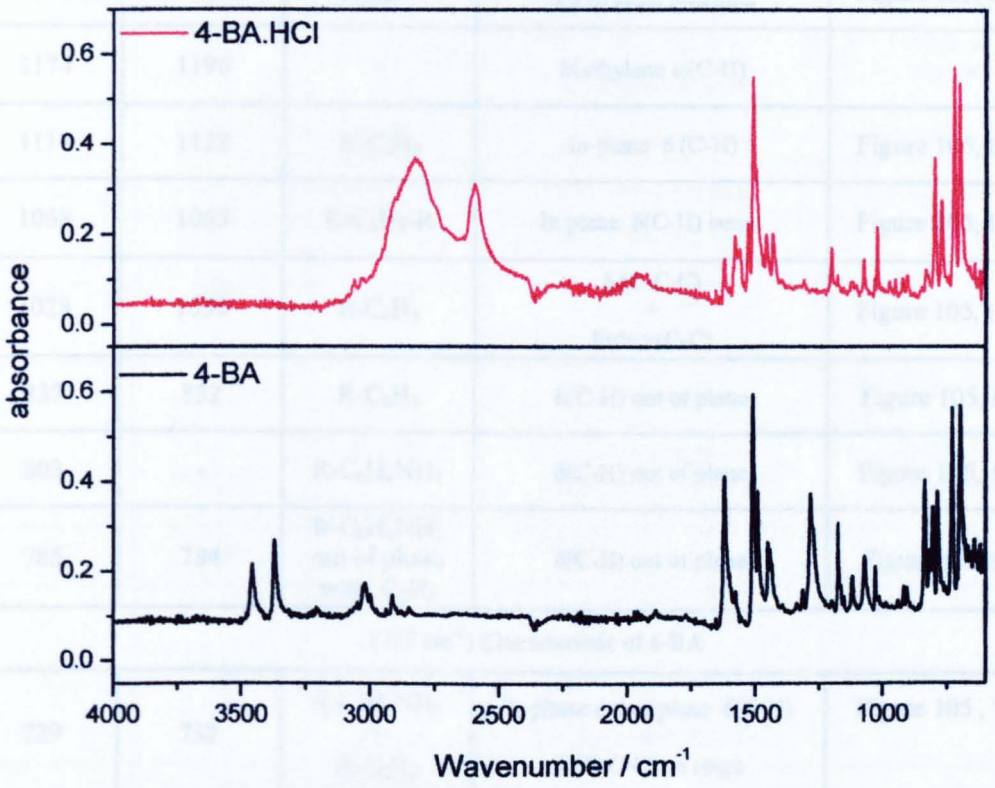

Figure 104 FTIR spectra of 4-BA and 4-BA.HCl

4-BA Band (cm^{-1})		Aromatic Ring	Assignment	Benzene ring equivalent / comment
FTIR	$Dmol^3$			
3500		-	ν(N-H)asymm	-
3390		-	ν(N-H)symm	-
1620	1649	$R\text{-}C_6H_4NH_2$	ν(C-C) in phase	Figure 106 a.
1577	1579	-	NH_2 scissors	(should be IR intense, but is on shoulder of 1620 cm^{-1})
1509	1514	$R\text{-}C_6H_4NH_2$	δ (N-H) + ν(N-C) + ν(C-C) semicircle	Semicircle stretch Figure 106 b
1489	1480	$R\text{-}C_6H_5$	ν(C-C) + bend(C-H) in-plane	Figure 105, 1500 cm^{-1}
1441	1444	$R\text{-}C_6H_4NH_2$	ν(C-C) out of phase	Figure 106, a.
1282	1291	$R\text{-}C_6H_5$	In plane δ(C-H) All in same direction	Figure 105, 1275 cm^{-1}
1174	1196	-	Methylene ω(C-H)	-
1118	1122	$R\text{-}C_6H_5$	In-plane δ (C-H)	Figure 105, 1156 cm^{-1}
1068	1065	$R\text{-}C_6H_5\text{-}R$	In plane δ(C-H) bends	Figure 105, 1073 cm^{-1}
1028	1030	$R\text{-}C_6H_5$	δ (C-C-C) + little ν(C-C)	Figure 105, 1027 cm^{-1}
837	832	$R\text{-}C_6H_5$	δ(C-H) out of plane	Figure 105, 835 cm^{-1}
803	-	$R\text{-}C_6H_4NH_2$	δ(C-H) out of plane	Figure 105, 835 cm^{-1}
785	784	$R\text{-}C_6H_4NH_2$ out of phase with C_6H_5	δ(C-H) out of plane	Figure 105 835 cm^{-1}
(785 cm^{-1}) Characteristic of 4-BA				
729	732	$R\text{-}C_6H_4NH_2$ + $R\text{-}C_6H_5$	In phase out of plane δ(C-H) + δ (C-C-C) on rings	Figure 105 , 750 cm^{-1}
697	-		In phase out of plane δ(C-H) + δ (C-C-C) on phenyl	Figure 105 750 cm^{-1}

Table 44 FTIR assignments for 4-BA (4000 – 600 cm^{-1}).

Definition of modes: ν - stretch, δ - deformation or bend, ρ - rock, ω - wag

4-BA.HCl Band (cm^{-1})		Aromatic Ring	Assignment		Benzene ring equivalent / comment
FTIR	Dmol[3]				
2934/2945		-	ν(N-H)	Esym	-
2921/2921				A	
2844/2844				Eanti	
2841/2841				Esym	
2770/2770				A	
2715/2715				Eanti	
2600			(NH_3) Fermi resonance		Combination: δ(N-H) and ρ(NH_3)
1620	1643	R-$C_6H_4NH_2$	ν(C-C) in phase		Figure 106 a
1570	1569	-	δ(NH_3) asymm		Degenerate if it was C_{3v}, but due to H-bonding it isn't
1525	-	-	δ(NH_3) asymm		
1505	1495	R-$C_6H_4NH_2$	δ(NH_3) symm + ν(C-C) out of phase		Semicircle stretch Figure 106 b
1456	1440	R-C_6H_5	ν(C-C) out of phase		Figure 105 1450 cm^{-1}
1431	1432	R-$C_6H_4NH_2$	ν(C-C) out of phase		Figure 105 1450 cm^{-1}
1202	1205	R-C_6H_5	Methylene wag(C-H) + ν(C_{ar}-C_{meth}) + δ(C-C-C) minor component		
1075	1070/1102	-	ρ(NH_3)		OR Figure 105 , 1073 cm^{-1}
1021	1034/1011	R-C_6H_5 / R-$C_6H_4NH_2$	δ (C-C-C) in phase Figure 105 , 1027 cm^{-1}	/	R-$C_6H_4NH_2$ Figure 105 , 1027 cm^{-1}
799	809	R-$C_6H_4NH_2$	δ(C-H) out of plane		Figure 105 835 cm^{-1}
769	766	R-$C_6H_4NH_2$ + R-C_6H_5 rings are in phase	δ(C-C-C) on phenyl + δ(C-C-C) on amine + Out of plane symm δ(C-H)		Figure 105 750 cm^{-1}
720	-	R-$C_6H_4NH_2$ + R-C_6H_5	In phase out of plane δ(C-H) δ(C-C-C) on rings		Figure 105 750 cm^{-1}
695	-	R-C_6H_5	In phase out of plane δ(C-H) δ(C-C-C) on phenyl		Figure 105 750 cm^{-1}

Table 45 FTIR assignments for 4-BA.HCl (4000 – 600 cm^{-1}).

Definition of modes: ν - stretch, δ - deformation or bend, ρ - rock, ω - wag

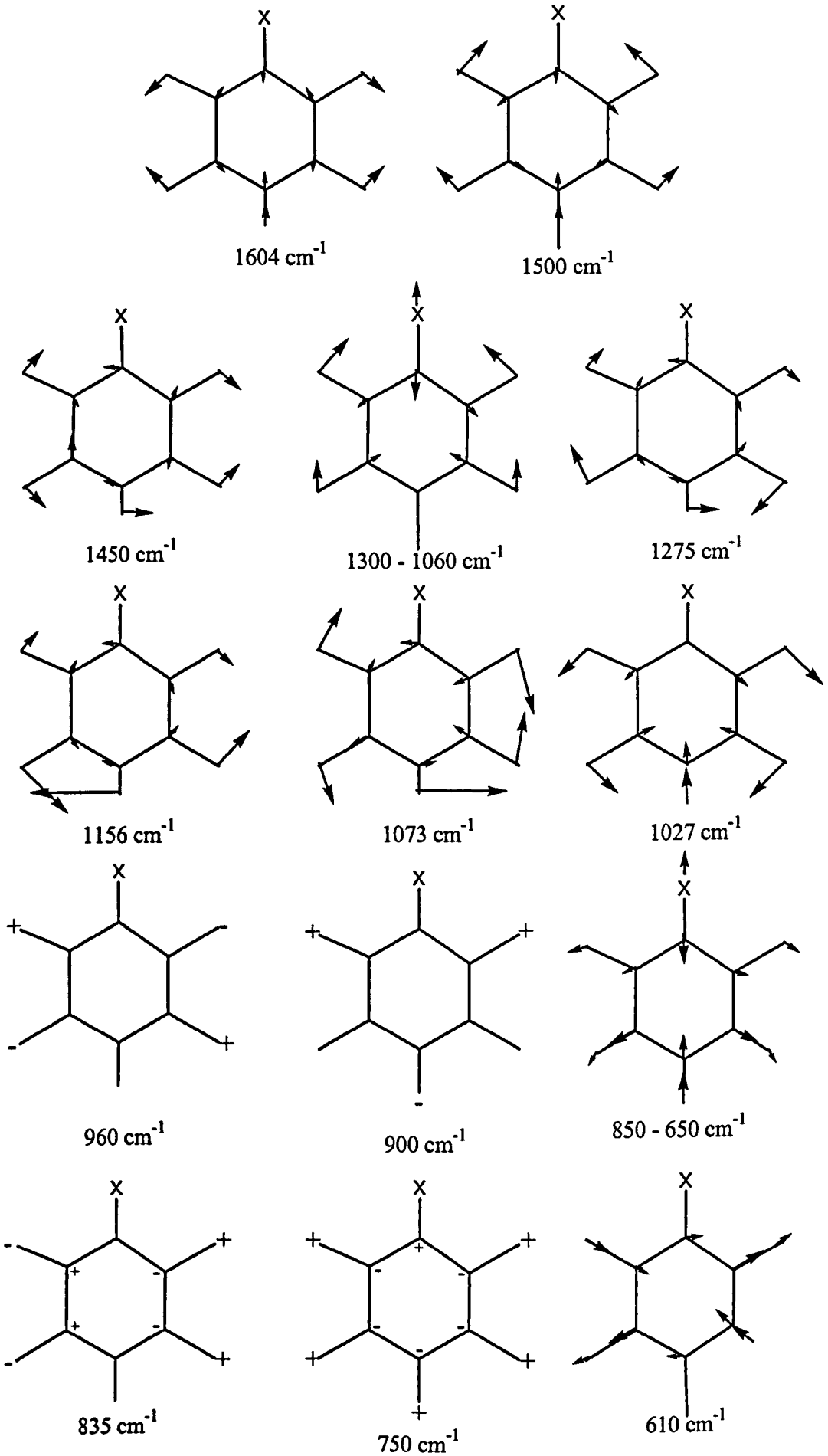

Figure 105 Benzene ring vibrational modes.[98]

4-BA: 4000 – 3000 cm-1

The symmetric and asymmetric NH stretching frequencies for 4-BA, observed at 3500 cm^{-1} and 3390 cm^{-1}, are characteristic of an aryl-NH_2 species.[98] The ν(C-H) stretch region at 3000 cm^{-1} has not been assigned due to difficulties with mixing of the vibrational modes which complicated the spectra. The INS and FTIR spectra of a sample of 4-BA where the amine protons have been exchanged for deuterium are currently being investigated. This work coupled with periodic DFT calculations on the deuterated compound should lead to a full vibrational assignment.

1620 – 697 cm^{-1}

Many of the bands in this region are related to the aromatic rings, and are assigned with reference to the literature on mono substituted benzenes as shown in Figure 105.[98] The quadrant stretch at 1620 cm^{-1} is the C-C ring stretch where the bonds in one quadrant stretch and the two carbons in the neighbouring quadrant contract. The N-H scissors mode is observed at a lower frequency than the literature suggests, observed at 1577 cm^{-1} compared with the literature value, 1638 – 1602 cm^{-1}. The band observed at 1509 cm^{-1} is a combination of the semicircle ν(C-C) stretch on the amine ring, Figure 106, the ν(C-N) and the δ(NH).

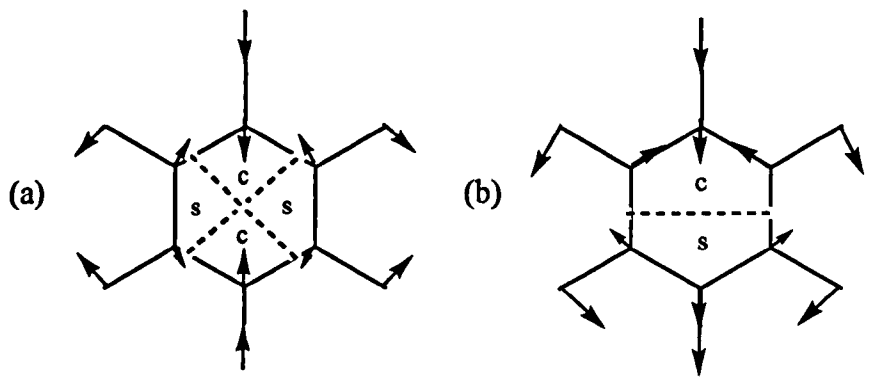

Figure 106 (a) Quadrant and (b) semi-circle stretch of benzene [98]

Where c – compressed region, s – stretching region

The most prominent difference in this region between the spectra of 4-BA and 4-BA.HCl is the intense band at 785 cm^{-1} assigned to the out of plane δ(C-H) on the amine ring of

4-BA. This band is not observed in the 4-BA.HCl spectrum, but could be in combination with the C-C-C bends on the phenyl and amine rings observed at 769 cm^{-1}.

4-BA.HCl: 3000 – 2000 cm^{-1}

There are two totally symmetric (A_1) and two doubly degenerate (E) N-H stretching vibrational modes expected for the NH_3 group.[84] The ν(N-H) bands appear between 2945 and 2715 cm^{-1} and their assignment is in agreement with the literature, being below 3000 cm^{-1} as expected for aryl primary amine salts. [98] The band at 2600 cm^{-1} is assigned as a Fermi resonance of a combination of deformation vibrations. [98] This broad peak at 2600 cm^{-1} appears to contain two bands; it is believed to be the result of the combination of the $\delta(NH_3)$ at 1525 cm^{-1} with the $\rho(NH_3)$ at 1075 cm^{-1} and the $\delta(NH_3)$ at 1505 cm^{-1} plus the $\rho(NH_3)$ at 1075 cm^{-1}. This is a combination band, which although normally expected to have low intensity, is strong due to its proximity to the strong ν(N-H) which allows it to 'borrow' intensity.[126] For this process to be permitted, one of the combining bands must also have the same symmetry as the ν(N-H). Complicated Fermi resonances have been assigned in the literature for methanol, which similarly, is a combination of the bending and rocking modes, but of the OH bend and $\rho(CH_3)$.[126] As with 4-BA, deuterated 4-BA.HCl has been prepared and is currently being investigated in order to assign the CH stretching region at 3000 cm^{-1}.

Although less common for aryl than alkyl primary amine salts,[98] an isolated band at approximately 2000 cm^{-1} is characteristic of these compounds. This band is a combination of the antisymmetric $\delta(NH_3)$ and the $\tau(NH_3)$ modes, the low intensity feature at 1950 cm^{-1} in the 4-BA.HCl spectrum could be assigned to this band.

1650 – 695 cm^{-1}

Many of the bands in this region are assigned with reference to the bands of mono-substituted benzene, Figure 105. The quadrant stretch at 1620 cm^{-1} is observed, Figure 106. For 4-BA.HCl the band observed at 1505 cm^{-1} has contributions from both the semicircle ν(C-C) stretch on the amine ring, Figure 106, and the δ(NH) mode.

The only mode in this region which appears to be characteristic of the hydrochloride salt is the asymmetric $\delta(NH_3)$ which appears at 1570 cm^{-1} but this almost coincides with the NH scissors at 1577 cm^{-1} of 4-BA and so, on its own, it is not a useful diagnostic band of hydrochlorination.

5.2.2 MDA and MDA.2HCl

The vibrational assignments of the FTIR spectra of MDA and MDA.2HCl, Figure 107, are listed in Table 46 and Table 47. MDA has a much higher symmetry than 4-BA having a C2 rotational axis at the methylene carbon, on the isolated molecule; since both aromatic rings are equivalent, resulting in a much simpler FTIR spectrum. This is also true for MDA.2HCl as both aromatic rings contain an NH_3^+ group in the *para* position.

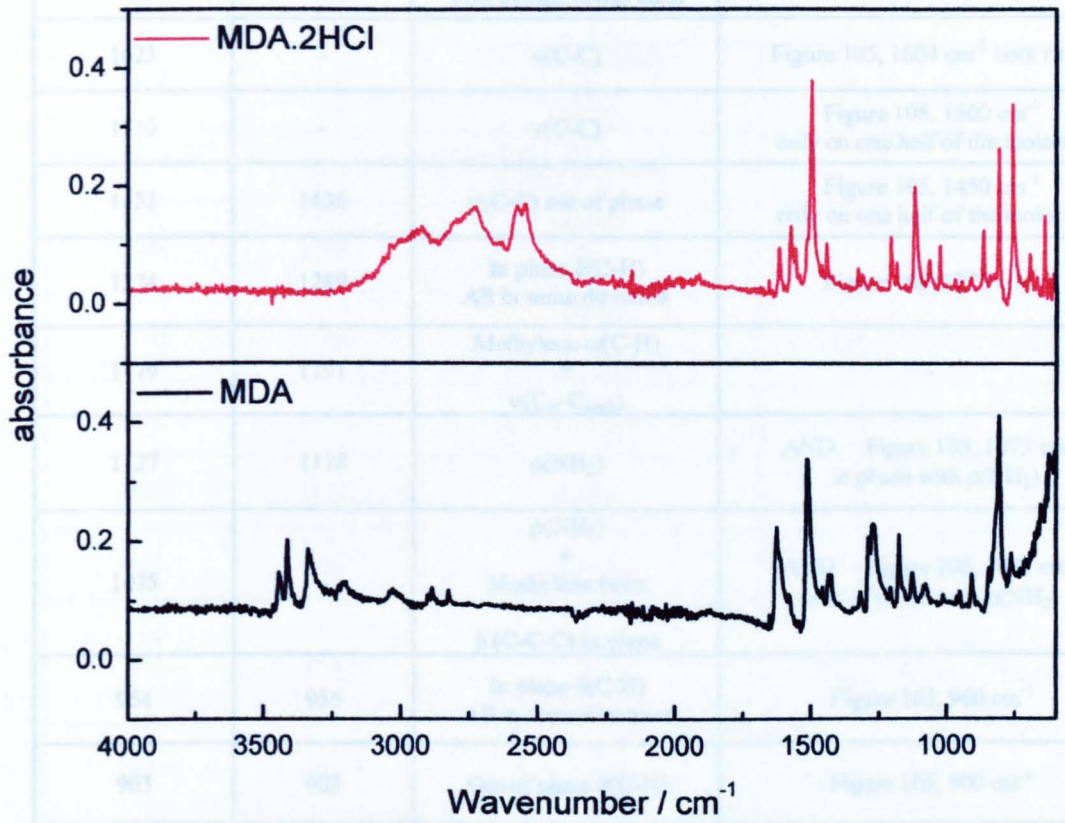

Figure 107 FTIR spectra of MDA and MDA.2HCl.

MDA Band (cm^{-1})		Assignment	Benzene ring equivalent
FTIR	$Dmol^3$		
3472	-	ν(N-H) asymm	-
3435	-	ν(N-H) asymm	-
3329	-	ν(N-H) symm Two modes, broad band	-
1623	-	ν(C-C)	Figure 105, 1604 cm^{-1} both rings
1510	-	ν(C-C)	Figure 105, 1500 cm^{-1} only on one half of the molecule
1433	1436	ν(C-C) out of phase	Figure 105, 1450 cm^{-1} only on one half of the molecule
1274	1289	In plane δ(C-H) All in same direction	Figure 105, 1275 cm^{-1}
1179	1191	Methylene ω(C-H) + $\nu(C_{ar}\text{-}C_{meth})$	-
1127	1118	$\rho(NH_2)$	AND Figure 105, 1073 cm^{-1} in phase with $\rho(NH_2)$
1075	-	$\rho(NH_2)$ + Methylene twist + δ (C-C-C) in plane	AND Figure 105, 1073 cm^{-1} out of phase with $\rho(NH_2)$
954	956	In plane δ(C-H) All in same direction	Figure 105, 960 cm^{-1}
903	903	Out of plane δ(C-H)	Figure 105, 900 cm^{-1}
803	805	$\omega(NH_2)$ in phase with δ(C-H) out of plane	Figure 105, 835 cm^{-1}
760	761	$\omega(NH_2)$ + δ(C-H) out of plane	Figure 105, 835 cm^{-1}
626	636	Two in plane δ (C-C-C) Out of phase	Figure 105, 610 cm^{-1}

Table 46 FTIR assignments for MDA (4000 – 600 cm^{-1}).

Definition of modes: ν - stretch, δ - deformation or bend, ρ - rock, ω - wag

MDA.2HCl Band (cm^{-1})		Assignment	Benzene ring equivalent
FTIR	Dmol[3]		
3240 - 2610	-	ν(N-H)	
2560	-	(NH_3) Fermi resonance	Combination: δ(N-H) and ρ(NH_3)
1619	-	ν(C-C)	Figure 105, 1604 cm^{-1} both rings
1571	1589	δ (NH_3) asymm	-
1498	1508	δ (NH_3) asymm + ν(C-C)	Figure 105, 1500 cm^{-1}
1437	1444	δ (NH_3) symm	-
1209	1229	ω(CH_2) + ν(C-N)	-
1179	1190	ω(CH_2) + In plane δ(C-H)	Figure 105, 1300 - 1060 cm^{-1}
1118	1118	ρ(NH_3) SHARP	-
1061	1059	ρ(NH_3)	-
1018	1012	δ (C-C-C)	Figure 105, 1300 - 1027 cm^{-1}
864	858	δ (C_5-C_4-C_3) + δ (C-C -C)	Figure 105, 850 - 650 cm^{-1}
808	806	δ(C-H) out of plane	Figure 105, 835 cm^{-1} purely ring
756	751	δ (C_5-C_4-C_3) + ν(C-N)	Figure 105, 850 - 650 cm^{-1}
695	698	δ (C_6-C_1-C_2)	Figure 105, 850 - 650 cm^{-1}
639	637	In plane δ (C-C-C)	Figure 105, 610 cm^{-1}

Table 47 FTIR assignments for MDA.2HCl (4000 – 600 cm^{-1}).

Definition of modes: ν - stretch, δ - deformation or bend, ρ - rock, ω - wag

MDA: 3500 – 2000 cm^{-1}

Compared with 4-BA there are two NH_2 groups and so there should be four ν(N-H) bands, two antisymmetric and two symmetric. The antisymmetric bands are observed at 3472 and 3435 cm^{-1} and the two symmetric bands coincide in the broad band at 3329 cm^{-1}. These bands are at lower frequency than the corresponding antisymmetric and symmetric ν(N-H) bands in 4-BA, which is consistent with the presence of H-bonding[127] in MDA but its absence in 4-BA, this is consistent with the XRD structures, Chapter 4. The ν(C-H) region has as yet not been assigned. The FTIR and INS spectra of deuterated MDA and MDA.2HCl are currently being investigated in combination with periodic DFT calculations of these materials. It is hoped that this approach will lead to the full vibrational assignment of these materials.

1623 – 626 cm^{-1}

The assignments of the substituted benzene ring modes are made by reference to the literature[98] and are shown in Figure 105. The major differences between MDA and 4-BA in this region are the two strongly absorbing C-C-C bending modes which appear in the 4-BA spectrum at 729 and 697 cm^{-1} but are not observed in MDA. There is one broad C-C-C bend in the MDA spectrum, which appears at the spectral cut-off, at 626 cm^{-1}. Another difference between the spectra of MDA and 4-BA is the coupling of the in-plane δ(C-H) at 1127 cm^{-1} with the ρ(NH_2) mode which is observed in MDA but not in 4-BA.

Other minor differences are slight changes in the modes of the ν(C-C) assignments, the appearance of the weak in-plane δ(C-H) band at 954 cm^{-1} and the incorporation of the NH_2 wag into the strongly absorbing out of plane δ(C-H) band at 803 cm^{-1}. A final difference is the lack of an NH_2 scissors mode, previously observed at 1577 cm^{-1} in 4-BA, as the low frequency shoulder of the ν(C-C).

MDA.2HCl: 3500 – 2000 cm^{-1}

By comparison with 4-BA.HCl, the bands between 3240 and 2610 cm^{-1} are assigned to the ν(N-H) modes. There are three δ(NH_3) and two ρ(NH_3), which could combine to make the Fermi resonance assigned as the two bands at 2574 and 2549 cm^{-1}. The two combinations which sum to give these frequencies are the δ(NH_3) at 1498 cm^{-1} plus the ρ(NH_3) at 1061 cm^{-1} and the δ(NH_3) at 1437 cm^{-1} plus the ρ(NH_3) at 1118 cm^{-1}. The symmetry of the deformation and rock modes is not known but it is assumed that one of

these modes shares the same symmetry as the ν(N-H) and so the enhancement of the combination band by Fermi resonance would be allowed.

The tentative assignment of the combination band of the $\delta(NH_3)$ and the $\tau(NH_3)$ modes appearing at 1950 cm^{-1} for 4-BA, is even more tenuous for MDA.2HCl as there is only a very weak broad feature in this region.

1620 – 639 cm^{-1}

There are three main differences in this region between MDA.2HCl and 4-BA.HCl; the sharp $\rho(NH_3)$ at 1118 cm^{-1} and the sharp C-C-C bend at 864 which are not present in the 4-BA.HCl spectrum; and the appearance of the in-plane C-C-C bend at 639 cm^{-1} which is not observed in 4-BA.HCl. Other minor differences include the combination of the ν(C-N) instead of the $\nu(C_{ar}-C_{me})$ with the CH_2 wag at 1209 cm^{-1} and the much reduced intensity of the C-C-C bend at 695 cm^{-1}. The ν(C-N) is lower in wavenumber than expected,[98] the literature states it should appear in the region 1330 – 1260 cm^{-1}. This difference is likely caused by the combination with the CH_2 wag at 1209 cm^{-1}, which is expected to appear anywhere between 1375 – 1150 cm^{-1}.[98]

There are four prominent peaks which differentiate MDA.2HCl from MDA in this region. These are the $\delta(NH_3)$ at 1571 cm^{-1}; the $\rho(NH_3)$ at 1118 cm^{-1}; the C-C-C bend at 1018 cm^{-1} which appears in MDA at 1075 cm^{-1} in combination with the $\rho(NH_2)$ and the strong band at 756 cm^{-1} assigned to the combination of the C-C-C bend and the ν(C-N).

5.2.3 Methylene dianilinie monohydrochloride (MDA.HCl)

The differences encountered between the calculated and experimentally obtained INS spectra of methylene dianiline monohydrochloride (MDA.HCl), have limited the use made of the calculations to assign the FTIR spectra. By comparison of the spectra of MDA and MDA.2HCl with MDA.HCl, Figure 108 and Figure 109, and the assignments of MDA and MDA.2HCl, a tentative assignment of MDA.HCl is given in Table 48.

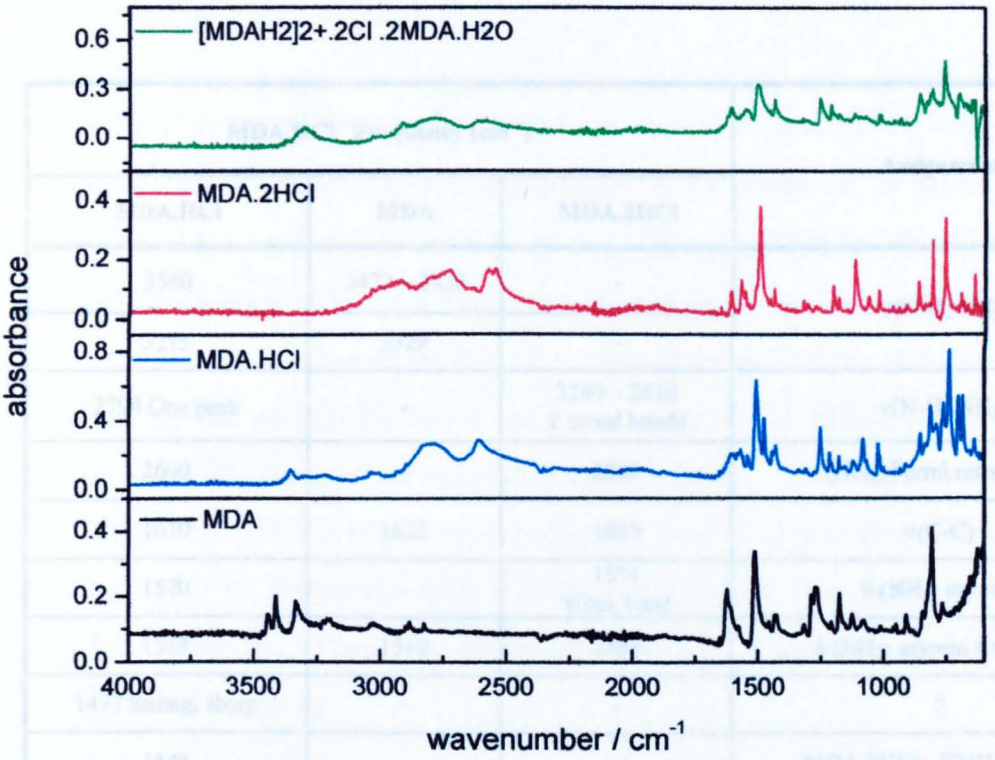

Figure 108 FTIR spectra of $[MDAH2]_2^+.2Cl^-.2MDA.H_2O$ and methylene dianiline monohydrochloride (MDA.HCl) compared with MDA and MDA.2HCl. (Full scan)

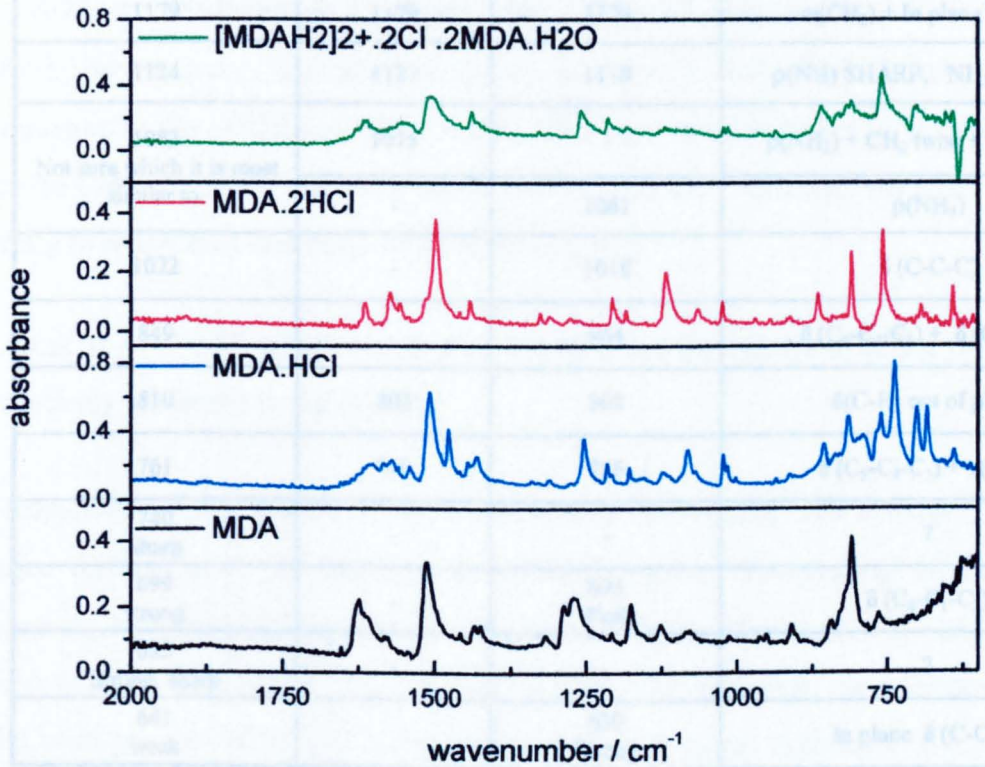

Figure 109 MDA series FTIR spectra, 2000 cm^{-1} to 600 cm^{-1}

MDA.HCl Frequency (cm^{-1})			Assignment
MDA.HCl	MDA	MDA.2HCl	
3360	3472 – 3435	-	ν(N-H) NH_2
3215	3329	-	
2794 One peak	-	3240 – 2610 2 broad bands	ν(N-H) NH_3
2600	-	2560	(NH_3) Fermi resonance
1610	1623	1619	ν(C-C)
1570	-	1571 Weak band	δ (NH_3) asymm
1514	1510	1498	δ (NH_3) asymm + ν(C-C)
1477 Strong, sharp	-	-	?
1446 Similar shape to MDA	1433	1437	MDA.2HCl: δ(NH_3) symm MDA: ν(C-C) out of phase
1248	1274	-	δ(C-H)
1215	-	1209	ω(CH_2) + ν(C-N)
1179	1179	1179	ω(CH_2) + In plane δ(C-H)
1124	1127	1118	ρ(NH) SHARP, NH_3 OR NH_2
1083 Not sure which it is most similar to.	1075	-	ρ(NH_2) + CH_2 twist + δ (C-C-C)
	-	1061	ρ(NH_3)
1022	-	1018	δ (C-C-C)
849		864	δ (C_5-C_4-C_3) + δ (C-C-C)
810	803	808	δ(C-H) out of plane
761	760	756	δ (C_5-C_4-C_3) + ν(C-N)
740 Sharp	-	-	?
699 strong	-	695 Weak	δ (C_6-C_1-C_2)
683 Strong, sharp	-	-	?
641 weak		639 Strong	In plane δ (C-C-C)

Table 48 Comparison of MDA.HCl frequencies with MDA and MDA.2HCl (4000 – 600 cm^{-1}).

Definition of modes: ν - stretch, δ - deformation or bend, ρ - rock, ω - wag

3500 – 2000 cm^{-1}

The most prominent differences in the spectra arise from the ν(N-H) modes. It appears that the antisymmetric ν(N-H) observed in MDA is not observed for MDA.HCl, but there is a band at 3215 cm^{-1} which is close to the symmetric ν(N-H) of MDA. This slight lowering of frequency of the ν(N-H) is consistent with H-bonding of the NH_2 group.[127] A shift to higher wavenumber of the δ(N-H) is also expected[98] if the NH_2 group is involved in H-bonding, but no δ(N-H) mode has been assigned for MDA, so this is not easily checked. The ν(N-H) region between 3420 and 2610 cm^{-1} in MDA.2HCl shows two broad bands, but in MDA.HCl it shows only one broad band. There is also a band at 2610 cm^{-1} which coincides in frequency with the band assigned to the Fermi resonance in the MDA.2HCl spectrum. These ν(N-H) assignments are consistent with MDA.HCl having both NH_3 and NH_2 groups.

1610 – 1641 cm^{-1}

Figure 109 focuses on the region between 2000 and 600 cm^{-1} where the major similarities to MDA are the bands at 1250 cm^{-1} and 1122 cm^{-1}, assigned in MDA as δ(C-H) and ρ(NH_2) respectively. The latter is closest in shape to that of MDA but is also close in frequency to the ρ(NH_3) of MDA.2HCl. The most similar bands to those in MDA.2HCl are the C-C-C bending modes at 1026, 702 and 862 cm^{-1}, although the latter two bands are strong in MDA.HCl and quite weak in MDA.2HCl.

A peak at 1477 cm^{-1} which is not observed in either the spectra of MDA or MDA.2HCl is tentatively attributed to the δ(N-H).

Comparison of the spectra of MDA.HCl with $[MDAH2]_2^+.2Cl^-.2MDA.H_2O$ shows the major differences to be found in the ν(N-H) region. Broadening of the ν(NH_2) and smearing of the ν(NH_3) region are consistent with the difference in H-bonding present in the crystals of $[MDAH2]_2^+.2Cl^-.2MDA.H_2O$ with that present in the solid powder material. The solid powder MDA.HCl used for the INS experiments is thought to contain no water molecules, and so is not likely to have bifurcated H-bonds, unlike the structure of $[MDAH2]_2^+.2Cl^-.2MDA.H_2O$ determined by XRD. The ν(NH_2) mode is also shifted down in wavenumber by 60 cm^{-1} which is confirmation that the NH_2 group is involved in H-bonding.[127] There is also a dramatic broadening of the previously sharp band at 1083 cm^{-1}, which is possibly the ρ(NH), from either the NH_2 or NH_3 group. This can be

attributed to the loss of freedom experienced by the NH_3 bonds when involved in H-bonding.

5.2.4 Summary of FTIR spectra

The complete assignment of the FTIR spectra of the amines and their hydrochloride salts allows easy identification of these compounds, the main diagnostic bands occurring in the ν(N-H) region. For example, the FTIR spectra were used to distinguish between products and reactants during the preparation of the hydrochloride salts as outline in Chapter 3. The differences in the ν(N-H) region are attributed to the added NH groups present in MDA and MDA.2HCl compared to 4-BA and 4-BA.HCl and the changes in intermolecular bonding. The differences between methylene dianiline monohydrochloride and $[MDAH2]_2^+.2Cl^-.2MDA.H_2O$ can be rationalised with respect to their different structures and very different H-bonding motifs.

Chapter 6

Investigations and development of the kinetic model of the dissolution and dissociation of 4-BA.HCl in chlorobenzene

6 Investigations and development of the kinetic model of the dissolution and dissociation of 4-BA.HCl in chlorobenzene

The main goal of this project was to understand the behaviour of the amine hydrochloride salts in the process solvent chlorobenzene and postulate a route by which the amine hydrochloride could be converted back to the valuable amine starting material. As methylene dianiline dihydrochloride salt (MDA.2HCl) could not be observed in solution (see Chapter 3), the investigation of the solution behaviour was limited to 4-benzylaniline hydrochloride (4-BA.HCl).

This chapter describes these investigations, from initial experiments, aimed at determining an overall equilibrium constant, which led to the postulation of a reaction mechanism, to the experiments which verified this kinetic scheme.

Sections 6.1 – 6.1.2 describe some preliminary experiments that indicated inconsistencies in the solvation/dissociation process. Section 6.1.3 identifies the primary origins for the observed inconsistencies and describes how these problems could be overcome. Section 6.2 describes the development of a reaction scheme for the solvation and dissociation of 4-BA.HCl$_{(s)}$. Sections 6.2.1 and 6.2.2 describe a series of, respectively, 'closed' and 'open' experiments. Finally, Section 6.3 describes the development of a kinetic model.

6.1 Investigations of the dissociation of 4-BA.HCl$_{(s)}$

The experiments described in this section include the preliminary investigation of the possible dissociation of 4-BA.HCl$_{(s)}$ to form the free amine [4-BA $_{(solv)}$], shown in Equation (62), over a range of temperatures, 323, 347 and 403 K. This was the initial aim of this project as outlined by our industrial sponsors.

$$\text{4-BA.HCl}_{\text{solid}} \underset{k_{-1}}{\overset{K_1 \; k_1}{\rightleftharpoons}} \text{4-BA}_{\text{solv}} + \text{HCl}_{\text{solv}} \qquad (62)$$

Also outlined in this section, the aim is to measure the conversion purely in solution of 4-BA.HCl$_{(solv)}$ to 4-BA$_{(solv)}$, shown in Equation (63).

$$\text{4-BA.HCl}_{solv} \underset{k_{-2}}{\overset{k_2}{\rightleftharpoons}} \text{4-BA}_{solv} + \text{HCl}_{solv} \qquad K_2 \qquad (63)$$

6.1.1 Dissociation of 4-BA.HCl$_{(s)}$

Determination of the equilibrium constant, K_1, was performed at 323, 347 and 403 K. A small mass of 4-BA.HCl$_{(s)}$ was heated in chlorobenzene for a number of hours in a round bottomed flask fitted with a condenser, as described in Chapter 2. A sample was taken and filtered before analysis by ^{1}H NMR. The CH_2 and NH_2 ^{1}H NMR integrals were used to calculate the concentrations of 4-BA$_{(solv)}$ and 4-BA.HCl$_{(solv)}$ and so determine the stoichiometric equilibrium constant, K_2, using Equation (64). The CH_2 signal represents both amine and hydrochloride salt, whereas the NH_2 signal only represents 4-BA$_{(solv)}$, and so by subtraction of the intensity of the NH_2 signal from that of the CH_2 signal, the concentration of 4-BA.HCl$_{(solv)}$ can be determined.

$$\begin{aligned} K &= [\text{4-BA}_{(solv)}]\,[\text{HCl}_{(solv)}] \;/\; [\text{4-BA.HCl}_{(solv)}] \\ &= [\,\delta\,\text{NH}_2\,]^2 / [\,\delta\text{CH}_2 - \delta\text{NH}_2\,] \\ &= [\text{4-BA}] \times [\text{HCl}] / [(\text{4-BA.HCl} + \text{4-BA}) - \text{4-BA}] \\ &\equiv \text{mmol L}^{-1} \end{aligned} \qquad (64)$$

These experiments were carried out before the solvent suppression ^{1}H NMR pulse program was optimised as described in Chapter 2. ^{1}H NMR spectra were obtained using a C_6D_6 insert, data was accumulated for up to 8 h to obtain reasonable signal to noise. The detection limit of free amine, as determined by the NH_2 proton resonance, was 0.1 mmol L^{-1}. This concentration of free amine corresponds to an equilibrium value, K_2, of 2.6×10^{-6} mmol L^{-1}, assuming the CH_2 signal was equivalent to a combined 4-BA and 4-BA.HCl concentration of 4 mmol L^{-1}. This implies that the smallest equilibrium constant which could be detected in these experiments was 2.6×10^{-6} mmol L^{-1}.

6.1.1.1 Dissociation of 4-BA.HCl$_{(s)}$ at 323 K

Three experiments carried out at 323 K (Table 49) showed only CH_2 signals in the ^1H NMR spectra, no NH_2 signals were observed. No equilibrium was detected; dissolution of 4-BA.HCl was the only process detectable at this temperature. The spectra are shown in Figure 110.

Experiment	A	B	C
Reaction time (h)	4.17	4.17	72
[CH_2] (mmol L^{-1})	4	5	7
[NH_2] (mmol L^{-1})	-	-	-

Table 49 Experiments A, B and C on the dissociation 4-BA.HCl$_{(s)}$ in chlorobenzene performed at 323 K.

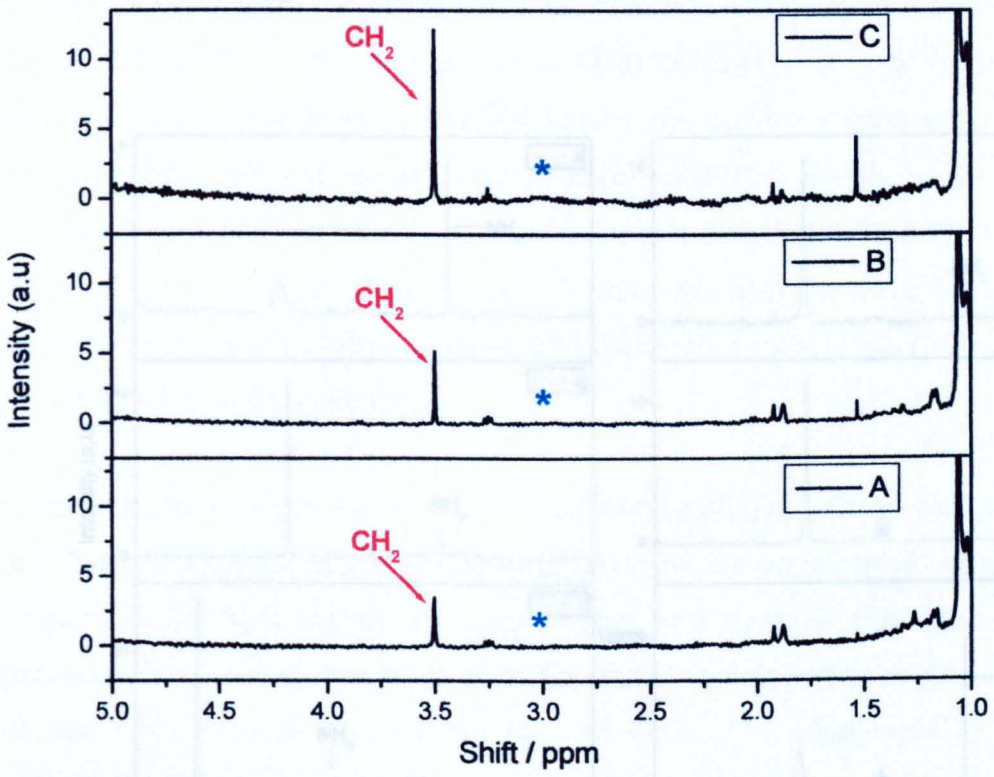

Figure 110 ^1H NMR spectra of experiments A, B and C on the dissociation 4-BA.HCl$_{(s)}$ in chlorobenzene performed at 323 K.

*** - indicates the region of the spectra where the NH_2 signal is expected to be observed.**

At 323 K no free amine, 4-$BA_{(solv)}$, was observed; the NH_2 proton resonance would be expected to be observed at 3 ppm, as indicated in Figure 110 by the asterisks. Therefore, there is no evidence of the dissociation of 4-BA.$HCl_{(s)}$ to form 4-$BA_{(solv)}$. However, this temperature is sufficient to form 4-BA.$HCl_{(solv)}$ as indicated by the observed CH_2 ^1H NMR signals, Figure 110. At 323 K 4-BA.HCl can be dissolved in chlorobenzene, but the dissociation to form 4-$BA_{(solv)}$ does not occur at detectable levels.

6.1.1.2 Dissociation of 4-BA.$HCl_{(s)}$ at 347 K

Six experiments were performed at 347 K, a temperature comparable to the industrial process. Five of these experiments were left at reaction temperature for 4 h, the other for only 30 min. This latter experiment of short duration was performed to give insight into the speed of reaction; how quickly does 4-BA.$HCl_{(s)}$ dissociate to a measurable extent? Results are shown in Figure 111 and summarised in Table 50.

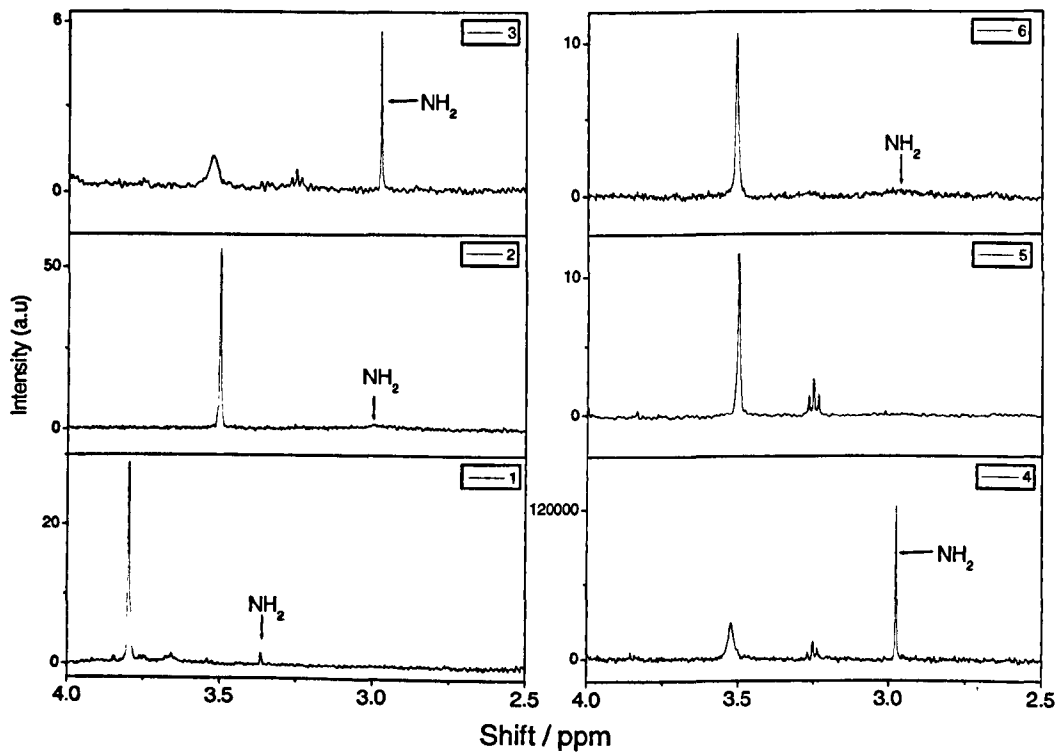

Figure 111 ^1H NMR spectra of experiments on the dissociation 4-BA.$HCl_{(s)}$ in chlorobenzene at 347 K.

Experiment	Reaction time (h)	FWHM of δ NH_2 (ppm)	Concentration (mmol L^{-1})		K (mmolL^{-1})
			4-BA.HCl	4-BA	
1	4	3.0 E-3	1.6	0.9	5.2 E-7
2	4	0.15	2.1	2.6	3.3 E-3
3	4	2.0 E-3	0.3	0.5	8.3 E-4
4	4.67	3.7 E-3	0.5	0.9	1.6 E-3
5	5	-	1.5	-	-
6	0.5	-	1.5	-	-

Table 50 Experiments on the dissociation of 4-BA.$HCl_{(s)}$ *in chlorobenzene at 347 K.*

FWHM – full width of the NH_2 signal measured at half of the maximum height, K – equilibrium constant.

All experiments were performed under identical conditions; however, the results obtained were not reproducible. Spectra from experiments 1, 2, 3 and 4 show the formation of small concentrations of amine. Spectra 5 and 6 are shown as examples of reactions which did not produce any 4-BA. After approximately 4 h at 347 K there is some discrepancy in the final measured concentrations of 4-BA.HCl and 4-BA between experiments. The spectra for experiments 3 and 4 show uncharacteristically broad CH_2 signals, as shown in Figure 111 . These signals are an order of magnitude broader than those observed in the standard 4-BA solutions (see Figure 25 in Chapter 2); this adds doubt to these two results. The average value of the equilibrium constant established after approximately 4 h, experiments 1 - 4, is 0.0143 +/- 0.0141 mmol L^{-1}.

Ignoring experiment 6, the width at half maxima of the NH_2 signals are consistent (column 3 in Table 50). Qualitatively, these are consistent with the overall trend shown in Chapter 2, Figure 25, the NH_2 signals are sharp at low concentrations (less than 1 mmol L^{-1} experiments 1, 3 and 4) and broader at the critical concentration required for optimal exchange with water in the solvent (3 – 6 mmol L^{-1}, experiment 2). However, quantitatively these signal widths are inconsistent with those of the standard 4-BA solutions. The NH_2 signals of these equilibrium experiments are either a factor of 10 narrower or a factor of 10 wider than their 4-BA solution counterparts. This disagreement could be due to differing environments of the NH_2. In the case of these dissociation experiments, the NH_2 of 4-$BA_{(solv)}$ could be in exchange with water protons and the protons of the NH_3^+ of 4-BA.$HCl_{(solv)}$. This could lead to differing line shape trends of the NH_2 resonance, as opposed to the relatively simple exchange of the NH_2 protons with water in the standard 4-BA solutions. Collectively these experiments at 347 K indicate

that the dissociation of 4-BA.$HCl_{(s)}$ to form free amine, 4-$BA_{(solv)}$ is viable but somewhat irreproducible under the experimental conditions used.

6.1.1.3 Variability in the 347 K experiments

A simple explanation of the variability in the data acquired from the 347 K experiments was not easily found. All possible sources of inconsistency were considered, purity of solvent, preparation of 4-BA.$HCl_{(s)}$, and reaction apparatus.

Reaction vessel, hotplate and oil bath were consistent for all experiments, and so these sources of inconsistency were immediately ruled out. Using distilled or non-distilled chlorobenzene could affect the concentration of the species in exchange with the NH_2 protons, which could account for the difference in line shape of the NH_2 signals observed. The sample preparations methods of 4-BA.$HCl_{(s)}$ were different; the samples used in experiments 3 and 4 were prepared in the solution phase using an overhead stirrer, experiments 1 and 2 used a sample prepared via the direct gas – solid route, and the sample for experiment 6 was prepared in solution with a magnetic stirrer bar (see Chapter 2). However, impurities in the 4-BA.$HCl_{(s)}$ samples are likely to be minor as all samples provided identical elemental analysis, ATR-FTIR spectra with no free amine ν(N-H) bands, and no unassigned features in the ^1H NMR spectra.

From the TGA measurements discussed in Chapter 3 it can be concluded that no thermal decomposition is observed at 347 K, and therefore the 4-$BA_{(solv)}$ observed in the dissociation experiments at this temperature was not produced via thermal dissociation of the solid. This is one source of variability which can be ruled out.

To rule out temperature as a source of inconsistency, the same experimental set up was used but at reflux. If the solvent used in one experiment was purer than in another, the temperature at which reflux occurred would be higher. Therefore, reaction time was measured from the point at which reflux commenced, regardless of the temperature which had been reached. The temperature difference between the four reflux experiments was in fact very slight (± 2 K).

6.1.1.4 Dissociation of 4-BA.HCl$_{(s)}$ at reflux, 403 K

Four experiments measuring the dissociation of 4-BA.HCl$_{(s)}$, Table 51, were performed under reflux, approximately 403 K, as described in Chapter 2. The amine signal is clearly observed in all four experiments, Figure 112. At this temperature increased concentrations of 4-BA$_{(solv)}$ were observed in comparison to the experiments at 347 K, suggesting the equilibrium position is shifted further to the product side. The average value of the equilibrium constant is 0.055 ± 0.029 mmol L^{-1}.

Reflux Experiment	Concentration (mmol L^{-1})		K (mmol L^{-1})
	4-BA.HCl	4-BA	
R1	8	20.7	0.05
R2	7.5	37.5	0.05
R3	4.5	20.5	0.09
R4	13	27	0.06

Table 51 Four experiments measuring the dissociation of 4-BA.HCl$_{(s)}$ in chlorobenzene at reflux.

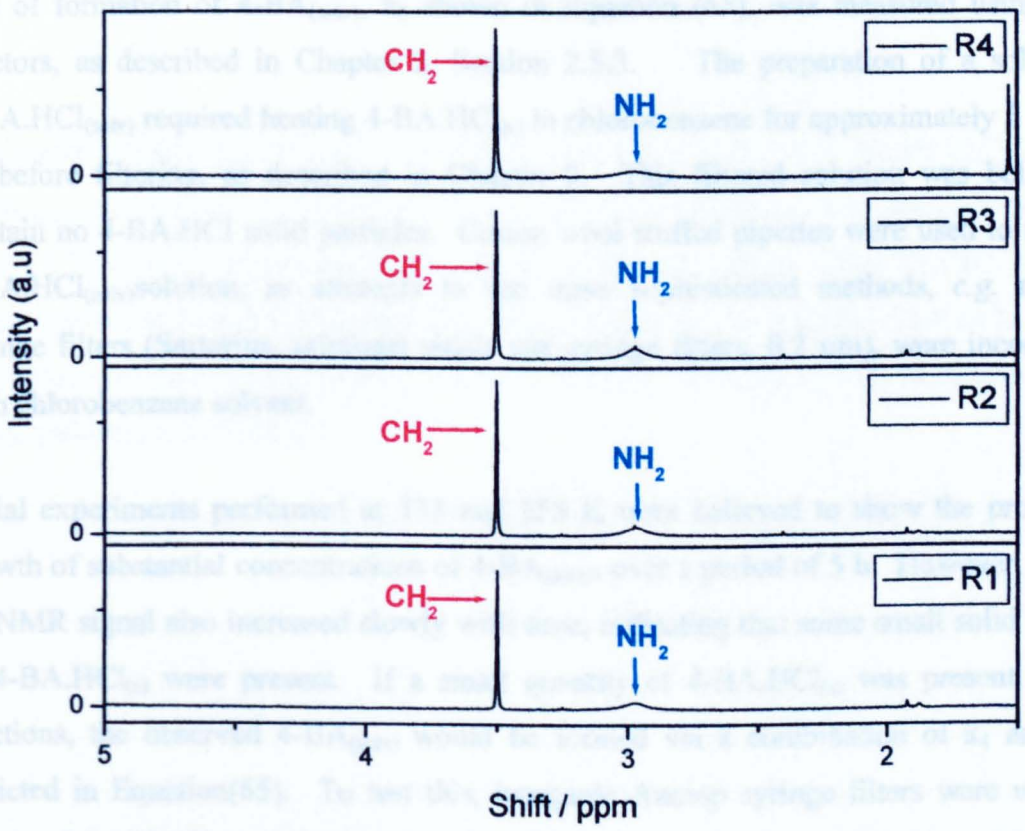

Figure 112 ^{1}H NMR spectra of the four experiments measuring the dissociation of 4-BA.HCl$_{(s)}$ in chlorobenzene at reflux.

However, the TGA data at 403 K (Chapter 3) show 100 % mass loss of the 4-BA.HCl$_{(s)}$ in 30 min. These equilibrium reactions were held at 403 K for only 15 min, but a possible contribution to the production of 4-BA$_{(solv)}$ from either the dissolution of 4-BA.HCl$_{(s)}$ from the vapourisation of the solid or the thermal dissociation of 4-BA.HCl$_{(s)}$ to form 4-BA cannot be excluded *(as shown by the blue arrows* in Equation (65)). Reaction at this temperature is therefore, likely to be a combination of solid-based and the solution processes (Equation (65)). Although it is noted that the TGA data can only be used as a guide in the solution reactions as the interactions of species with the solvent may be the determining factor in the mechanism.

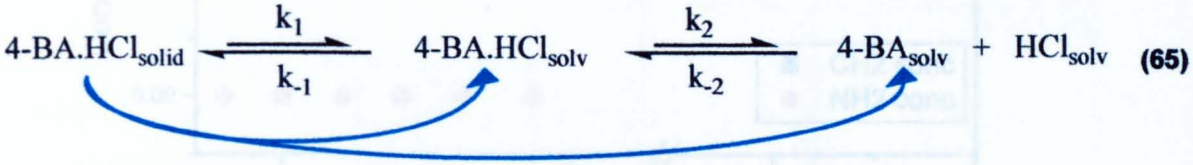

(65)

6.1.2 Solution reaction; 4-BA.HCl$_{(solv)}$ → 4-AB$_{(solv)}$

To test the hypothesis that thermal dissociation of the solid to form free amine plays no role in the solution phase experiments, a solution of 4-BA.HCl$_{(solv)}$ was prepared and the rate of formation of 4-BA$_{(solv)}$, k_2 shown in Equation (65), was measured using sealed reactors, as described in Chapter 2, Section 2.5.3. The preparation of a solution of 4-BA.HCl$_{(solv)}$ required heating 4-BA.HCl$_{(s)}$ in chlorobenzene for approximately 5 h at 323 K, before filtering, as described in Chapter 2. This filtered solution was believed to contain no 4-BA.HCl solid particles. Cotton wool stuffed pipettes were used to filter the 4-BA.HCl$_{(solv)}$solution, as attempts to use more sophisticated methods, *e.g.* millipore syringe filters (Sartorius, ministart single use syringe filters, 0.2 μm), were incompatible with chlorobenzene solvent.

Initial experiments performed at 333 and 353 K were believed to show the progressive growth of substantial concentrations of 4-BA$_{(solv)}$, over a period of 5 h. However, the CH_2 ^{1}H NMR signal also increased slowly with time, indicating that some small solid particles of 4-BA.HCl$_{(s)}$ were present. If a small quantity of 4-BA.HCl$_{(s)}$ was present in these reactions, the observed 4-BA$_{(solv)}$ would be formed via a combination of k_1 and k_2 as depicted in Equation(65). To test this, inorganic Anotop syringe filters were used in a repeat of the 353 K experiment. Figure 113 shows the reaction profile for this reaction, where 4-BA.HCl$_{(s)}$ solid particles (>0.2 μm) were removed by filtration, prior to reaction.

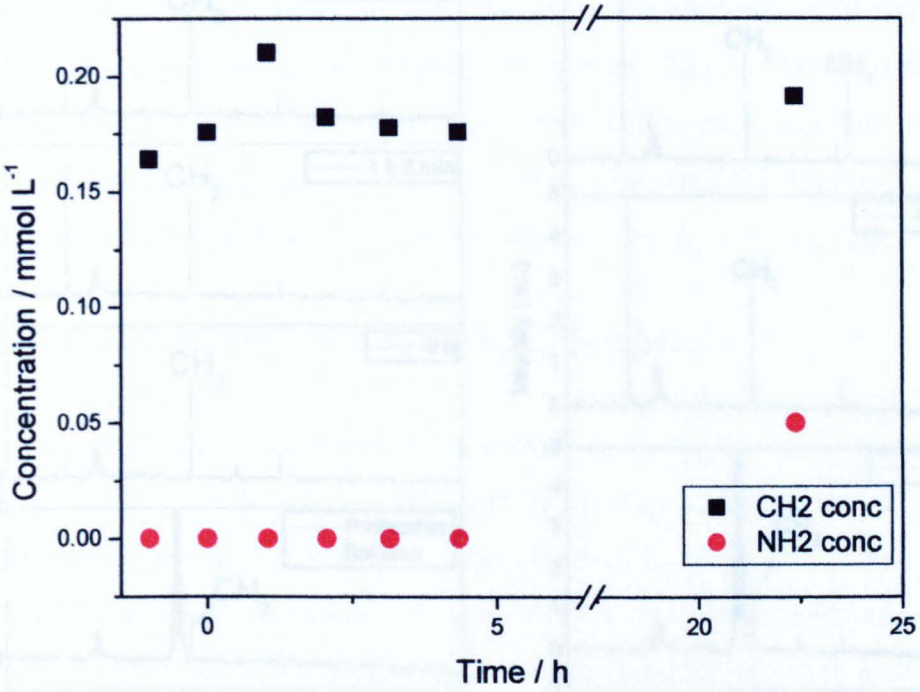

Figure 113 Reaction profile of a filtered solution of 4-BA.HCl in chlorobenzene at 353 K for 24 h, under closed conditions. (No solid particles greater than 0.2 μm present)

4-BA.HCl$_{(solv)}$ prepared by dissolving 4-BA.HCl$_{(s)}$ at 323 K for 5 h, then filtered using Anotop syringe filters. ■ - CH_2 concentration (concentration of 4-BA.HCl$_{(solv)}$ + concentration of 4-BA$_{(solv)}$), ● - NH_2 concentration (concentration of 4-BA.HCl$_{(solv)}$).

The pretreated solution (Figure 114, and the data point at -0.5 h in Figure 113) shows no 4-BA$_{(solv)}$ was observed. Before reaction at 353 K, no 4-BA$_{(solv)}$ was detected during the first 4.3 h, a small concentration is detected in the last sample, after 22.5 h. This NH_2 signal (shown in Figure 114) is small and approximates to the detection limit of free amine. It is concluded that the conversion of 4-BA.HCl$_{(solv)}$ to 4-BA$_{(solv)}$ in chlorobenzene does not occur under these conditions.

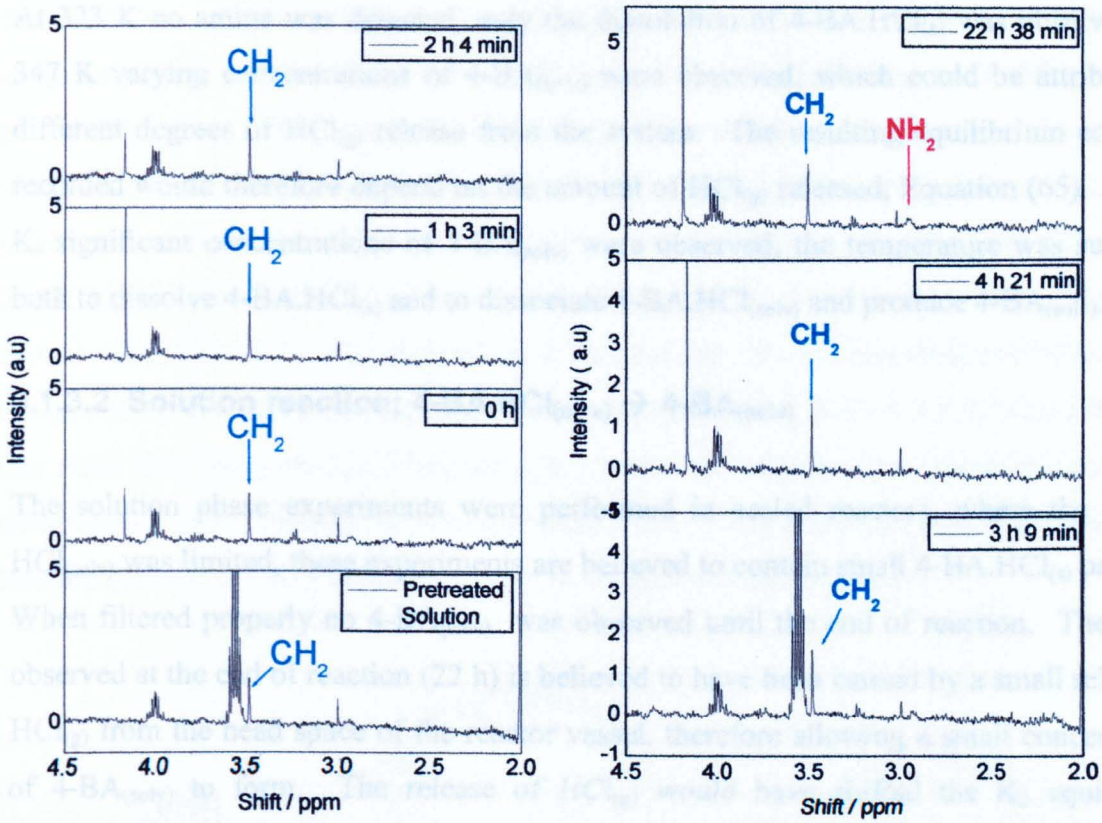

Figure 114 ^{1}H NMR spectra of samples from the reaction of a filtered solution of 4-BA.HCl in chlorobenzene at 353 K for 24 h, under closed conditions. (No solid particles greater than 0.2 μm present)

Using filtration through Anotop syringe filters.

6.1.3 Review of investigations of the dissociation of 4-BA.HCl$_{(s)}$

All of these dissociation and solution experiments were performed before optimisation of ^{1}H NMR spectroscopy; the detection limit of 4-BA$_{(solv)}$ at this time was poor, 0.1 mmol L^{-1}. This is believed to be the major cause of the inconsistencies observed in the 347 K dissociation measurements (Figure 111, Table 50).

6.1.3.1 Dissociation experiments of 4-BA.HCl$_{(s)}$ at 323, 347 and 403 K

These dissociation measurements were performed under open conditions, being conducted with a reflux condenser above a stirred volume of solution, allowing loss of gaseous material from the reaction system.[21] It is possible that HCl$_{(solv)}$ could partition into the gas phase and so these experiments cannot be measuring a true equilibrium when one of the salient species is escaping the system.

At 323 K no amine was detected, only the dissolution of 4-BA.$HCl_{(s)}$ was observed. At 347 K varying concentrations of 4-$BA_{(solv)}$ were observed, which could be attributed to different degrees of $HCl_{(g)}$ release from the system. The resulting equilibrium constants recorded would therefore depend on the amount of $HCl_{(g)}$ released, Equation (65). At 403 K, significant concentrations of 4-$BA_{(solv)}$ were observed; the temperature was sufficient both to dissolve 4-BA.$HCl_{(s)}$ and to dissociate 4-BA.$HCl_{(solv)}$ and produce 4-$BA_{(solv)}$.

6.1.3.2 Solution reaction; 4-BA.$HCl_{(solv)}$ → 4-$BA_{(solv)}$

The solution phase experiments were performed in sealed reactors, where the loss of $HCl_{(solv)}$ was limited, these experiments are believed to contain small 4-BA.$HCl_{(s)}$ particles. When filtered properly no 4-$BA_{(solv)}$ was observed until the end of reaction. The amine observed at the end of reaction (22 h) is believed to have been caused by a small release of $HCl_{(g)}$ from the head space of the reactor vessel, therefore allowing a small concentration of 4-$BA_{(solv)}$ to form. The release of $HCl_{(g)}$ would have shifted the K_2 equilibrium (Equation (63)) to the right hand side, allowing the formation of a detectable concentration of 4-$BA_{(solv)}$.

6.2 Reaction scheme

Combining the knowledge gained from the XRD, lattice energy calculations, TGA experiments and the investigations of the dissociation of 4-BA.$HCl_{(s)}$, the reaction scheme shown in Figure 115 was proposed.

FTIR analysis of the TGA samples (see Chapter 3) showed no evidence of thermal dissociation of 4-BA.$HCl_{(s)}$ to form 4-BA. At temperatures between 323 and 373 K, only a small mass loss was observed during the TGA experiments. This indicates 4-BA.HCl to be effectively thermally stable at the temperatures encountered in the solution reactions. However, the behaviour of the solid may be different when in solution. The energy required to overcome the dispersive forces of the solid lattice of 4-BA.HCl is 310 kJ mol^{-1} (see Chapter 4). An enthalpy of solvation of comparable size is required for the dissolution of 4-BA.$HCl_{(s)}$. At 323 K dissolution of 4-BA.$HCl_{(s)}$ was observed (Section 6.1.1.1). At temperatures below 323 K dissolution of 4-BA.$HCl_{(s)}$ is believed to be the only possible reaction.

Above 373 K substantial mass loss was observed during the TGA experiments. At these temperatures there is thought to be enough energy to break the ionic forces holding the ion pair, 4-BA.HCl$_{(solv)}$ (449 kJ mol^{-1}), together and release 4-BA$_{(solv)}$. However, the solution reactions (Section 6.1.2) suggest that without the release of HCl$_{(g)}$ the break up of the ion pair is not possible. Investigations of the dissolution of HCl in chlorobenzene (Chapter 3 Section 3.2.3) indicated that HCl is not easily dissolved in chlorobenzene, taking 30 min to saturate at 0.1 mol L^{-1}. The attempts at dissolution of HCl in chlorobenzene by trapping HCl$_{(g)}$ above chlorobenzene were not successful (Chapter 3 Section 3.2.2) which implies that once HCl has partitioned into the gas phase it is unlikely to go back into solution; therefore, K_3 lies to the right hand side (Figure 115). This is consistent with the low mole fraction (0.0319 at 1.013 bar) of HCl in chlorobenzene chlorobenzene.[27]

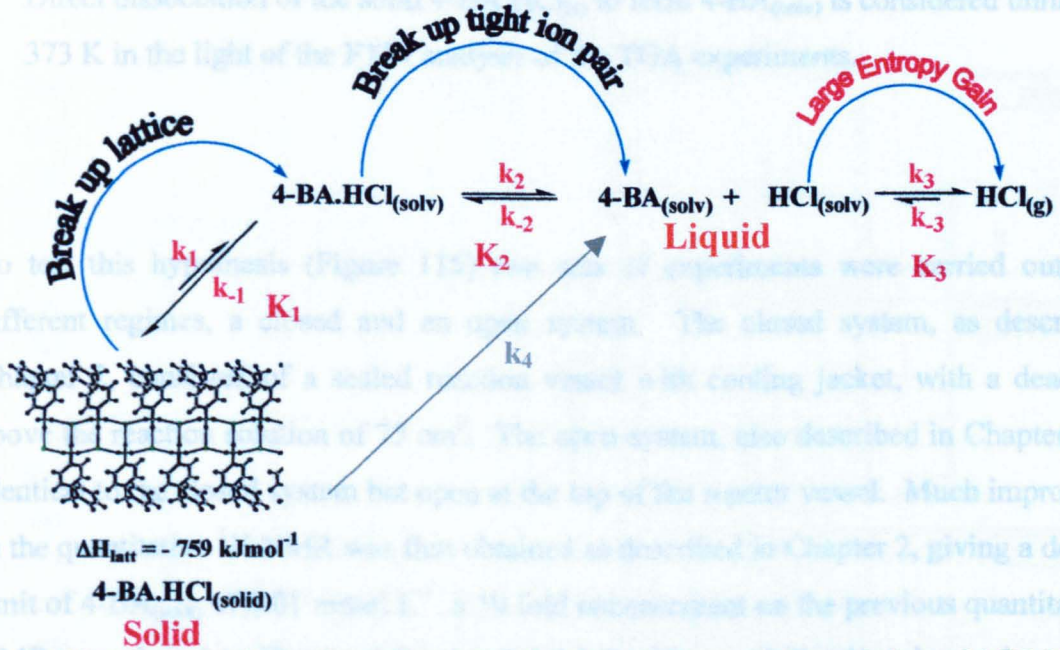

Figure 115 Proposed reaction scheme for the dissolution and dissociation of 4-BA.HCl$_{(s)}$ in chlorobenzene.

This reaction scheme moves away from a more generalised equilibrium between solid amine hydrochloride and solvated amine. It is proposed (Figure 115) that there are three equilibria involved in the solution based reaction:

Equilibrium K_1

The dissolution of 4-BA.HCl$_{(s)}$ in chlorobenzene resulting in the formation of a solvated 4-BA.HCl, a tight ion pair.

Equilibrium K_2

The break-up of the tight ion pair (4-BA.$HCl_{(solv)}$) to form 4-$BA_{(solv)}$ and $HCl_{(solv)}$. 4-$BA_{(solv)}$ should form when $HCl_{(solv)}$ can partition into the gas phase and escape from the system.

Equilibrium K_3

The partitioning of $HCl_{(solv)}$ into the vapour phase is thought to be the controlling step in the reaction scheme. If $HCl_{(solv)}$ can partition into the gas phase, under open reaction conditions, $HCl_{(g)}$ is not expected to re-dissolve in chlorobenzene. This implies the k_{-3} reaction is limited and so therefore is the k_{-2} reaction.

***Thermal dissociation of* solid, rate coefficient k_4**

Direct dissociation of the solid 4-BA.$HCl_{(s)}$ to form 4-$BA_{(solv)}$ is considered unlikely at 373 K in the light of the FTIR analysis of the TGA experiments.

To test this hypothesis (Figure 115) two sets of experiments were carried out, under different regimes, a closed and an open system. The closed system, as described in Chapter 2, consisted of a sealed reaction vessel with cooling jacket, with a dead space above the reaction solution of 75 cm^3. The open system, also described in Chapter 2, was identical to the closed system but open at the top of the reactor vessel. Much improvement in the quantitative ^1H NMR was first obtained as described in Chapter 2, giving a detection limit of 4-$BA_{(solv)}$ of 0.01 mmol L^{-1}, a 10 fold enhancement on the previous quantitative ^1H NMR procedure (see Chapter 2 Section 2.4.7.4.3). These solution based experiments were all performed using the Radleys carousel reaction station, (Chapter 2).

6.2.1 Experiments under closed conditions

Four experiments were performed at 373 K under closed conditions. Under these conditions only a slow dissolution of 4-BA.$HCl_{(s)}$ is observed, no amine is detected over a period of 24 h in all four experiments, the ^1H NMR spectra are shown in Figure 116, the blue asterisk indicates the region of the spectra, ~ 3 ppm, where the NH_2 signal would be observed. Figure 116 shows the data from Experiment A, a sequential growth in intensity of the CH_2 signal is observed, with a final concentration of 2.26 mmol L^{-1}; no amine signal

is observed. This result is consistent with the hypothesis that under conditions where the release of $HCl_{(solv)}$ to the gas phase is hindered, the formation of 4-$BA_{(solv)}$ is not possible.

Within the confines of a generalised equilibrium model (Equation (63)) using the revised detection limit of free amine of 0.01 mmol L^{-1} and a saturation concentration of 4-$BA.HCl_{(solv)}$ of 2.26 mmol L^{-1}, an upper limit of the equilibrium constant can be estimated (Equation (66)).

$$K_2 = \frac{[4\text{-}BA_{(solv)}]\,[HCl_{(solv)}]}{[4\text{-}BA.HCl_{(solv)}]} < 4.5 \times 10^{-8}\ \text{mol}\ L^{-1} \qquad (66)$$

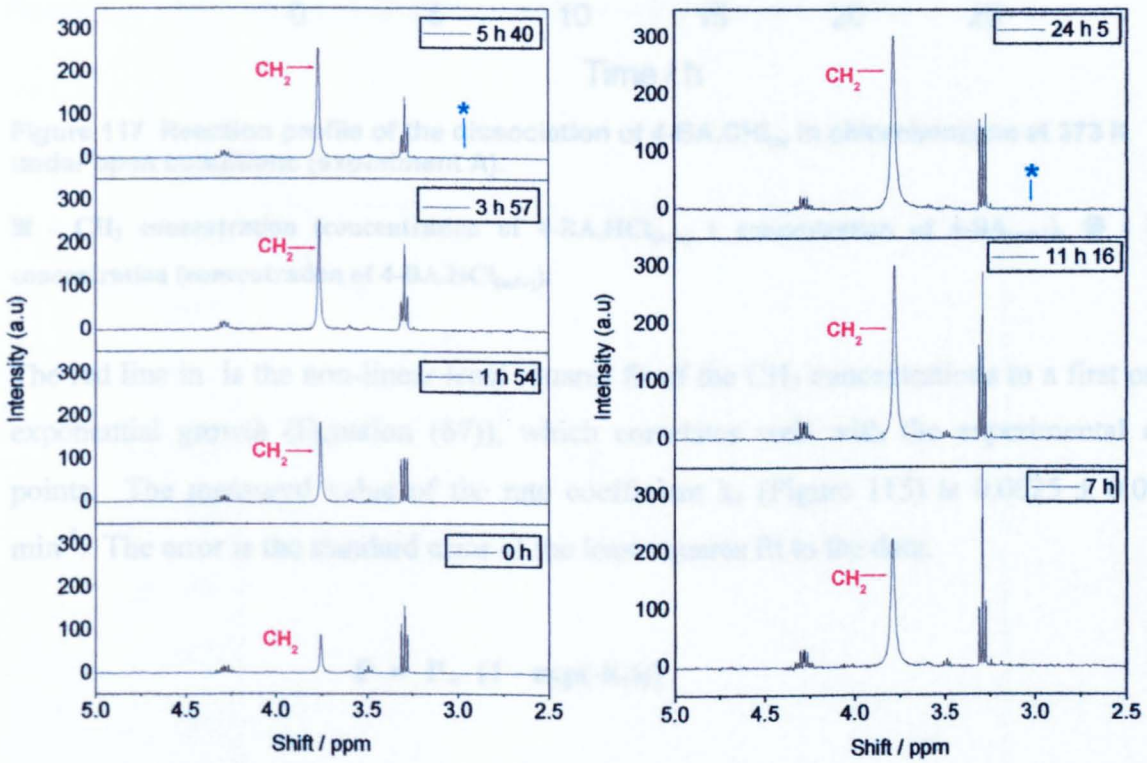

Figure 116 ^1H NMR spectra from the reaction of 4-$BA.HCl_{(s)}$ at 373 K under closed conditions, experiment A.

*** - the region of the spectrum where the NH_2 signal would be observed if 4-$BA_{(solv)}$ was formed.**

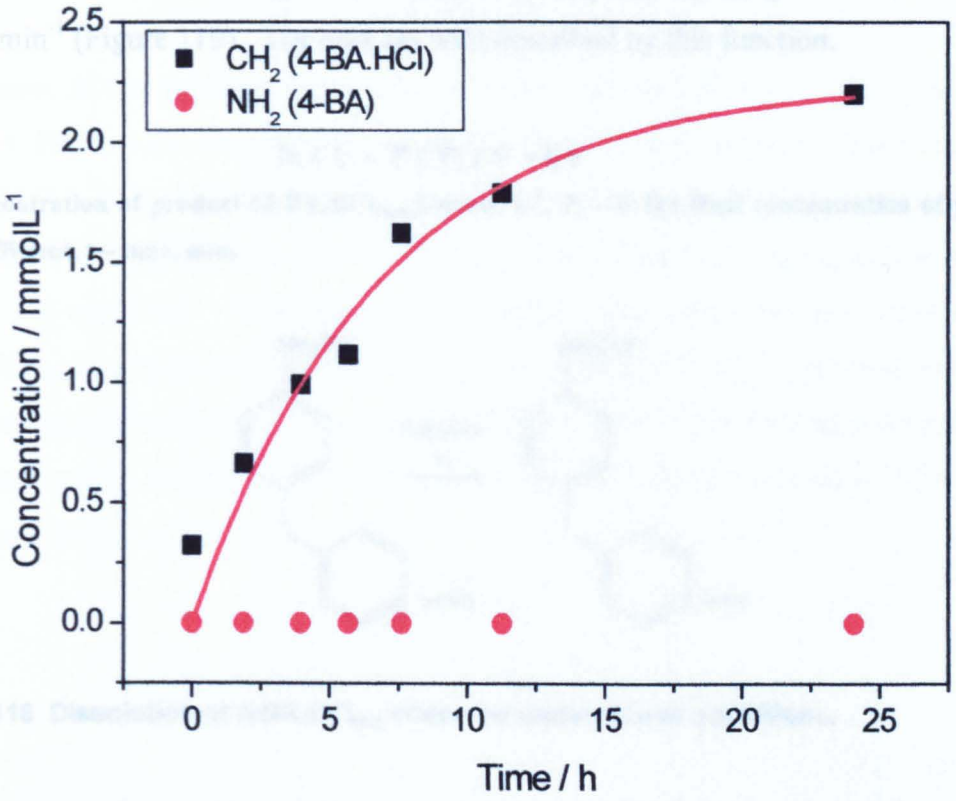

Figure 117 Reaction profile of the dissociation of 4-BA.CHl$_{(s)}$ in chlorobenzene at 373 K under open conditions (experiment A).

■ - CH_2 concentration (concentration of 4-BA.HCl$_{(solv)}$ + concentration of 4-BA$_{(solv)}$), ● - NH_2 concentration (concentration of 4-BA.HCl$_{(solv)}$).

The red line in is the non-linear least squares fit of the CH_2 concentrations to a first order exponential growth (Equation (67)), which correlates well with the experimental data points. The measured value of the rate coefficient k_1 (Figure 115) is 0.0025 ± 0.0005 min^{-1}. The error is the standard error of the least squares fit to the data.

$$P = P_\infty (1 - \exp(-k_1 t)) \quad (67)$$

P – concentration of CH_2, P_∞ - the final concentration of CH_2, k_1 – rate coefficient, t – time (h).

The rate coefficient of the k_1 reaction (Figure 118) with respect to the solid 4-BA.HCl, would be expected to be zero order, dissolution of a solid is thought to be a zero order process,[128] but the concentration of 4-BA.HCl$_{(s)}$ cannot be measured experimentally. The concentration of the product of the k_1 reaction (4-BA.HCl$_{(solv)}$) is measured, and is treated with first order kinetics as 4-BA.HCl$_{(solv)}$ formation is not continuous but hindered by its limited solubility in chlorobenzene. Fitting the dissolution of 4-BAHCl$_{(s)}$ to the integrated

rate equation for first order growth of a product (Equation (68)) gives a rate of 0.0025 ± 0.0001 min^{-1} (Figure 119). The data are well described by this function.

$$\ln (1 - P / P_t) = - k t \quad (68)$$

P – concentration of product (4-BA.HCl$_{(solv)}$) mmol L^{-1}, P_t – is the final concentration of product, k-rate coefficient, t – time, min.

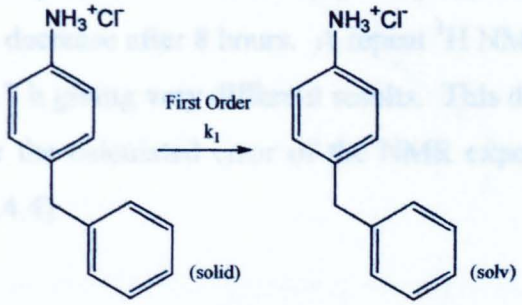

Figure 118 Dissolution of 4-BA.HCl$_{(s)}$, observed under closed conditions.

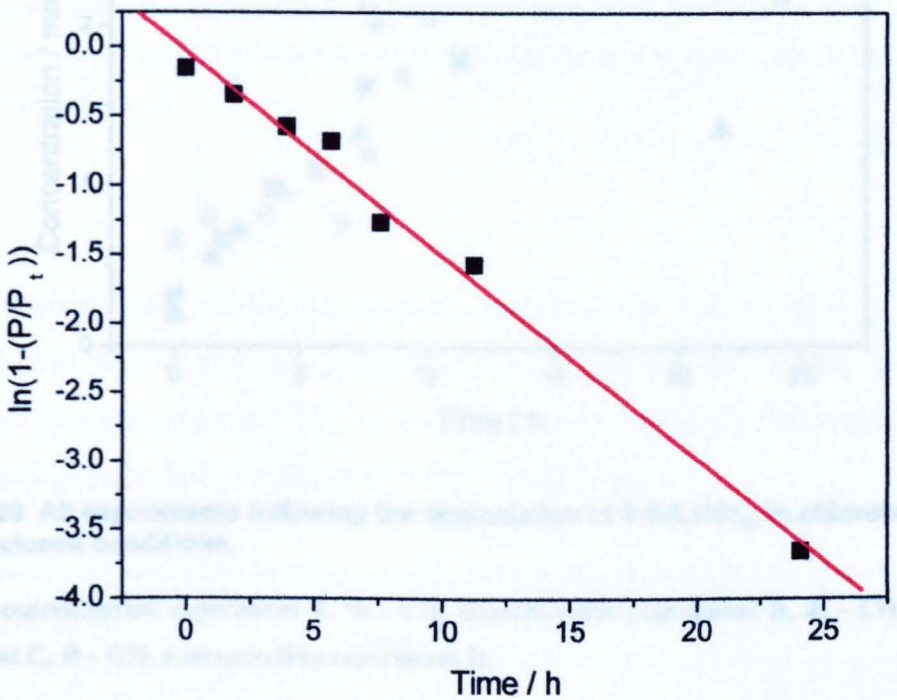

Figure 119 The dissolution of 4-BA.HCl$_{(s)}$ (experiment A) fitted to first order kinetics (Equation (68)).

■ - CH_2 concentration (concentration of 4-BA.HCl$_{(solv)}$) used as P in Equation (68).

6.2.1.1 Comparison of all k_1 experiments at 373 K

Experiment A was repeated three times, the data collected from all four experiments are shown in Figure 120. Excluding experiment D, all reactions appear to have similar initial rates of 4-BA.HCl$_{(s)}$ dissolution. Experiments A and B were run for over 20 h; both show the saturation of the solution of 4-BA.HCl$_{(solv)}$. Unreacted 4-BA.HCl$_{(s)}$ was present at the end of all reactions. Experiment D is initially very fast but the concentration of 4-BA.HCl$_{(solv)}$ appears to decrease after 8 hours. A repeat ^{1}H NMR spectrum was recorded for the sample taken at 6.7 h giving very different results. This difference cannot be easily explained, and is outside the calculated error of the NMR experiment of 0.23 mmol L^{-1} (Chapter 2, Section 2.4.7.4.4).

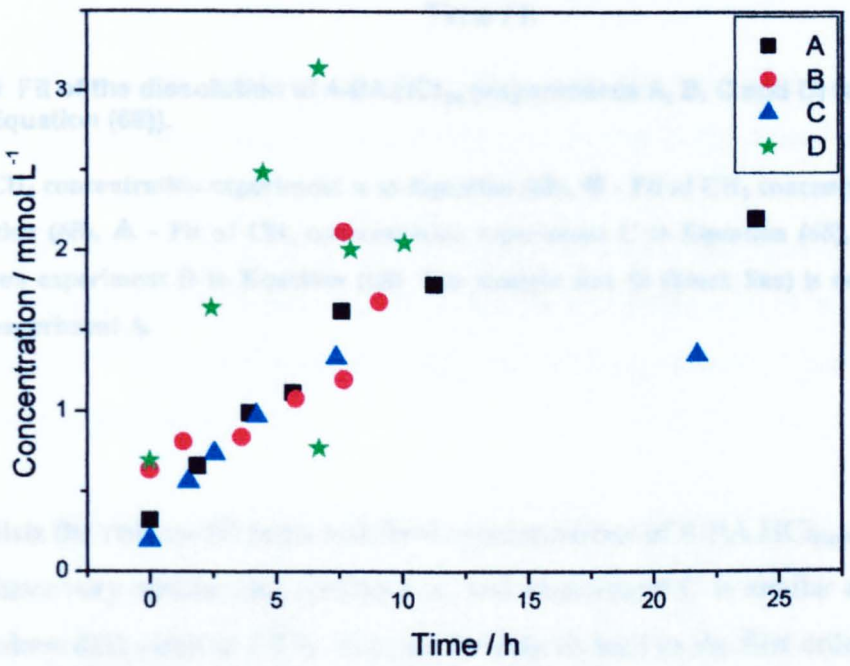

Figure 120 All experiments following the dissociation of 4-BA.HCl$_{(s)}$ in chlorobenzene at 373 K under closed conditions.

■ - CH_2 concentration experiment A, ● - CH_2 concentration experiment B, ▲ - CH_2 concentration experiment C, ★ - CH_2 concentration experiment D.

The data treated according to Equation (68), from all four experiments are shown in Figure 121. The straight line fit (the black line in Figure 121) is only applied to the data from experiment A. Comparing the data from all experiments, apart from one anomalous point from experiment C, the scatter in the data is small. All experiments appear to conform to first order growth of product, 4-BA.HCl$_{(solv)}$.

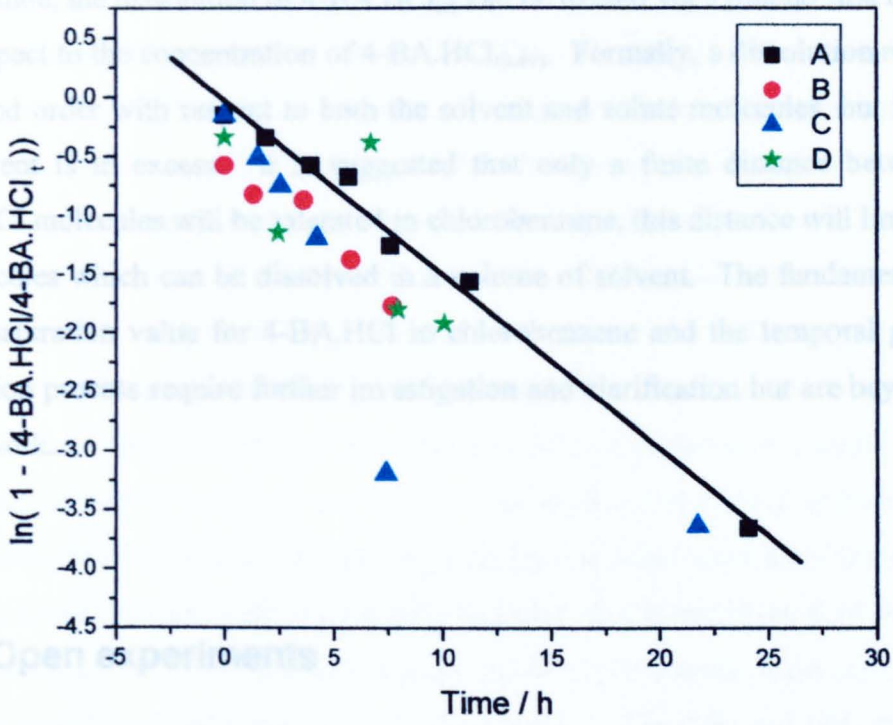

Figure 121 Fit of the dissolution of 4-BA.HCl$_{(s)}$ (experiments A, B, C and D) to first order kinetics (Equation (68)).

■ - Fit of CH_2 concentration experiment A to Equation (68), ● - Fit of CH_2 concentration experiment B to Equation (68), ▲ - Fit of CH_2 concentration experiment C to Equation (68), ★ - Fit of CH_2 concentration experiment D to Equation (68). The straight line fit (black line) is only applied to the data from experiment A.

Table 52 lists the rate coefficients and final concentrations of 4-BA.HCl$_{(solv)}$. Experiments A and B have very similar rate coefficients, and experiment C is similar also, apart from one anomalous data point at 7.5 h. Overall the data fit well to the first order rate equation, and have an average rate coefficient of 0.005 ± 0.003 min^{-1}.

Experiment	[4-BA.HCl$_{(solv)}$] (mmol L^{-1})	k_1 (min^{-1})
A	2.26	0.0025 ± 0.0002
B	1.44	0.003 ± 0.004
C	1.39	0.005 ± 0.001
D	2.4	0.01 ± 0.008

Table 52 Saturation values of 4-BA.HCl$_{(solv)}$ and rate coefficients for reactions of the dissociation of 4-BA.HCl$_{(s)}$ in chlorobenzene at 373 K under closed conditions, experiments A, B C and D.

To conclude, the dissolution of 4-BA.$HCl_{(s)}$ can be treated via a pseudo first order reaction, with respect to the concentration of 4-BA.$HCl_{(solv)}$. Formally, a dissolution reaction would be second order with respect to both the solvent and solute molecules, but in this system the solvent is in excess. It is suggested that only a finite distance between solvated 4-BA.HCl molecules will be tolerated in chlorobenzene, this distance will limit the number of molecules which can be dissolved in a volume of solvent. The fundamental principles on the saturation value for 4-BA.HCl in chlorobenzene and the temporal profile for the dissolution process require further investigation and clarification but are beyond the scope of this work.

6.2.2 Open experiments

Three experiments were performed under open conditions at 373 K, as described in Chapter 2. The reactor configuration was identical to that in the closed experiments (see Section 6.2.1) except the reaction vessels were open at the top, allowing any $HCl_{(solv)}$ formed to partition into the gas phase and be lost from the reaction system (Figure 122). In these experiments the CH_2 signal represents the total concentration of both 4-BA.$HCl_{(solv)}$ and 4-$BA_{(solv)}$, the NH_2 signal represents only the 4-$BA_{(solv)}$ species. Figure 123 shows the results from experiment 1.

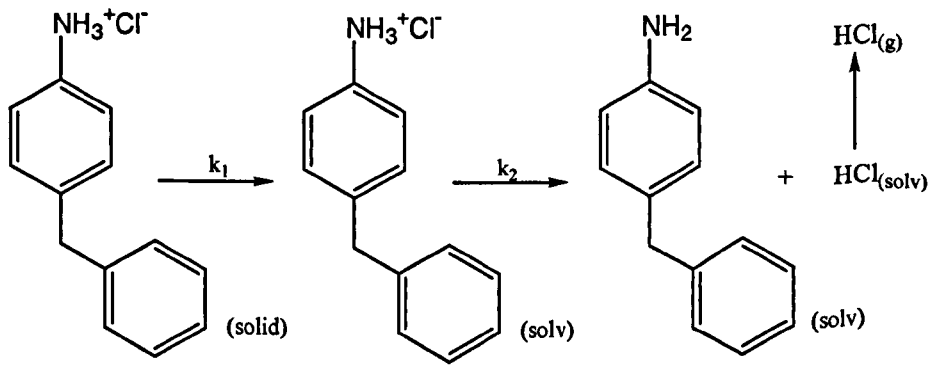

Figure 122 Open experiment reaction scheme.

The concentrations calculated by NMR analysis of all samples from experiment 1, except that at 7.6 h, were consistently low. Variance observed in the spectra obtained using the pre-saturation ^1H NMR pulse program gives standard deviations of CH_2 and NH_2 concentrations listed in Table 14, Chapter 2. Misalignment of the frequency of the pre-

saturation pulse with the resonance frequency of the chlorobenzene proton signals which are designated for suppression can cause spectra to be obtained which appear to have lower concentrations of solute than expected. A slight drift in the magnetic field of the spectrometer could cause this misalignment. This variance is thought to be the cause of the low concentrations recorded for the samples of experiment 1. To compensate for these consistently low measured concentrations, a normalisation procedure was followed; the concentrations of NH_2 and CH_2 signals were normalised with respect to the final concentration of CH_2 at completion of the reaction. The reaction was deemed to be complete when the integrals of the CH_2 and NH_2 signals were equal signifying full conversion of starting material to amine. For experiment 1, final concentrations were calculated by NMR as 4 mmol L^{-1} although the known initial concentration of 4-BA.$HCl_{(s)}$, (A_0) which had been completely converted to amine would have been 6.16 mmol L^{-1}. The concentration of the NH_2 and CH_2 signals in the 21 h sample were normalised to the starting concentration of 4-BA.$HCl_{(s)}$, 6.16 mmol L^{-1}. The CH_2 and NH_2 integrals of the remaining samples were then scaled according to this 21 h sample. This refinement of the data was performed in the belief that 100 % mass balance should have been achieved by comparison with the other two sets of experiments, which did achieve full conversion.

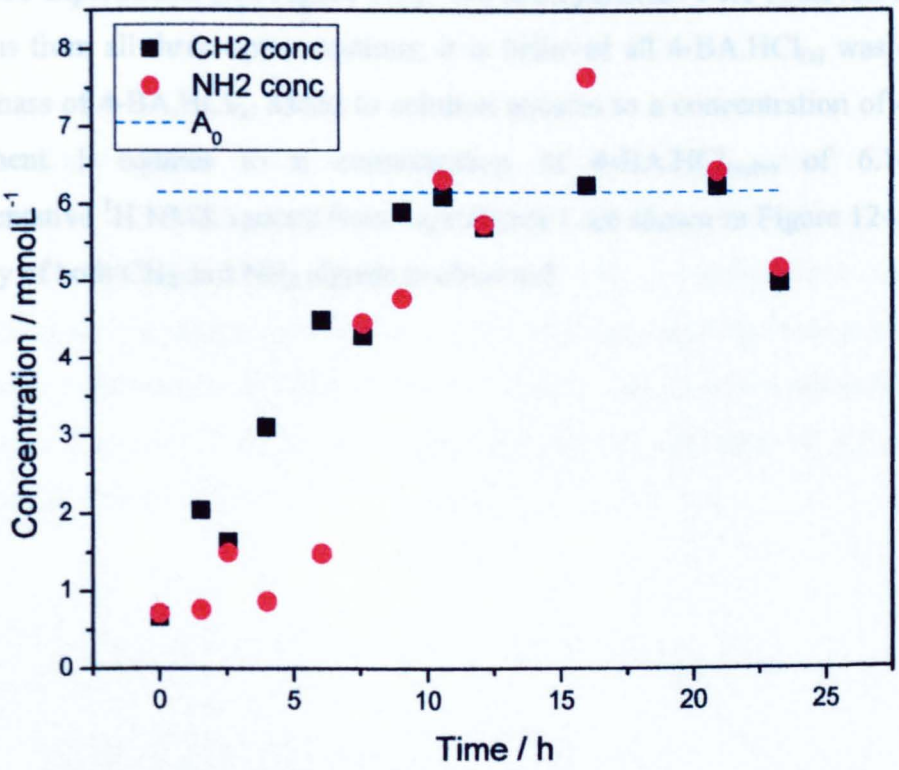

Figure 123 Reaction profile of the dissolution and dissociation of 4-BA.$CHl_{(s)}$ in chlorobenzene at 373 K under open conditions (experiment 1).

A_0 – the initial concentration of 4-BA.$HCl_{(s)}$, in this case 6.16 mmol L^{-1}, ■ - CH_2 concentration (concentration of 4-BA.$HCl_{(solv)}$ + concentration of 4-$BA_{(solv)}$), ● - NH_2 concentration (concentration of 4-BA.$HCl_{(solv)}$).

Figure 123 shows the rapid formation of 4-$BA_{(solv)}$ which reaches a final concentration equal to the CH_2 concentration after approximately 10 h, which is consistent with all 4-BA.$HCl_{(s)}$ having been converted to 4-$BA_{(solv)}$ the other two series of experiments reproduce this trend. During the initial stage of the experiment, 0 – 10 h, the concentration of 4-$BA_{(solv)}$ is always less than the CH_2 concentration, consistent with a consecutive process. The CH_2 concentration represents both 4-BA.$HCl_{(solv)}$ and 4-$BA_{(solv)}$ whereas the NH_2 concentration only represents the 4-$BA_{(solv)}$ species. If the reaction is a consecutive process 4-$BA_{(solv)}$ is produced from 4-BA.$HCl_{(solv)}$ and so its concentration can never exceed that of its starting material, 4-BA.$HCl_{(solv)}$. This does not prove this is a consecutive process; a lower concentration of 4-$BA_{(solv)}$ could also be a result from a concurrent process which formed 4-BA.$HCl_{(solv)}$ and 4-$BA_{(solv)}$ from 4-BA.$HCl_{(s)}$, as long as the rate coefficient of the 4-BA.$HCl_{(solv)}$ reaction was greater. This topic is discussed later in Section 6.3.1.

The final five data points (Figure 123) excluding that at 16 h, have nearly equal CH_2 and NH_2 concentrations, consistent with the full conversion of 4-BA.HCl to 4-BA. The final concentration of 4-$BA_{(solv)}$ is 6 mmol L^{-1}, much greater than the saturated solutions obtained in the closed experiments. The NH_2 profile is dramatically different from that of the closed experiments (see Figure 118). No solid particles were observed in the resulting solutions from all three open reactions; it is believed all 4-BA.$HCl_{(s)}$ was consumed, the initial mass of 4-BA.$HCl_{(s)}$ added to solution equates to a concentration of 4-BA.$HCl_{(s)}$ in experiment 1 equates to a concentration of 4-BA.$HCl_{(solv)}$ of 6.16 mmol L^{-1}. Representative ^1H NMR spectra from experiment 1 are shown in Figure 124; the growth in intensity of both CH_2 and NH_2 signals is observed.

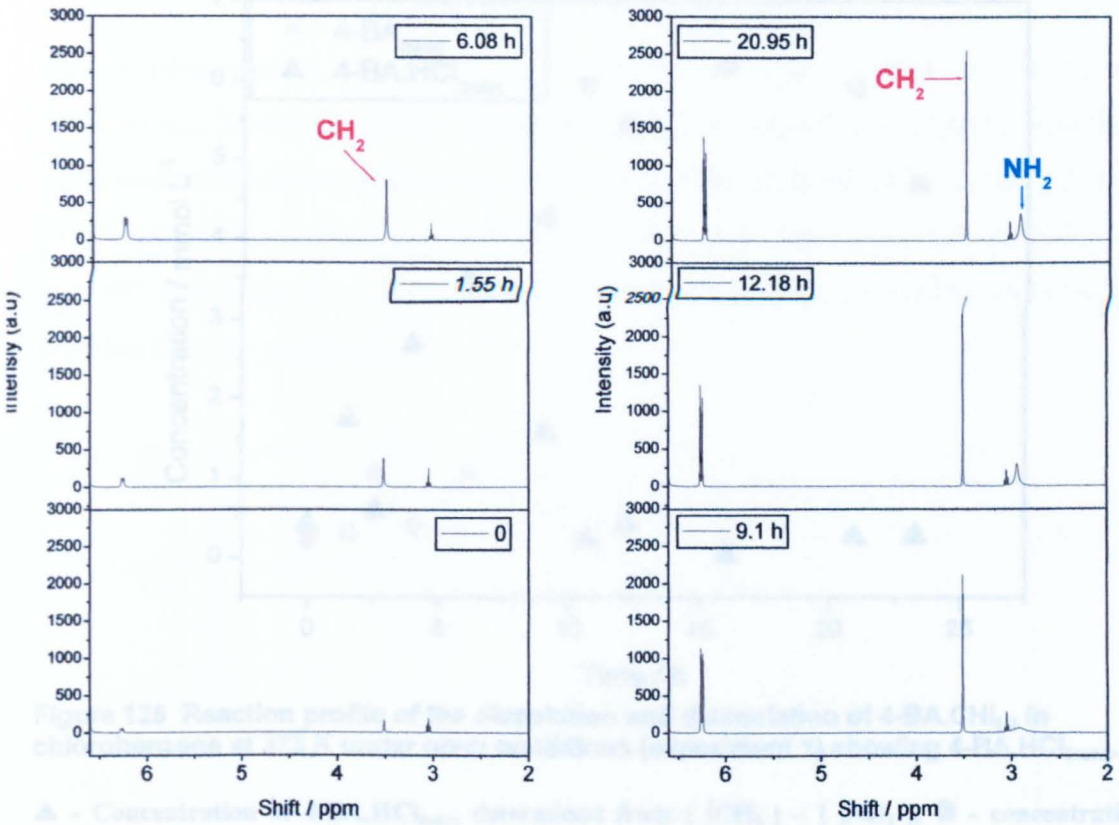

Figure 124 Example ^{1}H NMR spectra from experiment 1, reaction of 4-BA.HCl$_{(s)}$ in chlorobenzene at 373 K, under open conditions

The CH_2 signal represents both 4-BA.HCl$_{(solv)}$ and 4-BA$_{(solv)}$ whereas the NH_2 signal represents only the 4-BA$_{(solv)}$ species. This means the reaction profile of 4-BA.HCl$_{(solv)}$, can be calculated by the subtraction of the NH_2 concentrations from the CH_2 concentrations. The reaction profile of the 4-BA.HCl$_{(solv)}$ species is shown in Figure 125, and appears to behave as an intermediate, reaching a maximum concentration at 6 h, then dropping to 0 mmol L^{-1} at the same time that the concentration of 4-BA$_{(solv)}$ plateaus, signifying the end of reaction.

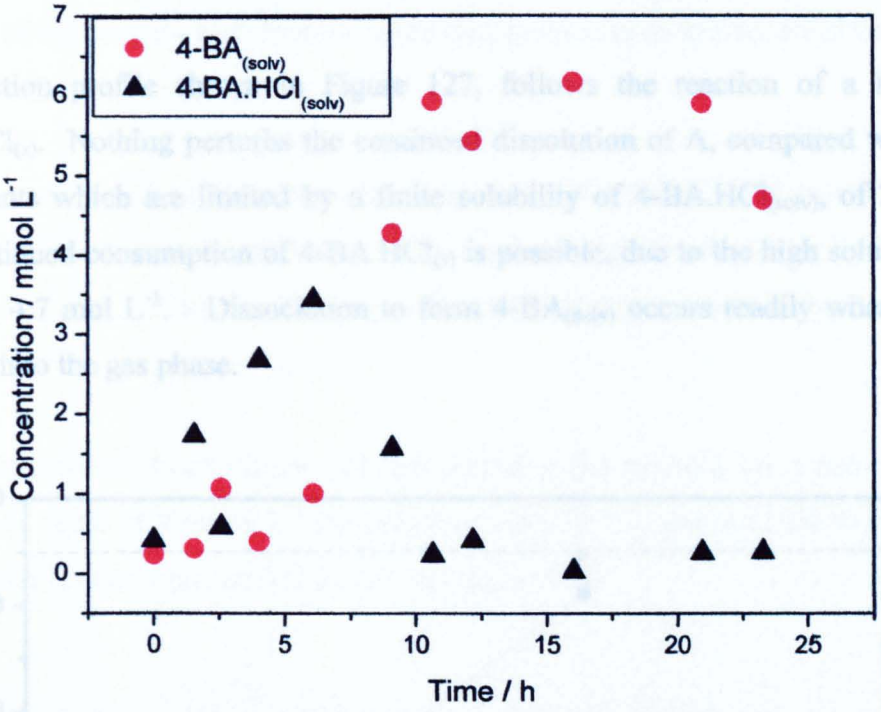

Figure 125 Reaction profile of the dissolution and dissociation of 4-BA.CHI$_{(s)}$ in chlorobenzene at 373 K under open conditions (experiment 1) showing 4-BA.HCl$_{(solv)}$.

▲ - Concentration of 4-BA.HCl$_{(solv)}$ determined from [∫CH$_2$] – [∫NH$_2$], ● - concentration of 4-BA.HCl$_{(solv)}$ determined from ∫NH$_2$.

6.3 Development of a kinetic model

The Open experiment reactions are believed to be a consecutive process (Figure 115) where the consumption of A, 4-BA.HCl$_{(s)}$, to form the intermediate B, 4-BA.HCl$_{(solv)}$is a zero order process, followed by the 1st order consumption of B to produce C, 4-BA$_{(solv)}$ (Figure 126).

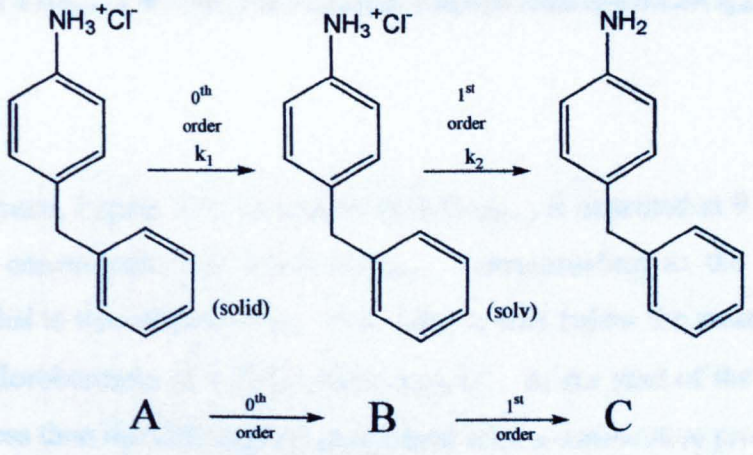

Figure 126 Consecutive reaction model, dissolution of 4-BA.HCl$_{(s)}$ followed by the dissociation of 4-BA.HCl$_{(solv)}$ to form 4-BA$_{(solv)}$.

6.3.1 Justification of first stage: 0th order

The reaction profile shown in Figure 127, follows the reaction of a large mass of 4-BA.HCl$_{(s)}$. Nothing perturbs the continued dissolution of A, compared with the closed experiments which are limited by a finite solubility of 4-BA.HCl$_{(solv)}$, of 2.2 mmol L^{-1}. This continued consumption of 4-BA.HCl$_{(s)}$ is possible, due to the high solubility of 4-BA in MBC, 4.7 mol L^{-1}. Dissociation to form 4-BA$_{(solv)}$ occurs readily when HCl$_{(solv)}$ can partition into the gas phase.

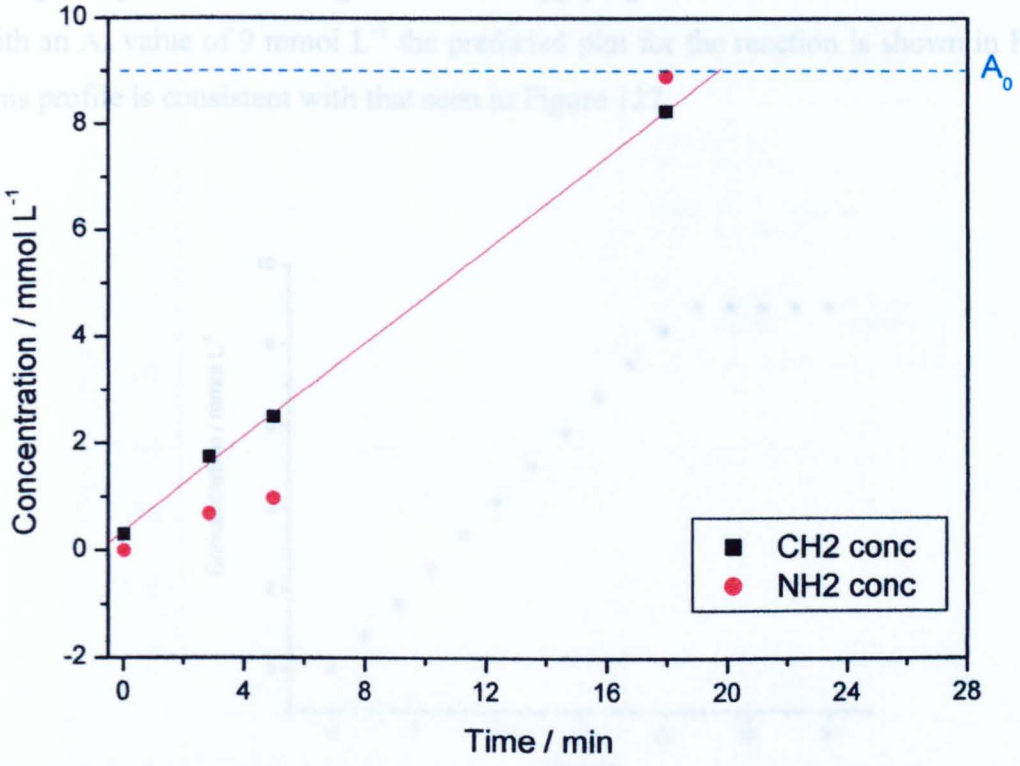

Figure 127 Reaction profile of the dissolution and dissociation of 4-BA.CHl$_{(s)}$ in chlorobenzene at 373 K under open conditions (experiment 2).

A_0 – the initial concentration of 4-BA.HCl$_{(solv)}$ (6.16 mmol L^{-1}) expected from the mass of 4-BA.HCl$_{(s)}$ added at the start of the reaction, ■ - CH_2 concentration (concentration of 4-BA.HCl$_{(solv)}$ + concentration of 4-BA$_{(solv)}$), ● - NH_2 concentration (concentration of 4-BA.HCl$_{(solv)}$).

In this experiment, Figure 127, saturation of 4-BA$_{(solv)}$ is expected at 9 mmol L^{-1}, equal to the expected concentration of 4-BA.HCl$_{(solv)}$ corresponding to the initial mass of 4-BA.HCl$_{(s)}$ added to the solution (A_0). This value is well below the saturation concentration of 4-BA in chlorobenzene of 4.722 ± 0.034 mol L^{-1}. At the start of the reaction the values of 4-BA are less than the CH_2 signals, consistent with a consecutive process. At the end of the reaction these concentrations are taken to be equal, all A has been converted to C. The

slight discrepancy observed between the CH_2 and NH_2 values of the final sample is the measure of uncertainty in determining the concentrations of species from the NMR signals at these concentration levels.

The linear plot of the CH_2 signals has a gradient of 0.007 ± 0.001 mmol L^{-1} min^{-1}. The reaction defines a zero order profile. It is expected that the slope will be sensitive to the degree of mixing. If we could measure the concentration of A directly, we would be able to determine k_1.

Using the gradient from Figure 127 and applying the formula for a zero order reaction, with an A_o value of 9 mmol L^{-1} the predicted plot for the reaction is shown in Figure 128. This profile is consistent with that seen in Figure 127.

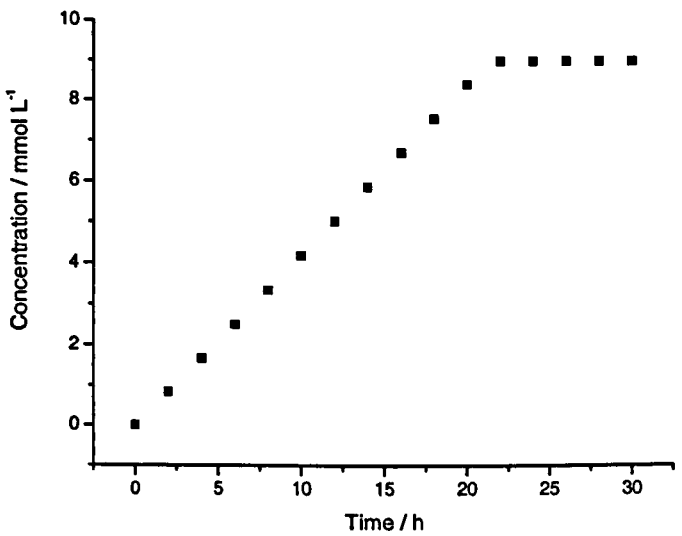

Figure 128 Zero order reaction.

Simulation of 4-BA.HCl$_{(solv)}$ concentration in chlorobenzene at 373 K assuming dissolution process of 9 mmol L^{-1} of 4-BA.HCl$_{(s)}$ to be zero order with an associated rate constant of 0.007 mmol L^{-1} min^{-1}.

6.3.2 Justification of second stage: 1st order

Figure 125 indicates that the concentration of 4-BA.HCl$_{(solv)}$, B, reaches a maximum at 6 h, then decays to 0 mmol L^{-1} by 10 h. This coincides with the concentration of C reaching a maximum. The decay of B between 6 and 10 h appears to follow a first order exponential decay, Figure 125. A non-linear least squares fit of the experimental values of B to a first

order exponential decay is obtained (see Equation (69) and Figure 129). The rate of this decay, which corresponds to k_2 in Figure 126 has a value of 0.006 ± 0.034 min^{-1}.

This is consistent with the second stage of the consecutive reaction being first order. After all of the 4-BA.HCl$_{(solid)}$ is consumed, B_{max}, the decay of B is a first order process, and therefore the production of 4-BA$_{(solv)}$, C, is first order.

$$B = A_0 \exp(-k_2 t) \quad (69)$$

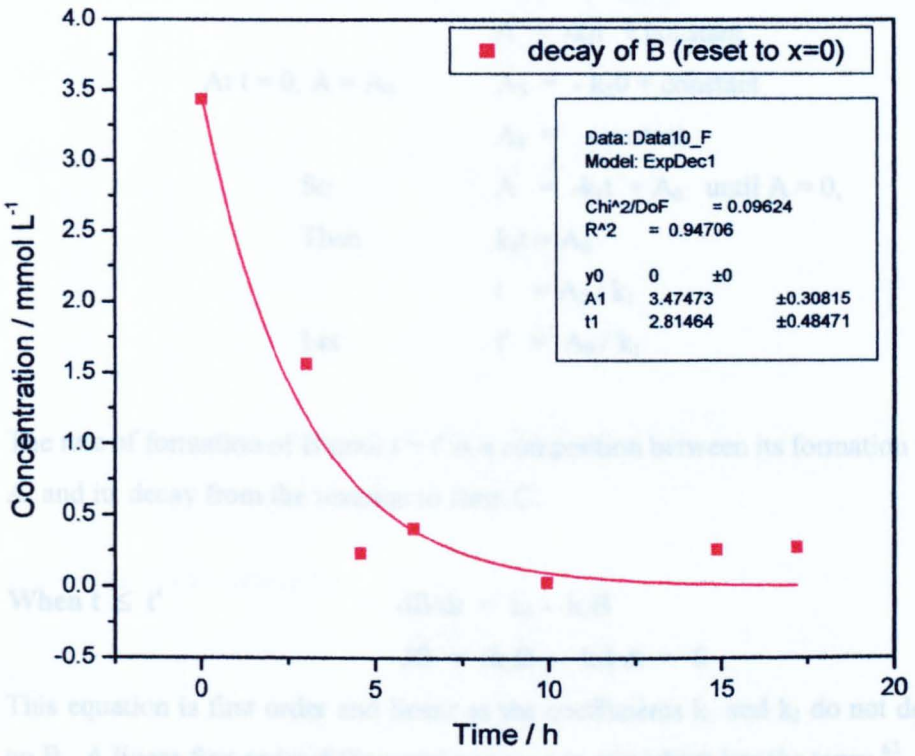

Figure 129 Fit of 1st order decay (Equation (69)) to 4-BA.HCl$_{(solv)}$ (B) after B_{max} (6 h) in experiment 1 (Figure 125).

■ - Concentration of 4-BA.HCl$_{(solv)}$ from experiment 1 between 6 and 10 h.

6.3.3 Derivation of the rate equations for a 0th, 1st order consecutive process

A search of the chemical literature for a 0th order followed by 1st order consecutive process provided no analytical expressions.[61, 62] The following kinetic model for 0th order followed by 1st order consecutive reactions was derived with assistance from Dr A Miller.[129] A, B

and C represent 4-BA.HCl$_{(s)}$, 4-BA.HCl$_{(solv)}$ and 4-BA$_{(solv)}$ respectively (Equation (70)). A condition is set, at time t', where the concentration of A is zero and B is B_{max}. After time, t', the concentration of B follows a first order decay.

$$A \xrightarrow[0^{th}\ order]{k_1} B \xrightarrow[1^{st}\ order]{k_2} C \qquad (70)$$

- The rate of decay of A is zero order: $dA/dt = -k_1$

$$A = -k_1 t + constant$$

At $t = 0$, $A = A_0$: $A_0 = -k_1 0 + constant$

$$A_0 = constant$$

So: $A = -k_1 t + A_0$ until $A = 0$,

Then: $k_1 t = A_0$

$$t = A_0 / k_1$$

Let: $t' = A_0 / k_1$

- The rate of formation of B until $t = t'$ is a competition between its formation from A, and its decay from the reaction to form C.

When $t \leq t'$

$$dB/dt = k_1 - k_2 B$$

$$dB + (k_2 B - k_1)\, dt = 0$$

This equation is first order and linear as the coefficients k_1 and k_2 do not depend on B. A linear first order differential equation is one which has the term: [63]

$$dy/dt + p(t)y = g(t)$$

The integrating factor is $\exp(\int p(t)dt) = e^{k_2 t}$ and the equation becomes:

$$e^{k_2 t}\, dB + (k_2 B - k_1)\, e^{k_2 t}\, dt = 0$$

This has the form: $N(t, B)dB + M(t, B)dt = 0$

Where: $M(t, B) = (k_2 B - k_1)\, e^{k_2 t}$

And: $N(t, B) = e^{k_2 t}$

This is exact as: $\frac{dM}{dB} = \frac{dN}{dt}$

Need to find a function: $dg/dt = M$ and $dg/dB = N$

The solution is: $g(B, t) = constant$

$$g(B, t) = B\, e^{k_2 t} - (k_1/k_2)\, e^{k_2 t}$$

So the solution is $B e^{k_2 t} - (k_1/k_2) e^{k_2 t} = \text{constant}$

Now, $B = 0$ at $t = 0$, gives $\text{constant} = -k_1 / k_2$

So the solution is $B e^{k_2 t} - (k_1/k_2) e^{k_2 t} = -k_1 / k_2$

$$B = \frac{k_1}{k_2}(1 - e^{-k_2 t})$$

When $t \geq t'$ the rate of decay of B is only dependent on its decay from the reaction to form C.

$$dB/dt = -k_2 B$$

$$\int \frac{1}{B} dB = \int -k_2 \, dt$$

$$\ln B = -k_2 t + \text{constant}$$

$$B = c_1 e^{-k_2 t}$$

At $t = t'$

$$B = \frac{k_1}{k_2}(1 - e^{-k_2 t})$$

So

$$\frac{k_1}{k_2}(1 - e^{-k_2 t'}) = c_1 e^{-k_2 t'}$$

$$c_1 = \frac{k_1}{k_2}(e^{k_2 t'} - 1)$$

$$\mathbf{B = \frac{k_1}{k_2}(e^{k_2 t'} - 1) e^{-k_2 t}}$$

- C also has a time constraint.

$$dC/dt = k_2 B$$

So

$$\frac{dC}{dt} = \begin{cases} k_1 (1 - e^{-k_2 t}) & t \leq t' \\ k_1 (e^{k_2 t'} - 1) e^{-k_2 t} & t \geq t' \end{cases}$$

When $t \leq t'$

$$dC/dt = k_1 (1 - e^{-k_2 t})$$

$$C = k_1 (t + \frac{e^{-k_2 t}}{k_2}) + c_1$$

When $t = 0, C = 0$

$$0 = k_1/k_2 + c_1$$

$$c_1 = -k_1/k_2$$

and so

$$C = k_1 (t + \frac{e^{-k_2 t}}{k_2}) - k_1/k_2$$

$$C = \frac{k_1}{k_2}(tk_2 + e^{-k_2 t} - 1)$$

When $t \geq t'$

$$dC/dt = k_2 B$$

$$dC/dt = k_2 \frac{k_1}{k_2}(e^{k_2(t'-t)} - e^{-k_2 t})$$

$$= k_1 e^{-k_2 t}(e^{k_2 t'} - 1)$$

So $$C = \frac{-k_1}{k_2} e^{-k_2 t}(e^{k_2 t'} - 1) + c_1$$

At $t = t'$ $$C = \frac{k_1}{k_2}(tk_2 + e^{-k_2 t} - 1)$$

So $$\frac{k_1}{k}(t'k_2 + e^{-k_2 t'} - 1) = \frac{-k_1}{k_2} e^{-k_2 t'}(e^{k_2 t'} - 1) + c_1$$

$$c_1 = \frac{k_1}{k_2}(tk_2 + e^{-k_2 t'} - 1 + 1 - e^{-k_2 t'})$$

$$= t'k_1$$

$$C = \frac{k_1}{k_2} e^{-k_2 t}(1 - e^{-k_2 t}) + tk_1$$

Check: $B + C = A_0$ at $t = t'$

$$\frac{k_1}{k_2}(1 - e^{-k_2 t'}) + \frac{k_1}{k_2} e^{-k_2 t'}(1 - e^{-k_2 t'}) + t'k_1 = B + C$$

$$\frac{k_1}{k_2}(1 - e^{-k_2 t'} - 1 + e^{-k_2 t'}) + t'k_1 = B + C$$

$$t'k_1 = A_0$$

- From Equation (70) the final equations for A, B and C at times before and after t' are listed in Equations (71), (72) and (73).

$$A = \begin{cases} -k_1 t + A_0 & t \le t' \\ 0 & t \ge t' \end{cases} \quad (71)^{129}$$

$$B = \begin{cases} k_1/k_2(1 - \exp(-k_2 t)) & t \le t' \\ k_1/k_2(\exp(k_2(t'-t)) - \exp(-k_2 t)) & \end{cases} \quad (72)^{129}$$

$$C = \begin{cases} k_1/k_2(tk_2 + \exp(-k_2 t) - 1) & t \le t' \\ (k_1/k_2)\exp(-k_2 t)(1 - \exp(k_2 t')) + t'k_1 & t \ge t' \end{cases} \quad (73)^{129}$$

6.3.4 Modelling the data to a 0th, 1st order consecutive process

Using these integrated rate equations (Equations (71), (72) and (73)) a non linear least squares analysis was set up to find k_1 and k_2, fitting to the experimental concentrations of C from experiment 1 (Figure 130). The turning point, t', is the time when the concentration of A is zero, in experiment 1 this is at 6 h.

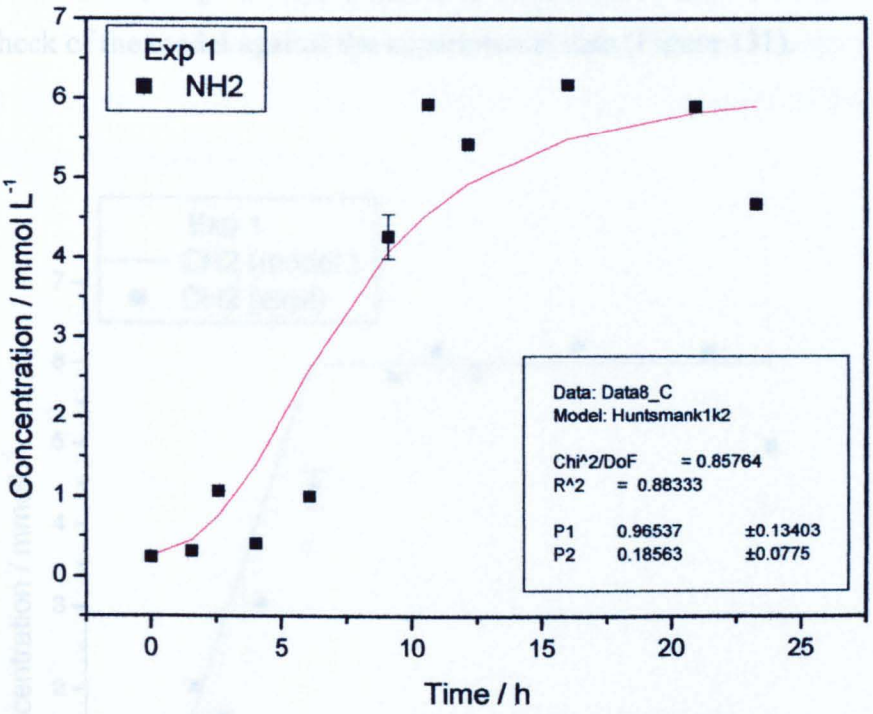

Figure 130 Non-linear least squares analysis of 4-$BA_{(solv)}$ concentrations from the reaction of the dissolution and dissociation of 4-BA.$HCl_{(s)}$ in chlorobenzene at 373 K under open conditions (experiment 1).

■ - The NH_2 concentrations represent experimentally obtained concentrations of 4-$BA_{(solv)}$ from experiment 1. The solid line is the non-linear least squares fit of Equation (73) to these data points, providing values for parameters k_1 and k_2.

The fit of the NH_2 concentrations to Equation (73) gives reasonable agreement. The errors represent the standard error in the fitting procedure.[130]

$k_1 = 0.016 +/- 0.0022$ mmol L^{-1} min^{-1} $\quad k_2 = 0.0033 +/- 0.0001$ min^{-1}

6.3.4.1 Comparison of Model with Experiment

Using these values for k_1 and k_2 and the equations for B, the concentration of 4-BA.HCl$_{(solv)}$ can be predicted. Adding this predicted concentration profile for B to the line generated for the NH_2 concentrations, which was derived from the non linear least squares fit (Figure 130) the CH_2 concentrations can be predicted, *i.e.* $CH_{2\,TOTAL}$ = 4-BA.HCl$_{(solv)}$ + 4-BA$_{(solv)}$. Thus a knowledge of k_1 and k_2 and via application of Equations (72) and (73), the concentrations of, respectively, B and C as a function of time can be calculated. This allows a check of the model against the experimental data (Figure 131).

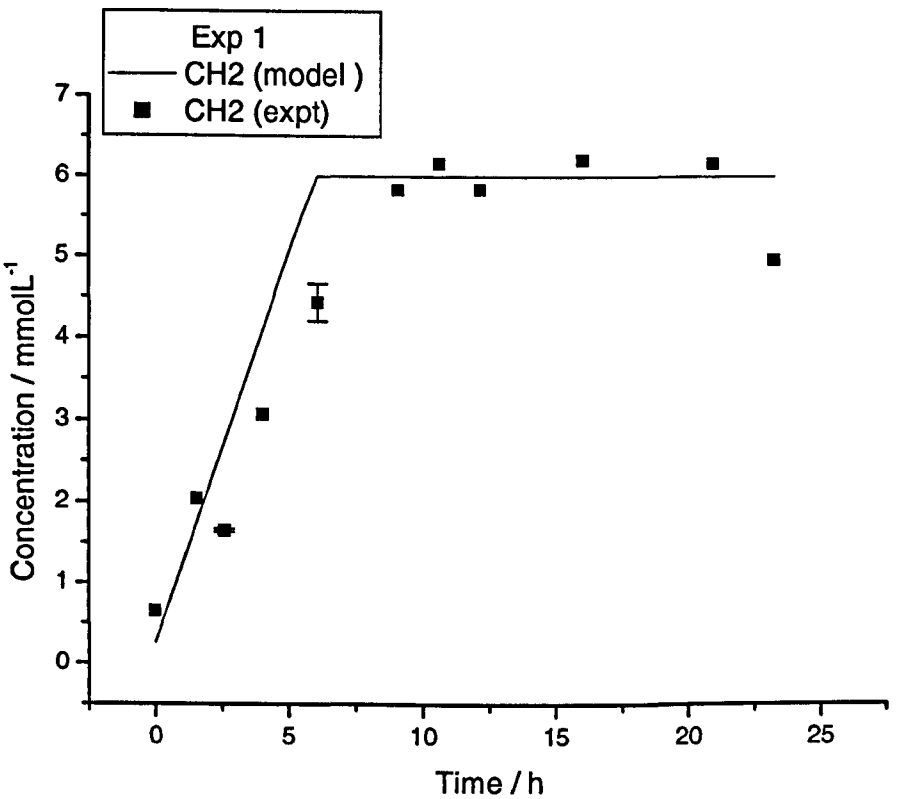

Figure 131 Non-linear least squares analysis of combined concentrations of 4-BA$_{(solv)}$ + 4-BA.HCl$_{(solv)}$ (CH_2) *from the reaction of the dissolution* and dissociation of 4-BA.HCl$_{(s)}$ in chlorobenzene at 373 K under open conditions (experiment 1, *Figure 125*).

■ - Experimental values of CH_2 concentrations. Black line - calculated CH_2 concentrations (using Equations (71), (72) and (73)).

The comparison of the model CH_2 with experimental CH_2 values shows excellent correlation. From the comparison it can be inferred that the predicted value of k_1 is

slightly large, as the model CH_2 data reaches a plateau *ca.* 3 h earlier than the experimental data. However, most of the other predicted data points are within the error of the experimental data. The error bars on the data points at 2.6 and 6 h are the standard deviations determined for 1.07 and 4.66 mmol L^{-1} 4-BA solutions respectively, using the pre-saturation ^1H NMR pulse program (as described in Chapter 2, Section 2.4.7.4.4).

The measured values of both the CH_2 and NH_2 concentrations with their associated error bars are compared with their predicted values in Figure 132. The error in the NH_2 and CH_2 values were calculated for concentrations of 1 and 4 mmol L^{-1}, as discussed in Chapter 2. The errors are largest for the 4 mmol L^{-1} solutions being 0.23 and 0.28 mmol L^{-1} for the CH_2 and NH_2 concentrations respectively.

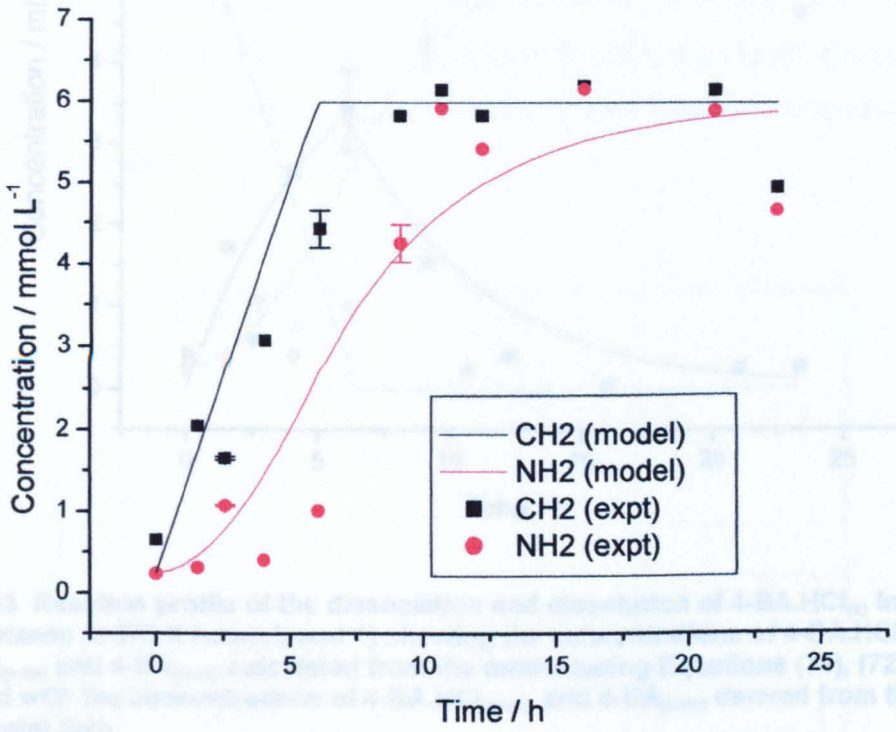

Figure 132 Non-linear least squares analysis of combined concentrations of 4-$BA_{(solv)}$ + 4-$BA.HCl_{(solv)}$ (CH_2) and the non-linear least squares analysis of the 4-$BA_{(solv)}$ (NH_2) concentrations from the reaction of the dissolution and dissociation of 4-$BA.HCl_{(s)}$ in chlorobenzene at 373 K under open conditions (experiment 1, Figure 125).

■ - Experimental values of CH_2 concentrations, black line - calculated CH_2 concentrations (using Equations (71), (72) and (73)), ● - experimental values of NH_2 concentrations, red line - calculated NH_2 concentrations from the model (using Equations (71), (72) and (73)).

The match between the experimental and model data is not exact but, considering the difficulties in the quantitative ^1H NMR measurements and the associated errors, this model is believed to be a good approximation to the real system.

Using the value for k_1 the consumption of A, 4-BA.HCl$_{(s)}$, can be predicted (Figure 133). The predicted concentrations of B compared with the experimentally determined concentrations, are also shown in Figure 133. The experimental B values are calculated by subtraction of the NH_2 concentrations from the CH_2 concentrations. The predicted value of B, is calculated from the subtraction of the predicted C values (Equation (73)) (Figure 130) from the predicted values of A (Equation (71)).

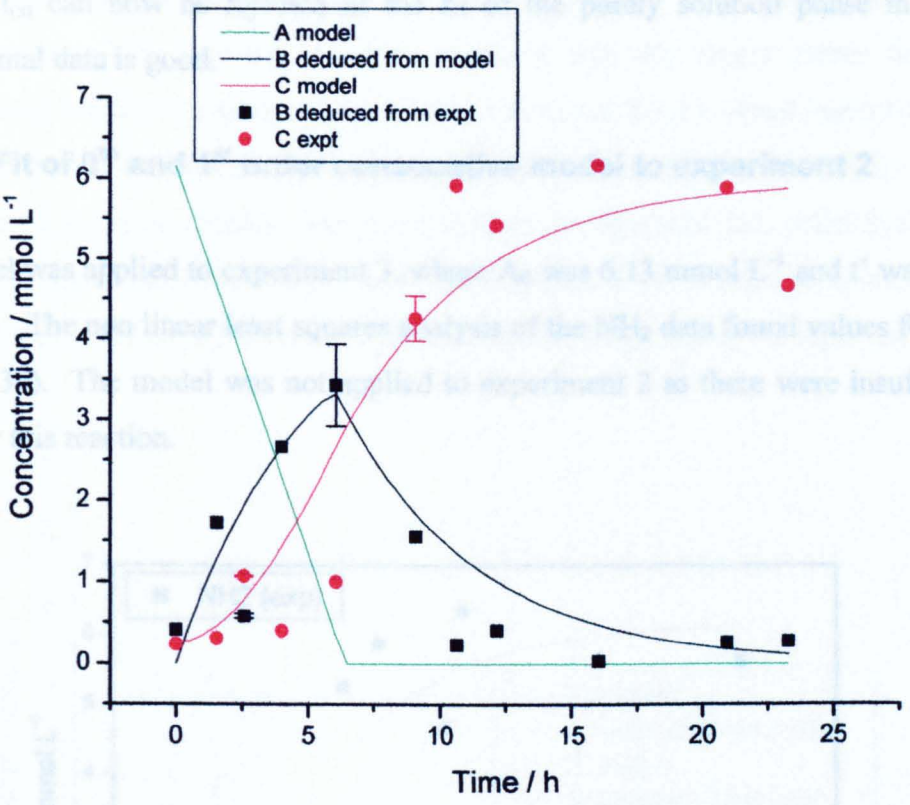

Figure 133 Reaction profile of the dissociation and dissolution of 4-BA.HCl$_{(s)}$ in chlorobenzene at 373 K (experiment 1) showing the concentrations of 4-BA.HCl$_{(s)}$, 4-BA.HCl$_{(solv)}$ and 4-BA$_{(solv)}$ calculated from the model (using Equations (71), (72) and (73)) compared with the concentrations of 4-BA.HCl$_{(solv)}$ and 4-BA$_{(solv)}$ derived from the experimental data.

■ - Experimental values of 4-BA.HCl$_{(solv)}$ concentrations (calculated by subtraction of NH_2 from CH_2 concentrations), black line - calculated 4-BA.HCl$_{(solv)}$ concentrations (using Equations (72)), ● - experimental values of 4-BA$_{(solv)}$ concentrations (calculated from the NH_2 concentrations), red line - calculated 4-BA$_{(solv)}$ concentrations from the model (using Equation (73)) and the green line - the calculated concentration of 4-BA.HCl$_{(s)}$ concentrations from the model (using Equation (71))

Comparing the experimentally deduced B with the predicted values for B, gives a fairly good agreement between the model and the experiment. The errors shown for B, are the propagated errors of the CH_2 and NH_2 signals for 4 mmol L^{-1} and 1 mmol L^{-1} solutions of 4-BA.

The maximum concentration of B is not expected to exceed the saturation limit of 2.2 mmol L^{-1} observed in the closed experiments (Figure 117). The maximum value observed in the Open experiment was 3.0 ± 0.51 $mmolL^{-1}$, which is not significantly different. Comparing the B values derived from the experiment with the predicted values for B, gives a fairly good agreement between the model and the experiment for the open system (Figure 133).

The hypothesis of a solid phase thermal dissociation route to form 4-$BA_{(solv)}$ from 4-BA.$HCl_{(s)}$ can now be rejected as the fit of the purely solution phase model to the experimental data is good.

6.3.4.2 Fit of 0th and 1st order consecutive model to experiment 2

The model was applied to experiment 3, where A_0 was 6.13 mmol L^{-1} and t' was estimated as 3.37 h. The non linear least squares analysis of the NH_2 data found values for k_1 and k_2 (Figure 134). The model was not applied to experiment 2 as there were insufficient data points for this reaction.

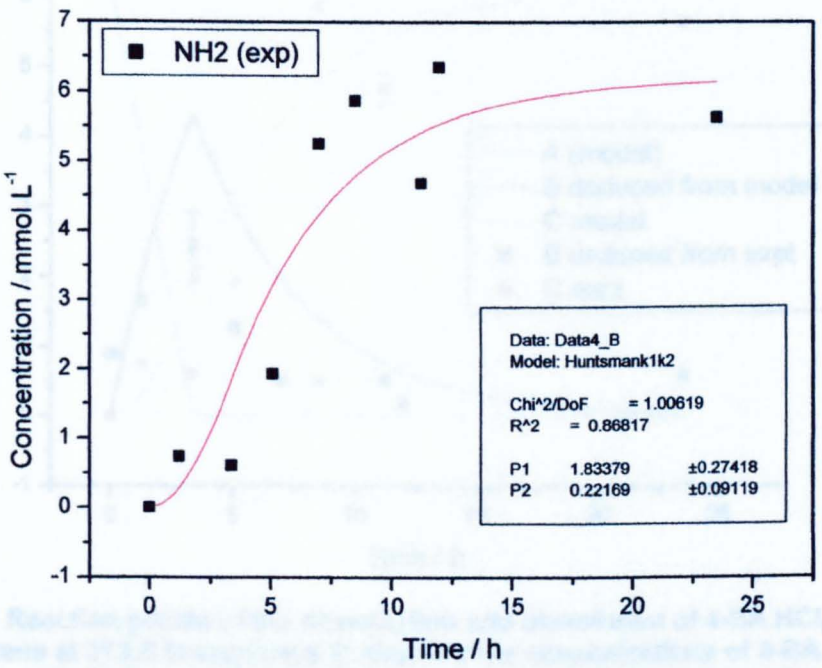

Figure 134 Non Non-linear least squares analysis of 4-$BA_{(solv)}$ concentrations from the reaction of the dissolution and dissociation of 4-BA.$HCl_{(s)}$ in chlorobenzene at 373 K under open conditions (experiment 3).

■ - The NH_2 concentrations represent experimentally obtained concentrations of 4-$BA_{(solv)}$ from experiment 1. The solid line is the non-linear least squares fit of Equation (73) to these data points, providing values for parameters k_1 and k_2.

$k_1 = 0.031 \pm 0.005$ mmol L^{-1} min^{-1} $k_2 = 0.004 \pm 0.002$ min^{-1}

The values obtained for k_1 and k_2 are significantly different from those determined using the data from experiment 3. Taking into account their associated errors, k_1 from experiment 3 is double that from experiment 1. The rate coefficient k_2 determined from experiment 1 is a little larger than that determined from experiment 3.

To compare the fit from both experiments the value of R^2, the correlation coefficient, must be compared. The closer this value is to 1, the better the fit. For experiment 1 R^2 is 0.883, for experiment 3 it is 0.868. This confirms that the model better describes the experimental results of experiment 1, which is also clear from a visual inspection of Figure 134 and Figure 135. Therefore, the rate coefficients obtained from the fit of the model to experiment 1 are more reliable. However, it must be stipulated that, collectively, these are challenging experiments working close to the extremes of the NMR spectrometer detection limits and some variability between separate, distinct datasets is to be expected.

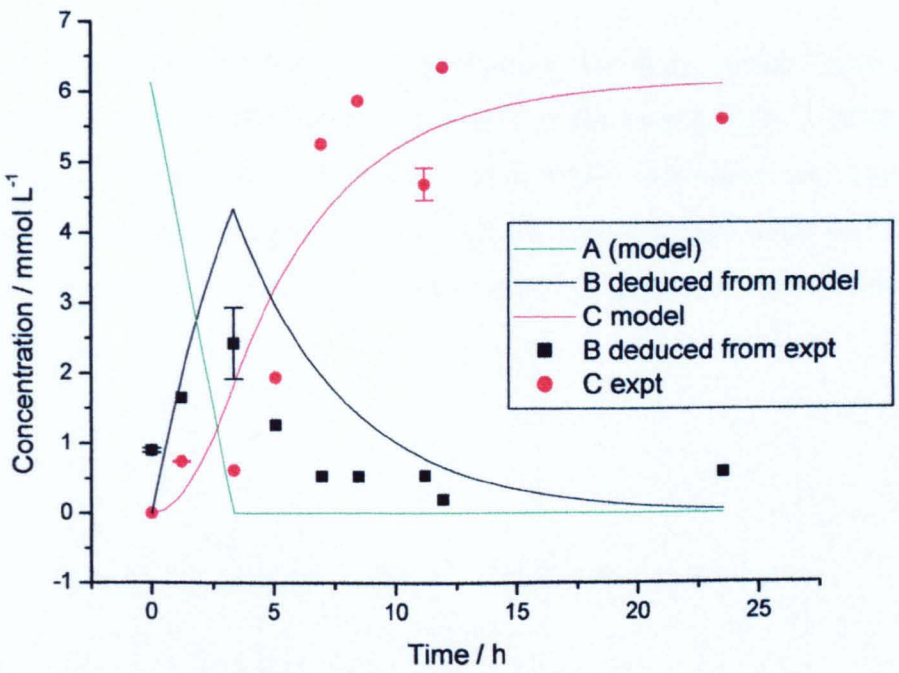

Figure 135 Reaction profile of the dissociation and dissolution of 4-BA.HCl$_{(s)}$ in chlorobenzene at 373 K (experiment 3) showing the concentrations of 4-BA.HCl$_{(s)}$, 4-BA.HCl$_{(solv)}$ and 4-BA$_{(solv)}$ calculated from the model (using Equations (71), (72) and (73)) compared with the concentrations of 4-BA.HCl$_{(solv)}$ and 4-BA$_{(solv)}$ derived from the experimental data.

■ - Experimental values of 4-BA.HCl$_{(solv)}$ concentrations (calculated by subtraction of NH_2 from CH_2 concentrations), black line - calculated 4-BA.HCl$_{(solv)}$ concentrations (using Equations (72)), ● - experimental values of 4-BA$_{(solv)}$ concentrations (calculated from the NH_2 concentrations), red line - calculated 4-BA$_{(solv)}$ concentrations from the model (using Equation (73)) and the green line - the calculated concentration of 4-BA.HCl$_{(s)}$ concentrations from the model (using Equation (71))

Nevertheless, the trends observed with experiment 1 (Figure 133) are essentially reproduced in experiment 3 (Figure 135), validating the generality of the postulated model. A third data set was recorded, experiment 2 (Figure 127) but is not complete and is therefore unsuitable for further analysis. It would be useful to obtain more data to check the robustness of the model and to evaluate the variability of the derived rate coefficients. Additionally, it is noted that these results were obtained under fixed and optimised mixing conditions. Experimental arrangements with improved mixing characteristics are expected to increase the magnitude of the rate coefficients.

6.4 Summary

The preliminary dissociation experiments of 4-BA.$HCl_{(s)}$ and the purely solution phase reactions of 4-BA.$HCl_{(solv)}$ provided clues to the reaction mechanism. At temperatures above 347 K, 4-$BA_{(solv)}$ was observed, however, in sealed reaction vessels the heating 4-BA.$HCl_{(solv)}$ at 353 K did not produce 4-$BA_{(solv)}$. These experiments combined with the understanding of the thermal stability gained from the TGA experiments, and the knowledge of the lattice energies allowed the development of a reaction mechanism for the solution phase conversion of 4-BA.$HCl_{(s)}$ to 4-$BA_{(solv)}$.

Under closed reaction conditions at 373 K, dissolution of 4-BA.$HCl_{(s)}$ is observed. The dissolution of 4-BA.$HCl_{(s)}$ is a first order process, reaching a saturation limit of approximately 2.2 mmol L^{-1}. Under these conditions no 4-$BA_{(solv)}$ is observed. The energy required to overcome the dispersive forces of the solid lattice of 4-BA.HCl is 310 kJ mol^{-1}, the enthalpy of solvation must be of comparable size to allow dissolution of 4-BA.$HCl_{(s)}$.

The open system favours the full conversion to 4-$BA_{(solv)}$, under these conditions the release of $HCl_{(solv)}$ to the gas phase is allowed, and the large energy binding the ion pair of 4-BA.$HCl_{(solv)}$ is overcome. Reaction under these conditions has been successfully modelled as a consecutive process, where the first stage is zero order and the second first order. The conversion to 4-$BA_{(solv)}$ is only limited by the concentration of 4-BA.$HCl_{(s)}$, A_0.

Chapter 7

Conclusions

7 Conclusions

A side reaction in the manufacture of isocyanates, producing highly insoluble amine hydrochloride salts, causes loss of starting material and costly downstream digestion in the industrial process. To gain insight into the possible conversion of these unwanted amine hydrochloride salts to valuable amine starting material in the solution phase; their solid state structure, thermal stability and solution phase behaviour were investigated. These investigations have culminated in the determination of a kinetic model for the recovery of starting material from the low solubility hydrochloride salt.

A major outcome of this work was the determination of the crystal structures of the five compounds. The intermolecular bonding present in the structure of the methylene dianiline series (MDA, MDA.2HCl and $[MDAH_2]^{2+}.2Cl^{-}.2MDA.H_2O$) compared with the 4-benzylaniline series (4-BA and 4-BA.HCl) was more extensive and stronger, as determined from the lattice energy calculations. These findings rationalised the previous difficulties encountered when investigating the solubility of MDA.2HCl in the process solvent (chlorobenzene) and directed the focus of the solution phase investigations and determination of a kinetic model on 4-BA.HCl. The extent of intermolecular bonding evident in the crystal structures also fuelled the desire for further characterisation of these solids; the full assignment of the FTIR spectra using the DFT calculations coupled with INS spectroscopy.

The initial aim of this project was to measure the rate of formation of amine from the amine hydrochloride with this reaction thought to represent one part of an equilibrium process between the solid amine hydrochloride and the solvated amine (Equation (74)). However, it was subsequently discovered that this simple equilibrium description as originally envisaged was incomplete due, principally, to complications with the dissolution of HCl. The chemical system needs to be reclassified in terms of an 'open' and 'closed' system.

$$\text{Amine.HCl}_{\text{solid}} \underset{k_{-1}}{\overset{K_1}{\overset{k_1}{\rightleftharpoons}}} \text{Amine}_{\text{solv}} + \text{HCl}_{\text{solv}} \qquad (74)$$

7.1 Reaction model

Due to the limited solubility of MDA.2HCl, which is representative of the structure of the industrial waste material, 4-BA.HCl was used as a model compound for the investigation of the behaviour of these salts in solution. The proposed reaction scheme (Figure 136) describes the conditions under which the dissociation of the unwanted by-product (4-BA.HCl) to the valuable industrial starting material (4-BA) can occur. Reaction in a closed system shows no amine production while reaction in an open system permits, within solubility limits, the complete consumption of solid waste to produce free amine. From these two extremes the conversion of waste hydrochloride salt in the industrial reactor can be rationalised.

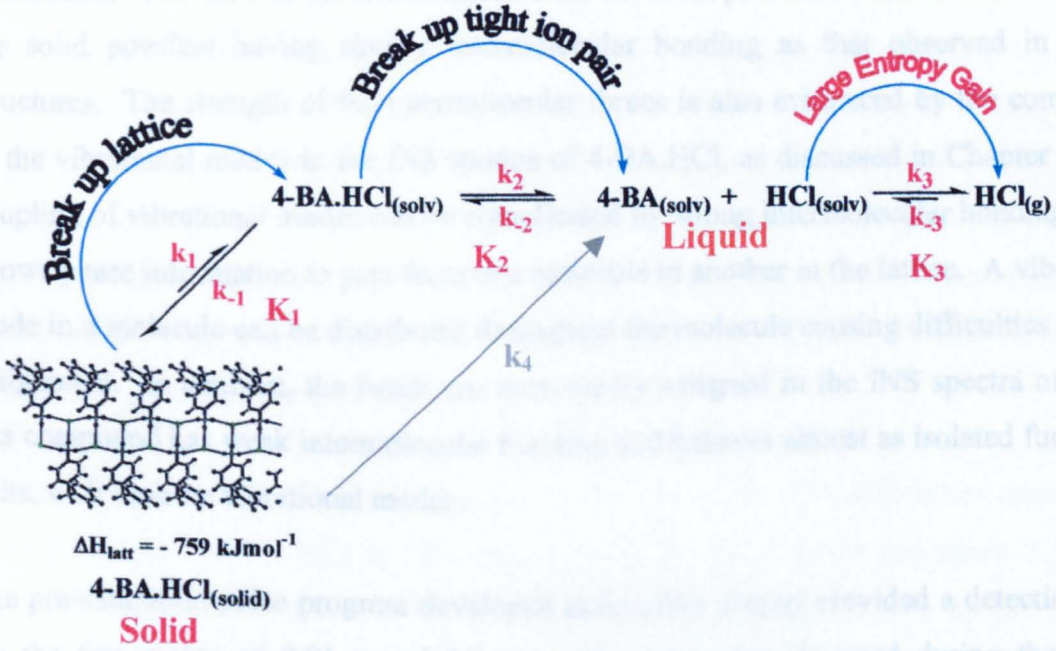

Figure 136 Proposed reaction scheme for the dissociation of 4-BA.HCl$_{(s)}$ to 4-BA$_{(solv)}$.

7.1.1 The closed system

A slow dissolution (0.005 ± 0.003 min^{-1}) of 4-BA.HCl$_{(s)}$ is observed at 373 K under closed conditions to a finite concentration of 2.2 mmol L^{-1}. No free amine is detected during a 10 hour mixing period. The constraint to higher solubility values is thought to be due to the favourable intermolecular bonding present in the solid state. The energy required to break the intermolecular bonds of 4-BA.HCl$_{(s)}$ can be approximated to the framework lattice energy of 310 kJ mol^{-1}. This energy represents the dispersion forces and H-bonding within

the solid lattice. This value is almost three times that of the total lattice energy of the amine starting material which has a solubility 5000 times that of 4-BA.HCl (4.722 +/- 0.034 mol L^{-1} at 293 K).

For free amine to be produced from these strongly bonded hydrochloride salts in the closed system, there must be a balance between the energy produced by solvation of the products (4-BA and HCl) in chlorobenzene and the energy required to break the tight ion pair ($4\text{-BA.HCl}_{(solv)}$, 449 kJ mol^{-1}). As no free amine is observed, it is deduced that the energy gained from solvation of 4-BA and HCl in chlorobenzene must be less than the energy required to break up the tight ion pair of $4\text{-BA.HCl}_{(solv)}$.

Good agreement was obtained between the INS spectra predicted from the DFT calculations with the INS spectra obtained from the solid powders. This is consistent with the solid powders having similar intermolecular bonding as that observed in crystal structures. The strength of the intermolecular forces is also evidenced by the complexity of the vibrational modes in the INS spectra of 4-BA.HCl, as discussed in Chapter 5. The coupling of vibrational modes can be complicated by strong intermolecular bonding which allows phase information to pass from one molecule to another in the lattice. A vibrational mode in a molecule can be distributed throughout the molecule causing difficulties in band assignment. In contrast, the bands are more easily assigned in the INS spectra of 4-BA; this compound has weak intermolecular bonding and behaves almost as isolated functional units, with discrete vibrational modes.

The pre-saturation pulse program developed during this project provided a detection limit for the free amine of 0.01 mmol L^{-1}. As no amine was observed during the closed experiments, this detection limit gives an upper limit of the equilibrium constant (K_2 in Figure 136) of 4.5×10^{-8} mol L^{-1}. From the discussion below, it is believed that this equilibrium exists; otherwise no amine would ever be produced. But, under these closed conditions the equilibrium lies far to the side of the tight ion-pair ($4\text{-BA.HCl}_{(solv)}$).

7.1.2 The open system

In complete contrast to the closed system, full conversion of $4\text{-BA.HCl}_{(s)}$ to $4\text{-BA}_{(solv)}$ is observed under open conditions. This reaction has been modelled as a consecutive reaction, the first step being a 0^{th} order production of $4\text{-BA.HCl}_{(solv)}$ and the second step,

the 1st order consumption of 4-BA.$HCl_{(solv)}$ to produce 4-$BA_{(solv)}$. The data are in good agreement with the consecutive model predictions. The release of $HCl_{(solv)}$ to the gas phase is proposed as the crucial difference between the closed and open systems. This model is based on a purely solution phase production of 4-BA, with no contribution from thermal decomposition of 4-BA.$HCl_{(s)}$, in agreement with the TGA results.

The consecutive reaction model is proposed with the 0th order dissolution of 4-BA.$HCl_{(s)}$, independent of its initial concentration with a calculated rate of 0.016 +/- 0.0022 mmol L^{-1} min^{-1}. This is consistent with there being no 4-BA.$HCl_{(s)}$ at the end of reaction, the saturation limit of 4-BA.$HCl_{(solv)}$ is not exceeded and the solid is entirely consumed. The maximum concentration observed in the open experiment was 3.0 ± 0.51 mmol L^{-1}, which is similar to the saturation limit of 2.2 ± 0.23 mmol L^{-1} observed in the closed experiments.

The second step, the conversion of 4-BA.$HCl_{(solv)}$ to 4-$BA_{(solv)}$, fits the profile of a first order reaction, with a calculated rate coefficient of 0.0033 +/- 0.0001 min^{-1}. The reaction is dependent on the concentration of 4-BA.$HCl_{(solv)}$ and is complete when 4-BA.$HCl_{(solv)}$ is consumed after approximately 10 h. For 4-$BA_{(solv)}$ to be produced in significant quantities, the energy of the tight ion pair (449 kJ mol^{-1}) of 4-BA.$HCl_{(solv)}$ must be exceeded. The factor contributing to the formation of 4-$BA_{(solv)}$ in the open system is believed to be the entropically favoured release of $HCl_{(solv)}$ to the gas phase.

HCl has a limited solubility in chlorobenzene (0.13 mol L^{-1}). The difficulties encountered when trying to dissolve HCl in chlorobenzene suggest once in the gas phase it will not readily dissolve back into the reaction solution. If $HCl_{(solv)}$ partitions into the gas phase in the open system, it will be lost from the reaction, preventing the back reaction to form 4-BA.$HCl_{(solv)}$.

7.2 Consequences of this work

MDA has a much lower solubility in the process solvent than 4-BA, and better represents the structure of the industrial polymeric amine starting material. An argument stands that 4-BA is possibly an inappropriate model system, and the rate data obtained is not applicable to the industrial case. Nevertheless, the proposed mechanism does give insight into the possible route by which waste hydrochloride salt is converted to valuable amine starting material. The 4-BA model is a good starting point to understanding the chemical transformations inherent in the *industrial amine.*

Using 4-BA.HCl as a model for the industrial waste material has permitted the deduction of a reaction scheme, where the loss or retention of $HCl_{(solv)}$ effectively acts as a chemical switch between complete or non waste conversion. This redefining of the parameters that describe the system and its surroundings for the dissociation of amine hydrochloride in chlorobenzene represent the most influential discovery of this project. This awareness offers enticing prospects for future waste minimisation strategies within the large-scale process.

8 References

1 A H Tullo, *C&EN,* **2007,** 85, 24-25.

2 D Randall and S Lee, *The polyurethanes book,* John Wiley & Sons, **2002,**

3 D C Miles and J H Briston, *Polymer Technology,* Temple Press Books, **1965,** London,

4 W B H Seymour, *Modern Plastics Technology,* **1975,**

5 Y Yakabe, K. M Henderson, W. C Thompson, D Pemberton, B Tury and R. E Bailey, *Environ. Sci. Technol.,* **1999**, 33, 2579-2583.

6 V Markovick and D A Hicks, *Philos Tr R Soc S-A,* **1997**, 355, 1415-1424.

7 A. Corma, P. Botella and C. Mitchell, *Chem. Commun.,* **2004**, 2008-2010.

8 P. A. Quadros, Jaam Castro and Cmsg Baptista, *Ind. Eng. Chem. Res.,* **2004**, 43, 4438-4445.

9 G. Wegener, M. Brandt, L. Duda, J. Hofmann, B. Klesczewski, D. Koch, R. J. Kumpf, H. Orzesek, H. G. Pirkl, C. Six, C. Steinlein and M. Weisbeck, *Appl. Catal., A,* **2001**, 221, 303-335.

10 K Weissermel and H-J Arpe, *Industrial Organic Chemistry,* Wiley-VCH, 3rd ed, **2003,**

11 A. de Angelis, P. Ingallina and C. Perego, *Ind. Eng. Chem. Res.,* **2004**, 43, 1169-1178.

12 E J Beckman, *Ind. Eng. Chem. Res.,* **2003**, 42, 1598-1602.

13 *Chemistry World,* **2006**, 16.

14 K. Y. Chen, J. F. Kuo and C. Y. Chen, *Biomaterials,* **2000**, 21, 161-171.

15 A. W. Smith, *Adv. Drug Delivery Rev.,* **2005**, 57, 1539-1550.

16 M Loenders and I Vermeesch, *Diaminodiphenylmethane (DADPM) hydrochlorides: determination of the solubility in monochlorobenzene.,* ICI Polyurethanes International research and technology, **1996,**

17 Z. H. Lin, L. L. Zhou, A. Mahajan, S. Song, T. Wang, Z. H. Ge and D. Ellison, *J. Pharm. Biomed. Anal.,* **2006**, 41, 99-104.

18 E. Thomas and J. Rubino, *Int. J. Pharm.,* **1996**, 130, 179-185.

19 S. F. Li, P. Doyle, S. Metz, A. E. Royce and A. T. M. Serajuddin, *J. Pharm. Sci.,* **2005**, 94, 2224-2231.

20 P W Atkins, *Physical Chemistry,* Oxford University Press, 6th ed, **1998,**

21 R J Silbey and R A Alberty, *Physical Chemistry,* John Wiley & Sons, 3rd ed, **2001,**

22 G Rayner-Canham, *Descriptive Inorganic Chemistry,* W H Freeman and Company, 2nd ed, **2000,**

23 F M Hall, *The theory of acids and bases,* **1964**, 1, 91-98.

24 J Barrett, *Inorganic chemistry in aqueous solution,* The Royal Society of Chemistry, **2003**, Vol.21, Cambridge,

25 N N Greenwood and A Earnshaw, *Chemistry of the Elements,* Pergamon Press, **1984**, Oxford,

26 J. L. Adcock, *J. Chem. Educ.*, **2001**, 78, 1495-1496.

27 P G T Fogg and W Gerrard, *Solubility of gases in liquids : A critical evaluation of gas/liquid systems in theory and practice,* John Wiley & Sons, **1991**,

28 K Burger, *Solvation, ionic and complex formation reactions in non-aqueous solvents,* Akademiai Kiado, **1983**, Vol.6, Budapest,

29 R C Weast, *Handbook of Chemistry and Physics,* The Chemical Rubber Co., 46th ed, **1964**, Ohio,

30 M. Z. Ilic and R. W. Cattrall, *J Inorg Nucl Chem,* **1981**, 43, 2855-2857.

31 D F Shriver, P W Atkins and C H Langford, *Inorganic Chemistry,* Oxford University Press, 2nd ed, **1994**, Oxford,

32 C Giacovazzo, H L Monaco, D Viterbo, F Scordari, G Gilli, G Zanotti and M Catti, *Fundamentals of Crystallography,* Oxford Science Publications, **1994**, Vol.2,

33 J E Huheey, *Inorganic Chemistry principles of structure and reactivity,* Harper and Row, 2nd ed, **1978**,

[34] J D Dunitz and A Gavezzotti, *Angew. Chem. Int. Ed,* **2005**, 44, 1766 - 1787.

35 A. Gavezzotti, *J. Phys. Chem. B,* **2002**, 106, 4145-4154.

36 A. Gavezzotti, *J. Phys. Chem. B,* **2003**, 107, 2344-2353.

37 P R Griffiths, *Chemical Infrared Fourier Transform Spectroscopy,* John Wiley & Sons, **1975**,

38 N B Colthup and L H Daly, *Introduction to Infrared and Raman Spectroscopy,* Academic Press, **1975**, New York,

39 J. Grdadolnik, *Acta Chim. Slov.*, **2002**, 49, 631-642.

40 W Clegg, *Crystal Structure Determination,* Oxford University Press, **1998**, Oxford,

41 J PGlusker, M Lewis and M Rossi, *Crystal structure analysis for chemists and biologists,* Wiley-VCH, **1994**, Weinheim,

42 J P Glusker and K N Trueblood, *Crystal Structure Analysis. A Primer,* Oxford University Press, 2nd ed, **1985**, Oxford,

43 G R Desiraju and T Steiner, *The Weak Hydrogen Bond,* Oxford Science Publications, **2001**, Vol.9,

44 G A Jeffrey, *An Introduction to Hydrogen Bonding,* Oxford University Press, **1997**, Oxford,

45 J B Foresman and A Frisch, *Exploring Chemistry with Electronic Structure Methods,* Gaussian Inc., 2nd ed, **1996**, Pittsburgh,

46 W Koch and M C Holthausen, *A Chemist's Guide to Density Functional Theory,* Wiley-VCH, **2000**, New York,

47 B. S. Hudson, *J. Phys. Chem. A,* **2001**, 105, 3949-3960.

48 A. J. Ramirez-Cuesta, *Comput. Phys. Commun,* **2004**, 157, 226-238.

49 D. Colognesi, M. Celli, F. Cilloco, R. J. Newport, S. R. Parker, V. Rossi-Albertini, F. Sacchetti, J. Tomkinson and M. Zoppi, *Appl. Phys. A: Mater. Sci. Process.*, **2002**, 74, S64-S66.

50 S F Parker, J Thomkinson, A J Ramiriz-Cuesta and D Colgnesi, *The TOSCA Users Guide,* **2003**,

51 P C H Mitchell, S F Parker, A J Ramirez-Cuesta and J Thomkinson, *Vibrational Spectroscopy with Neutrons, With applications in Chemistry, Biology, Materials Science and Catalysis,* World Scientific, **2005**, Vol.3,

52 P J Haines, *Thermal Methods of Analysis; Principles, Applications and Problems,* Blackie Academica & Professional, **1995**, Glasgow,

53 A Blazek, *Thermal analysis,* Van Nostrand Reinhold, **1973.**, London,

54 D H Williams and I Flemming, *Spectroscopic Methods in Organic Chemistry,* McGraw Hill, 5th ed, **1995**,

55 J W Akitt, *NMR and Chemistry An introduction to the Fourier transform-multinuclear era,* Chapman and Hall, 2nd ed, **1983**, London,

56 P J Hore, J A Jones and S Wimperis, *NMR: The toolkit,* Oxford University Press, **2006**,

57 R K Harris, *Nuclear Magnetic Resonance Spectroscopy,* Pitman Books, **1983**, London,

58 S. H. Smallcombe, S. L. Patt and P. A. Keifer, *J Magn Reson Ser A,* **1995**, 117, 295-303.

59 S Berger and S Braun, *200 and More NMR Experiments,* Wiley-VCH, 2nd, **2004**,

60 S. M. Zhang, X. B. Yang and D. G. Gorenstein, *J. Magn. Reson.*, **2000**, 143, 382-386.

61 A A Frost and R G Pearson, *Kinetics and Mechanism,* John Wiley & Sons, 2nd ed, **1961**,

62 D. W. Ball, *J. Chem. Educ.*, **1998**, 75, 917-919.

63 P Tebutt, *Basic Mathematics for Chemists,* John Wiley & Sons, 2nd ed, **1998**, New York,

64 E S Swinbourne, *Analysis of Kinetic Data,* Thomas Nelson & Sons, **1971**,

65 A. Khairuzzaman, S. U. Ahmed, M. Savva and N. K. Patel, *Int. J. Pharm.*, **2006**, 318, 15-21.

66 K. M. Picker, *Eur J Pharm Biopharm,* **1999**, 48, 267-268.

67 R E Walpole, *Introduction to Statistics,* Macmillan Publishing, 3rd ed, **1982**,

68 P R Hinton, *Statistics Explained,* Routledge, 2nd ed, **2004**,

69 J Leonard, B Lygo and G Procter, *Advanced practical organic chemistry,* Blackie Academic & Professional, 2nd ed, **1995**, London,

70 B. R. Tarr, *Inorg Syn,* **1950**, 3, 191-194.

71 G M Sheldrick, *SHELX97-Programs for Crystal Structure Analysis,* **1998**, (Release 97-2),

72 L J Farrugia, *J. Appl. Crystallogr.*, **1999**, 32, 837.

73 Z Otwinowski and W Minor, *Method Enzymol,* **1997**, 276, 307-326.

74 A. L. Spek, *J. Appl. Crystallogr.*, **2003**, 36, 7-13.

75 F L Hirshfeld, *Acta Crystallogr., Sect. A: Found. Crystallogr,* **1976**, 239-244.

76 B. Delley, *J. Chem. Phys.*, **2000**, 113, 7756-7765.

77 R J Fessenden and J S Fessenden, *Organic Laboratory Techniques,* Brooks/Cole Publishing, **1993**, Belmont, California,

78 A D Bain, D M Rex and R N Smith, *Magn. Reson. Chem,* **2001**, 39, 122-126.

79 S Meiboom, *J. Chem. Phys.*, **1961**, 34, 375-388.

80 F A L Anet and V J Basus, *J. Magn. Reson.*, **1978**, 32, 339-343.

81 J Reuben and D Fiat, *J. Chem. Phys.*, **1969**, 51, 4918-4927.

82 R P Bell, *J. Chem. Soc,* **1932**, 2905-2911.

83 S. H. Bauer, T. Yamazaki, K. I. Lazaar and N. S. Chiu, *J. Am. Chem. Soc.*, **1985**, 107, 743-747.

84 G Herzberg, *Molecular Spectra and Molecular Structure,* Krieger Publishing Company, **1991**, Vol.II: Infrared and Raman Spectra of Polyatomic Molecules,

85 J M Hollas, *Modern Spectroscopy,* John Wiley & Sons, **1987,**

86 W. West and R. T. Edwards, *J. Chem. Phys.,* **1937**, 5, 14-22.

87 C. E. Leberknight and J. A. Ord, *Phys Rev,* **1937**, 51, 430-433.

88 D. Williams, *Phys Rev,* **1936**, 50, 719-722.

89 J. P. Devlin, N. Uras, J. Sadlej and V. Buch, *Nature,* **2002**, 417, 269-271.

90 S. J. O'Brien and J. B. Byrne, *J. Am. Chem. Soc.,* **1940**, 62, 2063-2065.

91 H. C. Brown and J. D. Brady, *J. Am. Chem. Soc.,* **1952**, 74, 3570-3582.

92 I R Dunkin, *Matri-Isolation Techniques,* Oxford University Press, **1998**, Oxford,

93 A J Barnes, H E Hallam and G F Scrimshaw, *Trans. Faraday. Soc,* **1969**, 65, 3150-3158.

94 W. A. Herrebout and B. J. van der Veken, *J. Mol. Struct.,* **1998**, 449, 231-240.

95 A. C. Legon, P. D. Aldrich and W. H. Flygare, *J. Am. Chem. Soc.,* **1982**, 104, 1486-1490.

96 W. G. Read, E. J. Campbell and G. Henderson, *J. Chem. Phys.,* **1983**, 78, 3501-3508.

97 J A Pople, W G Schneider and H J Bernstein, *High-resolution nuclear magnetic resonance,* McGraw-Hill, **1959,**

98 D Lin-Vien, N R Colthup, W G Fateley and J G Grasselli, *The Handbook of Infrared and Raman Characteristic Frequencies of Organic Molecules,* Academic Press, **1991,** London,

99 I I Konstantinov, V D Selivanov and T I Melent'eva, *J Appl Chem-USSR,* **1975**, 48, 2099-2100.

100 F A Bovey, L Jelinski and P A Mirau, *Nuclear Magnetic Resonance Spectroscopy,* Academic Press, 2nd ed, **1988**, London,

101 Dr. K W Muir, Department of Chemistry, University of Glasgow,

102 F H Allen, *Acta Crystallogr., Sect. B: Struct. Sci,* **2002**, 58, 380-388.

103 D.A. Fletcher, R.F. McMeeking and D. Parkin, *J. Chem. Inf. Model.,* **1996**, 36, 746-749.

104 V K Bel'skii, V K Rotaru and M M Kruchinin, *Crystallogr. Rep.,* **1983**, 28, 695-698.

105 J. A. J. Jarvis and P. G. Owston, *J. Chem. Soc. D,* **1971**, 1403.

106 J W Swardstrom, D P Miller and L A Duvall, *Acta Crystallogr., Sect. B: Struct. Sci.,* **1972**, B28, 2510-2514.

107 J. Keegan, P. E. Kruger, M. Nieuwenhuyzen, J. O'Brien and N. Martin, *Chem. Commun.,* **2001**, 2192-2193.

108 G. B. Jones, *Tetrahedron,* **2001**, 57, 7999-8016.

109 C. J. Brown, *Acta. Cryst.,* **1949**, 2, 228-232.

110 G A Jeffrey and W Saenger, *Hydrogen Bonding in Biological Structures,* Springer-Verlag, **1991**, Berlin,

111 E O Schlemper, W C Hamilton and S J La Placa, *J. Chem. Phys,* **1971**, 54, 3990-4000.

112 K. Molcanov, B. Kojic-Prodic and N. Raos, *Acta Crystallogr., Sect. B: Struct. Sci.,* **2004**, 60, 424-432.

113 J C Speakman, *Struct Bond.,* **1972**, 12, 141-199.

114 P G Jones and B Ahrens, *Eur. J. Org. Chem.,* **1998**, 1998, 1687-1688.

115 C H MacGillavry and G D Rieck, *International Tabes for X-ray Crystallography, Physical and Chemical Tables,* Kluwer Academic Publishers, 2nd ed, **1999**, Vol.C. I.U.Cr, Dordrecht, The Netherlands, Table 9.5.1.1.

116 G. Portalone, *Acta Crystallogr., Sect. E: Struct. Rep. Online,* **2005**, 61, 3083-3085.

117 G. Plougsorensen and E. K. Andersen, *Acta Crystallogr., Sect. C: Cryst. Struct. Commun.,* **1985**, 41, 613-615.

118 M. Colapietro, A. Domenicano, C. Marciante and G. Portalone, *Acta Crystallogr., Sect. B: Struct. Sci.,* **1981**, 37, 387-394.

119 J D Dunitz, *X-ray analysis and the structure of organic molecules,* Verlag Helvetica Chimica Acta - VCH, 2nd ed, **1995**, New York,

120 C J Brown and M Ehrenberg, *Acta Crystallogr., Sect. C: Cryst. Struct. Commun.,* **1985**, 41, 441-443.

121 J. F. Malone, C. M. Murray, M. H. Charlton, R. Docherty and A. J. Lavery, *J Chem Soc Faraday T,* **1997**, 93, 3429-3436.

122 A. Gavezzotti, *J. Chem. Theor. Comp,* **2005**, 1, 834-840.

123 G. Filippini and A. Gavezzotti, *Acta Crystallogr., Sect. B: Struct. Sci.,* **1993**, 49, 868-880.

124 M. P. M. Marques, Laeb de Carvalho and J. Tomkinson, *J. Phys. Chem. A,* **2002**, 106, 2473-2482.

125 A. M. Amado, J. C. Otero, M. P. M. Marques and Laeb de Carvalho, *ChemPhysChem,* **2004**, 5, 1837-1847.

126 A. Predoi-Cross, R. M. Lees and J. W. C. Johns, *J. Mol. Spectrosc,* **1998**, 191, 348-361.

127 B P Straughan and S Walker, *Spectroscopy,* Chapman and Hall, **1976**, Vol.2,

128 A. Khairuzzaman, S. U. Ahmed, M. Savva and N. K. Patel, *Int. J. Pharm.,* **2006**, 318, 15-21.

129 Dr A. Miller, University of Glasgow, December 2006

130 Origin Manual, *Origin 7.5,* OriginLab Corp., **2003**, Northampton, MA,